DOE Office of Indian Energy - FINAL Progress Report

Recipient Organization:	**NANA Regional Corporation**
Project Title:	**Community-Scale Solar Deployment in the Northwest Arctic**
Covering Period:	September 1, 2016 – December 31, 2021
Date of Report:	April 30, 2022
Award Number:	**DE-IE0000034**
Technical Contact:	Sonny Adams 909 W. 9th Ave Anchorage, AK 99501 (907) 265-4185 sonny.adams@nana.com
Business Contact:	Kim Cunningham 909 W. 9th Ave Anchorage, AK 99501 (907) 265-3700 kimberly.cunningham@nana.com
Partners:	Kotzebue IRA Tribal Council Buckland IRA Tribal Council City of Buckland Deering IRA Council City of Deering Kotzebue Electric Association Ipnatchiaq Electric Company Northwest Arctic Borough Kikiktagruk Inupiat Corporation Deerstone Consulting LLC Advanced Microgrids LLC

Table Of Contents

Table of Contents

Table of Figures

Acknowledgements

This material is based upon work supported by the Department of Energy, Office of Indian Energy Policy and Programs, under Award Number DE- IE0000034.

Special thanks to NRC Village Energy Program Director Sonny Adams and NRC Energy Coordinator Terrell Jones, the City of Buckland Electric Utility, the Native Village of Buckland Tribal Council, Alaska Native Tribal Health Consortium (ANTHC) support staff working under the City of Buckland, the Ipnatchiaq Electric Company under the City of Deering, the Native Village of Deering Tribal Council, BoxPower, SMA, Inc., ABB, Inc., Kotzebue Electric Association, and DeerStone Consulting. Without your commitment to bring renewable energy to the Northwest Arctic region of Alaska, this project wouldn't have been possible.

Acronyms and Abbreviations

ANC	Alaska Native Corporation
ANRI	Alaska Native Renewable Industries
ANTHC	Alaska Native Tribal Health Consortium
AVEC	Alaska Village Electric Cooperative
BESS	Battery Energy Storage System
DOE-OIE	Department of Energy – Office of Indian Energy
IEC	Ipnatchiaq Electric Company (in Deering)
KEA	Kotzebue Electric Association
KIC	Kikktagruk Inupiat Corporation
NAB	Northwest Arctic Borough
NANA	NANA – Alaska Native Regional Corporation for the Northwest Arctic
NRC	NANA Regional Corporation
NRECA	National Rural Electric Cooperative Association
PV	Photovoltaic
WTP	Water Treatment Plant

Executive Summary

NANA Regional Corporation (NRC, or NANA) was formed as an Alaska Native Corporation (ANC) pursuant to the Alaska Native Claims Settlement Act of 1971. Our lands cover 39,000 square miles of the Northwest Arctic region of Alaska (Appendix A, Maps and Figures). We partner closely with the Northwest Arctic Borough (NAB) and our 11 remote communities on numerous projects and activities, especially around clean energy initiatives that improve quality of life and help to reduce extremely high energy costs experienced by the communities in our region. Collectively, the regional partnership has developed numerous successful solar, wind, biomass, and energy storage, distribution upgrade, and efficiency projects.

The Department of Energy-Office of Indian Energy (DOE-OIE) awarded NRC a $1 million Tribal Deployment Grant to install solar photovoltaic (PV) in three of the 11 NRC communities: Buckland, Deering, and Kotzebue; with an obligation for an additional $1 million in non-federal cost share from NANA and/or the other project participants. For this project, NRC worked directly with the three stand-alone electric utilities that serve Buckland, Deering, and Kotzebue.

The characteristics of the three participating communities are vastly different and illustrate the diversity across our region. Deering is an extremely small community of about 150 residents, whereas Kotzebue is by far the largest in our region with a population of almost 3,300 (Appendix B, Community Energy Profiles); Deering and Kotzebue are coastal communities, while Buckland's approximately 500 residents live over 15 miles inland on the Buckland River, which substantially impacts subsistence opportunities and activities as well as the cost and availability of imported commodities such as diesel fuel. However, by virtue of all three communities owning and operating their own electric utilities, they share at least one thing in common: all have a history of innovation in their pursuit of alternative and renewable energy projects, including wind energy, heat recovery, and small-scale solar on community water plants.

All three projects were successful and groundbreaking in various ways. The Buckland solar PV system, installed in 2018 at about 45 kW and using BoxPower's unique racking design on shipping containers and SMA inverters, became the first solar-wind-battery-diesel hybrid system to perform in diesels-off mode for substantial amounts of time. The Deering solar PV system, installed in 2019 at about 48.5 kW, used similar equipment but demonstrated significant cost savings by combining inverters, improved communications with ABB microgrid control technology, and reduced anchoring logistics and material requirements. Deering is also performing in diesels-off mode for hundreds of hours annually. The Kotzebue solar PV system, installed in 2020 at 576 kW, is the largest solar PV array in rural Alaska and is demonstrating high performance in replacing old, non-performing wind assets using the same communication lines and inverter housing that was originally established for older wind turbines. Kotzebue also successfully demonstrated the use of bi-facial solar PV panels to further increase performance with no cost additions. Kotzebue is not yet performing in diesels-off mode simply because the load is too high relative to their renewable energy generation and energy storage assets, but this solar PV array meaningfully advanced their march toward diesels-off and they continue to add renewable generation and storage.

Combined, these three systems have firmly demonstrated solar PV's role in the Northwest Arctic's renewable energy landscape. This DOE Tribal Deployment grant has also helped to create the template for future solar deployments in the region and across the state as we now see tremendous proliferation in the number and size of these projects, including Shungnak at 225 kW and Noatak at about 275 kW.

Introduction

NANA Regional Corporation (NRC, or NANA) was formed as an Alaska Native Corporation (ANC) pursuant to the Alaska Native Claims Settlement Act of 1971. Our lands cover 39,000 square miles of the Northwest Arctic region of Alaska. We partner closely with the Northwest Arctic Borough (NAB) and our 11 remote communities on numerous projects and activities, especially around clean energy initiatives that improve quality of life and help to reduce extremely high energy costs experienced by the communities in our region. Collectively, the regional partnership has developed numerous successful solar, wind, biomass, and energy storage, distribution upgrade, and efficiency projects. To further progress, we created the Northwest Arctic Energy Steering Committee to share and replicate these benefits across the region. NANA's mission is to provide economic opportunities for our more than 13,500 Iñupiat shareholders and to protect and enhance NANA lands.

With no roads in or out, all 11 communities in the region—Ambler, Buckland, Deering, Kiana, Kivalina, Kobuk, Kotzebue, Noatak, Noorvik, Selawik, and Shungnak—are completely isolated. The only access is via ship or airplane year-round, or snow machine or dog team in the winter. All commodities must be barged or flown in depending on the status of offshore and river ice. One of our communities, Noatak, must receive everything via air shipment since the course of the nearby river changed over a decade ago, rendering the waterway no longer navigable from the ocean. The NANA Regional Corporation and Land Status map in Appendix A shows the NANA region land status and our location and relative size within Alaska. It should be noted that NANA and the NAB shares the same boundaries.

All communities are served by stand-alone, islanded diesel electric microgrids except that Shungnak and Kobuk are electrically inter-connected by a 10-mile power line with a main power plant in Shungnak and a back-up plant in Kobuk in case of power line failure. Figure 1 below shows the energy installations for all 11 Tribal communities within our region (Noatak is in progress at the time of this report).

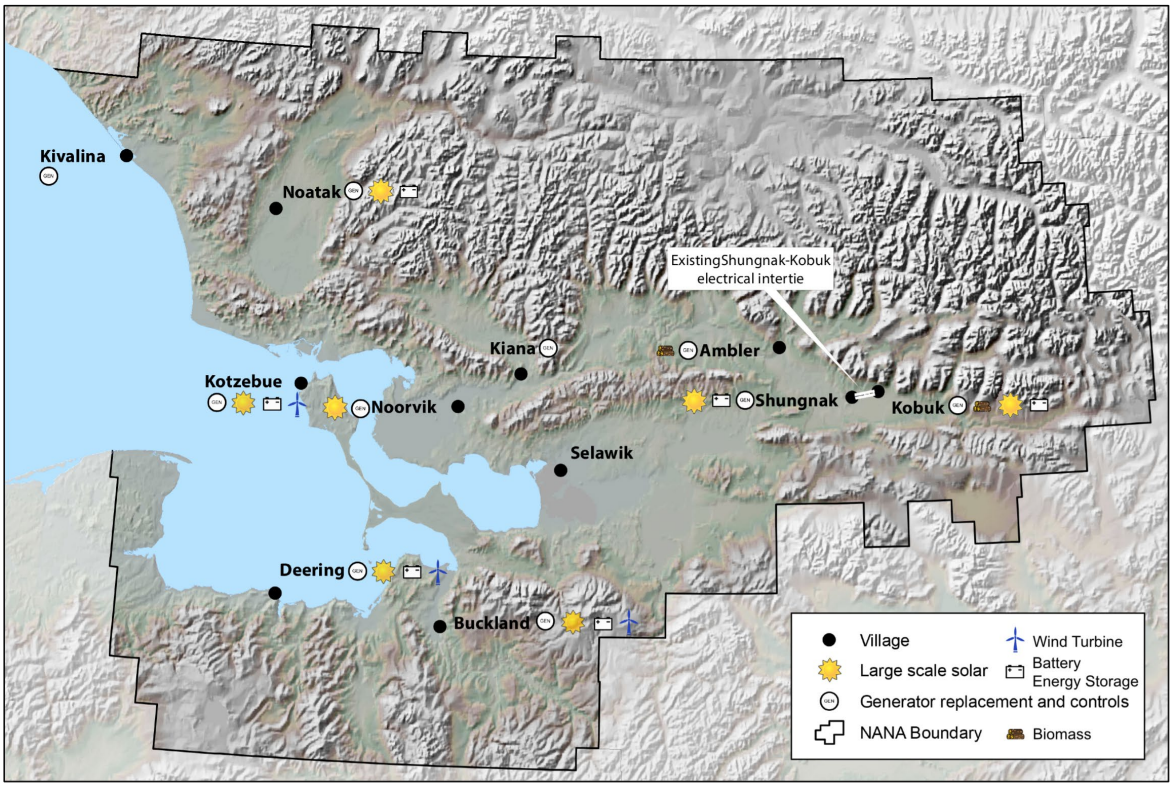

Figure 1 NANA Regional Energy Map

The Department of Energy-Office of Indian Energy (DOE-OIE) awarded NRC a $1 million Tribal Deployment Grant to install solar photovoltaic (PV) in the communities of Buckland, Deering, and Kotzebue, with an obligation for an additional $1 million in non-federal cost share from NANA and/or the other project participants. For this project, NRC worked directly with the three stand-alone electric utilities that serve Buckland, Deering, and Kotzebue. All three communities have both a federally recognized Tribal government and a state recognized City government serving their population, all of whom are NAB citizens and most of whom are also NANA shareholders. The electric utility in Buckland is owned and operated directly as a department of the City of Buckland. In Deering, the City has formed a separate sub-division known as Ipnatchiaq Electric Company (IEC) with its own board of directors and staff to manage the electric utility. In Kotzebue, the independent electric utility, Kotzebue Electric Association (KEA), is an electric cooperative with its own articles of incorporation, by-laws, board of directors and Staff, and is a member of the National Rural Electric Cooperative Association (NRECA). All eight other communities in the region are served by the same electric utility provider, Alaska Village Electric Cooperative (AVEC).

The characteristics of the three participating communities are vastly different and illustrate the diversity across our region. Deering is an extremely small community of about 150 residents, whereas Kotzebue is by far the largest in our region with a population of almost 3,300 (Appendix B, Community Energy Profiles); Deering and Kotzebue are coastal communities, while Buckland's approximately 500 residents live over 15 miles inland on the Buckland River, which substantially impacts subsistence opportunities and activities as well as the cost and availability of imported commodities such as diesel fuel. However, by virtue of all three communities owning and operating their own electric utilities, they share at least one thing in common: all have a history of innovation in their pursuit of alternative and renewable energy projects, including wind energy (Figure 2), heat recovery, and small-scale solar on community water plants.

Figure 2 Wind and Solar Energy Infrastructure in Kotzebue

Prior to this DOE funding opportunity only Kotzebue had a battery energy storage system (BESS) to stabilize their grid. However, at times, all three communities were operating high penetration renewable hybrid systems because of their wind energy contribution. Early data analysis of the wind energy systems in Deering and Buckland showed that any additional renewable energy installed on the system, such as solar PV, would augment the existing available energy enough to allow for operation of the entire grid in diesels-off mode (if a BESS could be obtained to handle the highly variable renewable production and

reduce impacts to the diesel generators, overall grid stability, and reliability). Hence, this DOE Tribal Deployment Grant to develop solar PV was accompanied by a separate effort to install batteries for both Buckland and Deering. Fortunately, both efforts secured funding around the same time, so it was possible to provide energy storage and grid stability through the BESS while increasing renewable energy contribution and creating periods of diesels-off operation. Due to the size of the community and energy load in Kotzebue, sufficient renewables or battery capacity could not be obtained to operate in diesels-off. However, KEA was interested in developing more solar PV to supplement their wind turbines, inching closer toward diesels-off operation in the future.

Grant Budget Overview

For budgeting purposes, we allocated $200,000 of DOE-OIE grant funds to both Deering and Buckland ($400,000 in total) and $600,000 to Kotzebue. All three communities provided at least one-to-one cost share, with Deering and Buckland using funds originally provided by NANA to all communities in the region (previously called "Village Economic Development" and now called "Village Economic Investment" funds) along with substantial in-kind contributions of local equipment, materials, labor, and local knowledge. KEA used funds originally provided by the NAB Village Improvement Fund, funds from its own internal budget, as well as in-kind contributions of labor, equipment, and expertise. Along with originally sourcing the cash match for Buckland and Deering, NANA contributed significant staff and contractor time for project development, community education and outreach, project management of contractors during construction, grant and financial management and reporting. NANA also leveraged other funds, organizations and expertise for production of educational and promotional videos of the projects in Buckland and Deering.

Project Description – Buckland

Buckland, Alaska was the first location to receive a solar PV system from this project, in the summer/fall of 2018. An updated Community Energy Profile for Buckland is included in Appendix B, which provides information on the community energy systems in Buckland along with community energy goals, milestones, and analyses of current and past performance.

The Buckland project team consisted of NRC Village Energy Program Director Sonny Adams and NRC Energy Coordinator Terrell Jones, the City of Buckland Electric Utility, the Native Village of Buckland Tribal Council, Alaska Native Tribal Health Consortium (ANTHC) support staff working under the City of Buckland, and DeerStone Consulting. Vendors included BoxPower, SMA, Inc., Talesun Solar Panels, and ABB, Inc. (now Hitachi). BoxPower staff were on-site to lead the installation and provided additional project management. The solar arrays were constructed on NANA land in the community of Buckland.

System Design Considerations

The system selected for Buckland consisted of three BoxPower modular arrays, each installed on a 20-ft shipping container (Figure 3). In the arctic environment, an above ground foundation design with additional gravel insulation greatly reduces the risk of permafrost disturbance and avoids costly geotechnical analysis prior to installation. By eliminating the need for heavy equipment required to drill or dig and backfill for a traditional foundation, we also avoided the high equipment mobilization costs for such a small system.

Figure 3 Complete Solar Arrays in Buckland

Each of the three shipping containers supported approximately 15 kW, for a total of 45 kW. The solar panels were Talesun TP672M-360, each at 360 Watts. There were three SMA TriPower 15 kW inverters, one for each modular array. Initially, each container was estimated to support about 20 kW of solar panels, for a total of 60 kW, but because of the more extreme tilt angle on the racking that was supported by the individual shipping containers, and the safety requirements associated with potential wind and snow loading for each container, we ultimately reduced the number of solar panels per container. Specifically, BoxPower's previous projects were all installed in locations much further south where the vertical tilt angle of the solar panels was generally 30 degrees. This allowed for more solar panels to be installed per shipping container because of less rotational force on the foundation.

In our case, because of the high latitude of Buckland and other arctic communities, we originally planned for a 60-degree vertical tilt angle, which would also shed more snow and reduce snow loading. Upon further analysis, winds can reach close to 100 mph in Buckland, so we were deterred from the ideal 60-degree tilt angle and ended up compromising with 45 degrees. The installed 45-degree tilt angle provided an acceptable safety margin for wind and snow loading and increased performance from 30 degrees. However, the 45-degree angle still placed more rotational force on the foundation/shipping container under high wind conditions as compared to 30 degrees, hence the reduced number of solar panels to reduce the rotational force vectors (Figure 4).

Figure 4 Crew Installing Racking at 45-degree Angle

Significant engineering was required to modify BoxPower's 30-degree racking design and to determine sufficient ballasting of the shipping containers. BoxPower retained Structural Engineering Excellence in California and Coffman Engineers in Alaska to calculate these modifications. It should also be noted that most commercial racking in the lower 48 for ground mount solar PV systems is only available with 30-degree tilt angle or less, so any arctic appropriate system designed for improved performance requires some customized racking if a larger tilt angle is desired.

In terms of ballasting, it was determined that almost the entire shipping container would need to be filled with material such as gravel or scrap metal (which was readily available in the community) to provide the necessary weight. This became logistically challenging in terms of moving and manipulating the gravel or scrap steel into the shipping container so as not to cause damage to the container or the heavy equipment while still maintaining structural integrity of the container. Protected space also had to be maintained in the container for the inverter and a person to view or work on the system. After much thought on how to best provide the required ballast and space, we realized that there was an excess of shipping containers in

the community, and we could simply fill one container completely with gravel as a foundation and then stack another container on top of it to support the solar PV and racking (Figure 5). We packed fill around the bottom container for additional support, so it was essentially buried above ground. Pre-engineered corner locks designed to stack shipping containers on top of each other were used to secure the containers to each other. This allowed the top container to support the solar PV system while maintaining clean interior space for the inverter and a person to monitor or repair it as needed.

Figure 5 Shipping Container Foundation (Blue Container is Buried)

The resulting system consisted of three stand-alone arrays, each using a stacked configuration of two shipping containers (Figure 5). The bottom container was filled with gravel and other scrap material and the top container supported about 15 kW of solar PV panels on the outside and a 15 kW SMA TriPower inverter on the inside. The power output was strung together into an SMA combiner box on the third pair of containers which transitioned to a buried conduit with conductor and fiber optics into the village power plant (Figure 6).

Figure 6 Trenching Conduit and Conductor into Existing Diesel Powerhouse

Figure 7 NRC Staff and Shareholder Terrell Jones Supporting BoxPower Installer

Figure 8 Installation Crew in Buckland

Figure 9 Installing Solar Panels in Buckland

Figure 10 Construction in Progress

Figure 11 Completed Solar Project Showing Power Generation Building

Performance

The detailed diesel, wind, and solar production data for Buckland starting from February 2021, to February 2022 is presented below, followed by graphical interpretation of the data. Because the SMA inverter, especially the combiner box, had difficulty communicating with the ABB microgrid controller(s), much of the early performance data was not captured in the ABB database. We were able to determine that solar PV production was occurring during this time, but we were not able to capture the output for long-term documentation. This was eventually resolved but unfortunately the first year or more of solar PV production data is not available. Further, it should be noted that once the SMA and ABB hardware and software were synced up through modbus mapping, the solar data was embedded with other generation assets, namely the wind and diesel generation. This is not a problem in terms of monitoring performance, but the result is that we have all three generation assets listed in the table below and illustrated in the graph below the table.

Date	Diesel Generation kWH	Solar PV kWh	Wind kWh	Total Generation kWh	Percent Renewables	Amount Renewables kWh
Feb-21	151490	0	25054	176544	14.2%	25054
Mar-21	151090	2545	44318	197953	23.7%	46863
Apr-21	137290	5891	27585	170766	19.6%	33476
May-21	130400	9510	19163	159073	18.0%	28673
Jun-21	105620	5839	8674	120133	12.1%	14513
Jul-21	110490	4406	14364	129260	14.5%	18770
Aug-21	127070	3931	13055	144056	11.8%	16986
Sep-21	131010	2561	20193	153764	14.8%	22754
Oct-21	145650	1424	19833	166907	12.7%	21257
Nov-21	195030	13	13646	208689	6.5%	13659
Dec-21	180590	8	22970	203568	11.3%	22978
Jan-22	204400	94	18209	222703	8.2%	18303
Feb-22	173900	808	22755	197463	11.9%	23563
TOTAL	1944030	37030	269819	2250879	13.6%	306849

Figure 12 Detailed Diesel, Wind, & Solar Production Data, Buckland (Feb 2021 - Feb 2022)

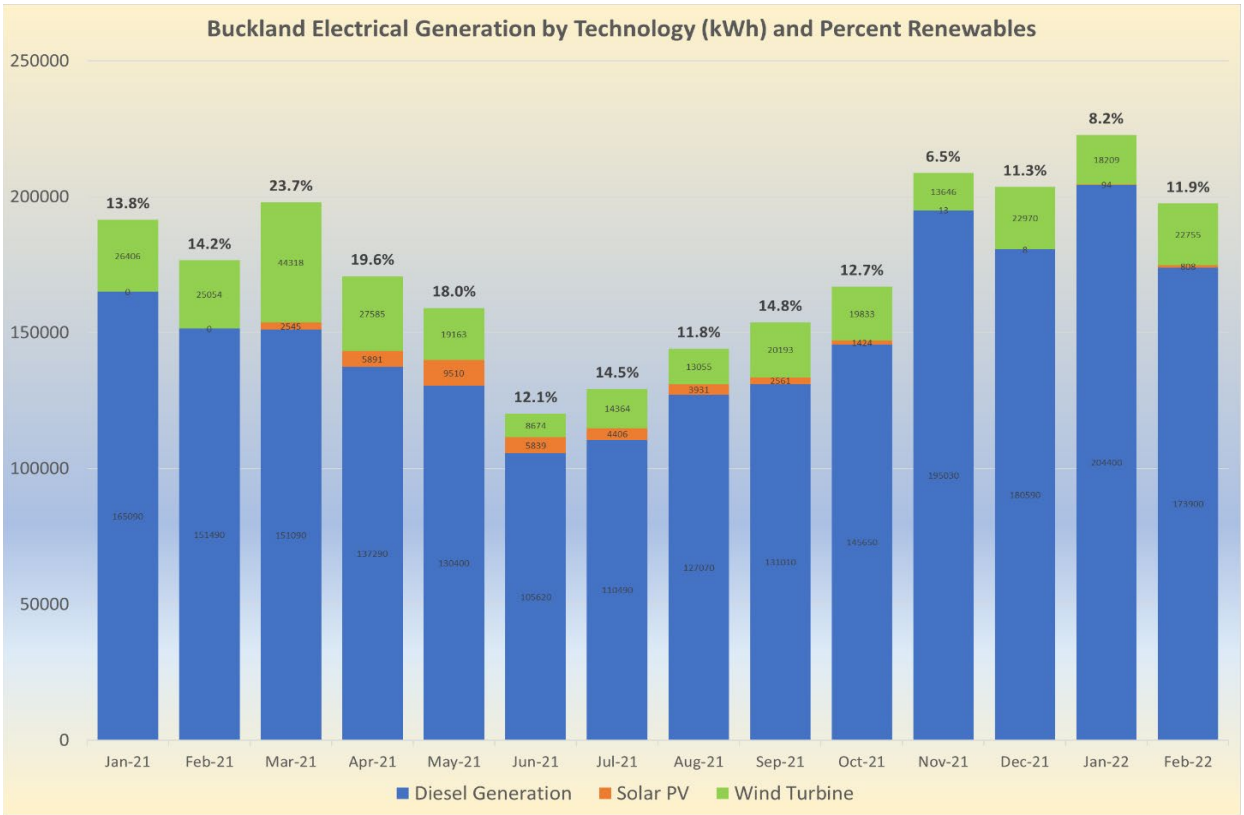

Figure 13 Graphical Representation of Power Data for Buckland (Feb 2021 – Feb 2022)

Challenges and Lessons Learned

Buckland was the first of three solar PV installations under this DOE project and the first-of-its-kind in many ways. Because this solar PV installation was part of a larger microgrid that included wind, batteries, electric boilers, diesel gen-sets, and heat recovery, the integration became challenging. Each of the microgrid components had an individual modbus protocol to coordinate through the ABB supervisory controller and each individual asset had an ABB device to translate to the supervisory controller. Though we anticipated this prior to and during installation, the actual digital communication required for this integration could only occur once all the assets were installed, and they did not all readily synchronize.

The first instance in which this became a problem was with the SMA cluster combiner of the three TriPower inverters trying to communicate with the ABB supervisory controller. Ultimately this required technical experts from SMA, ABB, BoxPower, and DeerStone Consulting with Specialty Electric, along with NRC staff and the powerplant operator from Buckland, all working together to perform modbus mapping, some remotely and some on-site. Because of the slow internet, this was not possible to completely synchronize remotely. While the solar PV was a stand-alone system, from a communications standpoint it needed to be part of a larger network to visualize all the inputs and optimize diesel and battery dispatch. The diagram on the next page (Figure 14) depicts the system, with the solar array and inverters bounded by the red line. This helped all project participants better understand their role and improved system performance and

optimization along with facilitating future troubleshooting.

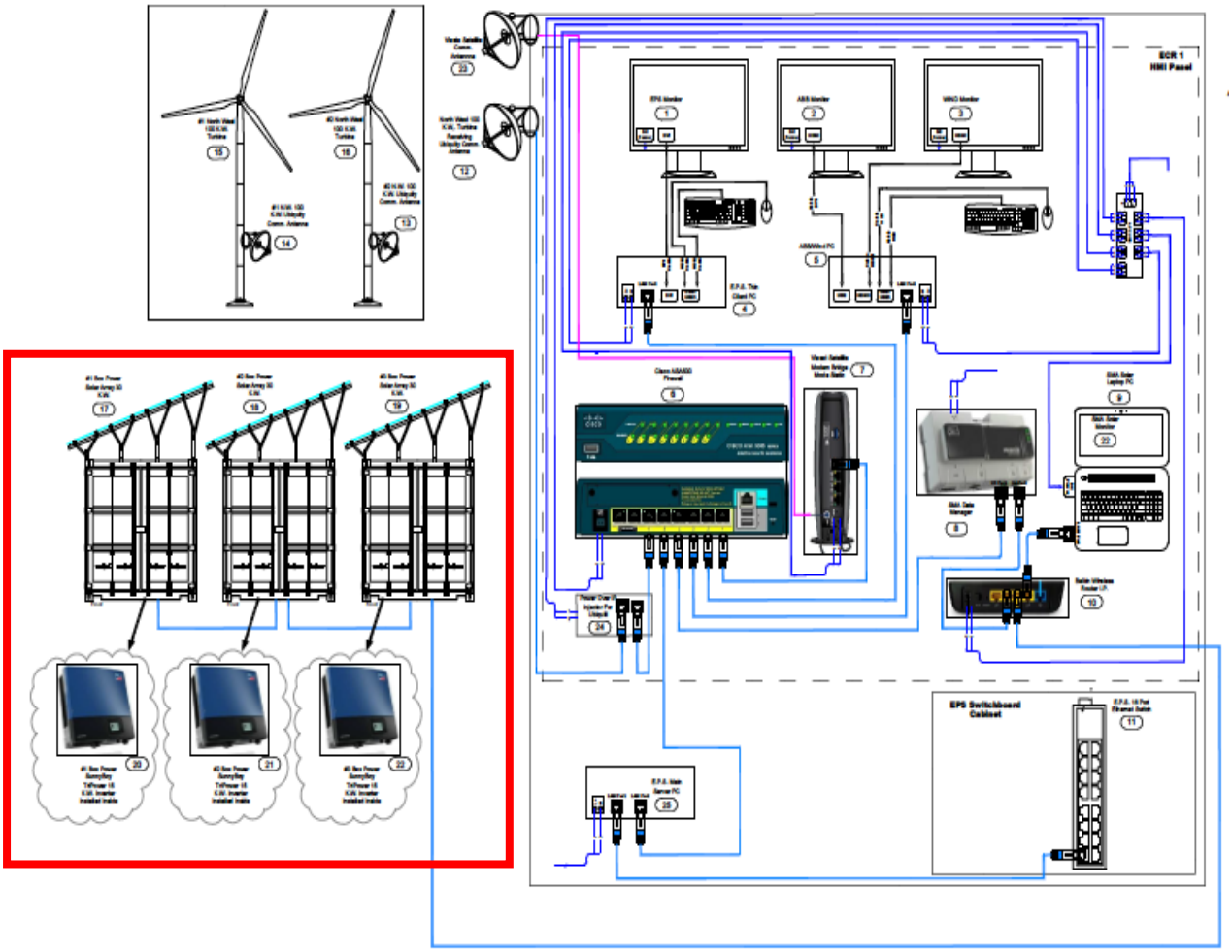

Figure 14 Diagram of Buckland Microgrid (Solar arrays and inverters bounded by red box)

See additional description of troubleshooting communications in Buckland in Appendix D.

Another design decision that manifested from a performance issue was the configuration of the individual arrays in a horseshoe. This was an outgrowth of several years of solar PV installations "in the round" across various villages in the region. The logic is that if all arrays are pointed directly due south, theoretically this would result in maximum production, but in practice, this also results in more severe voltage and power spikes when clouds create short-term variability in output as compared to if the arrays were arranged slightly offset from each other. When installing high penetration systems, the slight offset is gentler on the diesel generators that are required to ramp up and down to fill in the gap between load and solar PV output. Hence, a slight sacrifice in total annual output is traded for less impact on the diesel generators.

Project Description – Deering

The small community of Deering, Alaska was the second location to receive a solar PV system from this project, in the summer/fall of 2019. An updated Community Energy Profile for Deering

is included in Appendix A, which provides information on the community energy systems in Deering along with community energy goals, milestones, and analyses of current and past performance. The project team consisted of NRC Village Energy Program Director Sonny Adams and NRC Energy Coordinator Terrell Jones (who grew up in Deering), the Ipnatchiaq Electric Company under the City of Deering, the Native Village of Deering Tribal Council, and DeerStone Consulting. Vendors included BoxPower, SMA, Q Cells Solar Panels, and ABB (now Hitachi). BoxPower staff were on-site to lead the installation and provided additional project management during construction. The solar arrays were constructed on NANA land in the community of Deering.

Figure 15 Deering Power Plant Operator and Assistant with Inverter, atop shipping container, under array

After the installation was complete in Buckland and we were looking ahead to Deering, a major planning consideration was the lack of spare shipping containers. When we tried to apply the same foundation design that was used in Buckland (second shipping container mostly buried underground as foundation), both the shortage of extra containers and village concerns around ground disturbance due to a history of archeological finds of human remains in past projects, it became clear this was not going to be the right solution for Deering. We engaged PND Engineering to assist with load calculations and design considerations for an alternative foundation design. Their new design yielded a reduced amount of ballast in the form of gravel that could more easily fit inside the shipping container combined with duckbill anchors buried to a specified depth. To keep the gravel condensed into only a portion of the shipping container and to allow for working space inside the container as needed, we placed the gravel in supersacks and then, via telehandler, moved the filled gravel bags into the shipping container to provide the required ballasting (Figure 16).

Figure 16 Supersacks filled with gravel to contain ballasting weight inside container

System Configuration

In many ways this was a replication of the Buckland project from the year before. However, several significant changes were made to streamline the process, save money, improve performance, and address local constraints. Using the supersacks filled with gravel for ballasting combined with duckbill anchors (note yellow cable attached to underground duckbill anchor in Figure 17) reduced the amount of material handled, eliminated three shipping containers (out of six) and pre-engineered corner locks, and significantly reduced the labor required for the anchoring portion of the installation. The 45-degree tilt angle for the racking was complete and transferable from the Buckland project, so this was a sunk cost we were able to leverage for the second installation.

Figure 17 Two BoxPower solar PV arrays

The “surface area” from the racking available for installing solar panels was the same in Buckland and Deering, but because the solar PV industry continued to improve manufacturing efficiencies, standard-sized solar panels one year later generated 25 more watts per panel. The panels used in Deering were 385-Watt Q Cells, a superior product. At 42 panels per container array, this slight increase per panel resulted in an overall gain of >1 kW per array and >3 kW for the entire system. While each solar panel one year later could produce slightly more power, it was also slightly lower cost, so the outcome was more production for slightly less cost, at least from a solar panel perspective. When combined with the lower foundation material and handling requirements and resultant costs, this system, at higher output than Buckland’s, was installed for less money. However, some other costs associated with the system increased in the second year, such as shipping, which was beyond our control.

Figure 18 Construction in Progress in Deering

Another difference from Buckland was instead of three individual SMA inverters--one for each shipping container--we modified the design to a single inverter with more than three times the power rating of the three smaller inverters. We then wired all the power through a single unit instead of three individual inverters plus a combiner box. Because of the challenges in Deering with the compatibility of the SMA combiner box and the ABB microgrid controller, we completed the modbus mapping in advance and only had one inverter and one microgrid controller to coordinate. This resulted in a much simpler and less costly design that instantly went on-line and provided data collection of solar PV output in Deering. This was a direct result of lessons learned from Buckland.

We also replicated the horseshoe configuration of the three arrays in Deering, where the diesel generators were even more sensitive to sharp voltage and power output spikes that could result from shading solar PV panels in high penetration situations.

Figure 19 Solar Array in Deering

Figure 20 50 kW Inverter on top of single container, with Deering Power Plant Operator observing

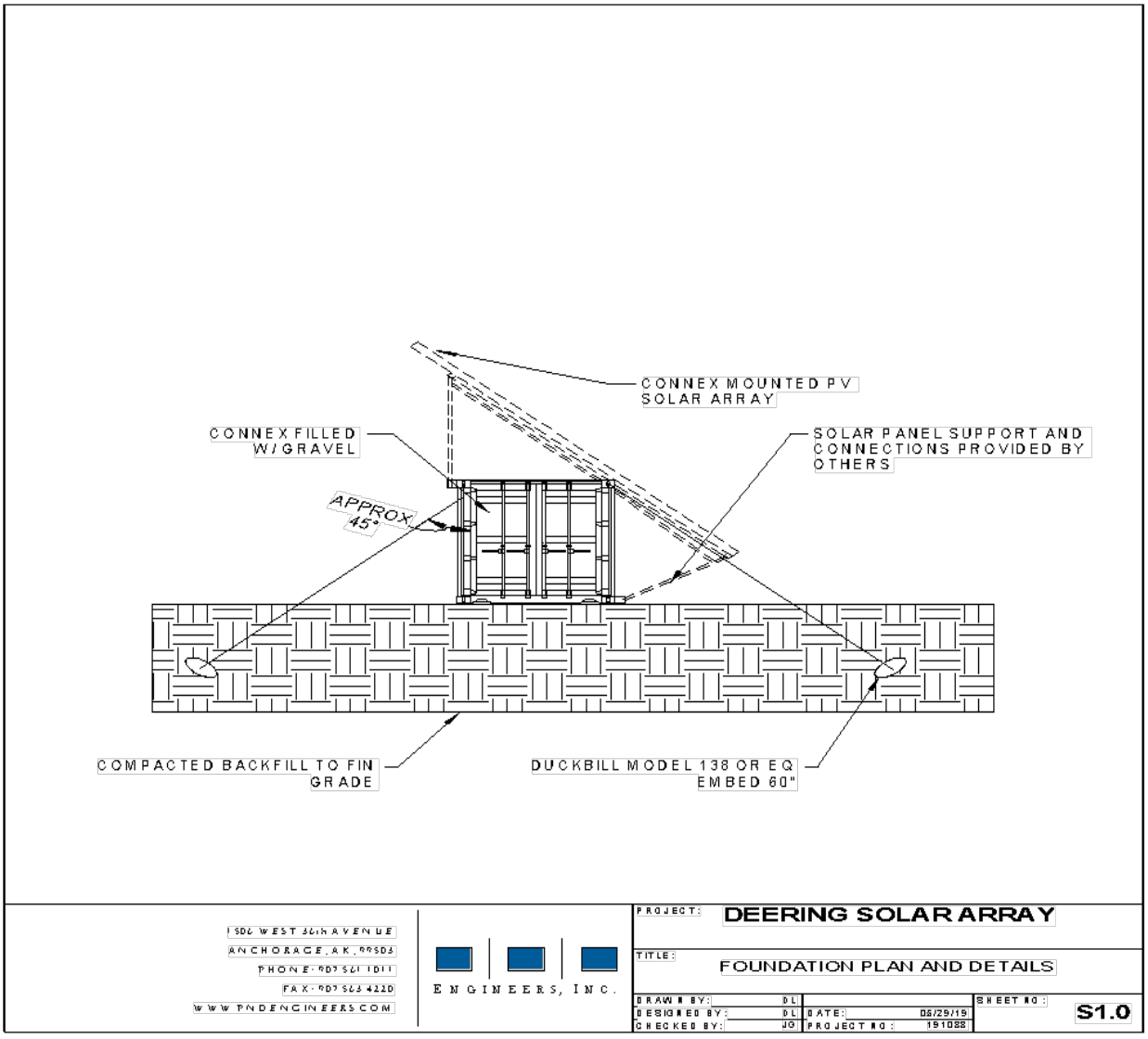

Figure 21 Foundation design with duckbill anchors

Performance

The detailed diesel, wind, and solar production data for Deering starting from February 2021 to February 2022 is presented below, followed by graphical interpretation of the longer-term data stretching back to November 2019 and then data analysis and discussion. As mentioned above with Buckland, because the solar PV was part of a larger microgrid that included wind, batteries, and diesel gen-sets, all the generation assets' contributions are listed below and are part of the overall system performance. Note that the wind turbines were off-line for part of this time, including in May and June 2021 when solar PV provided 17.8% of total generation for the month.

Date	Diesel kWh	Solar kWh	Wind kWh	Total kWh	Percent Renewables	Amount renewables kWh
Feb-21	70678	156	0	70834	0.2%	156
Mar-21	78689	3488	0	82177	4.2%	3488
Apr-21	61951	5803	0	67754	8.6%	5803
May-21	44393	9608	0	54001	17.8%	9608
Jun-21	29990	6506	0	36496	17.8%	6506
Jul-21	45990	4532	14334	64856	29.1%	18866
Aug-21	51100	3899	7483	62482	18.2%	11382
Sep-21	53030	2568	7027	62625	15.3%	9595
Oct-21	58340	1740	12555	72635	19.7%	14295
Nov-21	82300	540	3130	85970	4.3%	3670
Dec-21	70680	18	21413	92111	23.3%	21431
Jan-22	87260	5	11416	98681	11.6%	11421
Feb-22	76430	0	16955	93385	18.2%	16955
TOTAL	810831	38863	94313	944007		133176

Figure 22 Power Generation for Deering

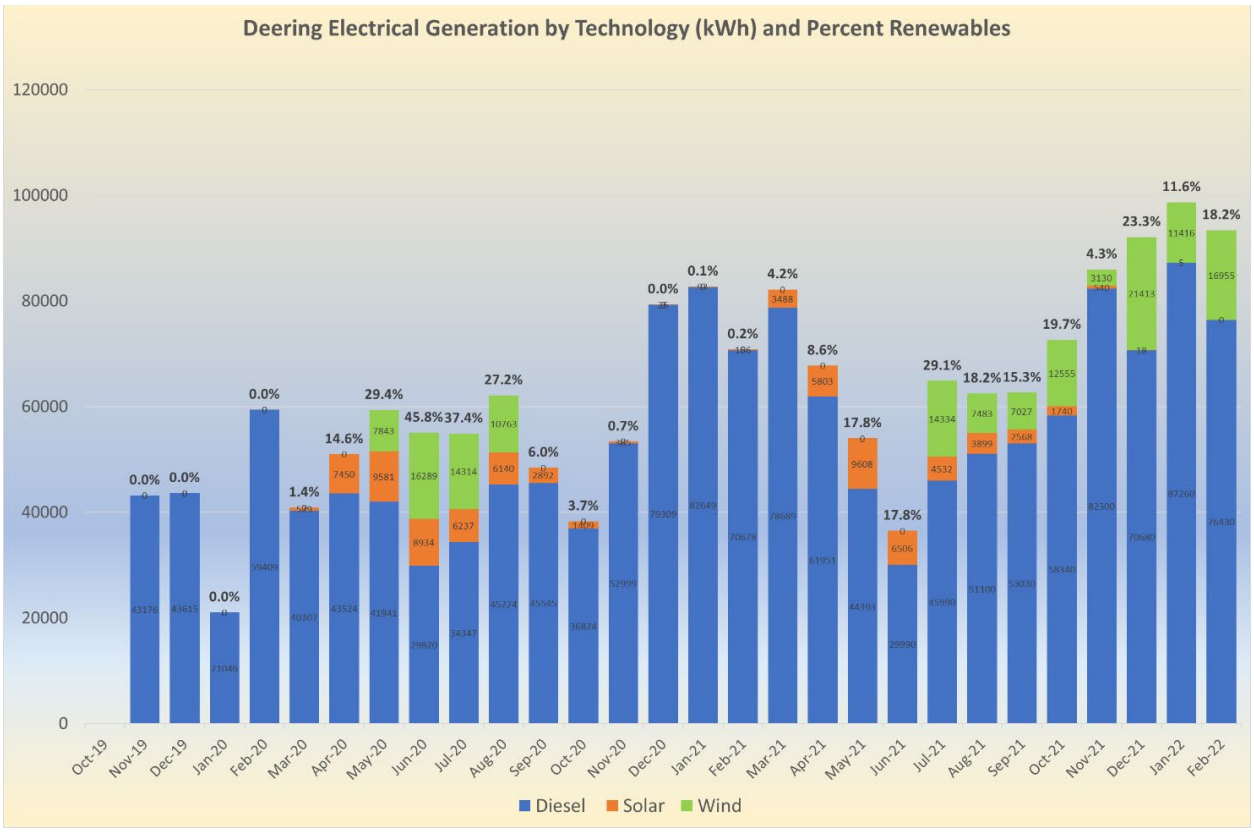

Figure 23 Graphical Power Generation Data for Deering

Challenges & Lessons Learned

Like in Buckland, Deering's solar PV system was part of a larger microgrid that included wind batteries, diesel generators, and heat recovery. Because of this more complex system, even if the solar PV was working perfectly, its impact was subject to the performance of, and integration into, the full microgrid. In Deering's case, this became an issue not because of the other renewable generation or storage assets, but because of the diesel generators that needed repair and/or replacement. In particular, the solar PV array was working as planned, but because one diesel generator was getting replaced and another needed significant repair, we couldn't fully commission the microgrid to operate in automatic mode to optimize dispatch and automatically turn off the diesel generators. This was a known condition and a new diesel generator and replacement parts for another generator were all secured, along with a diesel mechanic to perform the work, but because of Covid and other constraints, the diesel mechanic's site visit was delayed for over a year. During this time when the village was waiting for the mechanic to arrive on-site, the solar (and wind and batteries) could not perform to full capacity.

As well, during this time the wind turbine experienced an outage that was not easily diagnosed or repaired for many months. DeerStone Consulting worked on-site with Deering's Power Plant Operator and remote support from the wind turbine company that was responsible for annual maintenance of the turbines to ultimately diagnose and repair the turbine, but this also contributed to sub-optimal renewable performance for a significant period. As a testament to the reliability of solar power, there was a several month window where the main system that was performing as planned was the newly installed solar PV, waiting for the diesel generators and wind turbines to get repaired so the microgrid controller could be placed in automatic mode and fully leverage the benefits offered by the renewables and energy storage.

Another issue that we identified in Deering, and then realized was an issue in Buckland as well, was the energy consumption of the battery building that was constructed to house and protect the BESS. Again, this was not a direct outcome of the solar PV project, but the high penetration nature of the combined solar and wind production, which required a battery to manage properly, resulted in increased "station service" or parasitic load for the overall system because of the battery thermal requirements. The outcome of this analysis has been to re-design the battery building with more of a focus on thermal management and efficiency of the building--as much for cooling needs as for heating needs, since we found the battery building needing cooling even through large parts of the winter because of the heat generated by the isolation transformer, the battery itself, and the power conversion system. This was especially prominent in the summer, however, when the solar PV system could contribute much more to the cooling needs, which could be more justification for increasing the size of future solar PV systems.

Project Description – Kotzebue

Kotzebue is by far the largest community in our region. It also has the largest and most complicated energy system that includes several different types and sizes of wind turbines, multiple diesel generators, electric boilers to use excess wind to heat, a relatively large battery bank (950 kWh), and, prior to this DOE Tribal Deployment project, a small amount of solar PV installed behind the meter to support the City's water treatment plant (WTP). In fact, all communities in our region have solar PV installed behind the meter at the community WTP,

which provided the original technology validation for this project as these earlier installations have been in place for over a decade and have provided the longest-term production data for the region and likely the entire arctic.

An updated Community Energy Profile for Kotzebue is included in Appendix B, which provides information on the community energy systems in Kotzebue along with community energy goals, milestones, and analyses of current and past performance. The project team consisted of NRC Village Energy Program Director Sonny Adams and NRC Energy Coordinator Terrell Jones, Kotzebue Electric Association staff including General Manager Martin Shroyer and Lead Systems Engineer Matt Bergan, Kikiktagruk Inupiat Corporation (KIC), Alaska Native Renewable Industries (ANRI) as main system design and installers, and DeerStone Consulting. Vendors and equipment included LG Neon 400-Watt panels, Solar Edge inverters and optimizers, and AP Alternatives helical ground screws and racking.

System Configuration

KEA has been a clean energy leader and innovator in our region, across Alaska, and even nationally, demonstrating cold weather performance of wind turbines as an early adopter more than 20 years ago while a few years ago including demonstration of an electric vehicle in the arctic. The early wind turbine installations in Kotzebue yielded important data and provided valuable energy production, but these turbines have now reached their end of life, and when they experience issues that require significant maintenance, KEA is no longer repairing them. This end-of-life cycle resulted in the approach to the solar PV system, which was to use some of the existing infrastructure from the old wind turbines for the new solar. Specifically, there is not a lot of clear open land in the main town that could support a large solar array, but the wind farm in Kotzebue is a few miles out of town and already has digital communications wired from the farm back to the power plant along with small structures that housed inverters and transformers for the old wind turbines. It was decided to locate the solar array at the wind farm, remove several of the old wind turbines, and construct sub arrays of approximately 65 kW each, which was the nameplate rating on the small wind turbines that were being removed, and use the small structures to house the new solar inverters and wire into the transformers from the old wind turbines. This saved significant money by using some of the old equipment, reduced site control and permitting issues, and fit the DOE requirement of using Tribal land since the wind (and now) solar farm was located on KIC land. KIC is the local ANC Village ANCSA corporation based in Kotzebue.

The much larger system in Kotzebue compared to Buckland and Deering resulted in a decision to not use BoxPower shipping containers as the primary anchoring system since on a larger scale, shipping containers are more expensive than ground mount racking. However, because of Kotzebue's deep permafrost, ground mounting of the panels would require significant drilling and somewhat specialized equipment for both the drilling and the ground penetrations. ANRI, based in Huslia, Alaska, had previously installed a relatively large system in Hughes which also has deep permafrost and they had this experience prior to the Kotzebue installation. This past experience was a significant contributor to selection of ANRI as the general contractor based on an RFP issued by KEA. In the Hughes project, ANRI used ground penetrating helical piles

manufactured by AP Alternatives based in Pennsylvania, and it was decided to use the same equipment in Kotzebue.

Ground mounting the solar panels with these helical piles was the single most complicated and expensive part of the project. It required pre-drilling holes and then a specialized adapter head to a backhoe to screw the pilings into place, but this was necessary to avoid "frost jacking" from the freeze-thaw cycles exhibited by permafrost that often occurs with standard piles that do not have helical threads. This decision was based in part on research into the use of helical piles, a discussion of which part is included in Appendix C. The document is "Evaluation of Helical Piers for Use in Frozen Ground, Technical Report" by Zubeck and Liu (2002).

The final system in Kotzebue was 576 kW of solar that was divided into 8 separate sub-arrays, each using pre-existing infrastructure from the old, now replaced wind turbines. Like Buckland and Deering, the solar PV array in Kotzebue was part of a larger microgrid that included wind, batteries, diesel generators, and heat recovery, along with electric boilers, and required integration with ABB microgrid controllers and other components. Fortunately, the Solar Edge inverters and DC Optimizers communicated more easily with the other components in the Kotzebue system and the Solar Edge software allows for isolated data reporting on the solar PV system.

Figure 24 Solar PV Array and Wind Turbines in Kotzebue

Figure 25 Renewable Energy Generation in Kotzebue

Figure 26 Team in Kotzebue

Performance

The figure below shows KEA's solar energy production for all of 2021 and lifetime energy generated by the system from installation in May of 2020 through April 10, 2022. The table below was selected in part to demonstrate a full year's performance and validate a rough "rule of thumb" that we have observed from numerous solar PV installations in our region, which is that 1 kW of installed solar PV produces approximately 1 MWH of electricity annually. From the table below, we can see that in Kotzebue's case, the 576 kW nameplate rated system produced 579.59 MWH for all of 2021. It should be noted that we expect this number to slightly increase in future years because there were still some system optimization issues that we were dealing with in 2021 and some of the optimizers went offline, resulting in slightly reduced performance. Countervailing this expected future production, however, is the inevitable slight gradual decline of PV panel performance year over year due to UV degradation and other weathering, so the rough estimate of 1 MWH per installed kW seems to be a good generalization.

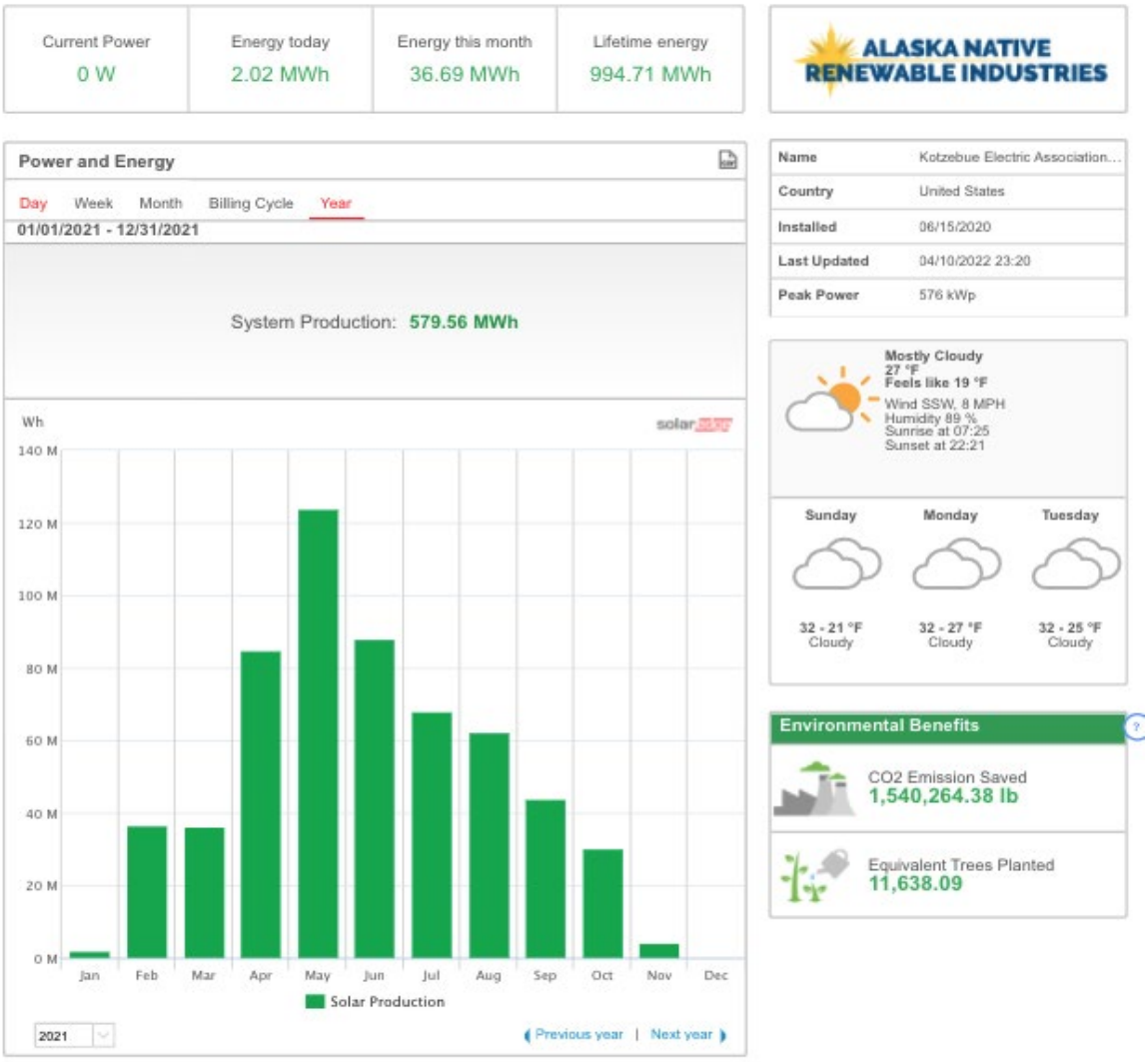

Figure 27 KEA's solar energy production for all of 2021

Outcomes & Conclusions

In general, it is hard to overstate the importance of these three projects, and DOE's contribution to them, in the evolution of solar PV development across the arctic and Alaska in general. They have been highly successful, widely observed, and exhibited the exact kind of progression we would expect, i.e., decreasing costs on a per unit basis, improved performance, streamlined construction, simplified design for more robust systems, and overall normalization of the technology. The results should be viewed not just from a conventional kWh performance basis, but also from the perspective of early adopters and ground breakers for what previously was viewed as a highly dubious proposition – solar power above the arctic circle.

DOE's contribution included not only financial support, but also ongoing technical support through the DOE-OIE Inter-Tribal Technical Support grant award and some staff time on very specific questions associated with optimization, potential expansion, and other issues. The progression of these three individual installations also contributed to the progression of the project participants and systemic learning that occurred in the region as a result of these efforts, Specifically, the project participants including NRC, the individual Tribes and Cities, and our main contractors, have all grown in understanding and maturity with regard to installing renewable energy systems in remote locations with legacy infrastructure that will always need updating and repair. Each challenge seemed initially daunting but over time as solutions emerged and expertise was gained, we have now created a highly functional operations team performing difficult troubleshooting and system optimization that will continue to yield significant benefits for our region over time.

One clear example of this is the recent project replication that is now occurring, which includes a fully operational high penetration solar PV and battery system in Shungnak (that also serves Kobuk, which is electrically inter-connected via a 10-mile tie-line) that is selling solar power generated by the local Tribes to Alaska Village Electric Cooperative, the largest electric utility in rural Alaska. That project was funded by the US Department of Agriculture and also selected ANRI as the general contractor, which is contributing toward an Alaska Native owned renewable energy business based in rural Alaska. The system design was very similar to what was used in Kotzebue under this DOE grant award. That system was fully installed in 2021.

More recently, the Native Village of Noatak and the Northwest Arctic Borough, with significant support from NANA, received a grant award from DOE-OIE to install a solar PV and battery system in that remote location. ANRI was once again selected under a competitive RFP process and will be using a similar design once again. Importantly, this project is benefitting from all the past projects in terms of how quickly we are now able to go from project concept to funding to construction. Most projects currently take years to move into construction, but in Noatak's case we were able to issue an RFP within weeks of final award agreements with DOE and have long lead-time equipment on order to hopefully avoid many of the delays experienced by other projects. We have working arrangements with AVEC, who is also the utility provider in Noatak, along with detailed system design issues, already resolved within a few months of finalizing the award. All of this saves time and money in situations where there is always a shortage of both.

Most recently (April 2022), we were notified that a joint Northwest Arctic Borough/NANA/multiple village application to the Alaska Renewable Energy Fund to streamline engineering and design of multiple solar PV-battery systems for all the remaining villages in the NANA region was recommended for funding. The final decision will be made by the Alaska State Legislature in the coming month or so, but we are expecting full funding to design and engineer another four solar PV and battery systems, much of which was based on the projects and lessons learned from these three installations.

With the three projects under this funding award, we can note some other important trends. These include installing larger systems for improved per unit costs through economies of scale; forming Tribal Independent Power Producers to increase capacity, create local jobs, and preserve the Power Cost Equalization payments in the community; and improved understanding of how solar PV can contribute to a larger microgrid system with multiple components, all of which require planning and coordination among vendors to streamline the digital communication requirements for improved monitoring and performance.

The success of these projects has been accompanied by increased interest in solar energy for our communities. This has been enhanced by an introductory solar PV training course co-sponsored by NANA and several others that was held in Kotzebue as a lead-up to these three installations. The course, "Solar PV 101," was taught by Solar Energy International and both NRC Village Energy staff members, Sonny Adams and Terrell Jones, attended the course along with several people from Deering, Buckland, Kotzebue, and other villages in our region. Many of these people ended up participating as local hires on the installations in their own villages. This has contributed to the region's embracing of the technology.

Finally, this overall effort has inspired people in the region and beyond to realize the potential of solar PV production even in what appear to be challenging resource conditions. It is important to understand the limits of solar PV, especially in the arctic where energy constraints are so severe in the winter when solar PV is not directly contributing to energy production, but because most communities receive just a few fuel shipments a year in the ice-free summer months, any diesel reduction contributed by solar in the spring and summer will result in less need for diesel overall and help to ensure diesel fuel is available in the winter when it is truly needed. These three installations are enduring statements to DOE's commitment to Tribal clean energy development and to our region's efforts to protect our culture, our resources, and our collaboration with each other and all stakeholders who want to contribute to sustainability in our region.

Thank you DOE for all your ongoing support and leadership.

Table of Appendices

Appendix A

Maps and Figures

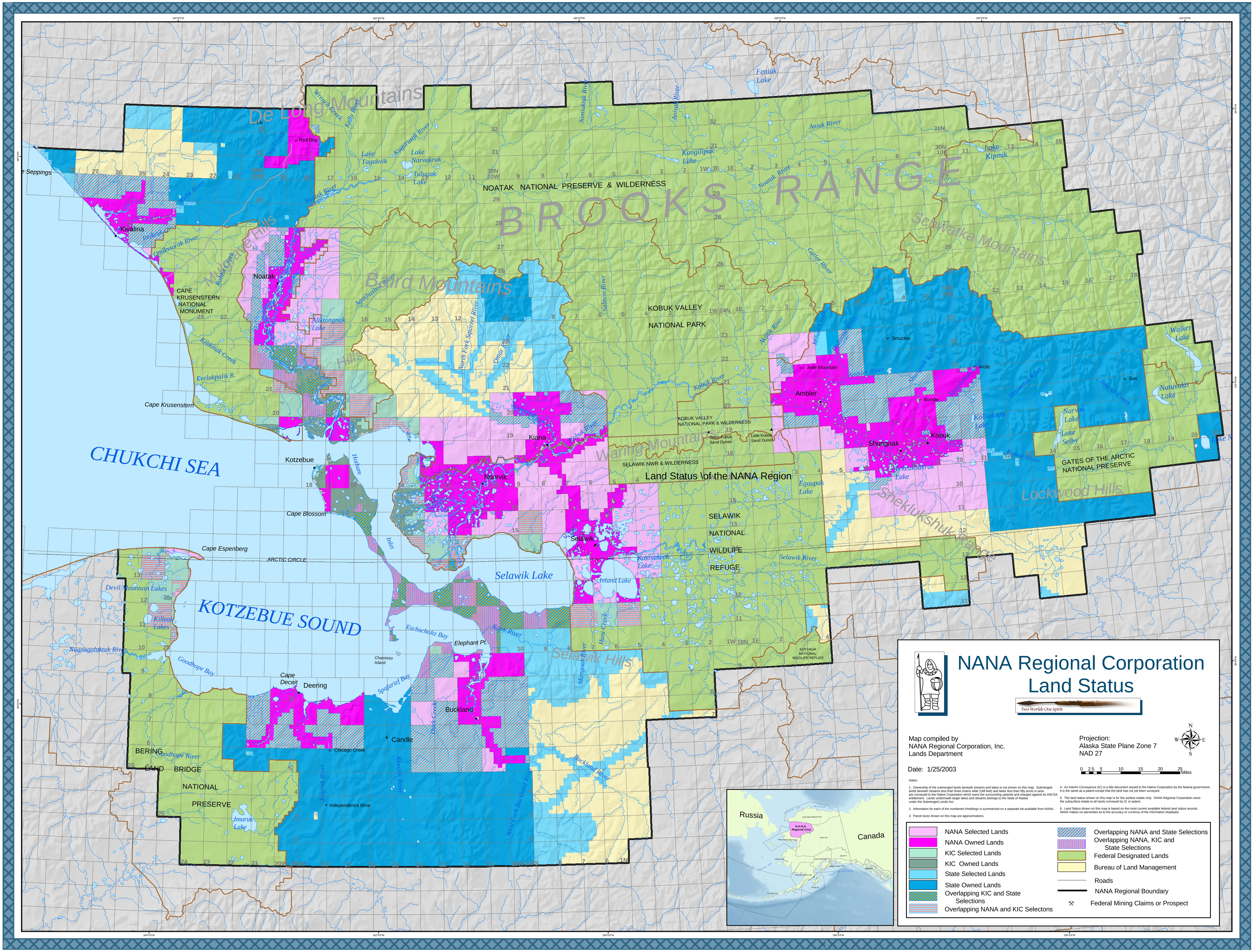

NANA Regional Corporation
Land Status
Two Worlds One Spirit
Map compiled by
NANA Regional Corporation, Inc.
Lands Department
Projection:
Alaska State Plane Zone 7
NAD 27
Date: 1/25/2003
0 2.5 5 10 15 20 25 Miles
Notes:
1. Ownership of the submerged lands beneath streams and lakes is not shown on this map. Submerged lands beneath streams less than three chains wide (198 feet) and lakes less than fifty acres in area are conveyed to the Native Corporation which owns the surrounding uplands and charged against its ANCSA entitlement. Lands underneath larger lakes and streams belongs to the State of Alaska under the Submerged Lands Act.
2. Information for each of the numbered inholdings is summarized on a separate list available from NANA.
3. Parcel sizes shown on this map are approximations.
4. An Interim Conveyance (IC) is a title document issued to the Native Corporation by the federal government. It is the same as a patent except that the land has not yet been surveyed.
5. The land status shown on this map is for the surface estate only. NANA Regional Corporation owns the subsurface estate to all lands conveyed by IC or patent.
6. Land Status shown on this map is based on the most current available federal land status records. NANA makes no warranties as to the accuracy or currency of the information displayed.
NANA Selected Lands
NANA Owned Lands
KIC Selected Lands
KIC Owned Lands
State Selected Lands
State Owned Lands
Overlapping KIC and State Selections
Overlapping NANA and KIC Selectons
Overlapping NANA and State Selections
Overlapping NANA, KIC and State Selections
Federal Designated Lands
Bureau of Land Management
Roads
NANA Regional Boundary
Federal Mining Claims or Prospect
Land Status \of the NANA Region
BROOKS RANGE
De Long Mountains
Baird Mountains
Schwatka Mountains
Waring Mountains
Selawik Hills
Lockwood Hills
Sheklukshuk Range
NOATAK NATIONAL PRESERVE & WILDERNESS
KOBUK VALLEY NATIONAL PARK
SELAWIK NATIONAL WILDLIFE REFUGE
GATES OF THE ARCTIC NATIONAL PRESERVE
CAPE KRUSENSTERN NATIONAL MONUMENT
BERING LAND BRIDGE NATIONAL PRESERVE
CHUKCHI SEA
KOTZEBUE SOUND
Selawik Lake
ARCTIC CIRCLE
Kivalina
Noatak
Kotzebue
Kiana
Noorvik
Selawik
Ambler
Shungnak
Kobuk
Buckland
Deering
Candle
Red Dog
Cape Krusenstern
Cape Blossom
Cape Espenberg
Cape Deceit
Elephant Pt.
Russia
Canada

BOXPOWER™

OWNER:	VILLAGE OF DEERING
LOCATION:	DEERING, AK

SITE LAYOUT

SIZE **B**	DRAWING NO. 30SB17 - 01	
SCALE NTS	DATE 6/28/2019	SHEET 1 OF (17)

KOTZEBUE SOUND

Magnetic North
13 1/4° E
True North

PROPOSED LOCATION OF
BOXPOWER SYSTEM

A-14(c) Plat No. 92-3

Quit Claim Deed to
Native Village of Deering
2003-000694-0
5/19/2003

DEERING TANK FARM
SUBDIVISION
Plat No. 2003-8

CITY OF
DEERING SUBD.
Plat No. 96-9

4' Utility
Easement

Quit Claim Deed to
City of Deering
Bk. 348, Pgs. 513-514
12/23/1997
Lots 29 & 30

Appendix B

Community Energy Profiles

Buckland
Nunatchiaq

Native Village of Buckland:
907-494-2171
City of Buckland:
907-494-2121

Demographics –
Native Village Status: Federally Recognized Tribal Council
Alaska Native Name: Nunachiak
Population: 511
Avg. Household Size: 5.02
Median Household Income: $41,932

Access –
Barge Access: Seasonal
Runway Ownership: State
Runway Surface: Gravel
Runway 1: 3,200 ft x 75 ft
Runway 2: None

Climate –
Average Summer Temperature: 52 °F
Average Winter Temperature: -2 °F
Heating Degree Days: 15,751

Heat & Power Costs (2021) –
Cost of Diesel Fuel: $6.15 per gal
Cost of Gasoline: $6.15 per gal
Cost of Electricity: $0.47 per kWh
Cost of Electricity, after PCE: $0.31 per kWh

Tank Farm -
Ownership: Native Village, City, School, AKDOT
Total Capacity: 297,300 gal
Status/Year Built: Acceptable

Electric Utility –
City of Buckland

Power Demand (2020) –
Average Summer Load: 180 kW
Average Winter Load: 250 kW
Peak Summer Load: 260 kW
Peak Winter Load: 350 kW
Total Power Generated: 1,626,621 kWh

Power System –
Fuel Efficiency (2020): 11.16 kWh/gal diesel
Line Loss (2018): 11.5%

Number of Community Buildings on PCE (2020): 12
Community PCE kWh Use of Total Allowed (2020): 28% (119,987 kWh - used / 429,240 kWh – total allowed)

Power Generation Infrastructure –
Diesel Engines:

Manufacturer	Model	Capacity	Year Built
Caterpillar	3456	475 kW	2006
John Deere	6135	400 kW	2021
John Deere	6135	310 kW	2021

Wind Turbine(s):

Manufacturer	Model	Capacity	Year Built
Northern Power Systems	Northwind 100	100 kW	2013
Northern Power Systems	Northwind 100	100 kW	2013

Solar PV:

Installer	Inverter	Capacity	Year Built
BoxPower	SMA Tripower	45.99 kW	2019

(Additional 10.13 kW installed for water plant, behind the meter)

Battery Storage System:

Manufacturer	Model	Capacity	Year Built
SAFT	Intensium Mini-M	277 kW / 218 kWh	2019

Heat Recovery –
Facilities Served: City office, new WTP, old WTP/Washeteria
Opportunity to Expand Waste Heat: Yes

Water & Wastewater –
Ownership: City of Buckland
Water System: Circulation Loop(s)
Wastewater System: Gravity

Selected Projects –

EPA DERA Generator Replacement – *Expected 2022*

- Replacement of two generators, 2021
  - John Deere 6135, 400 kW
  - John Deere 6135, 310 kW
- EPA Diesel Emissions Reduction Act & City of Buckland
  - $484,923 awarded from EPA in 2020
  - $96,665 from City of Buckland Cost Share

Solar PV Array and Inverter – *Completed 2019*

- Installed 45.99 kW solar PV and inverter, 2019
  - Solar PV & foundations by BoxPower
- Displaces 2,900+ gal/year diesel fuel
- Contributed to 130+ hours of diesels-off in 2020
- DOE Office of Indian Energy
  - $1 million awarded from DOE in 2016
  - $1 million match funding from NANA
    - Award for Kotzebue, Buckland, & Deering

Battery Storage and Controls – *Completed 2019*

- Installed 277 kW/218 kWh battery storage and controls
  - Necessary to make solar PV array effective
- Integrated solar PV & battery storage with microgrid, 2019
- Contributed to 130+ hours of diesels-off in 2020
- USDA High Energy Cost Grant Program
  - $1.6 million awarded in 2016
    - Award for Buckland and Deering

Wind/Diesel Microgrid – *Completed 2015*

- Installed two Northwind 100 kW wind turbines, 2013
- Integrated wind turbines with microgrid, 2015
- Displaces 18,000+ gal/yr diesel fuel
- Contributed to 130+ hours of diesels-off in 2020
- AK Energy Authority Renewable Energy Fund, Round 1
  - $10.5 million awarded in 2009
    - Shared award for Noorvik, Buckland, and Deering

LED Streetlight Retrofit Borough-Wide – *Completed 2015*

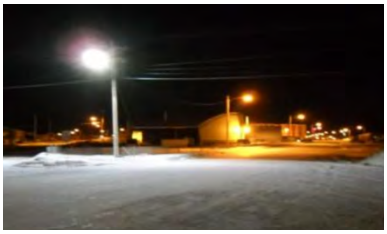

- Installed 8 LED streetlights in Buckland
- 25-year community savings: ~$870,000 & ~330,000 gal diesel
- State of Alaska, Grants to Municipalities
  - Funding awarded 2014
  - $200,000 awarded to Northwest Arctic Borough

Water Plant Solar PV – *Completed 2015*

- 10.3 kW solar PV installed
- Average 18 kWh/day; still operational
- Coastal Impact Assistance Program (CIAP)
    - Funding awarded 2009
    - $84,078 awarded

Future Projects –

Overhaul Generator 1

- Generator 1 is currently non-functional
- Overhaul generator 1 to enhance reliability and capacity to run system in automatic
    - Use Village Improvement Funding that is already allocated

Energy Audits

- Conduct additional energy audits of community buildings
    - Water treatment plant, washeteria, health clinic, school, sewer building, lift stations, City offices, City shop, City storage, teacher housing, armory, IRA building, and Native store.
- Conduct additional energy audits of residential buildings
    - Elders' homes and pastor home
- Conduct operational energy audits
    - Water treatment plant
        - Adjust heat add set points, utilize recovered heat, utilize electric boiler
- Complete energy efficiency recommendations to reduce heating and operational costs

Community-Wide Residential LED Lighting Upgrade

- Upgrade all residential lighting fixtures to energy efficient LED lighting
    - Survey type and quantity of lighting fixtures in all homes
    - Apply for Village Improvement Fund support
    - Procure and install energy efficient lighting
        - Reduce residential electricity costs

LED Streetlight Retrofit

- Install 30 new LED streetlights
- Upgrade 25 existing streetlights to LEDs
- Apply for Village Improvement Fund support
    - Hire local labor to install

Solar PV, Wind Turbines, and Battery Storage

- Increase capacity of solar PV array and battery storage
- Install additional wind turbine
    - Explore opportunity to use KEA's extra Northwind 100 wind turbine

- Displace additional diesel fuel and increase hours of diesels-off
    - Reduce the cost of electricity
- Enhance resiliency of system

Distribution System Upgrade

- Assess system to identify sources of high line loss
    - Replace and upgrade aging infrastructure, as required
        - Transformers, wires, etc.
- Straighten power poles that are leaning severely

Energy Milestones –

- Achieved diesels-off operation – *July 20th, 2019*
- Installed first solar PV in Buckland – *Completed 2015*

Community Goals –

- Reduce cost of residential space and water heating
    - Expand renewable energy microgrid
        - Solar PV, wind turbines, battery storage
    - Implement energy efficiency measures
    - Maintain and/or replace aging residential heating appliances
- Rebuild or replace diesel generator #1 to enhance reliability of power system
- Enhance energy efficiency of water and sewer systems
    - Repair and upgrade service lines to reduce frequency of freeze-ups
        - Dump Rd. sewer services freeze-up most frequently
- Create additional training opportunities for operators to enhance skills and understanding of microgrid
- Train back-up operator to expand the number of power system experts within the community
    - Provide relief for primary operator
    - Enhance reliability of power system
- Partner with Northwest Inupiat Housing Authority to implement policy changes to prioritize and invest in energy efficiency in newly constructed homes

Microgrid System Schematic –

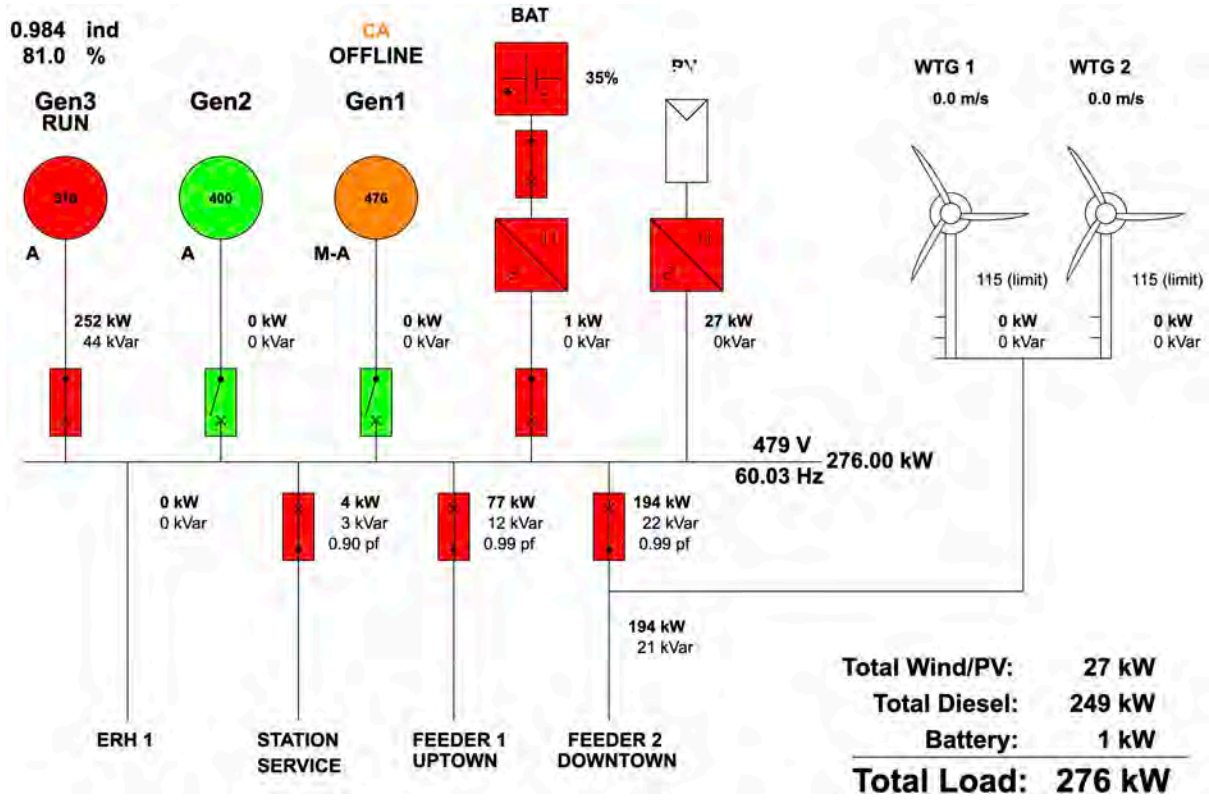

Energy System Trends –

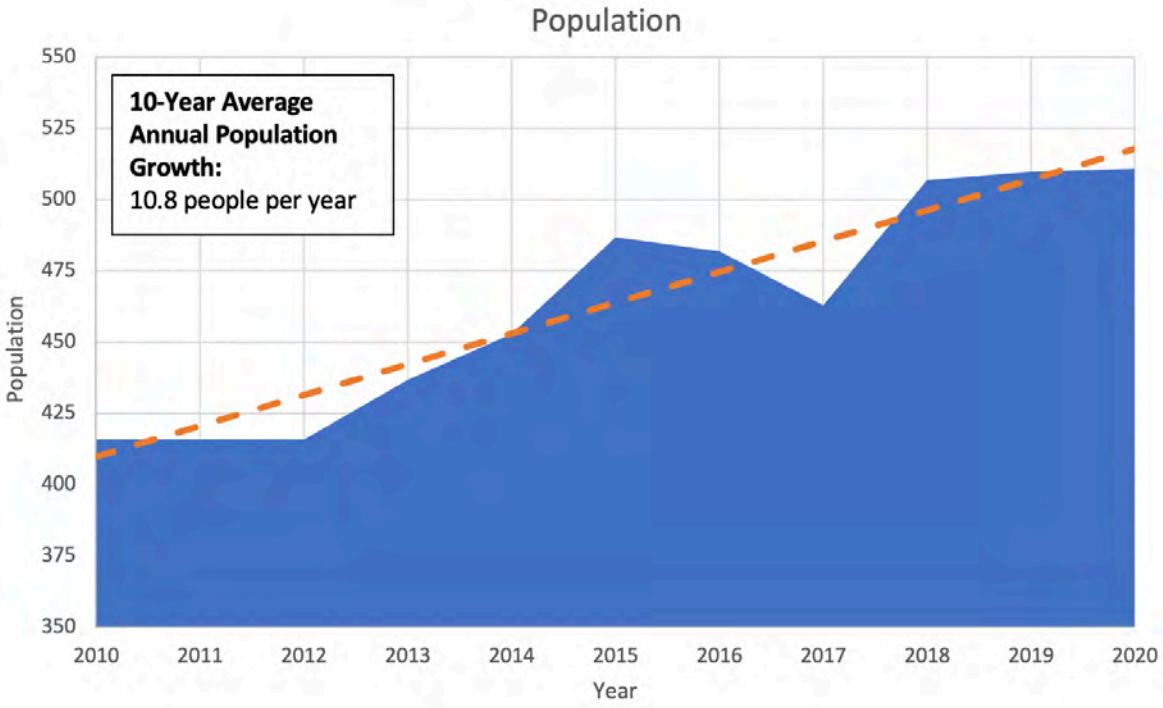

Dramatic changes in population impact the long-term community planning necessary to meet future power demand. The population in Buckland is not changing dramatically. Over the last ten years the population has increased an average of 2.6% each year.

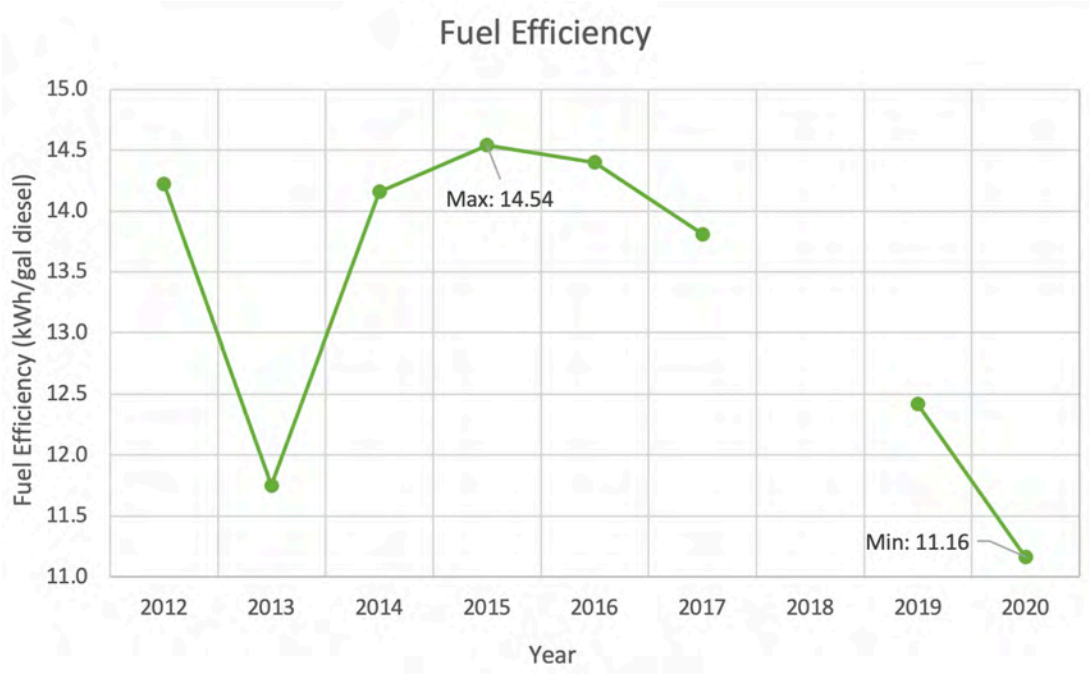

A higher fuel efficiency results in less diesel fuel use and a lower cost to generate power. A fuel efficiency below 12 kWh/gal is poor; a fuel efficiency above 14 kWh/gal is excellent. *From 2014 to 2017 the fuel efficiency in Buckland has been excellent, but in recent years it has been poor. Due to the method that is used to calculate this value in the PCE data, there are a variety of potential causes for this reduction in fuel efficiency. Further investigation is required to understand this decline in fuel efficiency. No data was available for 2018.*

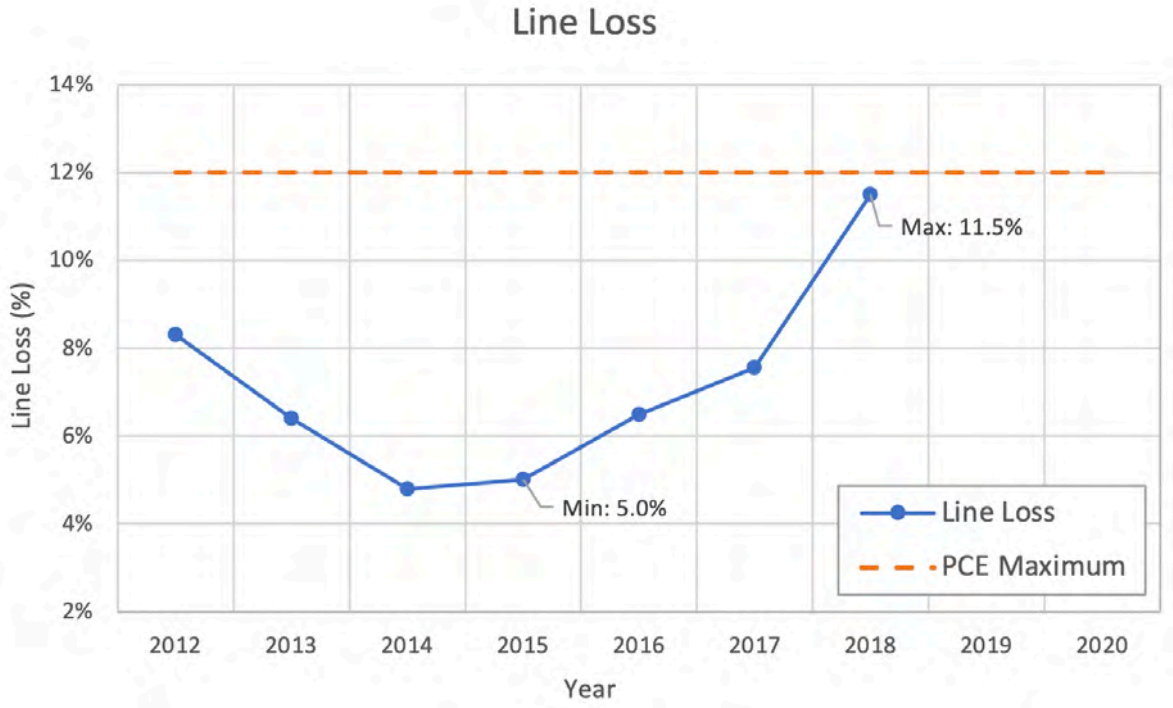

The maximum allowable line loss to maintain eligibility for PCE benefits is 12%. In Buckland, the line loss decreased steadily from 2012 to 2014, indicating the distribution system was in good condition and all power use is accounted for. Since then, the line loss has increased dramatically. Recent line loss values should be calculated and the system should be evaluated if high line loss persists. No data was available for 2019 and 2020.

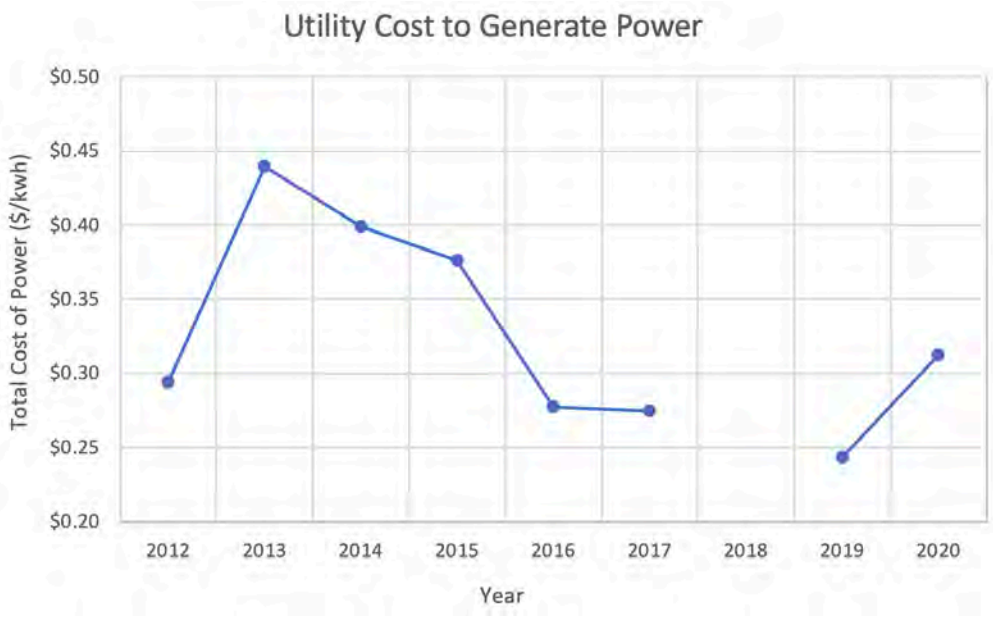

Over the long-term, a lower utility cost to generate power typically correlates with a lower cost of electricity for residents. The major factors that affect the cost to generate power are the cost of fuel, generator fuel efficiency, maintenance, and operations. Major system breakdowns may cause the cost to generate power to spike on a particular year, as will high fuel prices. In Buckland the cost to generate power has been trending lower each year since 2013, excluding the slight increase in 2020. Fuel savings from power generated by renewable energy sources are likely contributing to this reduction. No data was available for 2018.

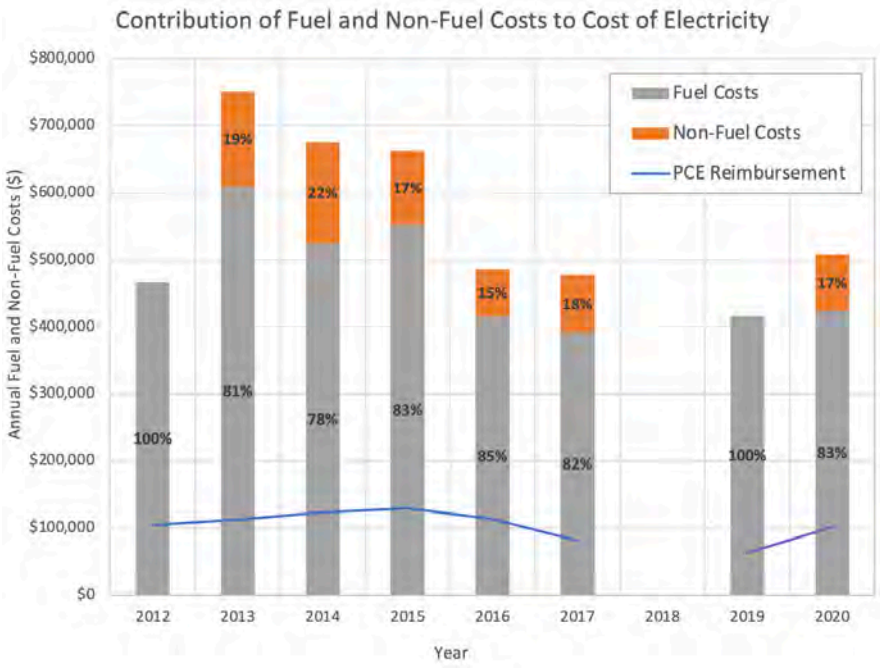

For many utilities, the non-fuel costs associated with generating power do not change dramatically each year. Fuel costs, on the other hand, are highly susceptible to annual fluctuations based on the global price of fuel, transportation costs, and the amount of power generated. PCE reimbursement is meant to offset the high fuel costs in rural Alaska. As the overall efficiency of the system increases, the PCE reimbursement offsets a larger portion of the total fuel costs. In Buckland, the reported portion of the costs spent on fuel is exceptionally high relative to other communities in the region. This is likely because in many of the other communities the Alaska Village Electric Cooperative (AVEC) owns and operates the local power plant. AVEC is able to buy fuel at a lower rate due to the volume of fuel they purchase for all the communities they serve. No data was available for 2018.

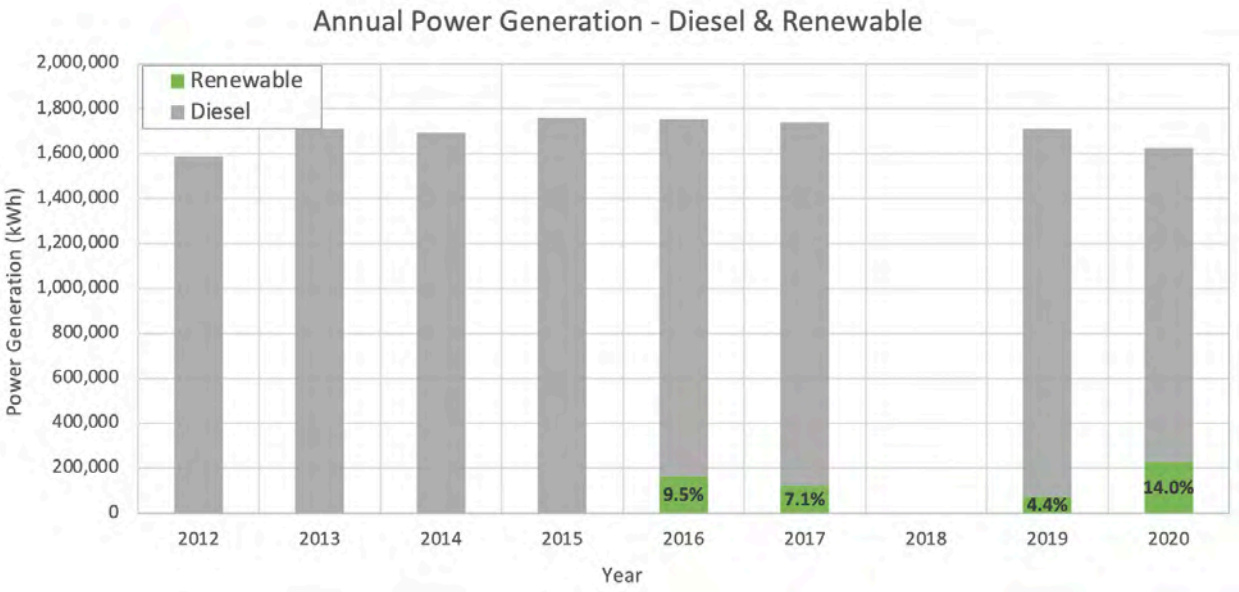

Renewable sources of power generation reduce diesel fuel use and can increase resiliency, in addition to offering many other benefits. The portion of power that is generated by renewable energy sources depends both on the capacity of the installed infrastructure as well as the performance of that infrastructure. In this way, the renewable energy generated may vary annually depending on the availability of the resource and availability of the equipment. In Buckland the portion of power generated by renewable energy sources has varied each year. No data was available for 2018.

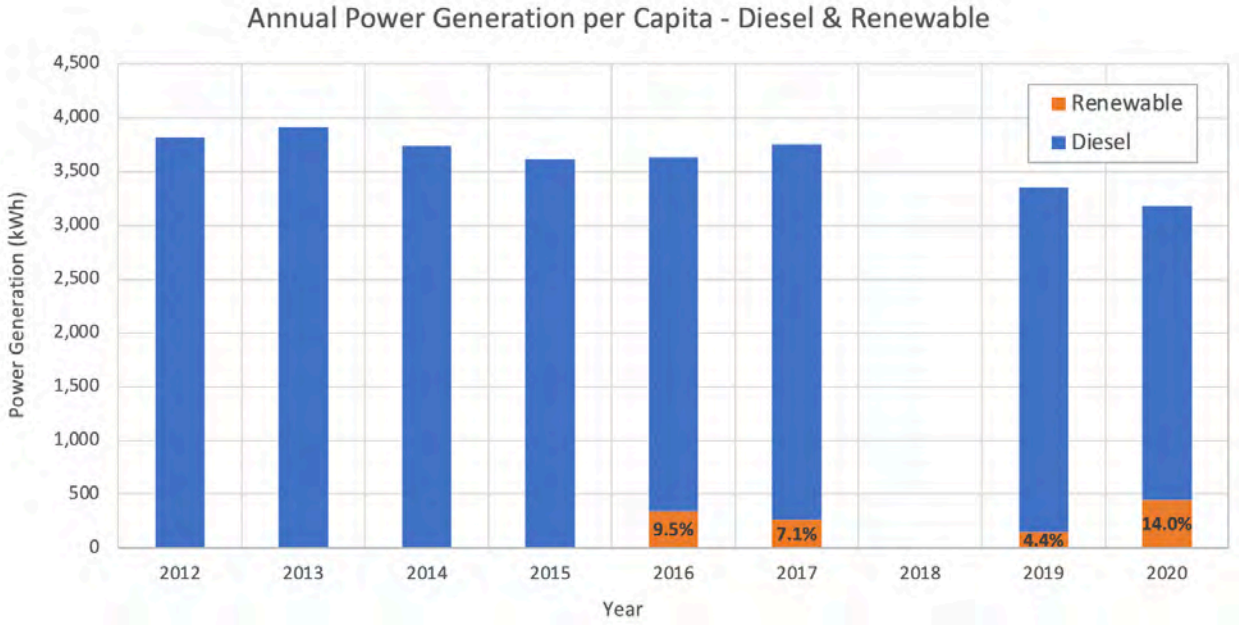

In general, people choose to power more electric devices each year, so the power generation per capita is expected to increase over time. When power generation per capita instead decreases over time, it is often correlated with reductions in power consumption as a result of energy efficiency upgrades. Power generation is also affected by the weather and corresponding heating needs each year. In 2019 and 2020 there were significant reductions in power generation per capita. No data was available for 2018.

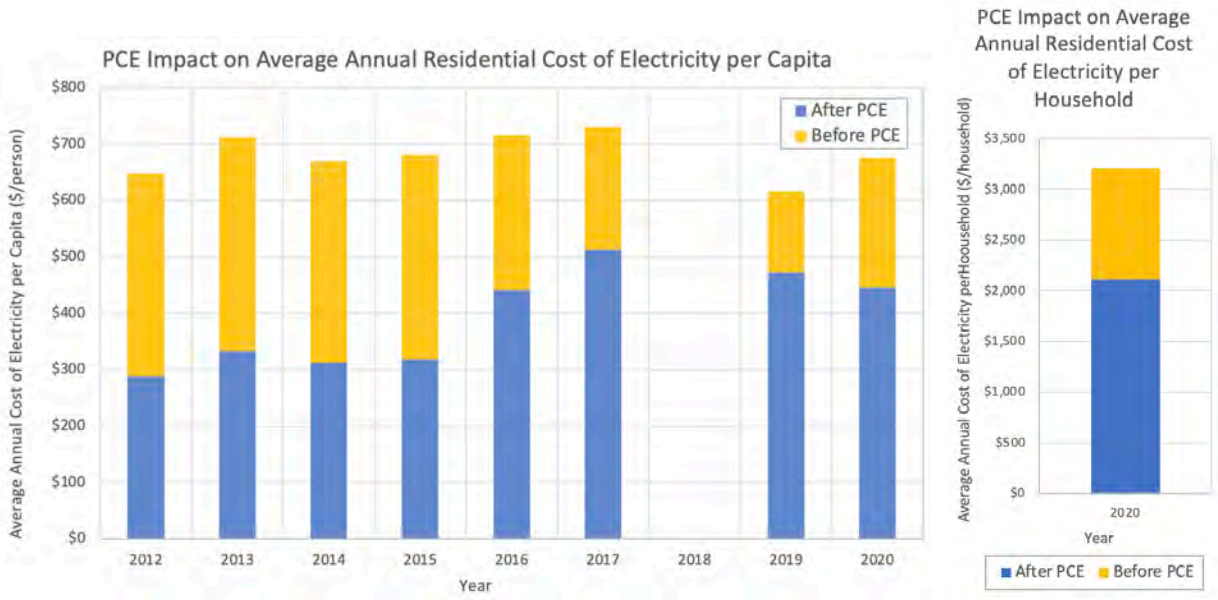

The PCE reimbursement reduces the residential cost of electricity by *a* different *amount* each year*. In communities where the main factor that affects the cost of power is the price of fuel, the PCE reimbursement will tend to levelize the residential cost of electricity from one year to the next. In Buckland, the residential cost of electricity per capita after PCE has varied dramatically over the last nine years from less than $300 per year to more than $500 per year. No data was available for 2018.*

Deering
Ipnatchiaq

Native Village of Deering:
907-363-2138
City of Deering:
907-363-2136
Ipnatchiaq Electric Company:
907-363-2157

Demographics –
Native Village Status: Federally Recognized Tribal Council
Alaska Native Name: Ipnatchiaq
Population: 168
Avg. Household Size: 3.53
Median Household Income: $44,375

Access –
Barge Access: Seasonal
Runway Ownership: State
Runway Surface: Gravel
Runway 1: 3,320 ft x 75 ft
Runway 2: 2,660 ft x 75 ft

Climate –
Average Summer Temperature: 50 °F
Average Winter Temperature: 0 °F
Heating Degree Days: 15,751

Heat & Power Costs (2021) –
Cost of Diesel Fuel: $4.12 per gal
Cost of Gasoline: $4.12 per gal
Cost of Electricity: $0.67 per kWh
Cost of Electricity, after PCE: $0.32 per kWh

Tank Farms -
Ownership: City of Deering, Northwest Arctic Borough School District (NWABSD), Ipnatchiaq Electric Company, Deering IRA
Bulk Fuel Capacity:

Owner	Fuel	Capacity (gal)
City of Deering	Diesel	63,000
NWABSD	Diesel	63,000
Ipnatchiaq Electric Company	Diesel	63,000
Deering IRA	Diesel	63,000
Deering IRA	Gasoline	63,000

Condition: Acceptable

Electric Utility –
Ipnatchiaq Electric Company (Subdivision of City)

Power Demand –
Average Load: 65 kW
Peak Summer Load: 150 kW
Peak Winter Load: 180 kW
Total Power Generated (2019): 699,769 kWh

Power System –
Fuel Efficiency (2019): 12.18 kWh/gal diesel
Line Loss (2017 - last reported): 3.2%
Number of Community Buildings on PCE (2020): 5
Community PCE kWh Use of Total Allowed (2020): 77% (108,384 kWh - used / 141,120 kWh – total allowed)

Power Generation Infrastructure –
Diesel Engines:

Manufacturer	Model	Capacity	Year Built
John Deere	6068TDW56	100 kW	2015
John Deere	6081AFM75	180 kW	2007
Cummins	LTA10G3	175 kW	1999
Cummins	LTA10G3	175 kW	1999

Wind Turbine(s):

Manufacturer	Model	Capacity	Year Built
Northern Power Systems	Northwind 100	100 kW	2014

Utility-Scale Solar PV:

Installer	Inverter	Capacity	Year Built
BoxPower	SMA Tripower	48.51 kW	2019

(Additional 11.13 kW installed for water plant, behind the meter)

Battery Storage System:

Manufacturer	Model	Capacity	Year Built
SAFT	Intensium Mini-M	277 kW / 109 kWh	2019

Heat Recovery –
Facilities Served: Washeteria/WTP
Opportunity to Expand Waste Heat: Yes

Water & Wastewater –
Ownership: City of Deering
Water System: Delivery; Washeteria
Wastewater System: Vacuum, Honey Bucket

Selected Projects –

EPA DERA Generator Replacement – *Expected 2022*

- Planned replacement of two generators, 2022
  - John Deere 4045, 100 kW; John Deere 6090, 200 kW
- Funding from EPA Diesel Emissions Reduction Act & Volkswagen Settlement Funding
  - $418,140 awarded from EPA in 2022
  - $129,056 from Volkswagen Settlement Funding

Distribution System Upgrade – *Expected 2022*

- Upgraded distribution system, started project in 2016
  - Installed new poles, transformers, and wires
- Reduced line loss and enhanced safety of distribution system
- USDA High Energy Cost Grant and Village Improvement Fund
  - $175,000 awarded from USDA HECG in 2016
  - $375,000 from Village Improvement Fund in 2017
  - $345,000 from Village Improvement Fund in 2021
  - $50,000 contributed by Ipnatchiaq Electric Company

Solar PV Array and Inverter – *Completed 2019*

- Installed 45 kW solar PV and inverter, 2019
  - Solar PV & foundations by BoxPower
- Displaces 4,300+ gal/year diesel fuel
- Contributed to 600+ hours of diesels-off from Apr ‘20 – Apr ‘21
- Department of Energy, Office of Indian Energy
  - $1 million awarded from DOE in 2016
  - $1 million match funding from NANA
    - Shared award: Kotzebue, Buckland, & Deering

Battery Storage and Controls – *Completed 2019*

- Installed 277 kW/109 kWh battery storage and controls
  - Necessary to make solar PV array effective
- Integrated solar PV & battery storage with microgrid, 2019
- Contributed to 600+ hours of diesels-off from Apr ‘20 – Apr ‘21
- USDA High Energy Cost Grant Program
  - $1.6 million awarded in 2016
    - Shared award: Buckland and Deering

Wind/Diesel Microgrid – *Completed 2015*

- Installed Northwind 100 kW wind turbine, 2014
- Integrated wind turbine with microgrid, 2015
- Displaces 7,200+ gallons diesel fuel annually
- Contributed to 600+ hours of diesels-off from Apr ‘20 – Apr ‘21
- AK Energy Authority Renewable Energy Fund, Round 1
  - $10.5 million awarded in 2009

        - Shared award: Noorvik, Buckland, & Deering

LED Streetlight Retrofit Borough-Wide – *Completed 2015*

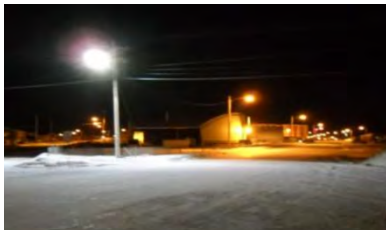

- Installed 15 LED streetlights in Deering
- 25-year community savings: ~$1.6M & ~630,000 gal diesel
- State of Alaska, Grants to Municipalities
    - Funding awarded 2014
    - $200,000 awarded to Northwest Arctic Borough

Water Plant Solar PV – *Completed 2013*

- 11.13 kW solar PV installed
- Average 21.9 kWh/day; still operational
- Coastal Impact Assistance Program (CIAP)
    - Funding awarded 2009
    - $86,833 awarded

Future Projects –

Energy Audits

- Conduct additional energy audits
    - Health clinic, school, sewer building, and City offices
- Complete energy efficiency recommendations to reduce heating and operational costs

Residential Heat Trace Design Upgrade

- Survey residential heat trace infrastructure and operation
- Design and implement improved system to maintain water system functionality in winter
    - Reduce energy consumption and enhance reliability

Community-Wide Residential LED Lighting Upgrade

- Upgrade all residential lighting fixtures to energy efficient LED lighting
    - Survey type and quantity of lighting fixtures in all homes
    - Apply for Village Improvement Fund support
    - Procure and install energy efficient lighting
        - Reduce residential electricity costs

Solar PV

- Increase capacity of solar PV array and battery storage
    - Displace additional diesel fuel and increase hours of diesels-off
        - Reduce the cost of electricity
    - Enhance resiliency of system

Energy Milestones –

- Achieved diesels-off operation – *October 11th, 2019*
- Installed first solar PV in Deering – *Completed 2013*

Community Goals –

- Reduce cost of residential space and water heating
    - Expand renewable energy microgrid
        - Solar PV, wind turbine
    - Implement energy efficiency measures
    - Maintain and/or replace aging residential heating appliances
- Upgrade diesel generators #1 and #3 to enhance reliability of power system
- Enhance energy efficiency of water and sewer systems
- Conduct feasibility study to determine how much additional solar PV and battery storage to install
- Create additional training opportunities for operators to enhance skills and understanding of microgrid
- Partner with Northwest Inupiat Housing Authority to implement policy changes to prioritize and invest in energy efficiency in newly constructed homes

Microgrid System Schematic –

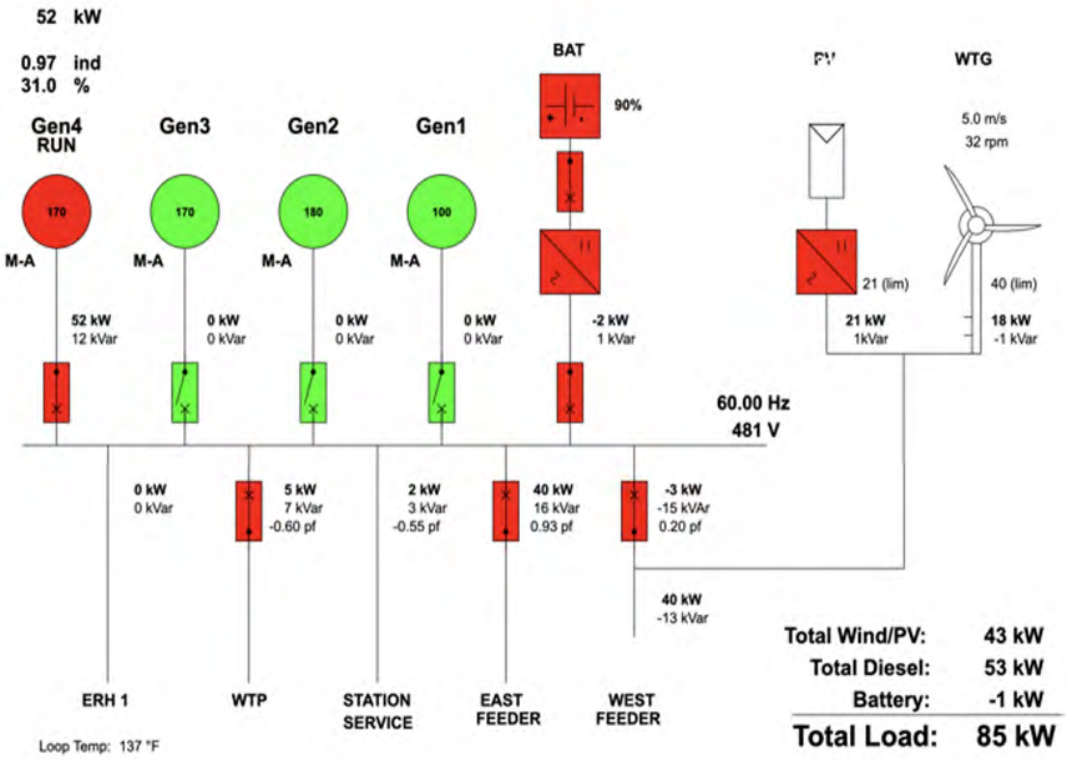

Energy System Trends –

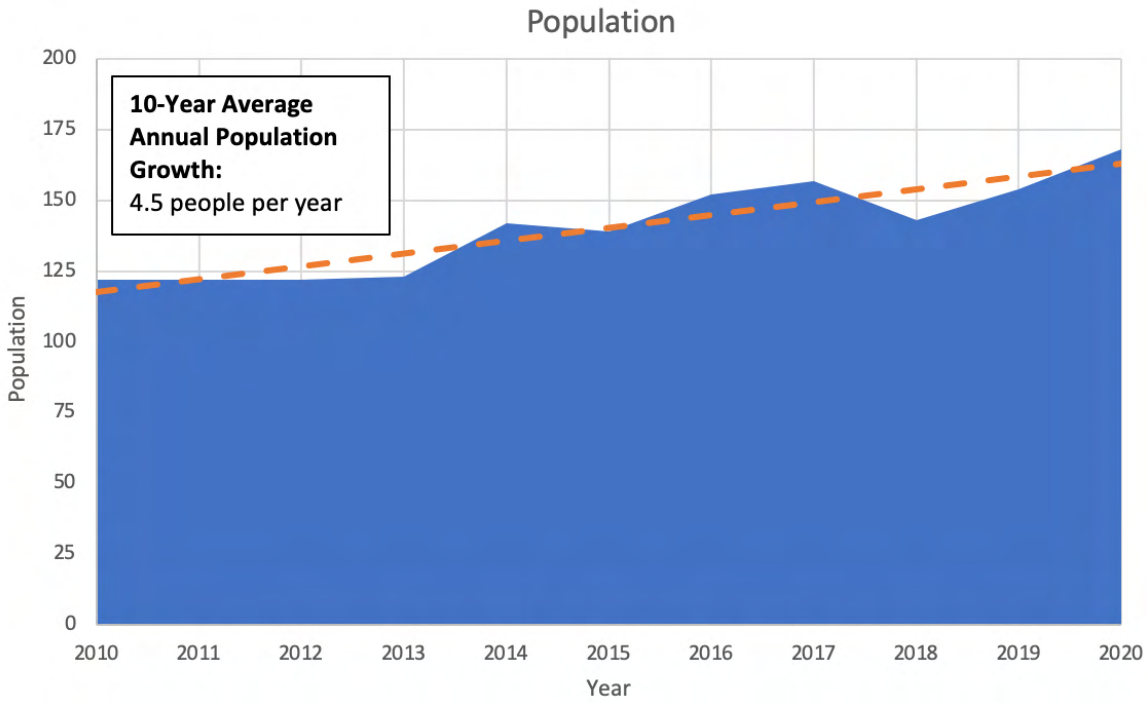

Dramatic changes in population impact the long-term community planning necessary to meet future power demand. The population in Deering is not changing dramatically. Over the last ten years the population has increased an average of 3.7% each year.

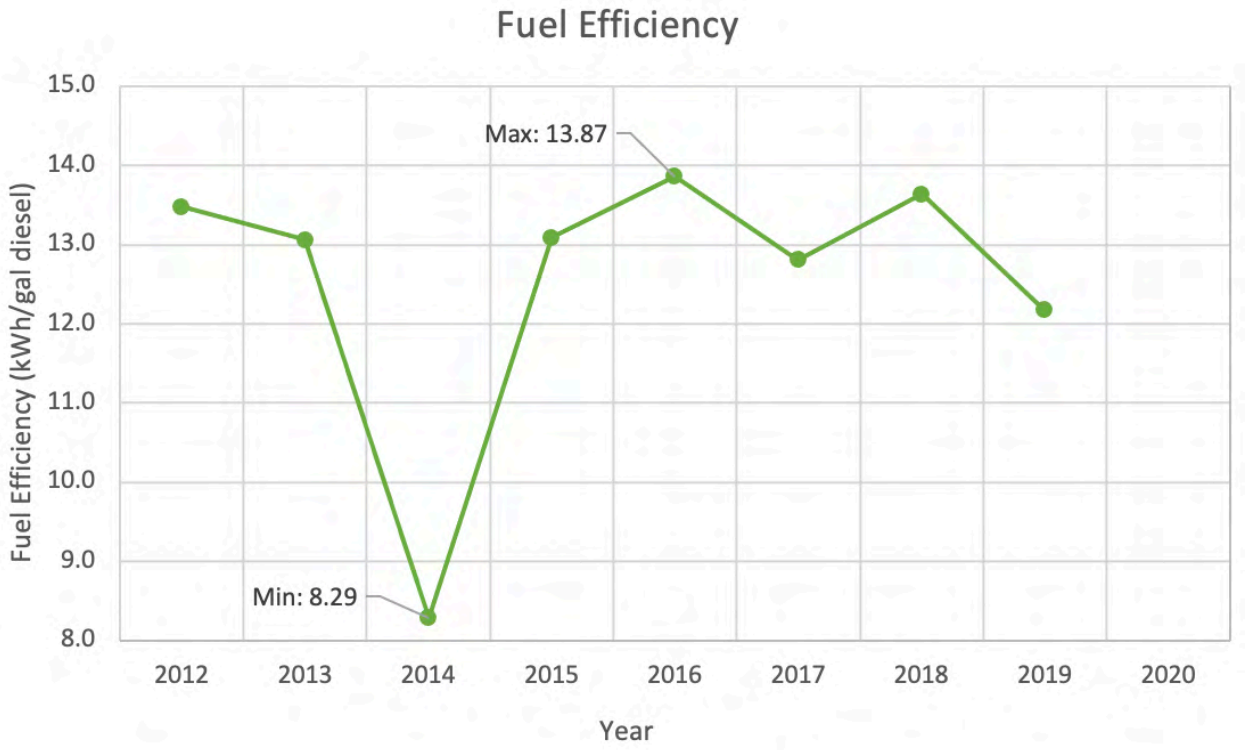

A higher fuel efficiency results in less diesel fuel use and a lower cost to generate power. A fuel efficiency below 12 kWh/gal is poor; a fuel efficiency above 14 kWh/gal is excellent. The fuel efficiency in Deering has typically been very good, but there is some variation year to year. The data for 2014 may be inaccurate as it is exceptionally low. No data was available for 2020.

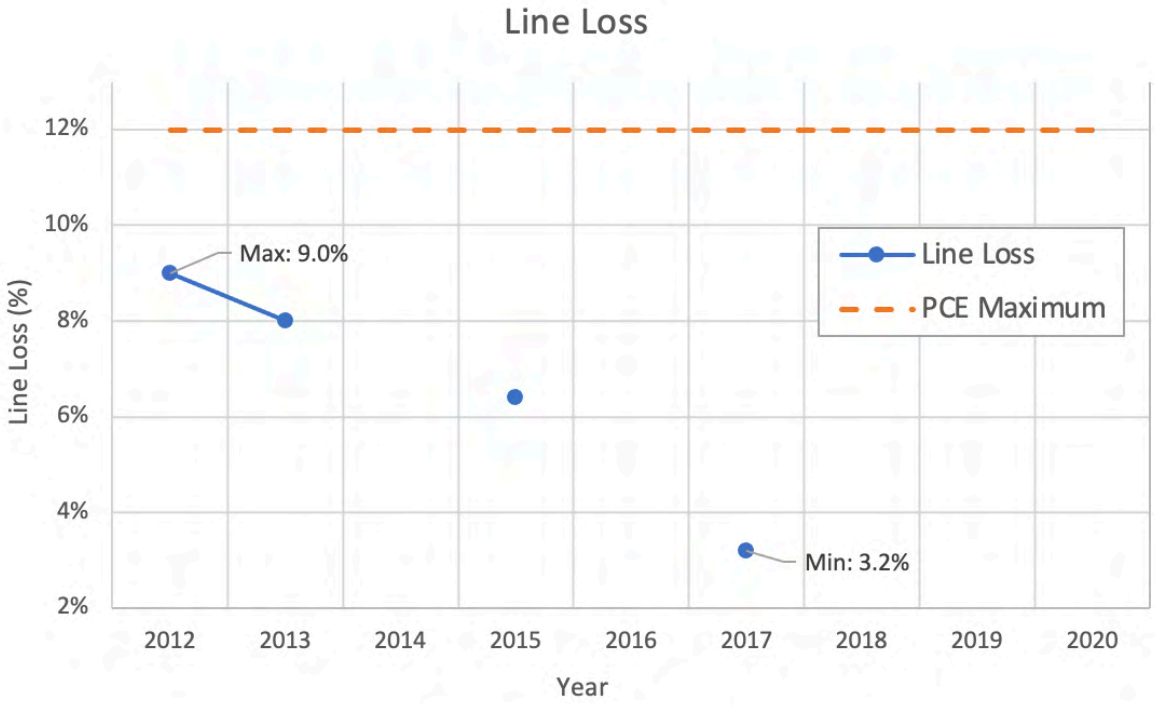

The maximum allowable line loss to maintain eligibility for PCE benefits is 12%. In Deering, the line loss has decreased dramatically since 2021 as a result of a distribution system capital upgrade. The gaps in the data indicate that either no data was available or the data was incorrect.

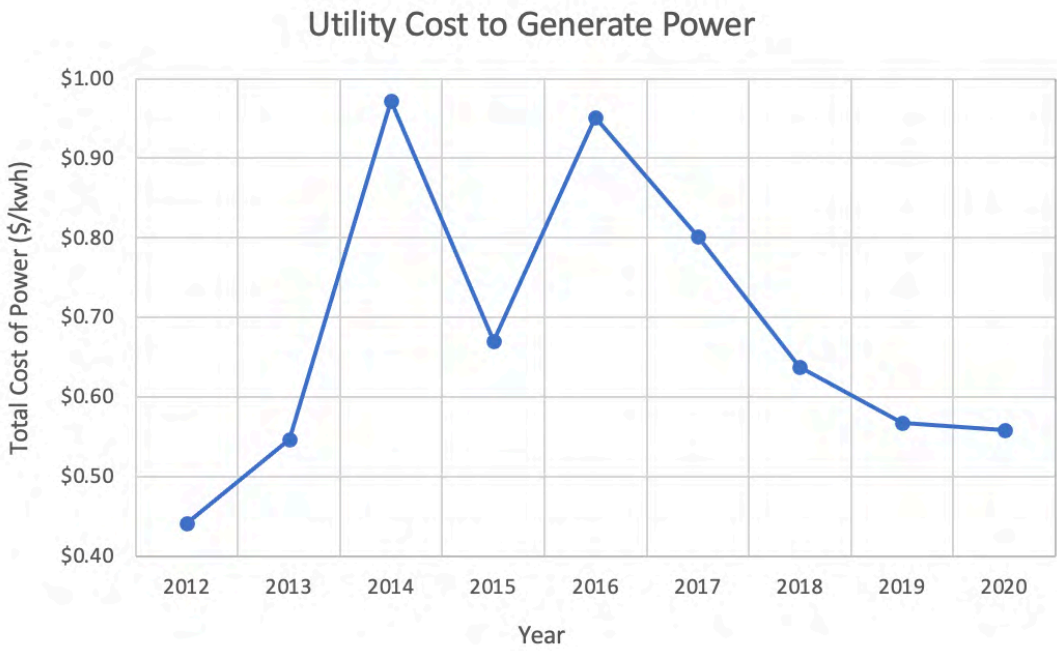

Over the long-term, a lower utility cost to generate power typically correlates with a lower cost of electricity for residents. The major factors that affect the cost to generate power are the cost of fuel, generator fuel efficiency, maintenance, and operations. Major system breakdowns may cause the cost to generate power to spike on a particular year, as will high fuel prices. In Deering the cost to generate power has been trending lower each year since 2016. Fuel savings from power generated by renewable energy sources are likely contributing to this reduction.

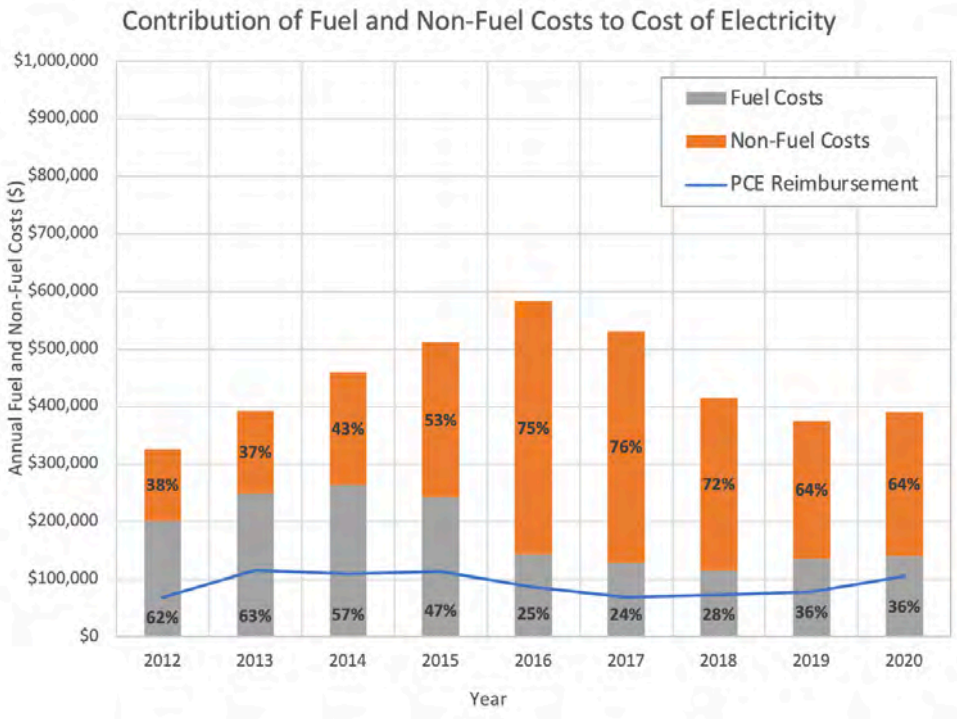

For many utilities, the non-fuel costs associated with generating power do not change dramatically each year. Fuel costs, on the other hand, are highly susceptible to annual fluctuations based on the global price of fuel, transportation costs, and the amount of power generated. PCE reimbursement is meant to offset the high fuel costs in rural Alaska. As the overall efficiency of the system increases, the PCE reimbursement offsets a larger portion of the total fuel costs. In Deering, the portion of the costs spent on fuel dramatically decreased in 2016, after the installation of the wind turbine. The portion of the costs spent on non-fuel costs as well as the total non-fuel costs increased dramatically in 2016, but have been decreasing since 2018.

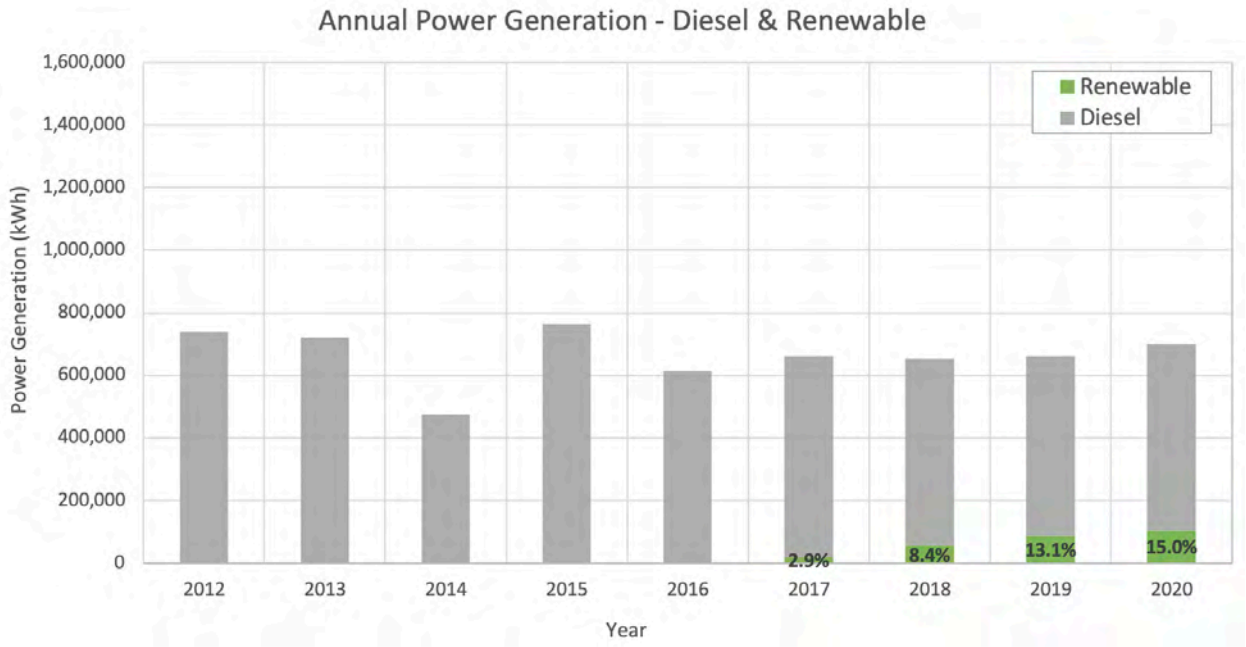

Renewable sources of power generation reduce diesel fuel use and can increase resiliency, in addition to offering many other benefits. The portion of power that is generated by renewable energy sources depends both on the capacity of the installed infrastructure as well as the performance of that infrastructure. In this way, the renewable energy generated may vary annually depending on the availability of the resource and availability of the equipment. In Deering the portion of power generated by renewable energy sources has increased each year since 2017.

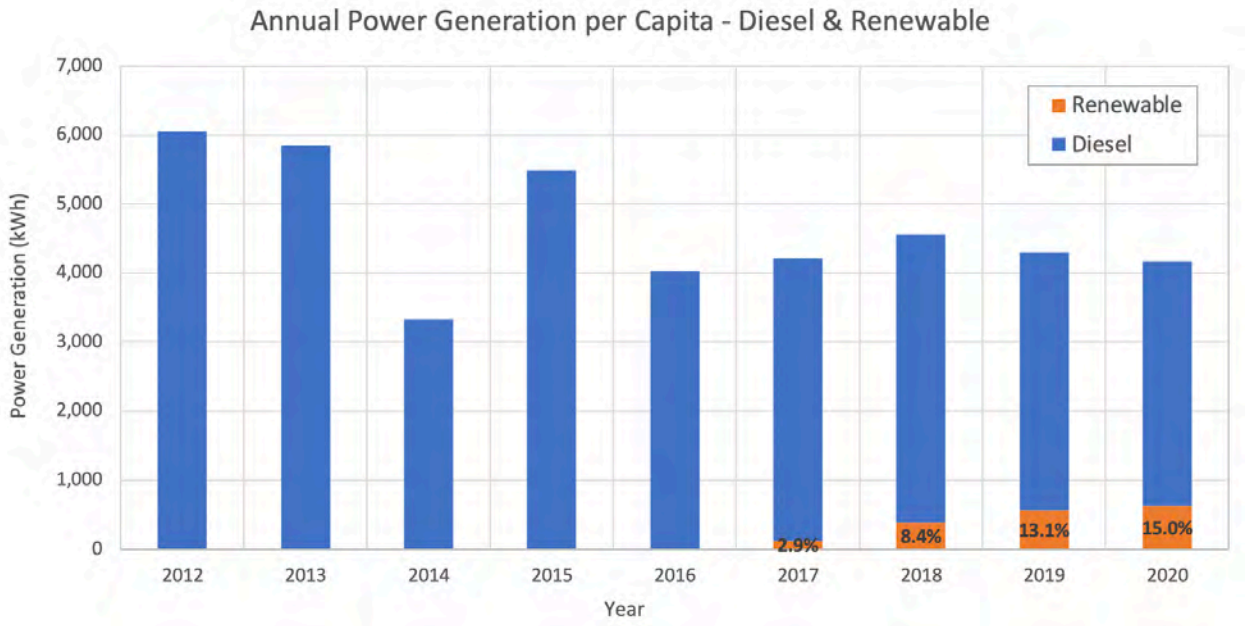

In general, people choose to power more electric devices each year, so the power generation per capita is expected to increase over time. When power generation per capita instead decreases over time, it is often correlated with reductions in power consumption as a result of energy efficiency upgrades. Power generation is also affected by the weather and corresponding heating needs each year. Excluding 2014, there was a dramatic step-down in power generation per capita in Deering in 2016.

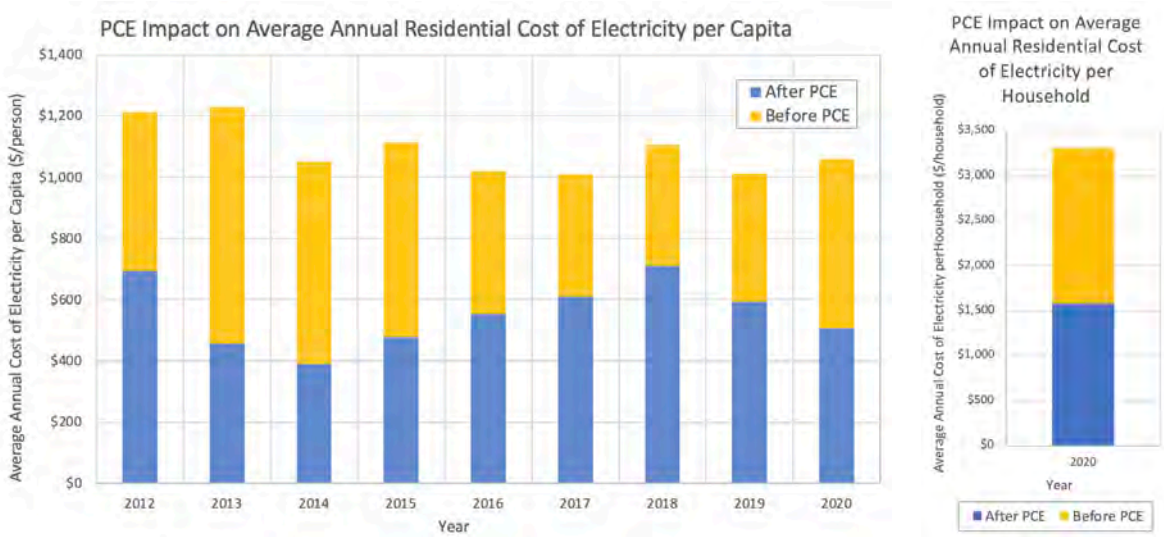

The PCE reimbursement reduces the residential cost of electricity by a different amount each year. In communities where the main factor that affects the cost of power is the price of fuel, the PCE reimbursement will tend to levelize the residential cost of electricity from one year to the next. In Deering, the residential cost of electricity per capita after PCE has varied dramatically over the last nine years from less than $400 per year to more than $700 per year.

Kotzebue
Qikiqtagruk

Native Village of Kotzebue:
907-442-3467
City of Kotzebue:
907-442-3401
Kikiktagruk Inupiat Corp.:
907-442-3165
Kotzebue Electric Association:
907-442-3491

Demographics –
Native Village Status: Federally Recognized Tribal Council
Alaska Native Name: Qikiqtagruk
Population: 3121
Avg. Household Size: 3.44
Median Household Income: $88,047

Access –
Barge Access: Seasonal
Runway Ownership: State
Runway Surface: Asphalt
Runway 1: 5,300 ft x 150 ft
Runway 2: 3,876 ft x 90 ft

Climate –
Average Summer Temperature: 51 °F
Average Winter Temperature: 0 °F
Heating Degree Days: 16,531

Heat & Power Costs (2021) –
Cost of Diesel Fuel: $5.87 per gal
Cost of Gasoline: $5.88 per gal
Cost of Electricity: $0.40 per kWh
Cost of Electricity, after PCE: $0.22 per kWh

Tank Farm -
Ownership: Kotzebue Electric Association (KEA) (Vitus – leasing a portion), Crowley
Bulk Fuel Capacity:

Owner	Fuel	Capacity (gal)
KEA	Diesel	2,150,000
Vitus	ULSD1	650,000 (leased from KEA)
Vitus	Gasoline	300,000 (owned by Vitus)
Crowley	Diesel Gasoline ULSD AV100LL Jet A	6,132,000

Condition: Deteriorating

Electric Utility –
Kotzebue Electric Association (KEA)

Power Demand (2020) –
Average Load: 2.5 MW
Peak Load: 3.4 MW
Total Power Generated: 19, 919,319 kWh

Power System (2020) –
Fuel Efficiency: 14.78 kWh/gal diesel
Line Loss: 3.1%
Number of Community Buildings on PCE: 26
Community PCE kWh Use of Total Allowed: 62% (1,632,934 kWh / 2,621,640 kWh)

Power Generation Infrastructure –
Diesel Engines:

Manufacturer	Model	Capacity
Caterpillar	3516	1135 kW
Caterpillar	C27	725 kW
EMD	8-710	1440 kW
EMD	16-710	2865 kW
EMD	16-710	2865 kW
EMD	20-710	3010 kW

Wind Turbine(s):

Manuf.	Model	Capacity	Qty	Status	Year Built
EWT	DW 54-900	900 kW	2	Functional	2012
Vestas	V15	65 kW	1	Needs Repair	2005
Northern Power Systems	Northwind 100	100 kW	1	Needs Repair	2000
AOC	15/50	66 kW	15	Needs Repair	1997 - 2005

Grid Stabilization:

Component	Manuf.	Model	Capacity	Year Built
STATCOM	ABB	PCS100	1MVAr	2012

Solar PV:

Installer	Inverter	Capacity	Year Built
Alaska Native Renewable Industries	Solar Edge	576 kW bifacial	2020

(*Additional 20 kW installed for water plant, behind the meter)*

Battery Storage System:

Component	Manuf.	Model	Capacity	Year Built
Battery	SAFT	IM-20	950 kWh	2015
Converter	ABB	PCS100	1,225 kW	2015
Microgrid Controller	EPS	Demand Control	-	2005

Electric Boiler:

Owner	Capacity	Year Installed
Maniilaq Health Center	450 kW	2014
National Park Service	108 kW	2022

Heat Recovery –
Facilities Served: Circulating water main – heat added in power plant to raise temp from 38°F to 50°F in winter months.
Opportunity to Expand Waste Heat: Yes

Water & Wastewater –
Ownership: City of Kotzebue
Water System: Piped; New water treatment plant – construction expected to conclude in fall 2022
Wastewater System: Piped

Selected Projects –

Battery Storage System Design – *Expected 2022*

- Design for ~4 MW/MWh battery storage system
- Design to integrate battery storage with microgrid to achieve diesels-off operation
- Alaska Energy Authority – REF 13; Kotzebue Electric Association
  - Grant awarded 2020
  - $325,000 awarded from AEA
  - $100,000 cost share from KEA

National Park Service Wind-To-Heat – *Expected 2022*

- Installed 108 kW electric boiler
- Excess wind energy powers NPS's electric boiler
- Finalizing agreement to buy excess wind power

Solar PV Array and Battery – *Completed 2020*

- Installed 576 kW bifacial solar PV and inverters
  - Average daily production: 1794 kWh/day
- Installed 950 kWh/1,130 kW battery storage system
- DOE; Village Improvement Fund; Kotzebue Electric Assoc.
  - Grant awarded 2019
  - $600,000 awarded from USDA
  - $600,000 awarded from VIF
  - $600,000 cost share from KEA

Biomass Feasibility Study – *Completed 2017*

- Evaluated opportunity to generate power from solid waste
  - Displace 30,000+ gallons of diesel fuel annually
  - Divert 300 tons of waste from landfill annually
- Determined to be a financially and technically viable project

Grid Stabilization Technology Upgrade – *Completed 2012*

- Installed ABB PCS 100 STATCOM 1MVAr
- Enhances microgrid stabilization
  - Increases power factor on genset during high-renewables operation

LED Streetlight Retrofit Borough-Wide – *Completed 2015*

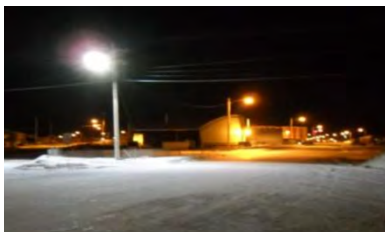

- Installed 275 LED streetlights in Kotzebue
- 25-year community savings: ~$30M & ~11.6M gal diesel
- State of Alaska, Grants to Municipalities
  - Funding awarded 2014
  - $200,000 awarded to Northwest Arctic Borough

Water Plant Solar PV – *Completed 2015*

- 21.06 kW solar PV installed
- Average 40.1 kWh/day; still operational
- Coastal Impact Assistance Program (CIAP)
  - Funding awarded 2009
  - $168,156 awarded

Wind/Diesel Microgrid Expansion – *Completed 2012*

- Installed two EWT 900 kW wind turbines
- Integrated wind turbines with microgrid
- Installed 450 kW electric boiler at hospital, 2014
  - Developed agreement for Maniilaq buy excess wind power
- AK Energy Authority Renewable Energy Fund, Rounds 1 & 3
  - Grants awarded 2008 & 2010
  - $8 million awarded total

Wind/Diesel Microgrid – *Completed 2005*

- Installed 15 AOC 66 kW wind turbines
- Installed 1 Vestas V15 65 kW wind turbine
- Installed 1 Northwind 100 kW wind turbine
- Integrated wind turbines with microgrid
- First successful cold temperature wind-diesel integration in US
- US Department of Energy
  - $4 million awarded in 1996

Future Projects –

Battery Storage

- Increase battery energy storage and inverter power capacity
- Funding secured for design work from Renewable Energy Fund, Round 13
    - Install an additional 4-8 MWh of battery storage and approximately 4 MW of inverter power capacity
- Need to secure procurement and installation funding

Solar PV

- Increase capacity of solar PV array
- Applied for Renewable Energy Fund, Round 14
    - Install an additional 500 – 600 kW of solar PV
    - Reuse infrastructure from old turbines (15 AOC's, maybe 1 Vestas)

Wind Turbines

- Expand wind energy with two additional turbines
    - 1,000 kW EWT turbines
- Funding secured for design work from Village Improvement Fund
- Need to secure construction funding

Community-Wide Residential LED Lighting Upgrade

- Upgrade all residential lighting fixtures to energy efficient LED lighting
    - Survey type and quantity of lighting fixtures in all homes
    - Apply for Village Improvement Fund support
    - Procure and install energy efficient lighting
        - Reduce residential electricity costs

Milestones –

- Installed largest solar PV array in rural Alaska – *Completed 2020*
- Installed first solar PV in Kotzebue – *Completed 2015*
- First utility-scale wind in the Arctic – *Completed 1997*

Community Goals –

- Reduce cost of residential space and water heating
    - Construct bulk fuel storage owned by City/Tribe
    - Expand renewable energy microgrid
        - Explore opportunities for dispatching excess wind for residential and commercial heating
            - Electric heating and/or heat pumps
    - Implement energy efficiency measures for residential and commercial buildings
    - Maintain and/or replace aging residential heating appliances
- Achieve diesels off operation after installation of additional battery storage
- Optimize diesel genset operation through installation of additional renewable energy generation sources and community-scale energy storage

    - Reduce wind curtailment
    - Reduce restrictions on use of smallest diesel generator
- Continue to optimize operation of bifacial solar installation to maximize energy generation
- Partner with NANA to organize electricians, mechanics, and additional technical expertise to serve the region
    - Utilize Kotzebue as a hub to offer trainings and service mobile equipment
- Explore opportunities to develop Cape Blossom Port to site additional wind turbines
- Enhance Native Village of Kotzebue, Kikiktagruk Inupiat Corp., and City of Kotzebue level of interest and involvement in Kotzebue's energy systems and energy efficiency opportunities
    - Further support reductions in the residential cost of energy for heat and electricity
    - Enhance community resilience

Energy System Trends –

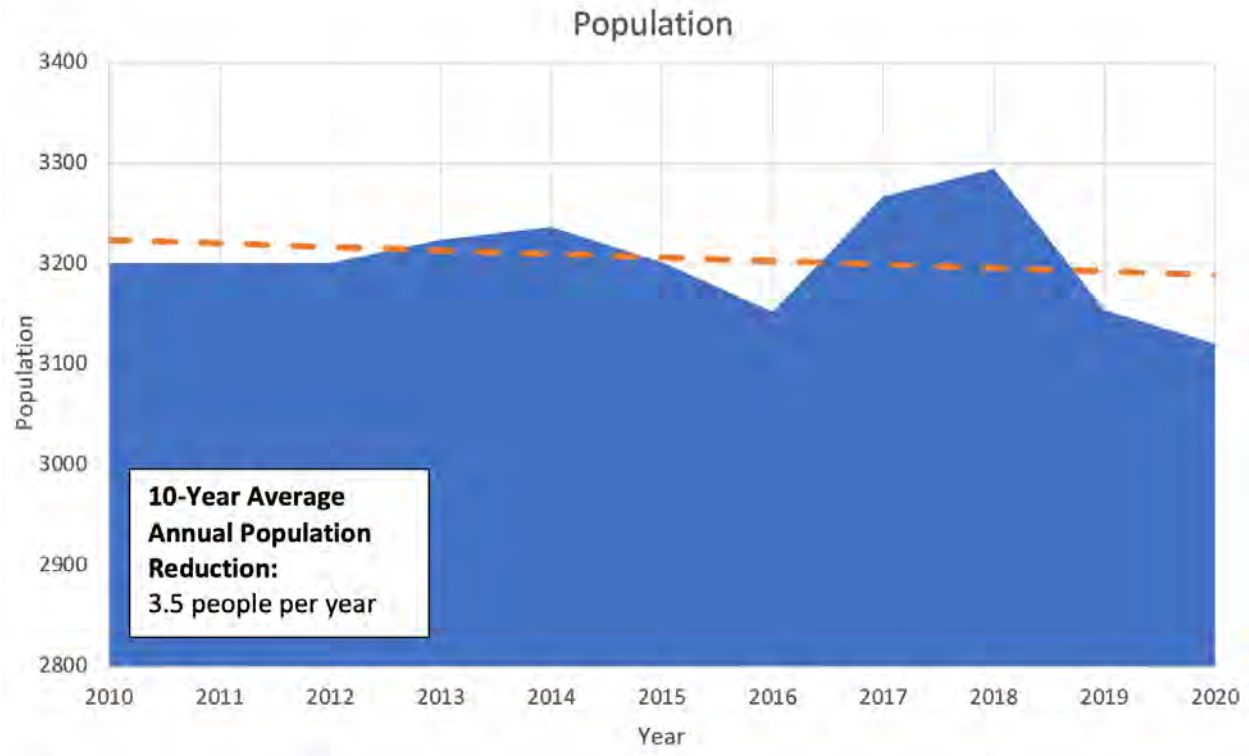

Dramatic changes in population impact the long-term community planning necessary to meet future power demand. The population in Kotzebue has fluctuated year-to-year. Over the last ten years the population has decreased an average of 0.1% each year.

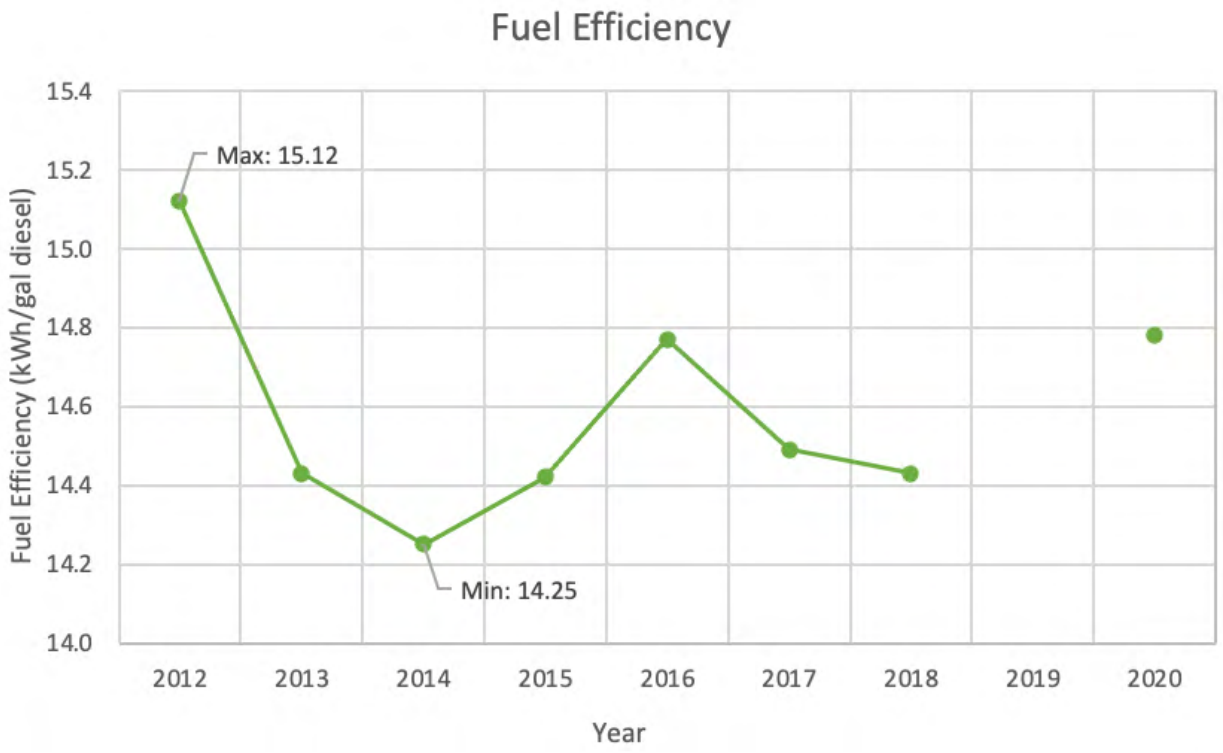

A higher fuel efficiency results in less diesel fuel use and a lower cost to generate power. A fuel efficiency below 12 kWh/gal is poor; a fuel efficiency above 14 kWh/gal is excellent. The fuel efficiency in Kotzebue has been excellent with values that are typically greater than 14 kWh/gal. No data was available for 2019.

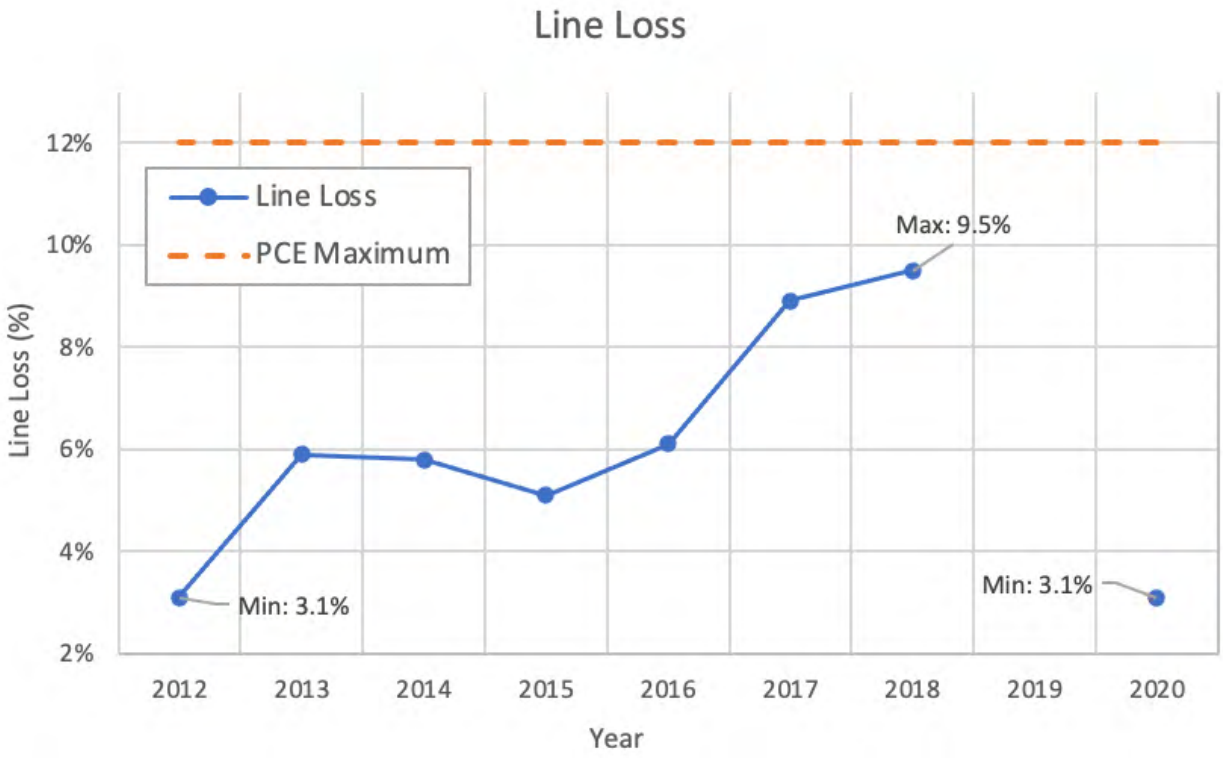

The maximum allowable line loss to maintain eligibility for PCE benefits is 12%. In Kotzebue, the line loss increased steadily from 2012 to 2018. In 2020 the line loss decreased dramatically. It is unclear what caused this dramatic reduction in line loss. No data was available for 2019.

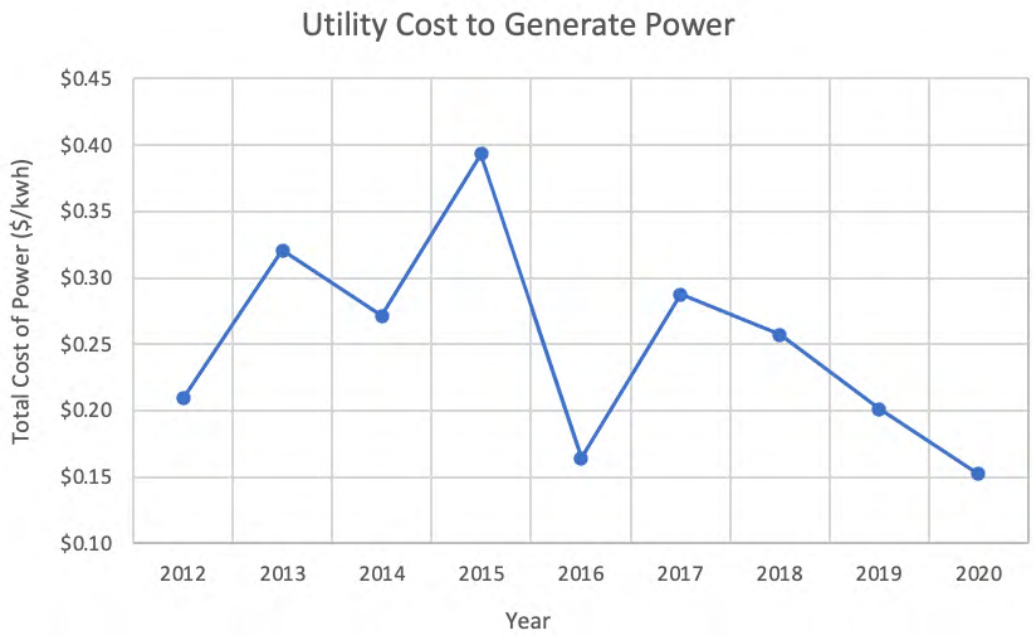

Over the long-term, a lower utility cost to generate power typically correlates with a lower cost of electricity for residents. The major factors that affect the cost to generate power are the cost of fuel, generator fuel efficiency, maintenance, and operations. Major system breakdowns may cause the cost to generate power to spike on a particular year, as will high fuel prices. In Kotzebue the cost to generate power has fluctuated substantially over the last nine years, but it has decreased in 2017 and 2018 and it is now at a very low value relative to other communities in the region and across the state. In 2016, 2019, and 2020 the cost to generate power does not include the non-fuel costs (as shown below) and therefore underestimates the actual cost to generate power. This is due to a PCE reporting error.

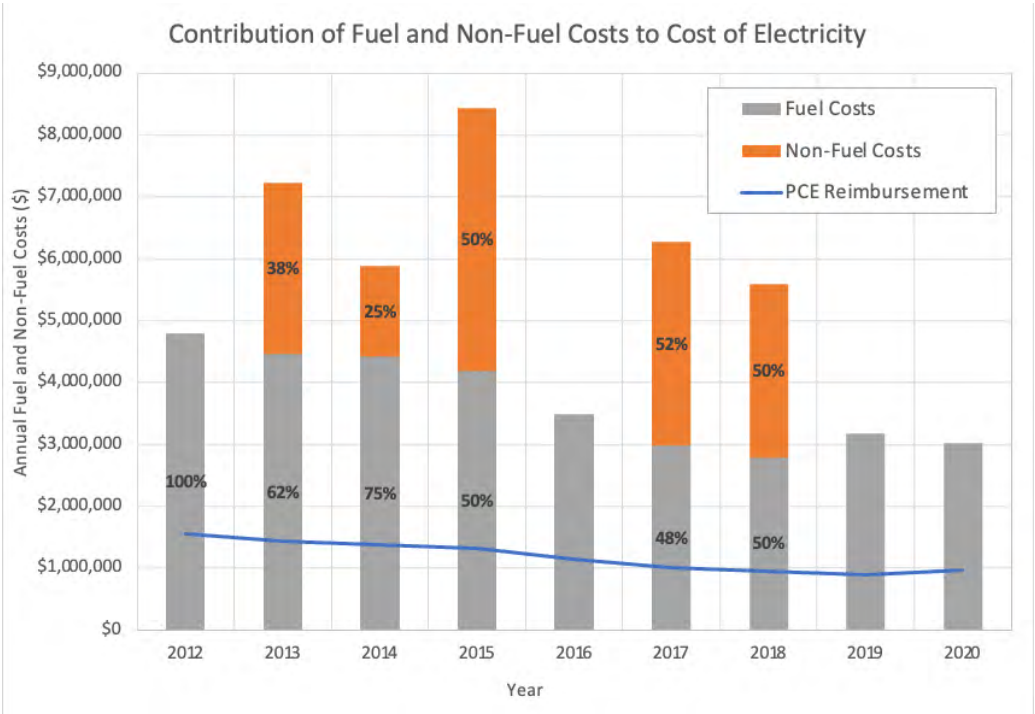

For many utilities, the non-fuel costs associated with generating power do not change dramatically each year. Fuel costs, on the other hand, are highly susceptible to annual fluctuations based on the global price of fuel, transportation costs, and the amount of power generated. PCE reimbursement is meant to offset the high fuel costs in rural Alaska. As the overall efficiency of the system increases, the PCE reimbursement offsets a larger portion of the total fuel costs. In Kotzebue, the reported non-fuel costs fluctuate dramatically year-to-year. It should be verified this is not a calculation error. The fuel costs have decreased dramatically since 2012 and have steadied in the last four years.

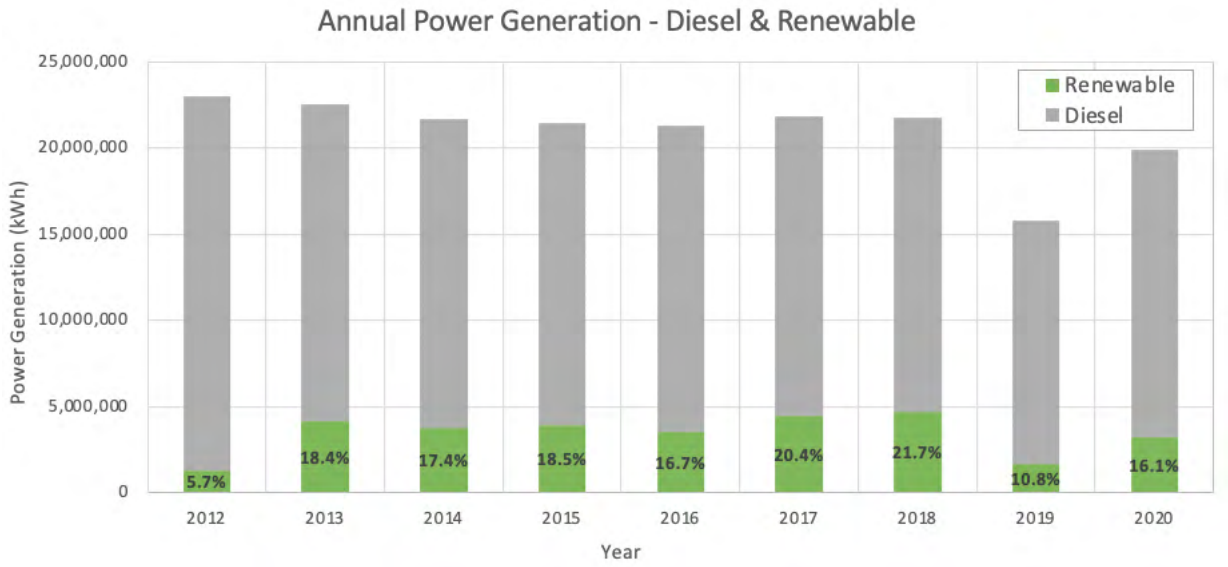

Renewable sources of power generation reduce diesel fuel use and can increase resiliency, in addition to offering many other benefits. The portion of power that is generated by renewable energy sources depends both on the capacity of the installed infrastructure as well as the performance of that infrastructure. In this way, the renewable energy generated may vary annually depending on the availability of the resource and availability of the equipment. In Kotzebue the portion of power generated by renewable energy sources grew dramatically in 2013 and modestly in 2017. In 2019 and 2020 the renewable energy generation decreased substantially, likely indicating downtime of renewable infrastructure.

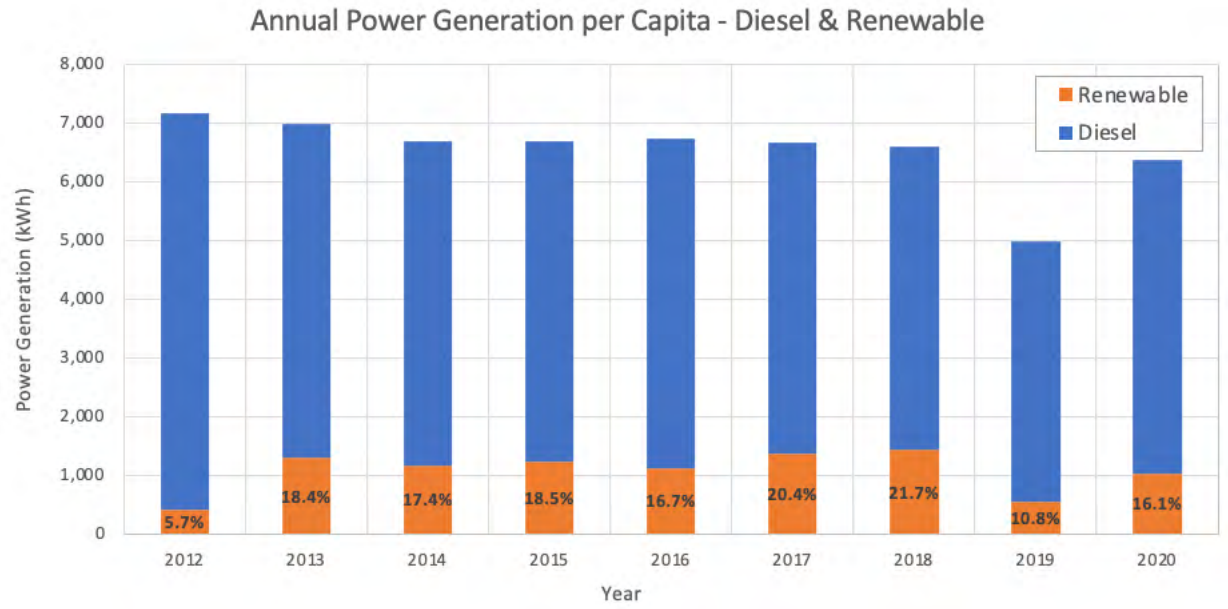

In general, people choose to power more electric devices each year, so the power generation per capita is expected to increase over time. When power generation per capita instead decreases over time, it is often correlated with reductions in power consumption as a result of energy efficiency upgrades. Power generation is also affected by the weather and corresponding heating needs each year. Power generation per capita in Kotzebue was exceptionally steady from 2014 to 2018, with slightly higher values preceding this interval and slightly lower values in recent years. In 2019 there were significant reductions in power generation per capita. It should be verified this is not a calculation error.

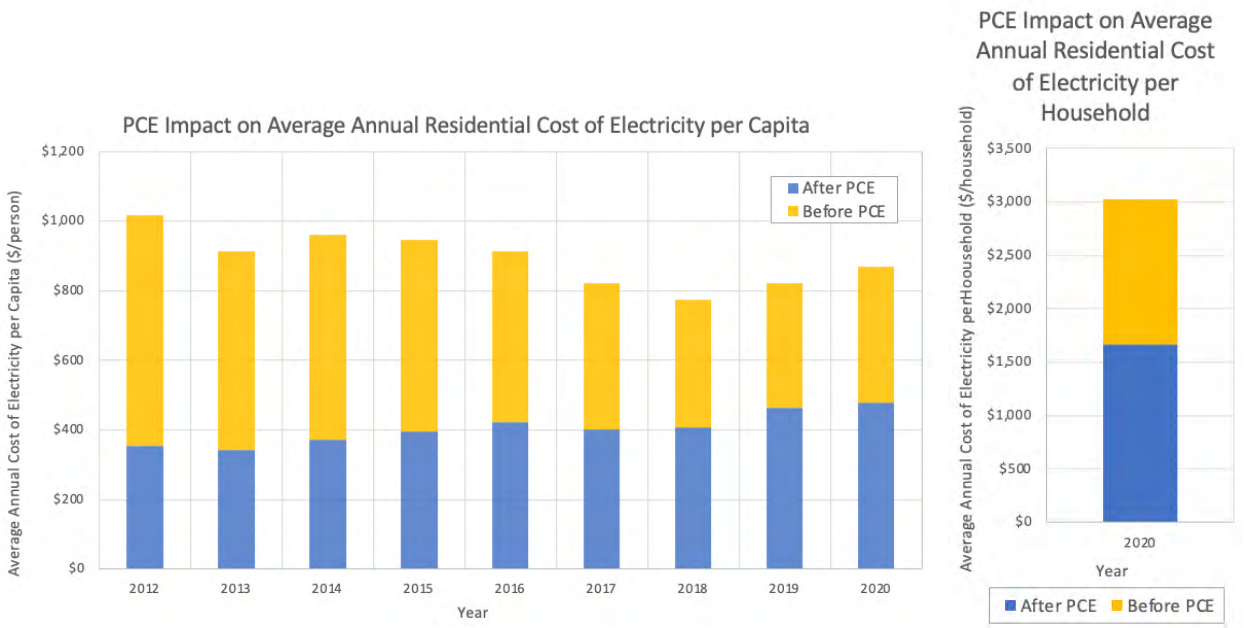

The PCE reimbursement reduces the residential cost of electricity by a different amount each year. In communities where the main factor that affects the cost of power is the price of fuel, the PCE reimbursement will tend to levelize the residential cost of electricity from one year to the next. In Kotzebue, the residential cost of electricity per capita after PCE has increased over the last nine years, while the cost before PCE has decreased. This reduction in PCE funding primarily reflects the increasing price of electricity on the Railbelt—which is used to calculate PCE reimbursement levels statewide—not a reduction in PCE rate due to KEA operations.

Appendix C

Helical Pile Performance in Frozen Permafrost Soil

Evaluation of Helical Piers for Use in Frozen Ground

Technical Report

by

Hannele K. Zubeck
School of Engineering
University of Alaska Anchorage
3211 Providence Drive
Anchorage, AK 99508

He Liu
School of Engineering
University of Alaska Anchorage
3211 Providence Drive
Anchorage, AK 99508

April, 2002

TABLE OF CONTENTS

TABLE OF FIGURES

TABLE OF TABLES

1. INTRODUCTION

1.1 Background

Foundation design in areas with frozen ground is more challenging than in warm areas. The additional challenges are due to frost action and creep of ice rich frozen soil. Also, construction, including excavation, transportation of materials, compaction, and any installation is more difficult and expensive than in temperate regions. Long distances to remote villages and facilities magnify these problems. Therefore, it is important to choose a foundation type for frozen ground that will perform satisfactorily in the harsh conditions, and is easy to transport and install.

Helical piers (Figure 1.1) are a potential alternative for traditional piles commonly used in frozen ground. The piers are installed by screwing them into the ground with a rotating head attached to an excavator (Figure 1.2) or with hand held equipment. The load from the superstructure is transferred into the surrounding soil through the helix or helixes attached to a shaft. They work in compression and tension and are ideal for fence poles, boardwalks, light poles, decks and even buildings (Figure 1.3). The ease of installation, lightweight, compact volume, small ground disturbance and minimal freeze-back time are the features of helical piers (Figure 1.4). The benefits of using helical piers are consequently decreased construction costs and preserving of the natural terrain.

1.2 Problem Definition

The helical piers have been used in remote villages by hundreds for foundations for utilidors and boardwalks (Figure 1.5). However, their use could be increased, if engineers would have confidence specifying them in their projects. They feel that neither design guidelines nor recorded performance data exist for helical piers. Therefore, Alaska Science and Technology Foundation (ASTF) funded this research project to develop guidelines for design of helical piers in frozen ground.

1.3 Objectives

The purpose of this research is to evaluate the performance of helical piers and to create installation and design guidelines. This is done by conducting a literature review, creating a finite element model for the piers, running a full-scale test in the U.S. Army Cold Regions Research and Engineering Laboratory (CRREL), and observing and recording existing pier projects.

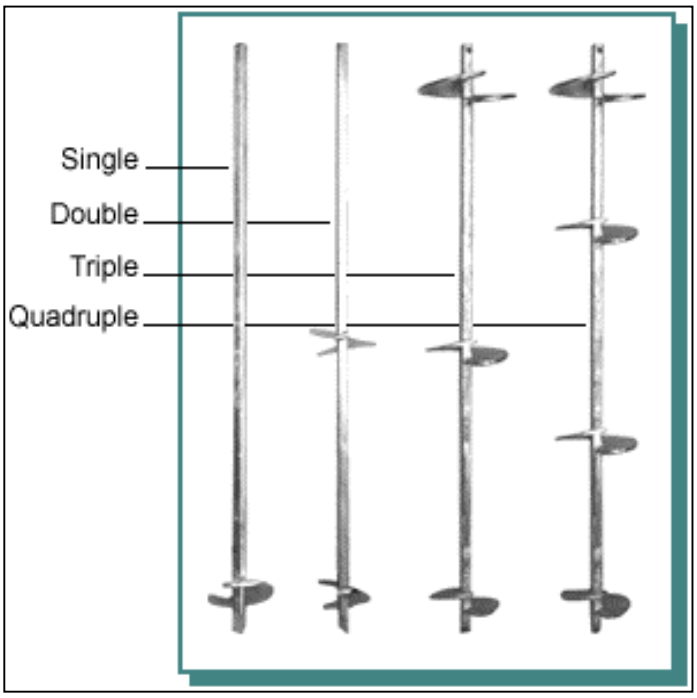

Figure 1.1 Helical Piers (A. B. Chance Co. 1996)

Figure 1.2 Installation of Helical Pier with Excavator and Rotation Head

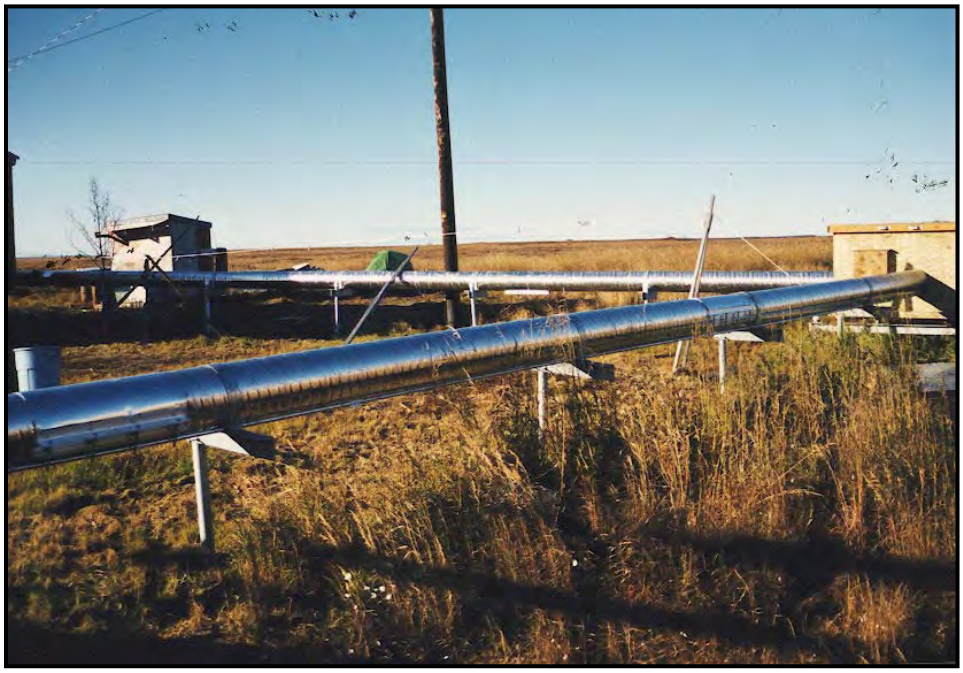

Figure 1.3 Utilidor Supported by Helical Piers in Selawik, Alaska

Figure 1.4 Insignificant Ground Disturbance

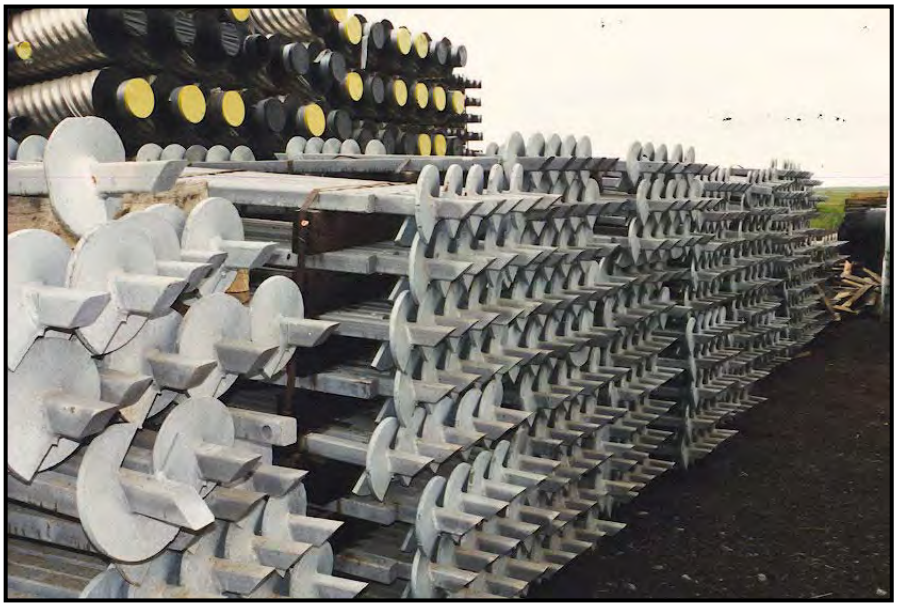

Figure 1.5 Helical Pier Stockpile in St. Michael, Alaska

1.4 References for Introduction

A.B. Chance Co.,1996, Helical Pier Foundation System Technical Manual, Bulletin 01-96

2. LITERATURE REVIEW

2.1 Introduction

Publications regarding the application of helical anchors and piers in both warm and frozen ground will be covered in the following sections. Much more research has been done on friction piles in permafrost. This work will be considered also since pile-design principles may have some application to helical pier design.

2.2 Applications of Helical Anchors and Piers in Warm Soils

2.2.1 Analysis of Helical Foundations in Warm Soils

Helical foundations are always considered deep foundations for design purposes. According to the A. B. Chance Co. (1996), a manufacturer of helical piers, for a single helix foundation there is good agreement that the failure mode is in bearing. That is, the ultimate bearing capacity of the soil is applied to the area of the helix to determine the theoretical ultimate capacity.

Multi-helix foundations are more complex. Two theories have been applied. One theory suggests that failure occurs when the applied load equals the sum of the bearing capacity of the bottom helix and the friction resistance of a cylinder of soil with a diameter equal to the average diameter of the remaining helixes and a length equal to the distance between the top and bottom helixes. The Chance Co. recommends using the other theory that suggests the capacity of the foundation is equal to the sum of the capacities of the individual helixes. The unit bearing capacity of the soil is applied to the area of each helix. A critical spacing of at least 3 times the helix diameter between each helix is sufficient to prevent one helix from affecting the performance of another.

For calculating the bearing capacity of a helical foundation the Chance Co. uses a modified bearing capacity equation for point bearing capacity as shown in Equation 2.1.

$$Q_h = A_h\left(9c + qN_q\right) \le Q_s \qquad \text{Equation 2.1}$$

Where: Q_h = Individual helix bearing capacity
A_h = projected helix area
c = soil cohesion
q = effective overburden pressure
N_q = bearing capacity factor
Q_s = upper limit determined by helix strength

The bearing capacity factor for cohesionless soils, N_q, is dependent upon the angle of internal friction, ϕ, and is taken from a chart based upon Meyerhoff's bearing capacity factors for deep foundations. The Chance Co. has empirically modified Meyerhoff's factor to reflect the performance of helical foundations (Figure 2.1).

The Chance Co.'s design theory does not consider creep in frozen soil, and therefore its validity for piers in frozen soil has not been determined.

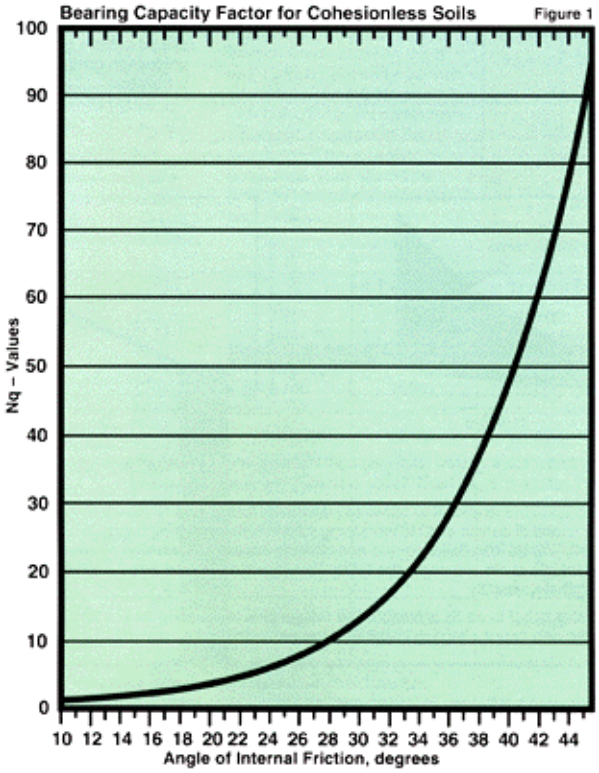

Figure 2.1. Bearing Capacity Factor, N_q, for Cohesionless Soils (A. B. Chance Co. 1996)

Some of the mechanical properties of deep foundations in warm soils may have application to helical piers in permafrost. For the installation of piles in warm soils, Randolph and Wroth (1978) proposed separate deformation patterns for the upper and lower soil levels. The upper layer of soil will be deformed exclusively by the load transferred from the pile shaft and the lower layer will be deformed exclusively by the pile base load. This model requires a slenderness ratio, l/r_0, greater than 20. Deformation around the soil shaft can be described by the shearing of concentric cylinders (Cooke, 1973). Randolph and Wroth's approach is only approximate, but compared favorably with numerical solutions.

2.2.2 Helical Anchors and Piers in Sand

Pullout resistance of single-screw helical anchors in dry sand is most dependent upon sand characteristics, anchor diameter, and installation depth (Adams and Hayes, 1967). In dry sand, failure of deep helical anchors is characterized by a failure plane formed completely inside the sand with no movement evident on the surface. The shear strength along the failure surface provides the greatest resistance to pullout load. The overburden of the failing soil mass is a small fraction of the resistant force. Ghaly et al.

(1991-I) determined an equation to calculate the ultimate pullout capacity (Q_u) of anchors in dry sand based upon a defined inverted failure cone (Figure 2.2 and Equation 2.2). Ghaly et al. also tested various screw shapes without significantly affecting the uplift capacity.

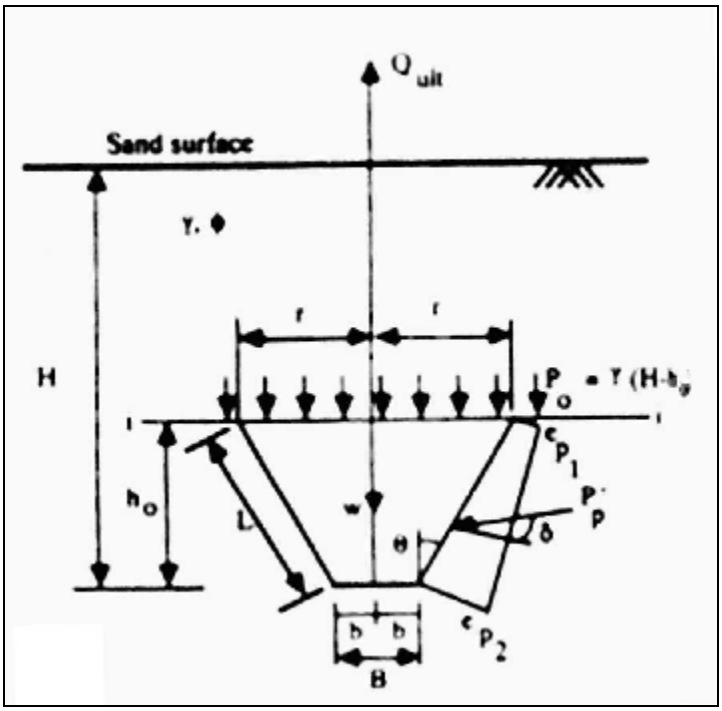

Figure 2.2. Forces Acting on Assumed Failure Surface (Ghaly et al., 1991-I)

$$Q_u = P_p + W + N \qquad \text{Equation 2.2}$$

Where: P_p = vertical component of total passive earth pressure; dependent upon the surface inclination angle of inverted failure cone, θ,
W = weight of sand wedge within failure surface,
N = downward force due to vertical earth pressure.

In a companion paper, Ghaly et al. (1991-II) evaluated the performance of helical anchors under hydrostatic and flow conditions. For deep anchors, the pullout load is almost the same as for dry sand, i.e., sand submersion has little effect on screw anchors installed to deep depths. As with dry sand the sand shearing resistance is the main component acting against uplift. Robertson and Carle (1995) successfully installed screw anchors in muskeg swamps to control pipeline buoyancy. Muskeg is organic material with low shear strength and low density.

Installations of multiple anchors in dense sand require a critical horizontal spacing (Shaheen and Demars, 1995). The spacing ratio should be at least 5 times the average

helix diameter. Varying the anchor depths within a group does not substantially increase pullout capacity for the group.

For inclined helical screw anchors in sand, Ghaly and Clemence (1998) found that pullout capacity depends on the installation depth, sand characteristics, and inclination angle. The failure surface is complex. The boundaries of the failure surfaces are segments of logarithmic spiral curves. The authors determined a method of calculating the ultimate pullout capacity of inclined anchors as a function of the pullout capacity of vertical anchors (Equation 2.3).

$$Q_{ui} = K\left(\frac{Q_{uv}}{\cos\frac{2\alpha}{3}}\right) \qquad \text{Equation 2.3}$$

Where: Q_{ui} = ultimate pullout load of inclined anchor,
Q_{uv} = ultimate pullout load of vertical anchor installed to depth H,
α = angle of inclination of anchor,
K = coefficient of embedment depth = 1.015-0.002(H/Bcos(α/2),
H = installation depth,
B = anchor diameter.

2.2.3 Helical Anchors and Piers in Clay

Mooney et al. (1985) determined the uplift capacity of a helical anchor in cohesive soils to be dependent upon the spacing of the helixes on the anchor shaft. As the helical plate spacing is reduced anchor capacities are increased. For spacing ratios greater than 1.5 times the diameter the failure surfaces are not cylindrical. Mooney et al. give Equation 2.4 for the capacity of a helical anchor in clay.

$$P = \pi DLC_u \qquad \text{Equation 2.4}$$

Where: P = net ultimate uplift capacity
D = diameter of helical plate
L = distance between top and bottom helical plates
C_u = measured shear strength of clay

In cohesive soils, Narasimha Rao and Prasad (1993) determined a method to predict capacities in cases where the helixes are spaced too far apart to produce a cylindrical failure surface. They proposed multiplying the uplift capacity with a nondimensional spacing factor, S_F. Where S_F is the ratio of experimental uplift capacity to measured uplift capacity. For anchors with varying size helical plates a satisfactory spacing ratio can be calculated using average diameters.

For lateral loads on helical piers in cohesive soils, Prasad and Narasimha Rao (1996) found that capacity increases with embedment depth and soil shear strength.

Capacities of helical piles are greater than for single pile shafts and capacity increases with the number of helical plates.

Narasimha Rao and Prasad (1991) also studied the effects of repetitive vertical loads on helical anchors in soft marine clay. The anchors are subject to static pull and repetitive tensile loading caused by the rocking and bobbing motion of buoyant superstructures subjected to wind and wave action. Anchor displacement is affected by loading period. As the period increases, upward movement increases at the same number of cycles. This may be attributed to creep of the marine clay.

2.3 Analysis of Deep Foundations in Frozen Soils

2.3.1 Creep in Frozen Soils

Failure of a foundation in frozen soils includes rupture and excessive deformation. The mode of failure depends upon soil type, temperature, strain rate, and confining pressure. It can range from failure in a brittle manner similar to weak rock through brittle-plastic with the formation of a single or several failure planes to a completely plastic failure without visible strain discontinuities. Plastic failure, i.e. excessive creep deformation, is typical for warm permafrost (Andersland and Ladanyi, 1994).

The strength and stability of deep foundations in permafrost is most dependent upon the creep strength of the soil. The creep strength is the compressive stress level at which rupture or tertiary creep occurs in the soil. Ladanyi (1972) adapted an engineering theory to express the time, temperature, and stress dependent deformation of frozen soils using creep theories for metals. The main purpose for Ladanyi's theory is to be used as a basis for solving bearing capacity problems with data taken from a set of constant-stress creep tests. Equation 2.5 is a power law approximation for pseudo-instantaneous creep ($\varepsilon^{(i)}$) and Equation 2.6 is a power law approximation for secondary creep rate ($\dot{\varepsilon}^{(c)}$).

$$\varepsilon^{(i)} = \varepsilon_k \left(\frac{\sigma}{\sigma_{k\theta}} \right)^k \qquad \text{Equation 2.5}$$

$$\dot{\varepsilon}^{(c)} = \dot{\varepsilon} \left(\frac{\sigma}{\sigma_{c\theta}} \right)^n \qquad \text{Equation 2.6}$$

Where: $\sigma_{k\theta}$ = temperature-dependent total deformation modulus, corresponding to the reference strain, ε_κ,
$\sigma_{c\theta}$ = temperature-dependent creep modulus, corresponding to the reference strain rate,
k = empirical exponent, less than or equal to 1,
n = experimental creep exponent, greater than or equal to one.

According to Ladanyi and Johnson (1974), it is not appropriate to analyze deep circular foundations in frozen soils on the basis of a Prandtl-type bearing capacity equation and separate settlement analysis using Boussinesq's stress-distribution theory and compressibility of soil. In frozen soil, the temperature and undrained creep become predominant in the determination of allowable foundation pressures. Therefore, Ladanyi and Johnson developed a method for predicting the time and temperature dependent creep settlement and the bearing capacity of frozen soil under deep circular loads. The adaptation of the cavity expansion model uses experimentally determined frozen soil parameters and is intended to be applicable to the design of deep circular footings as well as circular plate and screw anchors embedded deeply in frozen soil.

The cavity expansion model more accurately describes observations in field and laboratory tests of deep foundations in frozen soils. The failure surfaces in the tests were not similar to Prandtl-type failure surfaces. Nor was upward movement of the soil observed. They found that a cone of dense soil develops below the foundation without any observed failure surfaces. The indentation due to loading creates a plastic nucleus which, even after unloading, keeps the surrounding elastic mass in equilibrium and prevents the hole from closing.

The solution is only valid when the footing behavior is essentially unaffected by the free surface, since it is based on a theory of cavity expansion in an infinite medium. The limiting depth is about 4 times the footing diameter for clays, and about 7-9 times the diameter for sands.

Ladanyi and Johnson's description of the relationship of cavity expansion to stress and the temperature-dependent creep modulus is given in Equation 2.7. It determines the radial displacement rate of the cavity wall. Figure 2.3 diagrams the notation used in the model.

$$\frac{\dot{u}_i}{r_i} = \frac{\dot{\varepsilon}_c}{2}\left[\frac{p_i - p_o}{2n\sigma_{cu\theta}/3}\right]^n \qquad \text{Equation 2.7}$$

Where: $\dot{u}_i$ = radial displacement rate,
r_i = radius of the cavity,
$\dot{\varepsilon}_c$ = creep rate,
p_i = cavity expansion pressure,
p_o = average total original ground stress at the footing level,
n = exponent in creep equation,
$\sigma_{cu\,\theta}$ = creep modulus in uniaxial compression at freezing temperature θ,
θ = number of degrees Celsius below 0°C.

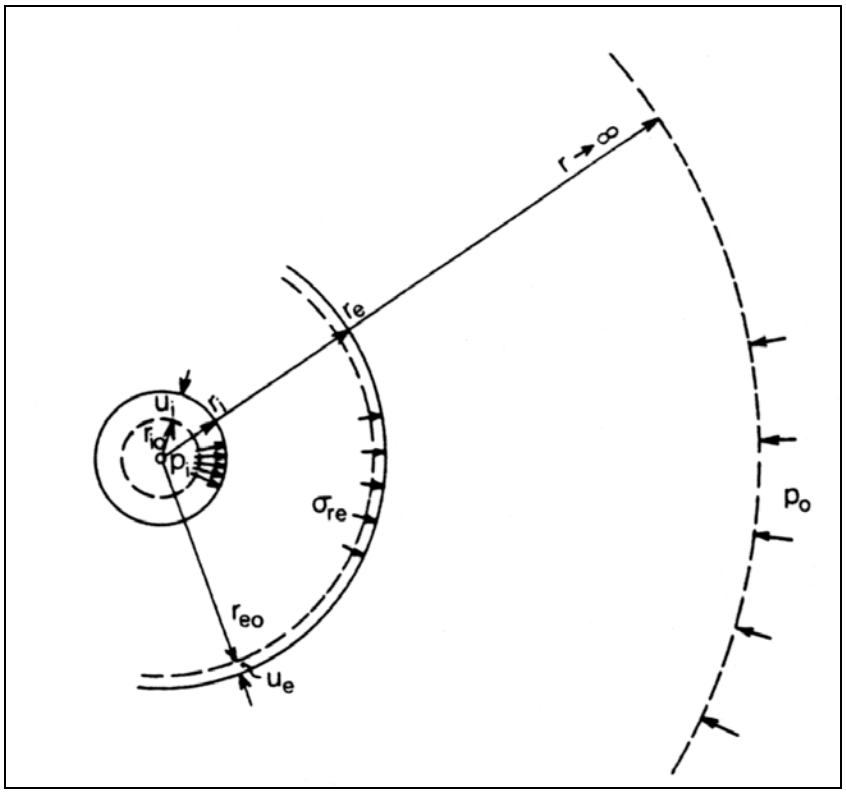

Figure 2.3 Notation in Cavity Expansion (Ladanyi and Johnston, 1974)

2.3.2 Helical Anchors in Frozen Ground

In 1974, Johnston and Ladanyi published the only known study of helical anchors in permafrost to compare actual data from screw anchors installed in northern Manitoba with the model of cavity expansion. They found that pullout loads for screw anchors are similar to what would be expected from deep footings of similar size. The anchors showed nonlinear load displacement and load-displacement rate relationships. Anchors attained their ultimate bearing capacities in a hyperbolic manner. Large displacements were required before the anchors attained ultimate bearing capacity. Prandtl failure planes are not evident under pullout loads.

The creep equation parameters, n and k, for the test site were determined in-situ and applied to the cavity expansion model. Creep rates and capacities were reasonably predicted.

According to Johnston's and Ladanyi's study in a single soil, single-helix anchors had relatively low pullout capacity when compared with grouted rod anchors. They could not predict if multiple-helix anchors would provide a significant increase in capacity although larger diameter helixes could increase pullout capacity. The authors stated that screw anchors are installed more easily with less soil disturbance than grouted rod anchors.

No literature exists currently on analysis on helical piers under compression in frozen ground. This warrants a need for this research project.

2.3.3 Adfreeze Piles in Frozen Ground

For piles in frozen ground, failure is defined as rupture of the adfreeze bond and excessive settlement at the pile tip. Long-term deformation behavior may be characterized by secondary creep in ice-rich soils and by primary creep in ice-poor soils. The required depth of embedment of a pile is dependent upon the adfreeze bond strength and temperature (Crory, 1975).

Nixon and McRoberts (1976) compared 2 models of end bearing creep: (1) a circular footing on a viscous half-space, and (2) an expanding spherical cavity in an infinite viscous medium, similar to Johnson and Ladanyi's (1974). The first model was only applicable to surface loads, but they found the expanding cavity model can simulate creep behavior at depth. Equation 2.8 was developed to determine the displacement rate of a pile based upon the cavity expansion model. Nixon and McRoberts found reasonable agreement between their model and the case history of a pile foundation in Fairbanks, Alaska. Increasing pile diameter appears to lower allowable stress for equal creep rates, i.e. under equal adfreeze stress, a large diameter pile will settle faster than a smaller pile.

$$\dot{u}_a = \frac{3^{(n_1+1)/2} B_1 \tau_a{}^{n_1} a}{n_1 - 1} + \frac{3^{(n_2+1)/2} B_2 \tau_a{}^{n_2} a}{n - 1} \qquad \text{Equation 2.8}$$

Where: $\dot{u}_a$ = pile displacement rate,
B, n = constants determined from uniaxial creep data for the frozen soil (Table 2.1),
τ_a = applied shaft shear stress
a = pile radius

Table 2.1 Creep Constants (Morgenstern 1980)

Temperature °C	B ($kPa^{-n}year^{-1}$)	n
-1	4.5×10^{-8}	3.0
-2	2.0×10^{-8}	3.0
-5	1.0×10^{-8}	3.0
-10	5.6×10^{-9}	3.0

Ladanyi and Paquin (1978) compared the results of a series of laboratory deep circular footing tests with the cavity expansion model developed in 1974 by Johnston and Ladanyi. Results of triaxial tests on frozen sand were the basis of the comparison. When frozen sand is loaded by a deep circular load, the rate of penetration is affected by the load and loading history, but becomes practically independent of history once the

penetration resistance has been mobilized. The theory based upon cavity expansion satisfactorily predicts penetration rates.

Parameswaran (1979) performed laboratory creep tests on model piles in frozen sand. The rate of displacement of piles under constant load has a power law creep-rate dependence upon the shear stress at the pile-soil interface. Parameswaran's results compared favorably with Johnston and Ladanyi's (1974) pullout tests on grouted rod anchors. These pile tests are a measure of the creep along the adfreeze. Lowering the test temperatures from –6 ° to –10 °C decreased the steady-state creep by almost an order of magnitude.

Morgenstern, et al., (1980) proposed a flow law for piles in ice or ice-rich soils at temperatures colder than –1°C as shown in Equation 2.9. They were able to adequately predict pile velocities with results of long-term creep tests using Equation 2.10. The creep constants for these equations are defined in Table 2.1. Using this method, substantially higher loads are permitted than recommended by Nixon and McRoberts (1976).

$$\dot{\varepsilon}_e = B\sigma_e^{\,3} \qquad \text{Equation 2.9}$$

Where: $\dot{\varepsilon}_e$ = strain rate,
B = creep parameter dependent upon temperature, defined in Table 2.1
σ_e = effective shear stress.

$$\frac{\dot{u}_a}{a} = \frac{3^{(n+1)/2} B \tau_a^{\,n}}{n-1}, \qquad \text{Equation 2.10}$$

Where: $\dot{u}_a$ = pile velocity,
τ_a = average applied adfreeze load,
a = pile radius,
n = stress exponent, defined in Table 2.1, ground temperature is assumed constant.

After reviewing long-term creep tests on frozen soils and proposed creep laws, Weaver and Morgenstern (1981) concluded that end-bearing support is negligible for piles in all types of homogeneous permafrost. The fraction of load supported in end-bearing by a pile in ice is, typically, less than 1%. For piles in ice-poor soils it is less than 2%. However, end-bearing support may be realized if the stiffness of the permafrost increases significantly with depth. Pile design in ice-rich soils should be governed by settlement and pile design in ice-poor soils should satisfy both settlement and strength criteria. Weaver and Morgenstern did not consider helical piers that function in a different way than traditional piles and transfer the load from the superstructure to the soil at helix by "end bearing."

Piles can be installed in frozen ground by dry auguring an oversized hole and backfilling the annulus with a slurry. A lengthy freezeback time is required to produce the necessary adfreeze bond. Open-ended pipe and H-piles can be driven in frozen ground under the right conditions and require very little freezeback time (Crory, 1982).

Nottingham and Christopherson (1983) reviewed data and experience from 5,000 piles driven into warm and cold permafrost. They concluded that piles can be placed much more accurately and with much less soil disturbance by driving than by the drill and slurry method. Piles cannot be driven efficiently at temperatures colder than –0.5 to –1.0 °C without pilot holes. In colder permafrost pilot hole needs to be thermally modified. This usually entails modifying permafrost temperature of a small pilot hole with non-circulated hot water. Freezeback times are typically less than 2 days.

Manikian (1983) conducted extensive testing and research and selected the thermally modified pile driving method as the fastest and most economical method of pile installation. As a result, all the piles installed for the aboveground oil pipeline in the Kuparuk Field were installed by this method. Recommended water temperature is 66°C with a thaw time of 30 minutes for granular soils and 60 minutes for fine-grained soils. For the determination of adfreeze strengths, soil type is more important than installation method. Different methods produced comparable adfreeze strengths. However, piles driven in frozen gravelly soils indicate lower adfreeze values than ice-rich silty sands. The author suggested this is because gravelly soils are located near rivers and subject to warmer ground temperatures. Manikian concluded the significant factors affecting pile performance are soil temperature, pile diameter, and creep. For design purposes, two conditions should be considered, short-term loading and long-term creep.

Linell and Lobacz (1980) published experimentally determined values for average sustained and average peak adfreeze bond strengths for steel pipe piles in frozen silt slurries. The bond strengths are dependent on permafrost temperature around the pile at the warmest time of the year and apply for soil temperatures down to -4°C (25°F). The authors provide correction factors for type of piles and for sand slurries.

Foundation design based on adfreeze strength between the pile and the frozen slurry or soil is not applicable for design of helical piers, since the capacity of the helical pier comes from the helix and not from the pile shaft.

2.3.4 Laterally Loaded Piles in Frozen Ground

For laterally loaded vertical piles in permafrost Neukirchner and Nixon (1987) found that the behavior of the pile changes from that of a flexible (long) pile to a rigid (short) pile as it attains its long-term equilibrium condition. The change in pile behavior is caused by creep of the surrounding soil. In long-term performance, laterally loaded piles that exhibit secondary creep rotate about a definable point at a uniform rate. Nixon (1984) established a model to define the point of pile rotation and for calculating the pile creep rate.

Vertical helical piers are not intended to support large lateral loads. Therefore, if lateral forces need to be considered, piers are often placed on a batter (installed at an angle).

2.4 Conclusions for Literature Review

The design and performance of helical anchors and piers in warm soils is analyzed using simple formulas that predict the field behavior adequately. However, the behavior of warm sands and clays differs greatly from the behavior of frozen ground. The extent to which design principles for helical piers in warm soil applications are applicable to frozen ground is not currently understood.

The behavior of piles in frozen ground is routinely estimated using adfreeze strength along the pile length. If the strength is mobilized along the entire pile length needs to be further studied. Successful installation of adfreeze piles in permafrost has become a routine procedure. The design principles and mechanics for adfreeze piles can not be directly applied to helical piers. Prediction of the pile capacity for piles and helical piers may utilize similar models but more research needs to be done.

2.5 References for Literature Review

A. B. Chance Co., 1996, *Helical Pier Foundation System Technical Manual*, Bulletin 01-9601.

Adams, J.I. and Hayes, D.C., 1967, "The Uplift Capacity of Shallow Foundations," *Ontario Hydro Res. Quarterly*, Vol. 19, No. 1, pp. 1-13.

Andersland, O. B. and Ladanyi, B., 1994, *An Introduction to Frozen Ground Engineering*, Chapman and Hall, New York.

Cooke, R.W. and Price, G., 1973,"Strains and Displacements around Friction Piles," *Proceedings*, Eighth International Conference on Soil Mechanics and Foundation Engineering, Moscow, U.S.S.R.

Crory, F.E., 1975, "Bridge Foundations in Permafrost Areas, Moose and Spinach Creeks, Fairbanks, Alaska," *CRREL Technical Report 266*, p.36.

Crory, F.E., 1982, "Piling in Frozen Ground" *Journal of the Technical Council on Cold Regions Engineering*, ASCE, Vol. 108, No. 1, pp. 112-124.

Ghaly, A. and Clemence, S., July 1998, "Pullout Performance of Inclined Helical Screw Anchors in Sand," *Journal of Geotechnical and Geoenvironmental Engineering*, ASCE, Vol. 124, No. 7, pp. 617-627.

Ghaly, A., Hanna, A., and Hanna, M., May 1991, "Uplift Behavior of Screw Anchors in Sand. I: Dry Sand," *Journal of Geotechnical Engineering*, ASCE, Vol. 117, No. 5, pp. 773-793.

Ghaly, A., Hanna, A., and Hanna, M., May 1991, "Behavior of Screw Anchors in Sand. II: Hydrostatic and Flow Conditions," *Journal of Geotechnical Engineering*, ASCE, Vol. 117, No. 5, pp. 794-807.

Johnston, G. H. and Ladanyi, B., August 1974, "Field Tests of Deep Power-Installed Screw Anchors in Permafrost," *Canadian Geotechnical Journal*, Vol. 11, No. 3, pp. 348-358.

Ladanyi, B., 1972, "An Engineering Theory of Creep of Frozen Soils," *Canadian Geotechnical Journal*, Vol. 9, No. 1, pp. 63-80.

Ladanyi, B. and Johnston, G.H., 1974, "Behavior of Circular Footings and Plate Anchors Embedded in Permafrost," *Canadian Geotechnical Journal*, Vol. 11, pp. 531-553.

Ladanyi, B., and Paquin, J., 1978, "Creep Behaviour of Frozen Sand under a Deep Circular Load," *Proceedings*, Third International Conference on Permafrost, Edmonton, Vol. 1, pp. 679-686.

Linell, K. A., and Lobacz, E. F., 1980, "Design and Construction of Foundations in Areas of Deep Seasonal Frost and Permafrost," US Army, Corps of Engineers, Cold Regions Research and Engineering Laboratory, Special Report 80-34, pp.211-212.

Manikian, V., 1983, "Pile Driving and Load Tests in Permafrost for the Kuparuk Pipeline System," *Proceedings*, Fourth International Conference on Permafrost, Fairbanks, Alaska, Vol. 1, pp. 804-810.

Mooney, J.M., Adamczak, S., and Clemence, S.P., 1985, "Uplift Capacity of Helical Anchor in Clay and Silt; Uplift Behaviour of Anchor Foundations in Soil," *Proceedings*, ASCE, pp. 48-72.

Morgenstern, N.R., Roggensack, W.D. and Weaver, J.S., 1980, "The Behaviour of Friction Piles in Ice and Ice-Rich Soils." *Canadian Geotechnical Journal*, Vol 17, No. 3, pp. 405-415.

Narasimha Rao, S. and Prasad, Y.V. N., Jul.-Dec. 1991, "Behavior of a Helical Anchor under Vertical Repetitive Loading," *Marine Geotechnology*, ASCE, Vol. 10, pp. 203-228.

Narasimha Rao, S. and Prasad, Y.V. N., February 1993," Estimation of Uplift Capacity of Helical Anchors in Clays," *Journal of Geotechnical Engineering*, ASCE, Vol. 119, No. 2, pp. 352-357.

Neukirchner, R.J. and Nixon, J. F., 1987, "Behavior of Laterally Loaded Piles in Permafrost," *Journal of Geotechnical Engineering Div.*, ASCE, Vol 113, No. 1, pp. 1-14.

Nixon, J.F. and McRoberts, E.C., 1976, "A Design Approach for Pile Foundations in Permafrost," *Canadian Geotechnical Journal*, Vol. 13, pp. 40-57.

Nixon, J.F., 1984, "Laterally Loaded Piles in Permafrost," *Canadian Geotechnical Journal*, Vol. 21, pp. 431-438.

Nottingham, D. and Christopherson, A.B., 1983, "Driven Piles in Permafrost: State of the Art," *Proceedings,* Fourth International Conference on Permafrost*,* Fairbanks, Alaska, pp. 928-933.

Parameswaran, V.R., 1979, "Creep of Model Piles in Frozen Soil," *Canadian Geotechnical Journal*, Vol.16, pp. 69-77.

Prasad, Y.V. N. and Narasimha Rao, S., November 1996, " Lateral Capacity of Helical Piles in Clays," *Journal of Geotechnical Engineering*, ASCE, Vol. 122, No. 11, pp. 938-941.

Randolph, M.F. and Wroth, P.C., 1978, "Analysis of Deformations of Vertically Loaded Piles," *Journal of the Geotechnical Engineering*, ASCE, Vol. 104, pp. 1465-1488.

Robertson, R. and Carle, R., 1995, "Screw Anchors Economically Control Pipeline Buoyancy in Muskeg," *Oil & Gas Journal*, pp. 49-54, April 24.

Shaheen, W.A. and Demars, K.R., October – December 1995, "Interaction of Multiple Helical Earth Anchors Embedded in Granular Soil," *Marine Georesources and Geotechnology*, Vol. 13, No. 4, pp. 357-374.

Weaver, J.S. and Morgenstern, N.R., 1981, "Pile Design in Permafrost," *Canadian Geotechnical Journal*, Natural Resource Council Canada, Vol. 18, No. 3, pp. 357-370.

3. CRREL EXPERIMENT

3.1 Introduction

The purpose of this project was to monitor creep in permafrost under helical piers in controlled environment. The outcome of the study was to be used 1) to calibrate the FEA models using field results and soil tests, and 2) to gain more information on the installation and behavior of helical piers in frozen ground.

To conduct the test, a test cell was constructed at the US Army Engineer Research & Development Center, Cold Regions Research & Engineering Laboratory (CRREL) in Hanover, New Hampshire. The test cell was instrumented to collect data on environmental conditions and the effects of pier loading. The following sections present the test cell construction and instrumentation, test procedure, and the test results.

3.2 Materials

3.2.1 Helical Piers

Helical piers with double and single helix were used in this investigation (Figure 3.1.) The piers are composed of solid square steel 44 mm (1.75 in) in width and approximately 1.6 m (66 in) in length. The diameter of the single helix is 203 mm (8 in). On the double helix pier, the upper helix is 254 mm (10 in) and the lower helix is 203 mm (8 in) in diameter. The distance between the upper and lower helixes is 609 mm (24 in). Plain extensions were attached to the pier during the installation. Similar to the pier, the extension is also a solid steel square bar, just under 1 m (38 in) in length that attaches to the pier with a threaded adapter. Mr. Tom Metlicka from Alaska Foundation Technology, Inc., Eagle River, Alaska, was in charge of the pier installation.

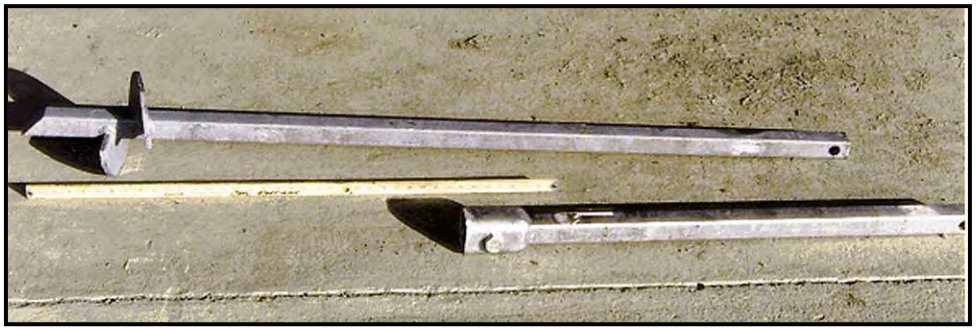

a. Single Helix Pier with Extension

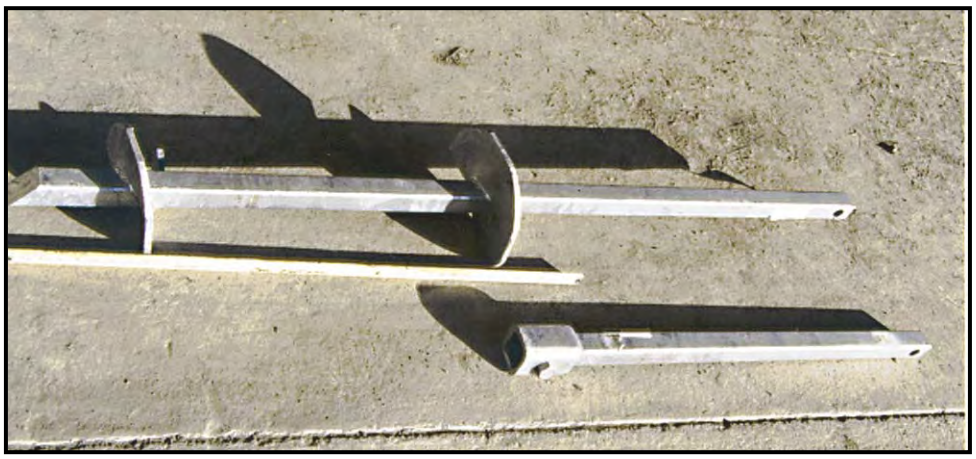

b. Double Helix Pier with Extension

Figure 3.1 Helical Piers and Extensions Installed in Test Cell

3.2.2 Test Soil

The soil used in the test cell was classified as an AASHTO A-4, USCS CL. Based on the Corps of Engineers criteria, this material is classified in the highest frost-susceptibility category (U.S. Army Corps of Engineers, 1997). The AASHTO test methods used for soil testing are given in Table 3.1. The soil properties are given in Table 3.2 and Figures 3.2 to 3.4.

Table 3.1 AASHTO Test Methods Used for Soil Testing

Code	Test
T 88-90	**Particle Size Analysis of Soils**
T 99-90	Standard Method of Test for the Moisture-Density Relations of Soils Using a 5.5 lb. (2.5 kg) Rammer and a 12 in. (305 mm) Drop
M 145-87	Recommended Practice for the Classification of Soils and Soil-Aggregate Mixtures for Highway Construction Purposes
T 89-90	Standard Method of Test for Determining the Liquid Limit of Soils
T 90-87	Standard Method Determining the Plastic Limit and Plasticity Index of Soils
T 100-90	Standard Method of Tests for Specific Gravity of Soils
T 265-86	Standard Method of Test for Laboratory Determination of Moisture Content of Soils
T 193-81	**Standard Method of Test for the California Bearing Ratio**

Table 3.2 Soil Properties

Atterberg Limits	**w (%)**
Liquid Limit	28
Plasticity Index	8
Specific Gravity	2.73

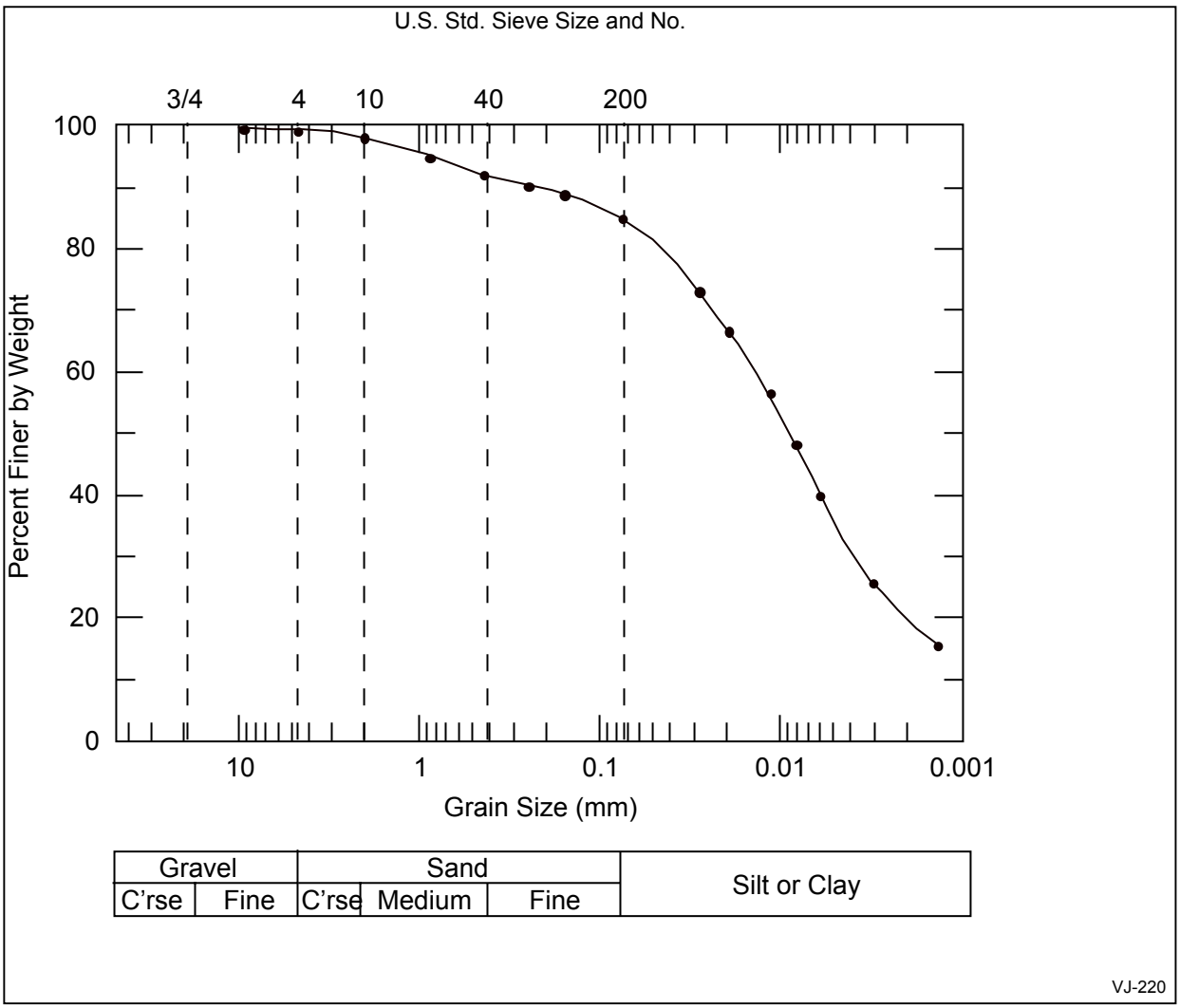

Figure 3.2 Sieve Analysis Results

After each layer of soil was placed in the cell, compaction of the soil was accomplished with a vibratory plate compactor. Density and water content tests were conducted using a Troxler nuclear gauge. Table 3.3 gives the average dry densities and water contents for each layer. During construction of the test section, the Troxler malfunctioned and readings for soil layers 4-6 were not recorded.

3.3 Test Procedure

3.3.1 Scope of Work

To simulate a permafrost condition, the soil in the test cell was frozen prior to installation of the piers. To obtain a frozen block of soil, freezing panels were placed on all sides of the test cell and the temperature was dropped to -4°C (25°F). Three helical piers were installed into the frozen soil. The testing was conducted under two soil temperature conditions: at -4°C (25°F) and at -1°C (30°F).

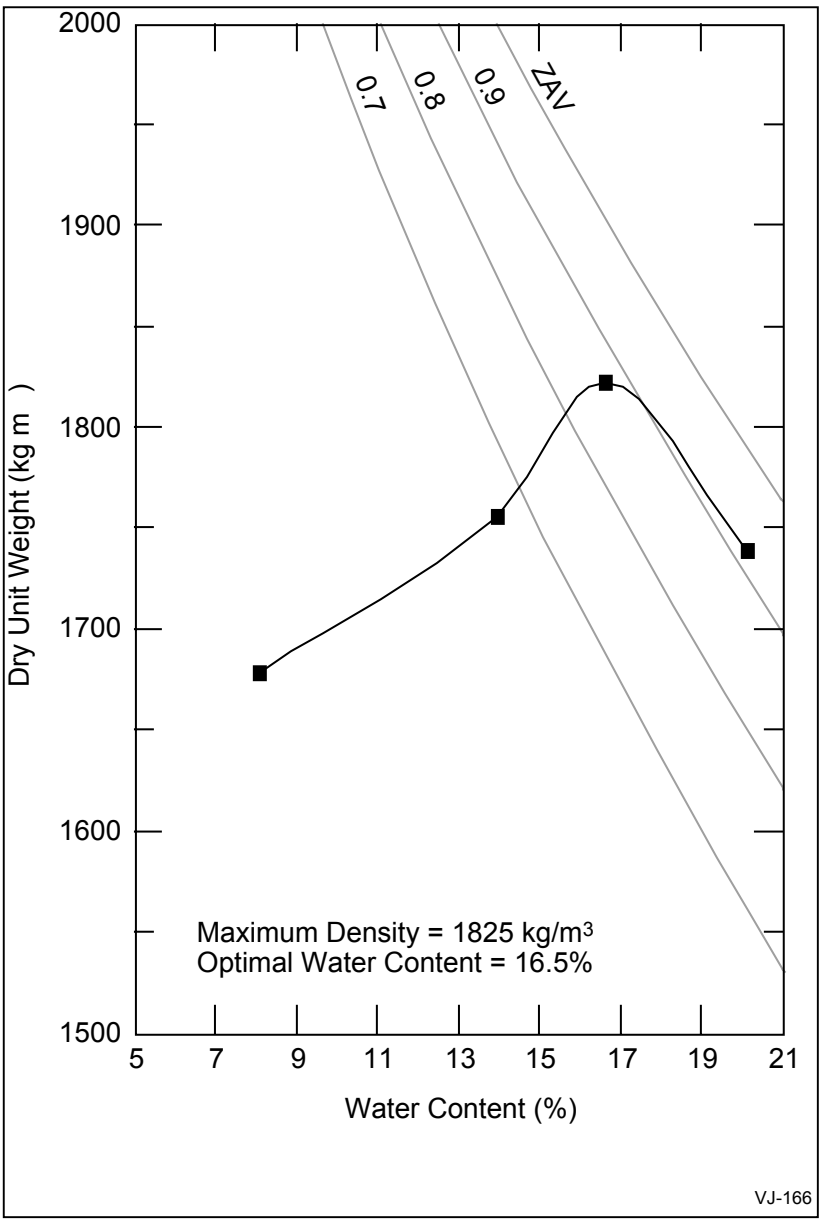

Figure 3.3 Standard Proctor Test Results

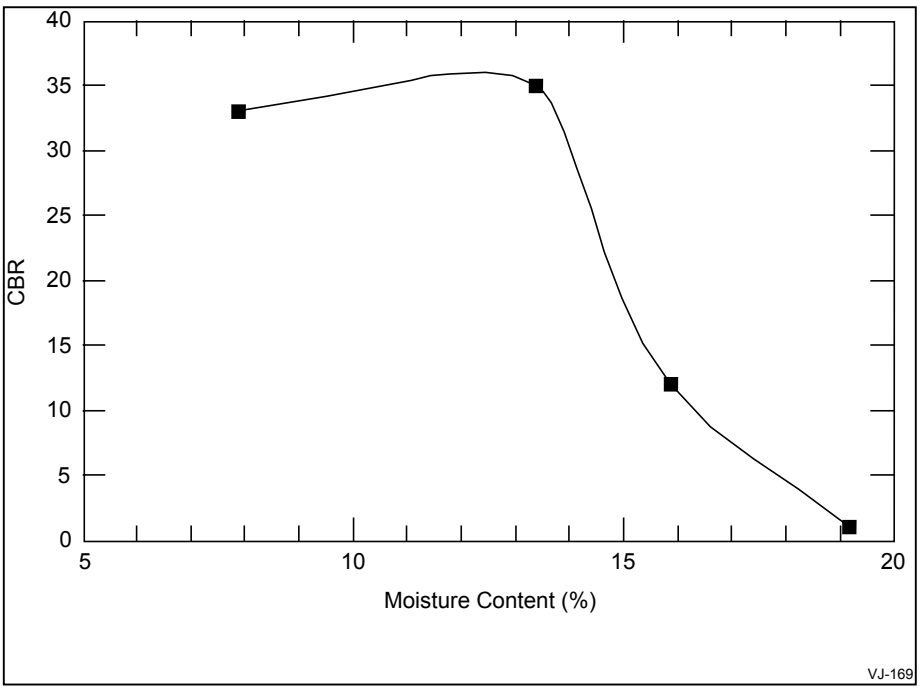

Figure 3.4 Results for California Bearing Ratio

Table 3.3 Average Troxler Readings for Each Soil Layer

Soil Layer	Water Content %	Dry Density (kg/m^3)	Dry Density (pcf)
1	15.6	1551.9	96.88
2	16.0	1537.1	95.96
3	14.4	1562.4	97.54
4	------	------	------
5	------	------	------
6	------	------	------
7	15.0	1501.1	93.71
8	13.1	1495.5	93.36
9	13	1566.9	97.82
10	13.9	1513.9	94.51
11	13.9	1494.5	93.30
12	13.6	1586.9	99.07
13	14.0	1500.8	93.69

To accomplish loading of the piers, a steel plate was placed on top of the piers and then loaded with concrete blocks weighing approximately 19.6 kN (4,400 lbs) each and measuring 0.76 m^3 (1 yd^3) in size. The load increments were added in the following pattern: 1) a single block in the center of the steel plate, 2) stacked double blocks in the center, 3) three single blocks – one centered over each pier, 4) three double stacked blocks – one stack centered over each pier. This loading sequence was used for both testing temperatures. Once the blocks were set into position, the configuration was monitored for any settlement. If no movement was seen after a designated time period, the loading was increased. Temperature and unfrozen water content were recorded regularly to monitor the state of freezing and thawing in the test cell.

3.3.2 Frost Effects Research Facility

The test cell was constructed in the CRREL's Frost Effects Research Facility (FERF). The FERF is a working laboratory where full-scale test sections can be constructed and tested under varying environmental conditions. The overall facility is 56 meters (183 ft) long by 31 meters (102 ft) wide. Within the 2,700 m^2 (29,000 ft^2) facility are twelve testing basins that may be used to conduct individual tests or combined to accommodate larger projects (Figure 3.5). The facility is capable of controlling the environmental effects on the test area. The ambient air temperature may be controlled from –7°C to +24°C (20 to 75°F). Attaining more extreme temperatures for subsurface freezing or thawing requires the use of surface panels, which permit temperatures as low as -38°C (-36 °F) or as high as +38°C (100 °F). Freezing and thawing rates of approximately 25 mm (1 inch) per day are typical by using the panels.

The test cell TC-8 was used in this investigation. It was modified to be 8 m (27 ft) long, 7 m (23 ft) wide and 3 m (9 ft) deep. A water table was installed to facilitate formation of ice lenses as moisture is drawn up to the freezing front during the freezing process. The test section was then to be frozen at a rate of approximately 25 mm (1 inch) per day to the full depth.

A ramp, located directly to the south of TC-8, was filled with gravel and used by heavy equipment to access the test section for anchor installation, core sampling, and as a staging area to place the concrete loading blocks when not in use. Figure 3.6 provides a plan view of the completed test section indicating the locations of instrumentation and the piers. Figure 3.7 shows a profile view of the test cell with the locations of the instrumentation and the installed piers.

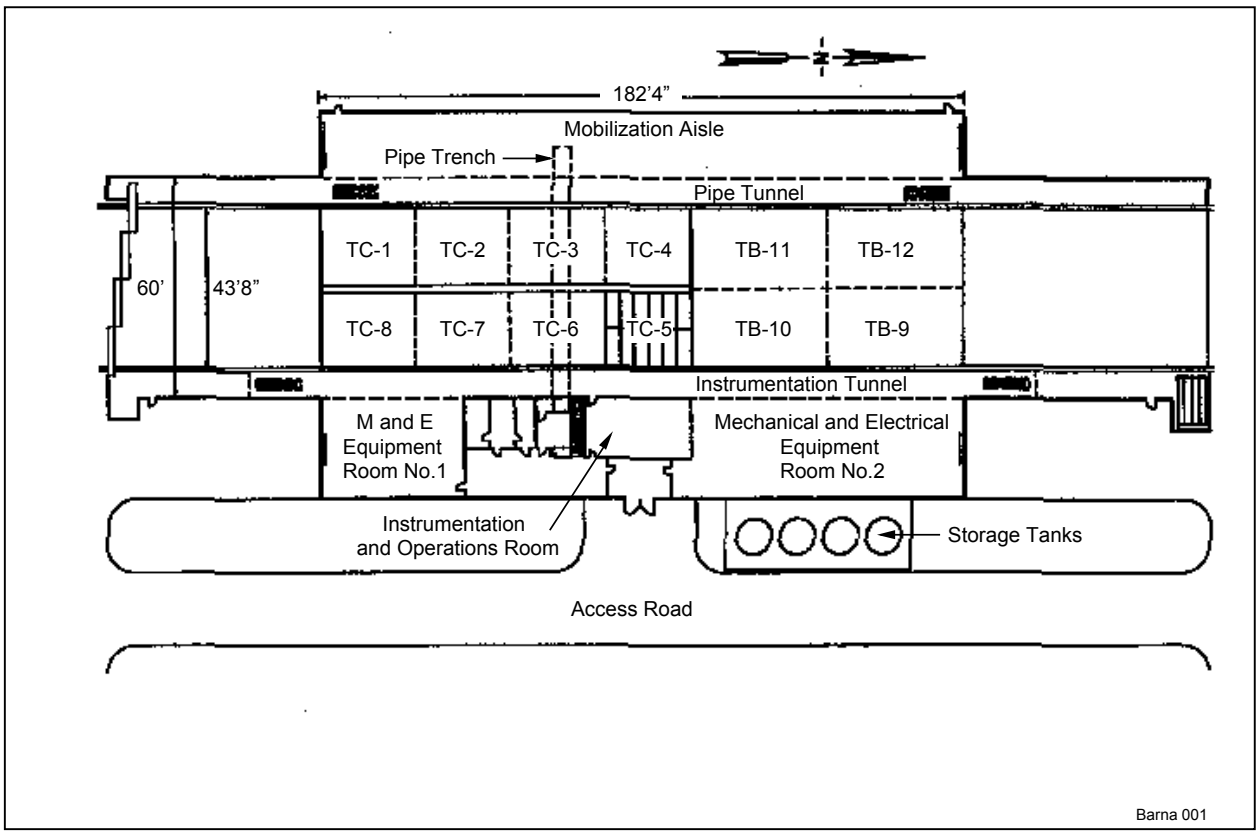

Figure 3.5 Plan View of FERF

A wooden bulkhead was constructed to full depth on both the north and south ends of TC-8 to section off the single test cell. Both the East and West sidewalls are 2.5 m (8ft) high, made of concrete and taper from top to bottom. The bottom of the sidewalls is 150 mm (6 in) thicker than the top. The taper in the wall assists with upward frost heaving during freezing. The interior of the sidewalls was lined with 25 mm (1 in) of rigid insulation to reduce the effect of the temperature gradient between the soil and walls. The bulkhead walls were lined with 50 mm (2 in) of rigid insulation for the same purpose. The concrete floor slopes slightly toward the center of the basin from the sidewalls and connects to a below-grade drainage system.

To minimize the heat loss and to better control the freezing of the soil, freezing panels were installed on the bottom of the test cell and along all sidewalls. The freezing panels are made of steel and measure roughly 2 m (6.5 ft) in length, 1.2 m (4 ft) in width and are 180 mm (7 in) thick. They contain coils on the surface backed with insulation to allow the glycol brine mixture to flow through and control the temperature. The test basin is equipped with a metal frame for holding the panels in place vertically along the wall and horizontally 406 mm (16 in) above the floor. The space between the floor and the bottom of the freezing panels was filled and leveled with sand. The panels were then positioned horizontally and the spaces between filled with sand. A protective layer of sand followed by a rubber membrane was placed above the panels to protect the panels from being punctured.

The water table, which consisted of crushed rock, was placed above the rubber membrane. Plastic 0.10 m (4 in) diameter stand pipes, for monitoring and controlling the water level in the water table were placed at each of the four corners of the test basin. In the subsurface, perforated 0.10 m (4 in) drain pipes ran along the edge and through the center of the test section. For the water table, crushed rock was filled to a depth of 203 mm (8 in), followed by a geotextile. Approximately 2.4 m (8 ft) of silty soil was then placed over the geotextile.

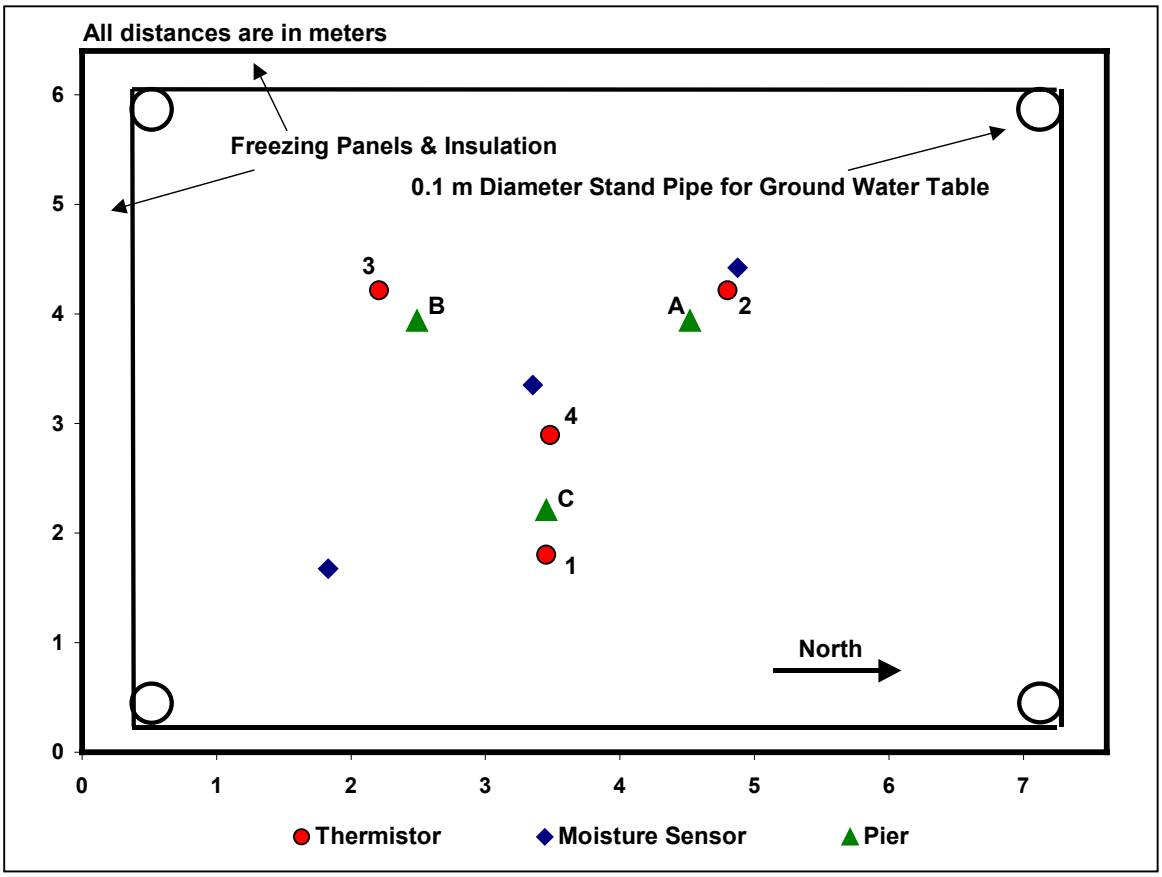

Figure 3.6 Plan View of Test Section

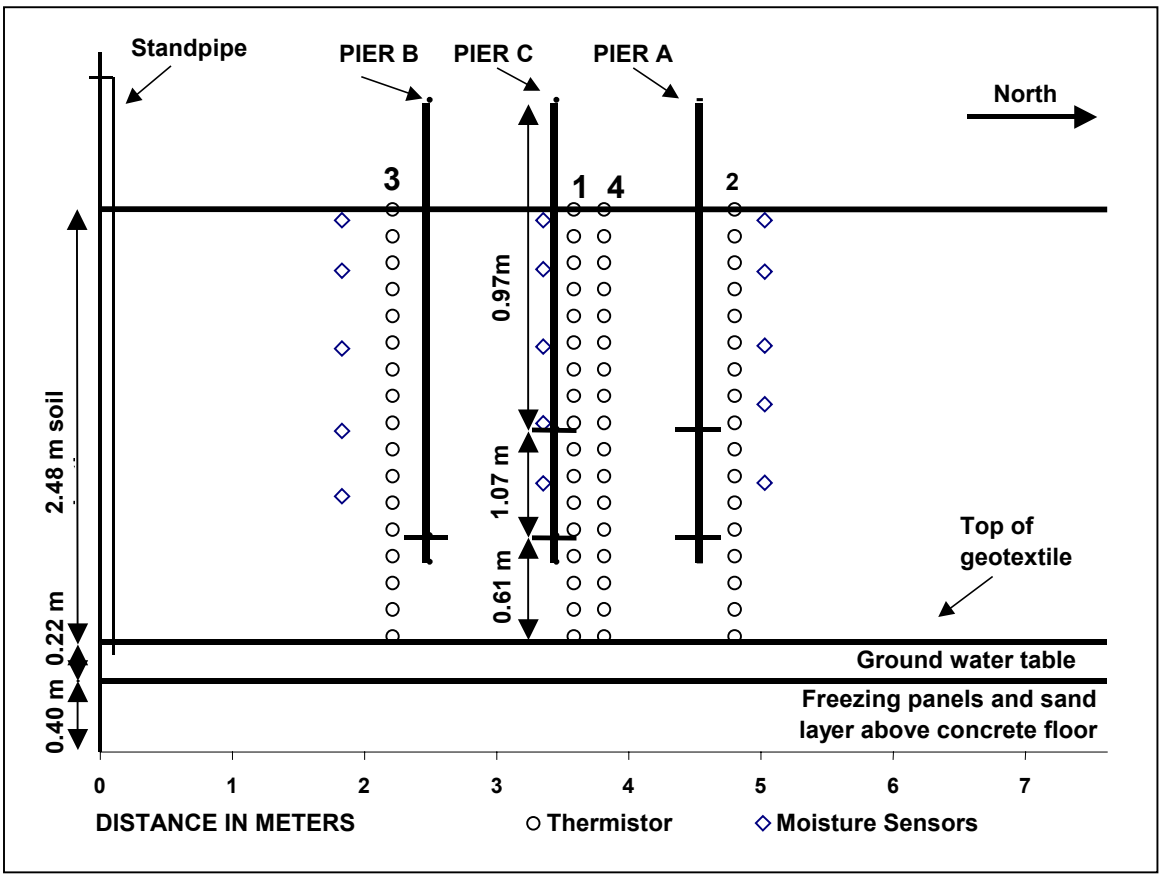

Figure 3.7 Profile View of Test Section

To achieve a 2.4 m (8 ft) depth of soil, wooden framing was built above the concrete center wall to build up the western side of the test section to the correct height. The framing was lined with fiberglass insulation. Framing was installed at the northern and southern ends of the test section to create a safety railing and provide a stable support for the reference beam used for the settlement devices. The finished soil test section measured 6.7 m (22 ft) in length, 6.1 m (20 ft) in width and a depth of just over 2 m (8 ft) (Figure 3.8).

3.3.3 Instrumentation

Temperature and moisture measurements in the soil were continuously monitored as the test section was both freezing and thawing. Each pier was monitored for any settlement in the vertical direction using a piezoelectric ultrasonic proximity sensor made by Banner®. Any tilting of the pier was measured by the AccuStar® II Dual axis clinometer.

Figure 3.8 Frozen Test Cell Prior to Pier Installation (from South)

Thermocouples: Thermocouples were used to monitor the temperatures of the freezing panels at the bottom and all sides of the test section in order to control the freezing process. The thermocouples manufactured at CRREL are accurate within ± 0.5 °C (± 0.9 °F). Prior to placing the sand layer, the strings were run individually and attached in the middle of the side refrigeration panels at a distance of 750 mm (30 in) above the concrete floor. These sensors were not attached to the surface panels since the panels were removed for the installation of the piers. Lead wires from each of the thermocouples were wired into a Campbell Scientific CR10 datalogger.

The datalogger collected ten readings in an hour. Nine of the readings were temperatures from the eight refrigeration panels and a reference temperature built into the datalogger. The last reading recorded the datalogger battery voltage. Figure 3.9 shows the average daily temperature readings during the freezing process and throughout the testing phase. Initially the temperature of the panels was stepped down to begin the freezing process in August 1999. The temperature was then held at 0°C (32°F) through September 1999. During the months of October and November 1999 the temperature was decreased and held at -4°C (25°F), then dropped again and held at -12°C (10°F) to produce ice lensing in the soil. However, as evident from Figure 3.11, the bottom of the basin froze about October 15th after which no ice lenses were formed. The piers were installed when a uniform soil temperature of –4 °C (25 °F) was reached. Pier installation occurred in December 1999.

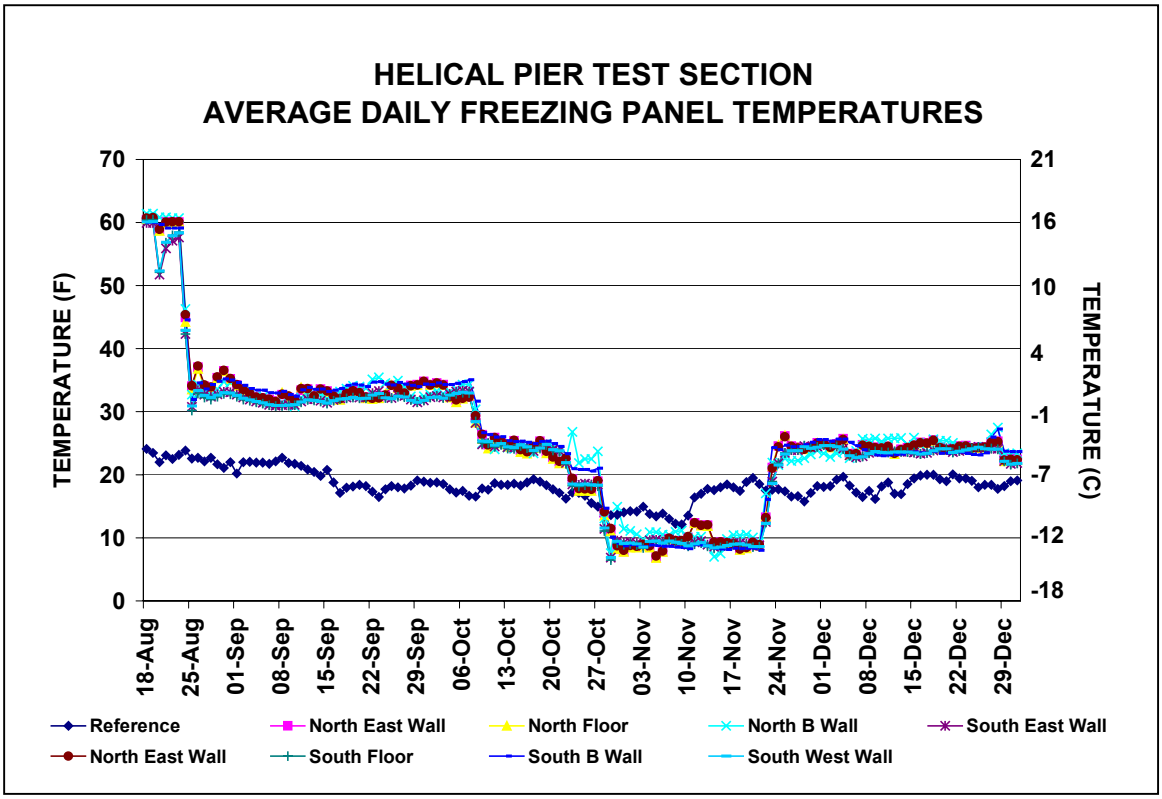

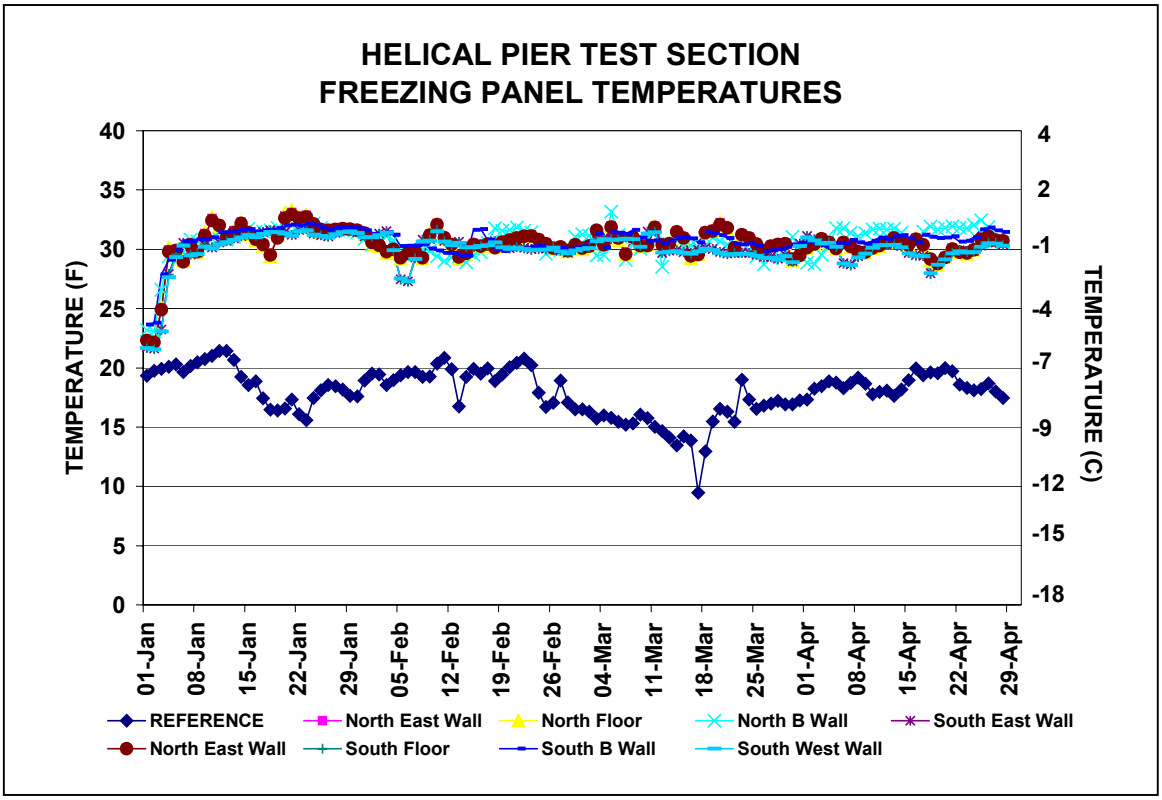

Figure 3.9 Average Daily Thermocouple Readings

Thermistors: Within the test section, soil temperatures were monitored using thermistor rods. The accuracy of thermistors is generally ± 0.7 °C (± 1.26 °F). These instruments used in the test cell were also manufactured at CRREL. The center of the rod is milled to house the thermistor nodes and accompanying wires. The nodes were spaced 150 mm (6 in) apart beginning from the top of the rod to an overall depth of 2,440 mm (96 in). Potting compound is filled in the slot to seal the nodes (Figure 3.10).

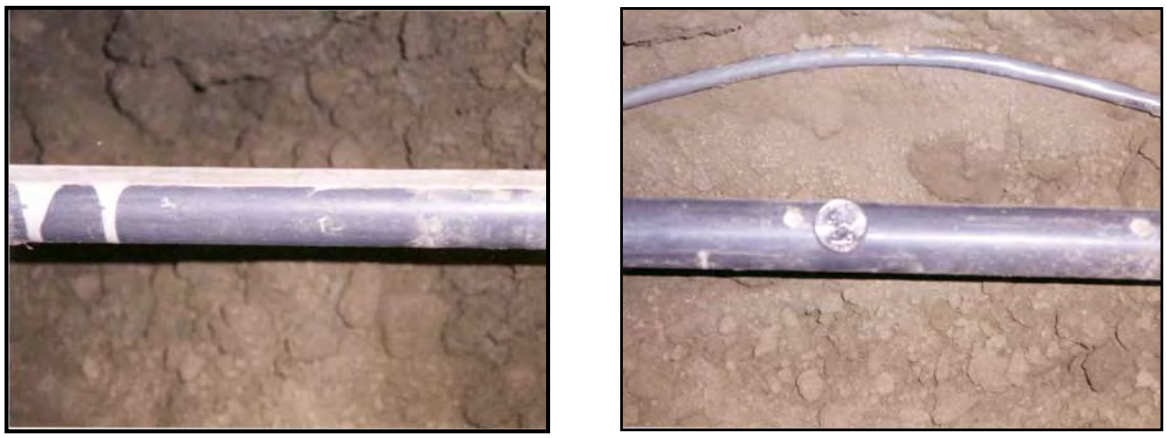

a. Milled Rod with Potting Compound b. Node Spacing

Figure 3.10 Thermistor Rod

Four thermistors were installed in the test section, 40 mm (16 in) away from each pier, and one in the center of the test section (Figure 3.6). The thermistor strings were positioned as close to the location of the piers as possible so they were not damaged when the piers were installed. The center thermistor was used to monitor temperature uniformity within the block of soil. Thermistor nodes were located at depths of 1,219 mm (48 in) and 1,829 mm (72 in) to correspond to the locations of the upper helixes on the double helix piers, and the lower helixes on all of the piers, respectively.

Average daily thermistor data was plotted as shown in Figures 3.11 to 3.14. It was assumed that the soil freezes at 0°C (32°F). Shortly after installation of Thermistor 3, the node at 1524 mm (60 in) gave unreasonable values. Water may have seeped through the potting compound and affected the node.

Moisture Sensors: Fifteen Campbell soil moisture probes were installed in the test section. Three columns of five sensors were located in a diagonal pattern to measure a soil moisture profile throughout the test cell (Figures 3.6 and 3.7).

Hourly data was collected and the average daily water content reported. As the water in the soil turns to ice, the probe interprets this change as a reduction in water. As the soil warms, the moisture content returns to pre-freeze levels (Figure 3.15).

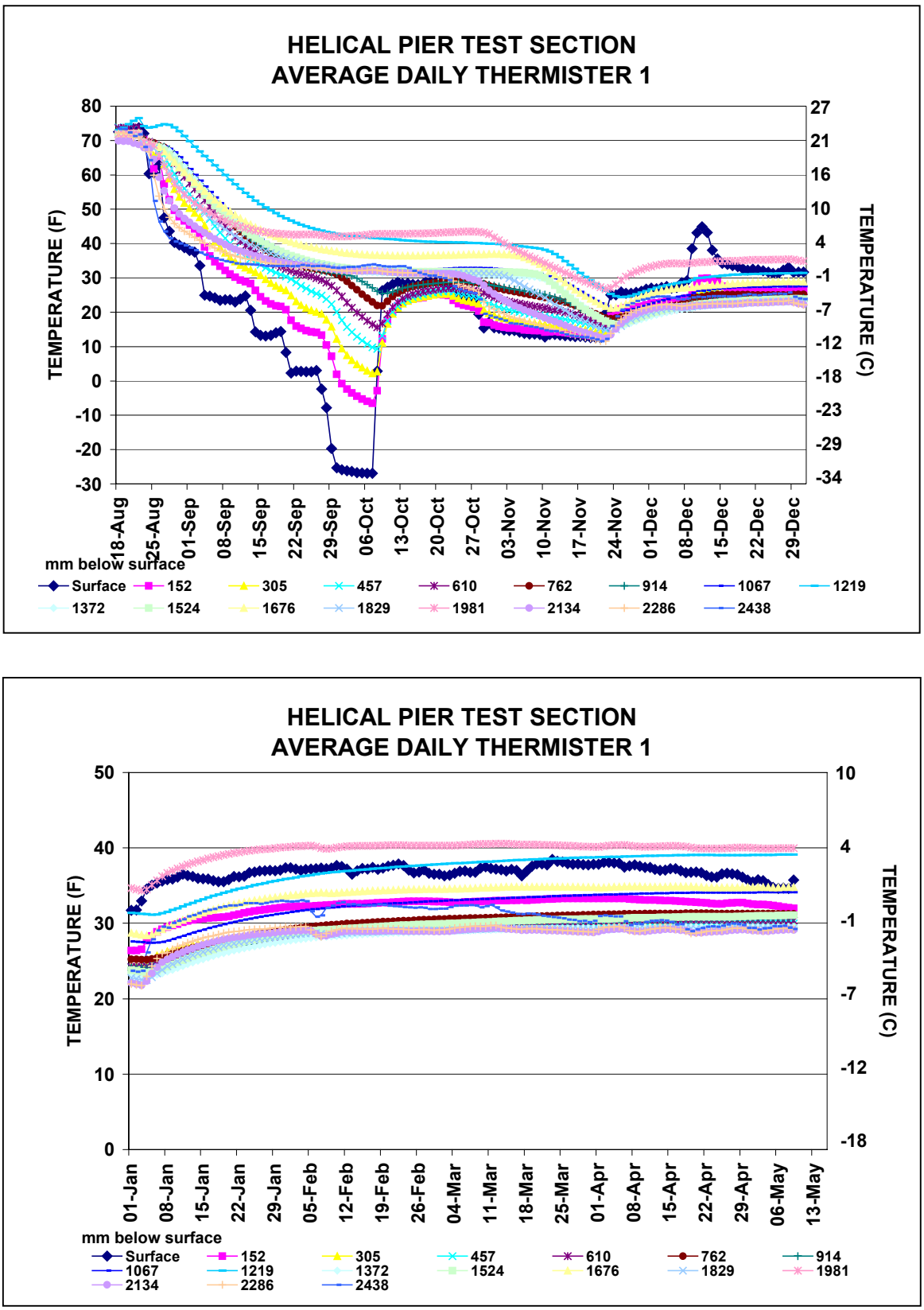

Figure 3.11. Average Daily Thermistor 1 Temperatures throughout Testing Period

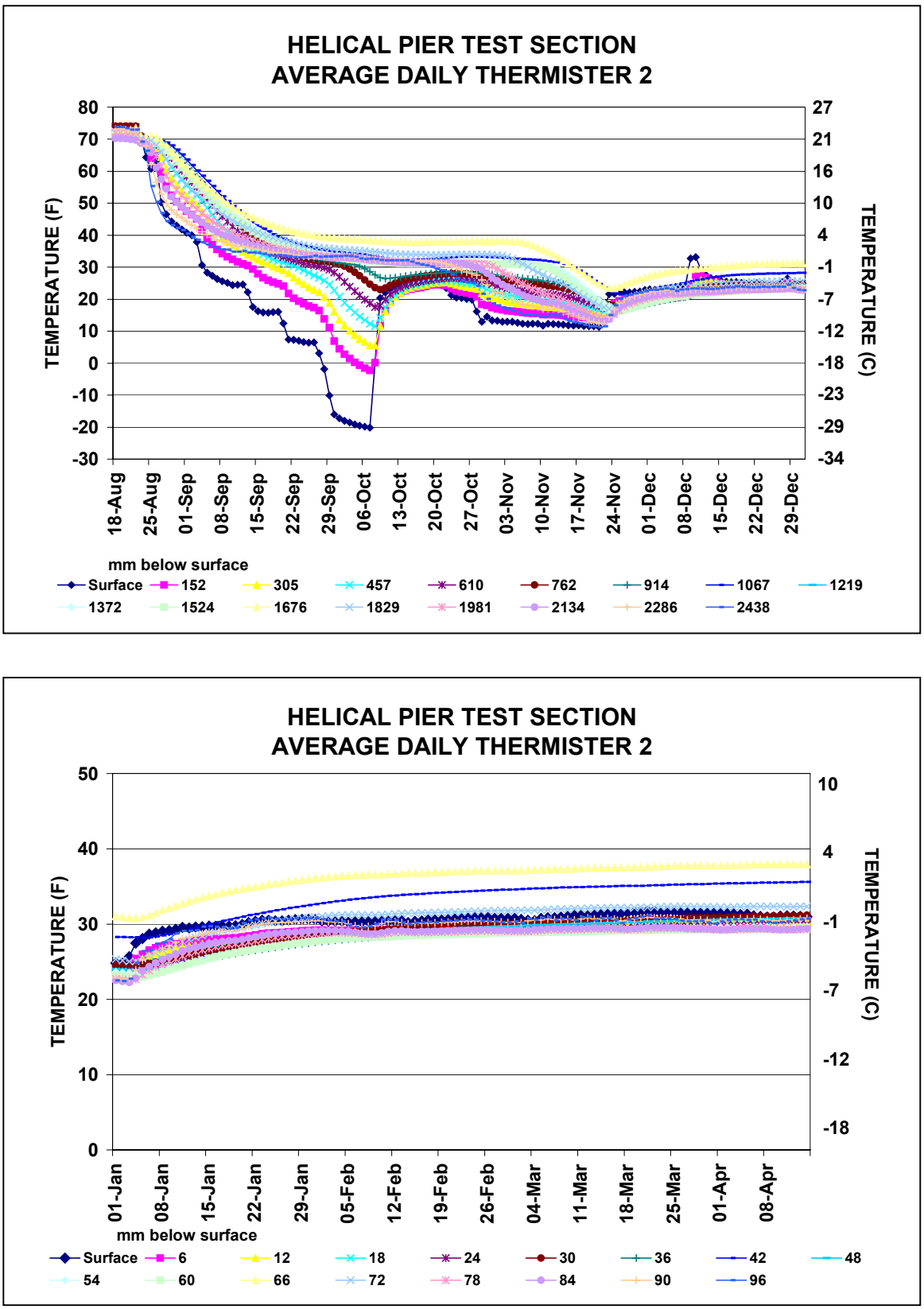

Figure 3.12. Average Daily Thermistor 2 Temperatures throughout Testing Period

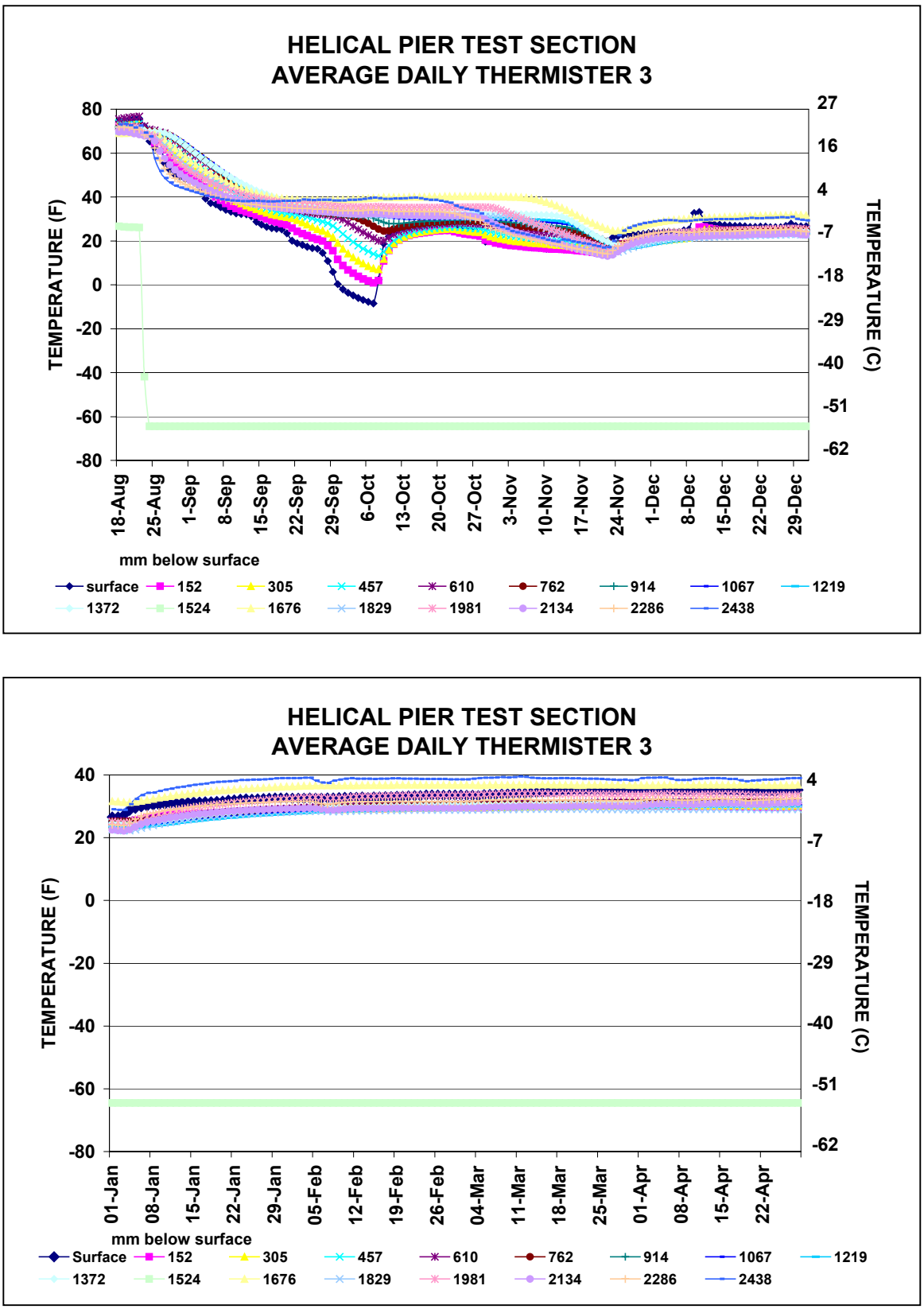

Figure 3.13. Average Daily Thermistor 3 Temperatures throughout Testing Period

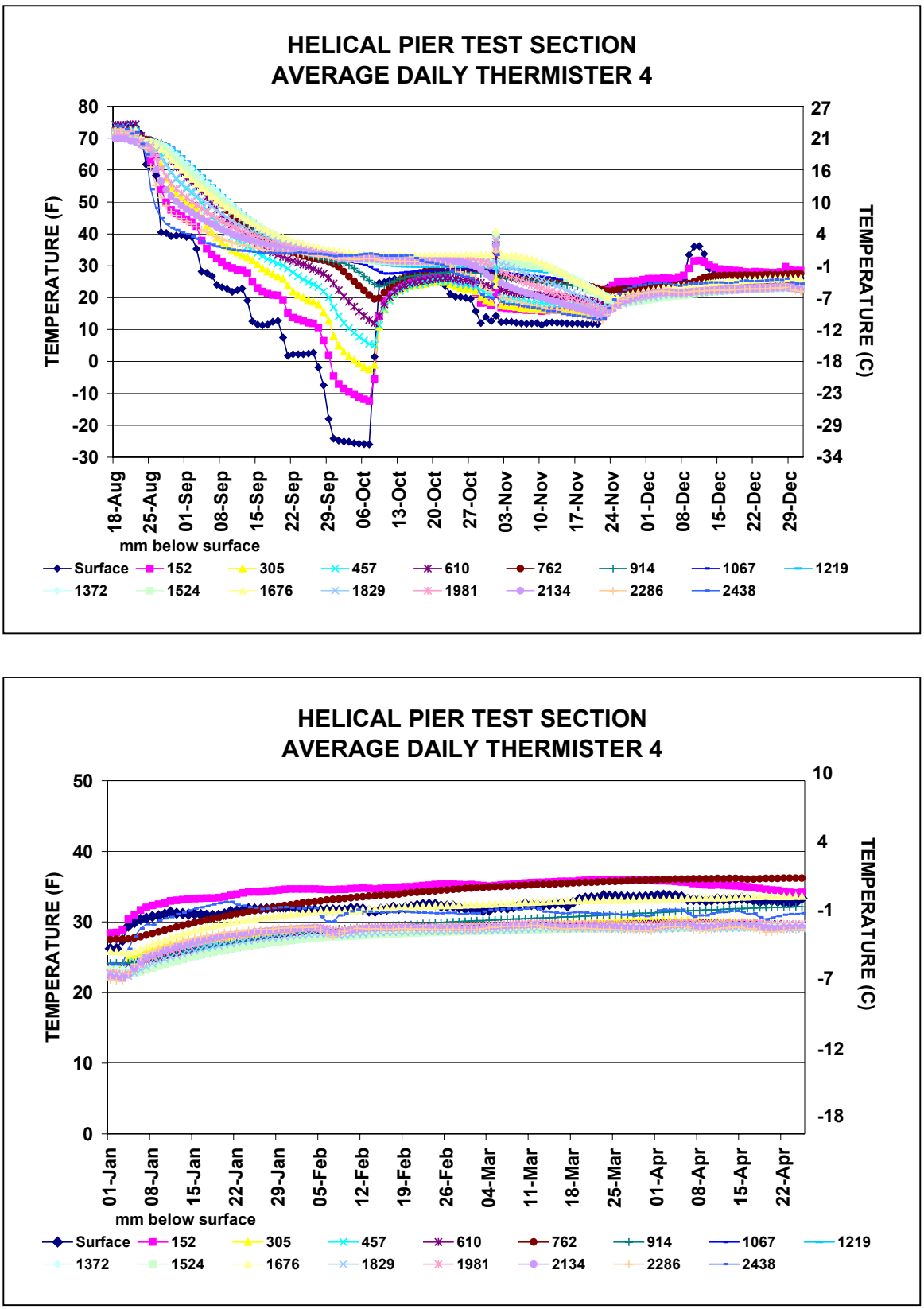

Figure 3.14. Average Daily Thermistor 4 Temperatures throughout Testing Period

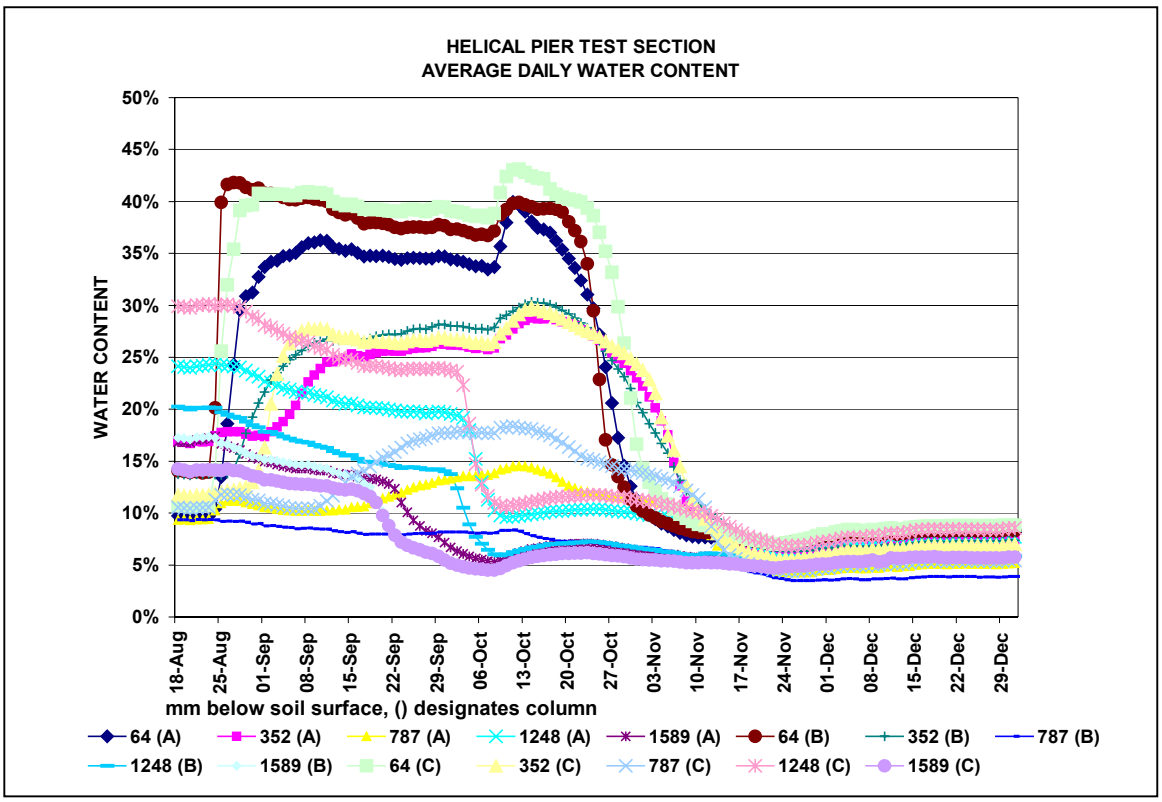

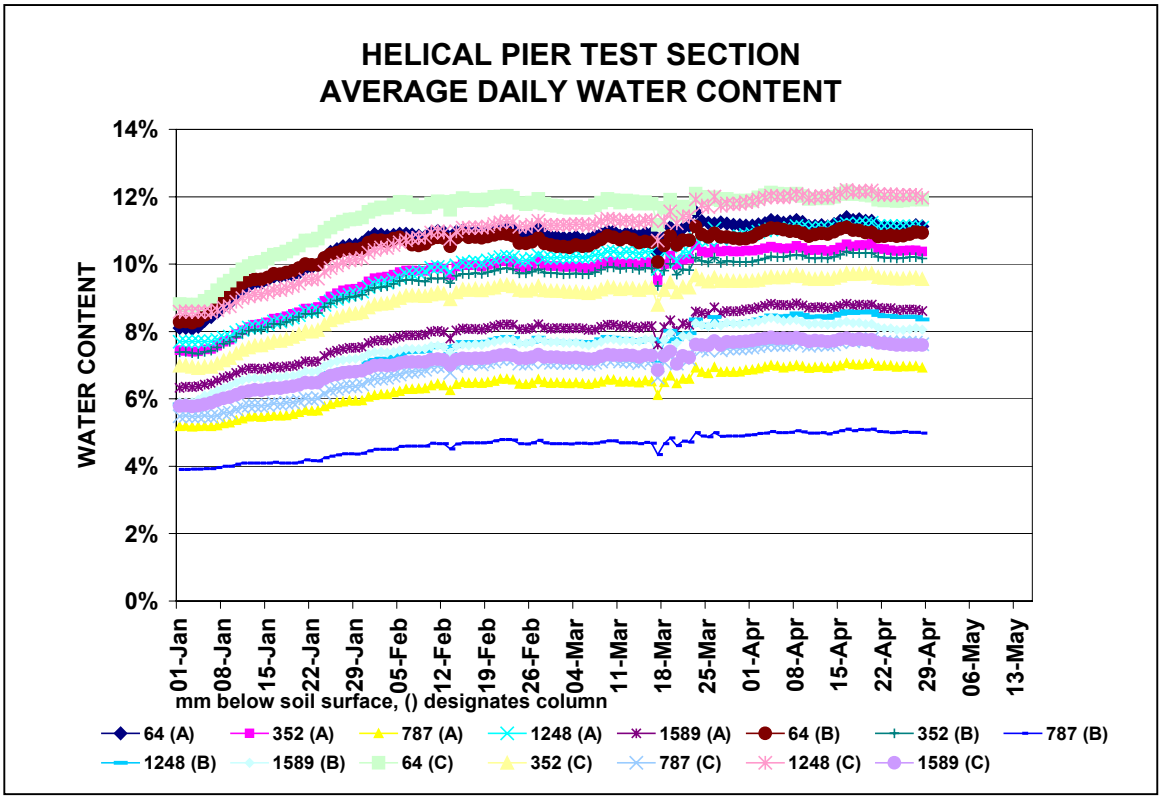

Figure 3.15 Average Daily Moisture Content throughout Testing Period

Creep Sensors: Pier settlement was measured using two devices. For vertical settlement the Banner® Sonic OMNI-BEAM™ piezoelectric ultrasonic proximity sensors were used (Figure 3.16a). Any tilting of the piers was measured using the AccuStar® II dual axis clinometer (Figure 3.16b).

Banner® Sonic OMNI-BEAM™: The operating range and temperature of the proximity sensor is 100 – 660 mm (4 - 26 in) and between 0 to 50 °C (32 to 122 °F), respectively. It was noted during testing that while the sensor operated within the specified temperature range, there was an effect in the readings from the ambient air temperature. To correct for the fluctuations in temperature, a fourth stationary range sensor was used. Since the reference sensor's location was fixed, the effects of temperature were corrected as a percent change from the reference distance.

To make sure that the OMNI-BEAM™ was reading the effects of the loading of the piers and not moving with the piers, it was necessary to develop an independent system where the range readers were not attached to the steel plate (Figure 3.17). A reference beam system was constructed to hold the range readers. An aluminum collar 127 mm (5 in) in diameter was placed over each pier and bolts were tightened on each side of the pier to hold the collar in place (Figure 3.18). An aluminum plate 914 mm (36 in) long and 152 mm (6 in) wide was secured to the collar. These collars and plates were attached to the piers so that the end of the plate was located under the main reference beam and away from the center of the test section. It was the distance between this aluminum plate and the OMNI-BEAM™ device where vertical settlement was measured (Figure 3.19). The aluminum reference beams were secured to the framing on the north and south ends of the test section.

Figure 3.16a OMNI-BEAM™

Figure 3.16b AccuStar®

Figure 3.17 Support System for OMNI-BEAM™

Figure 3.18 Aluminum Collar Bolted to Sides of Pier to Support Arm for Settlement Measurements

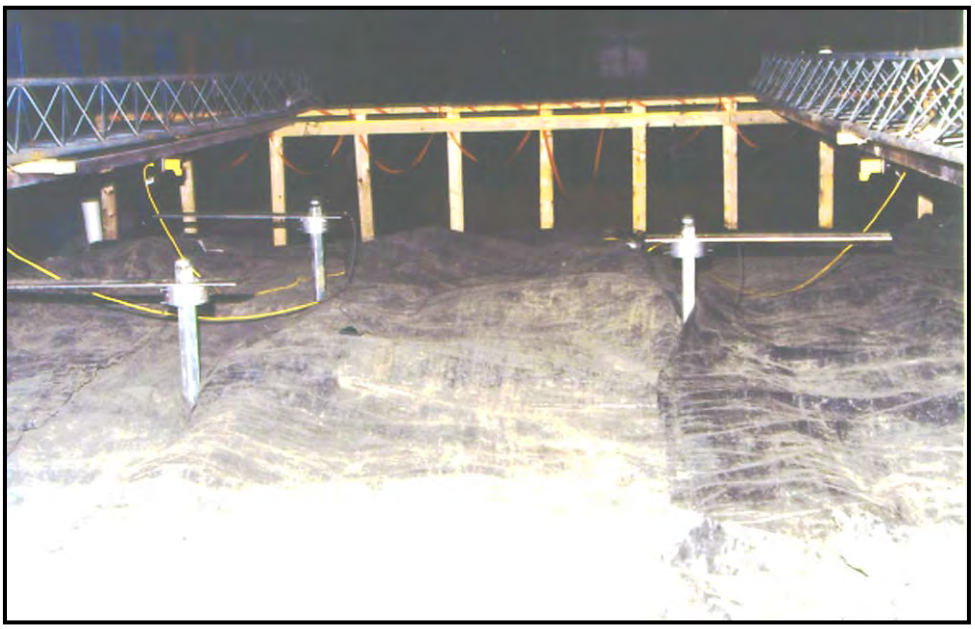

Figure 3.19 View from South End Showing Completed Test Cell and Piers before Concrete Blocks are Loaded

AccuStar® II dual axis clinometer: The tilt indicators operated over a range of ± 20 axial degrees. The operational temperature range is from –40 to +85 °C. The tilt indicators were placed on the aluminum arm, as close to the pier as possible (Figure 3.16b).

3.3.4 Pier Installation

Surface freezing of the test section began on August 18, 1999. After the freezing panels were connected to the refrigeration system and leak tested, the temperatures of the sides and bottom panels was decreased to –1°C (30°F) and held until October 7. Over the next two days, the temperature was decreased again to -4°C (25°F) and then finally dropped to –18°C (0°F) to accelerate the freezing process through the test cell and reach a uniform temperature of -4°C (25°F).

On December 9, 1999 the surface freezing panels were removed for the installation of the piers for a period of approximately 24 hours. All remaining freezing panels on the sides and bottom of the test section remained at a temperature of -4°C (25°F) during the installation. With the surface panels removed, the amount of thaw from the surface was less than 152 mm (6 in).

For the installation, the test section was cleaned off, the locations of the piers were located and painted, and elevations shot on the three intended pier locations (Figure 3.6). The ambient temperature of the FERF was approximately 18 – 21°C (65 – 70°F) during the installation. Figure 3.8 shows the frozen test cell before the piers were installed.

The bottom helix for each pier was not to be less than 610 mm (24 in) above the geotextile to ensure that there was some soil for creeping under the pier. The geotextile was located at a depth of approximately 2.48 m (8.2 ft) below the soil surface. The length of the helix was 1.6 m (5.5 ft) and the length of the extension was 0.9 m (3.2 ft). The pier extensions were marked 635 mm (25 in) from the top, which would be the amount exposed above the surface.

According to Mr. Metlicka, the supervisor of the installation, the procedure used in the FERF was similar to installations done in the field. A power auger mounted on a backhoe was used for the installation procedure (Figure 3.20). A double helix pier, designated as "Pier A", located in the Northwest quadrant of the test section was installed first. Once the drill rig was set and the correct fitting for the top of the pier attached, the pier was set over the location and checked for vertical alignment. Then the pier was drilled down into the soil. During the installation of pier A, the 8,135 N·m (6,000 lb-ft) shear pins exceeded their maximum torque rating and broke. The pins were replaced with 10,846 Nm (8,000 lb-ft) shear pins that did not brake. This means that the installation torque was between 8 and 11 kNm (6000-8000 lb-ft). The pier extension was then secured to the top of the pier using a bolt and locking nut (Figure 3.21). Installation continued until 635 mm (25 in) of the pier extension was above the surface of the soil. Piers B and C were installed using the same procedure. After each pier was installed, the soil was leveled around the pier and water was poured around the extension.

After the installation, core samples were collected and the surface freezing panels were replaced to refreeze the top soil. The panels were situated in such a way as to not interfere with the piers, but to still permit freezing. Thermal blankets were placed over any exposed surface to minimize temperature loss.

Figure 3.20 Pier Installation

Figure 3.21. Pier Extension is Attached

3.3.5 Core Samples

Two core samples were taken to verify ice forming in the soil. Core A was located on the southern side of the test section, and Core B was on the north side (Figure 3.22).

Core A was drilled to a total depth of 2 m (6.75 ft); core B to 2.2 m (7.08 ft). The samples were sliced into segments approximately 152 mm (6 in) in length and 38 mm (1.5 in) in diameter. The samples were weighed and placed in an oven to dry for a minimum of 24 hours. Table 3.4 gives water contents for each sample. According to Figure 3.15, the unfrozen water contents at the moment of the coring (December 10th) were from 3 to 8%. The unfrozen water contents varied from 10-30% in the beginning of the test to 5-40% in the end of October. The total water contents in Table 3.4 do not match with the high water contents in Figure 3.15.

The soil from core A appeared dry and crumbly with many air voids and gaps up to a depth of 762 mm (30 in) when it appeared more dense and solid. Core B was similar for the upper portion of the test hole, and was more compacted toward the bottom of the test hole. There were no prominent ice lenses observed in either of the core samples. Figure 3.23 shows what a typical core looked like during the sampling.

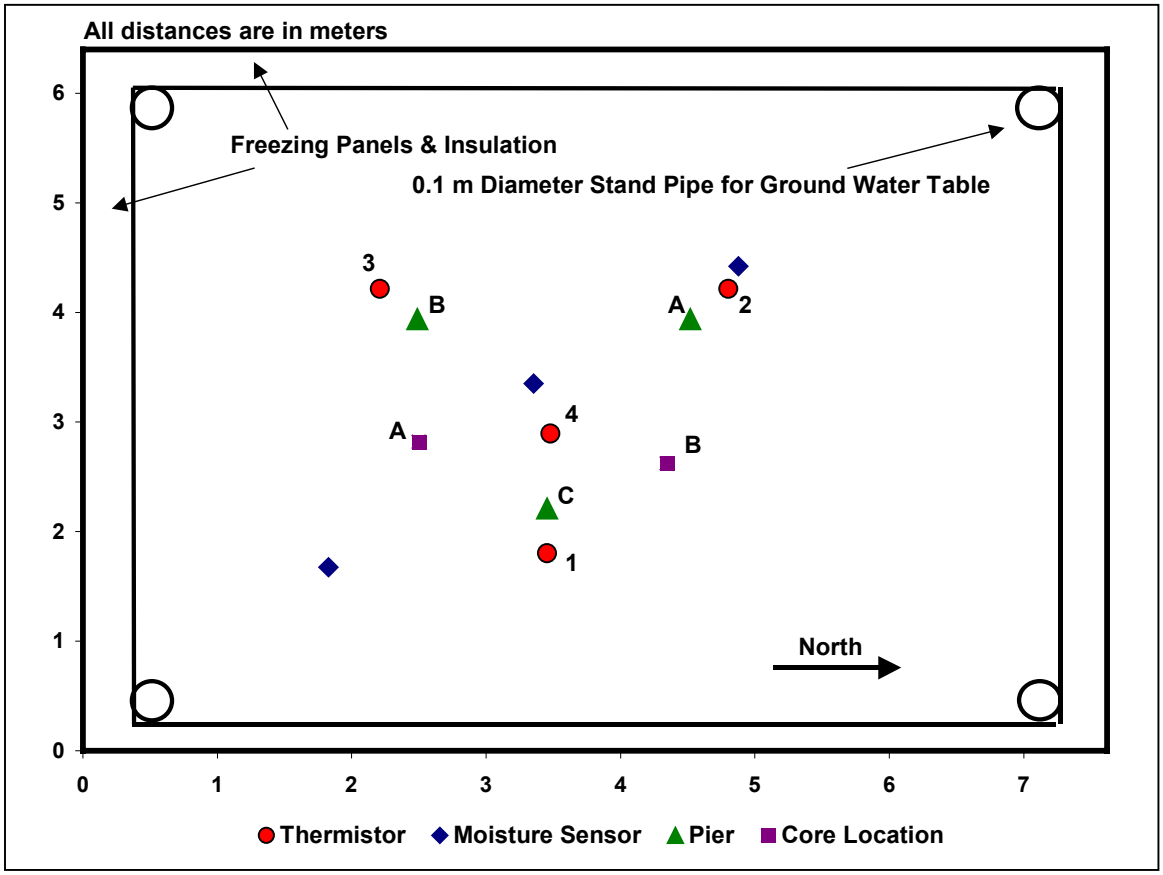

Figure 3.22 Locations of Core Samples

Table 3.4 Core Sample Water Contents

Core A Depth (mm)	Water Content (%)	Core B Depth (mm)	Water Content (%)	Average Water Content (%)
150	17.14	150	16.84	17.0
300	15.89	300	15.65	16.8
450	16.48	450	16.86	16.7
600	15.87	600	16.49	16.2
750	16.00	750	16.45	16.2
900	16.27	900	16.23	16.2
1050	16.64	1050	20.08	18.4
1200	16.66	1200	21.27	19.0
1350	14.59	1350	21.95	18.3
1500	16.03	1500	16.43	16.2
1650	13.83	1650	17.54	15.7
1800	18.28	1800	18.28	18.3
1950	16.90	1950	18.93	17.9
		2100	23.12	23.1

Figure 3.23 Core Samples

3.3.6 Pier Loading

After installing the piers and collecting the core samples, the freezing panels were replaced on the surface to refreeze the top soil. A moisture barrier was placed between the soil surface and the freezing panels to prevent the soil from sticking to the panels. The panels did not touch the piers. Three sets of single panels were placed on the West side of the test cell around Piers A and B. Two sets of 5 panels (or a 5-pack) were placed on the East side of the test cell on either side of Pier C. The freezing panels were re-connected to the glycol refrigeration system and set to –4°C (25°F) to refreeze the soil surface. Thermal blankets were placed over any exposed surface to minimize temperature loss.

To ensure vertical loading, rounded endcaps were glued to the top of the piers with epoxy and allowed to set for approximately 24 hours (Figure 3.24). Elevations of the piers with the endcaps were recorded.

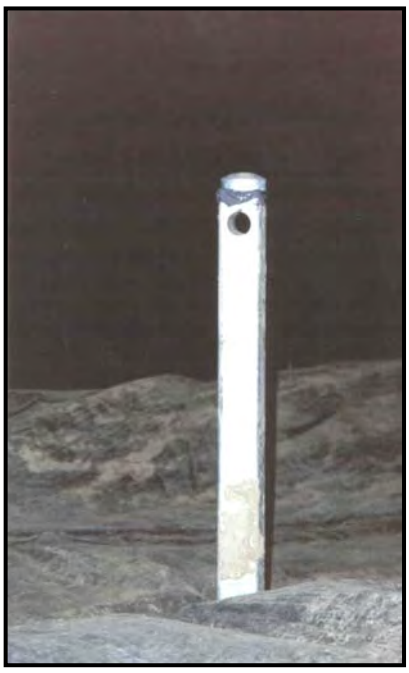

Figure 3.24 Installed Pier with Endcap

Once the soil reached the desired temperature, a steel plate 2.4 m wide by 3 m long by 25.4 mm thick, and weighing 14.7 kN (8 ft wide by 10 ft long by 1 in thick, weighing 3,300 lbs) was loaded onto the piers. Lines were drawn on the plate to line up the piers as the plate was placed. Outlines of the blocks were also marked on the plate to minimize the amount of time needed to place the blocks. A crane was used to pick up each block and place it on the steel plate. To guide the block into position and disconnect each block from the crane, at least one person was needed to be standing on the steel plate. Given the current set up, it was not possible to load the piers using a fully automated system to capture the instant deformation when the pier was loaded. The OMNI-BEAM™ proximity sensors measured movement on the plate while the

blocks were placed. The blocks were loaded one at a time using configurations given in Table 3.5 for the both testing temperatures.

Table 3.5 Loading Configurations

Configuration	Total Load (kN)	Load per Pier (kN)
Steel Plate	15.2	5.1
Single block placed in the center of the steel plate	33.0	11.0
Double block, stacked in center of steel plate	50.8	16.9
Single block over each pier	68.7	22.9
Double blocks, stacked over each pier	122.1	40.7

There was not much clearance between the antennas, where the OMNI-BEAM™ devices were mounted, and the steel plate. Care was used not to hit the antennas while trying to place the blocks, since it was reflected in the data. Even so, the additional movement on the plate was read by the instrumentation and should not be used for analysis.

When changing the block configurations from the stacked blocks in the center, the top block was moved and placed over Pier A. The bottom block was placed over Pier C and a third placed over Pier B. Moving and placing the blocks required some time, up to 30 minutes, to move everything into position and set it down. Figures 3.25 and 3.26 show the loaded piers with single blocks and double blocks.

After the blocks were set, data was collected for 24 hours. If no movement was observed in the data, the blocks were moved into the next configuration. Just prior to placing the first block, the data collection system was started and it collected readings every 10 seconds during the first hour, every minute during the second hour and every 15 minutes for 22 hours. The following day, the data was reviewed for any settlement. Results from the data are given in the next section. Based on the data, concrete blocks were then added to load the piers and monitor the response.

Figure 3.25 Loading Piers with Three Concrete Blocks (view looking North)

Figure 3.26 Loading Piers with Six Concrete Blocks

3.4 Test Results

3.4.1 Test at –4°C

On December 16, 1999 the steel plate was set on the piers. Data was collected for 24 hours to see the response of the piers before the blocks were loaded. The output from the OMNI-BEAM™ sensors was in inches. As mentioned previously, these sensors measured the distance from the device to the aluminum arm. Table 3.6 gives the initial readings of the sensors.

Pier loading began the morning of December 17, 1999 when the single block was placed in the center of the steel plate. Figure 3.27 shows the results of loading the single block. The spike seen after loading is believed to be from the change in temperature in the FERF when the South doors were opened and the outdoor temperature was much lower than that of the FERF. This was when a reference sensor was installed and the data was corrected for the effects of temperature. No changes were seen in the data and the second block was loaded on December 18, 1999 (Figure 3.28).

On the morning of December 20, 1999 the blocks were moved, one over each pier. The top block from the center stack, was placed on Pier A and the bottom block moved to Pier C. Pier B was loaded last with a third block. Again, the data suggest no settlement by the piers (Figure 3.29). Since there was no change in the data, the second layer of blocks was placed about an hour and a half later on December 20. Pier A was loaded first and the response was watched for a few minutes to check the stability of the plate. Pier A did show an increase in vertical distance after the block was loaded and then it leveled off. Pier C showed no change when loaded. Pier B (single helix) did show a small amount of change (Figures 3.30 and 3.31). No change was seen from any of the block configurations. The blocks stayed in position until December 21, 1999 when all of the blocks and the steel plate were removed. The blocks were removed from the piers in the same order as they were placed. After the blocks and plate were removed, elevations of the piers were taken. The piers showed no change in elevation, signifying no settlement during the test at -4°C. The test section remained dormant to see if there was any rebound by the now unloaded piers. The test concluded on January 3, 2000 and the temperature of the panels was increased to -1°C (30°F) to warm the soil for the next testing condition.

Table 3.6 Initial Readings of OMNI-BEAM™ Sensors

	Distance (mm)	Distance (in)
Pier A	205.5	8.09
Pier B	222.8	8.77
Pier C	214.4	8.44

Figures 3.31 through 3.38 show the readings for the tilt meters for the test at -4°C. For all piers, the X-direction shows movement in the East-West direction and the Y-direction shows movement in the North-South direction. The output values for the tilt meters were in millivolts (mV). A change of 56 mV is equivalent to 1 degree of axial movement. Each tilt meter was calibrated with 2,500 mV as dead center. Once the meters were set at each pier, the initial reading was used for the baseline to track any movement. Table 3.7 shows the initial tilt meter readings. The only movement registered by the tilt meters was caused during placement of the blocks. When someone stood on the plate to guide the block in place and right after placement of the block, a ‘wiggle’ movement could be felt. As shown in the results, no changes in tilt occurred during the test.

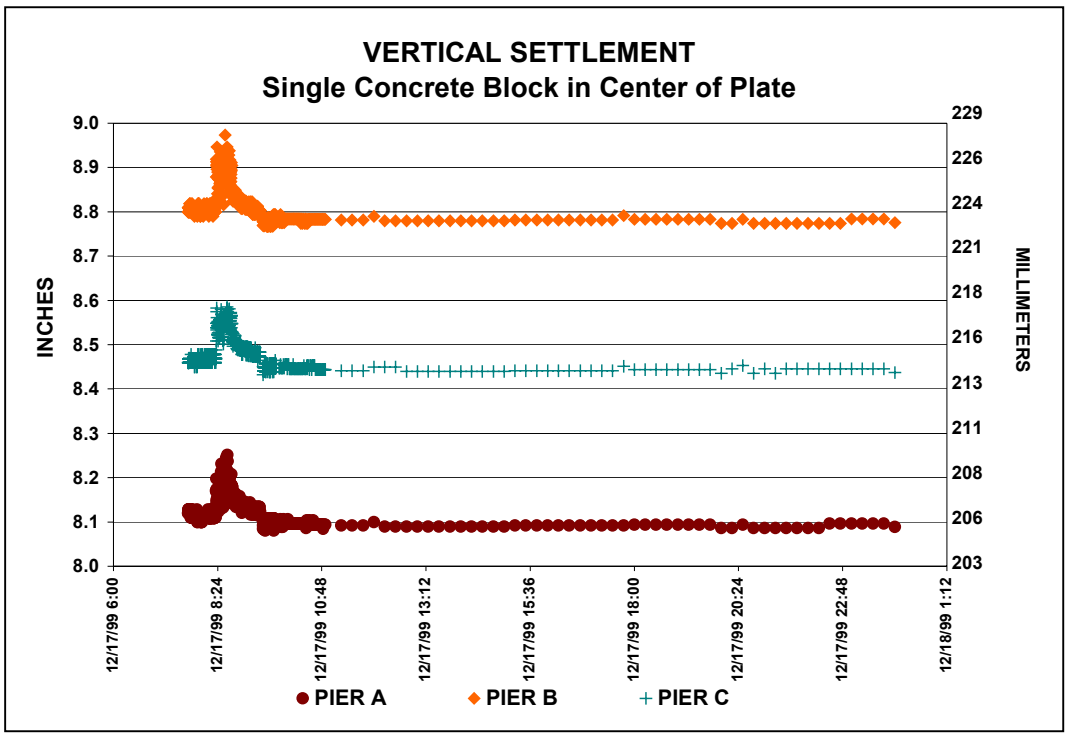

Figure 3.27 Pier Settlement at -4°C with Concrete Block Placed in Center of Steel Plate

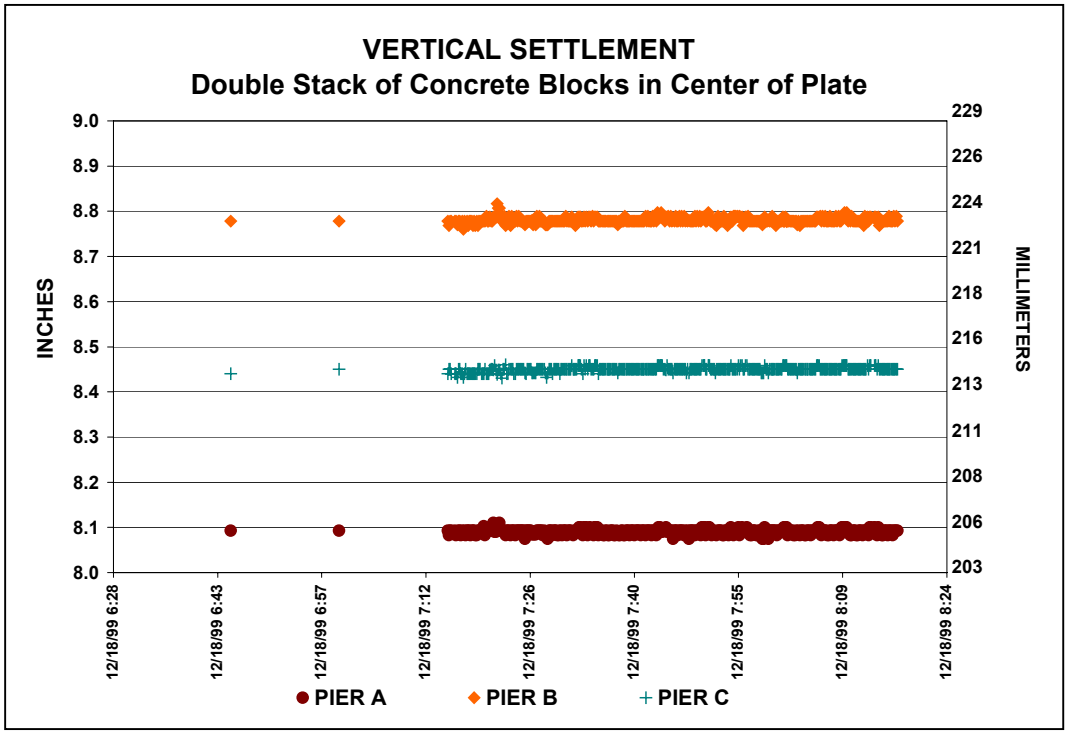

Figure 3.28 Pier Settlement at -4°C with Two Concrete Blocks Placed in Center of Steel Plate

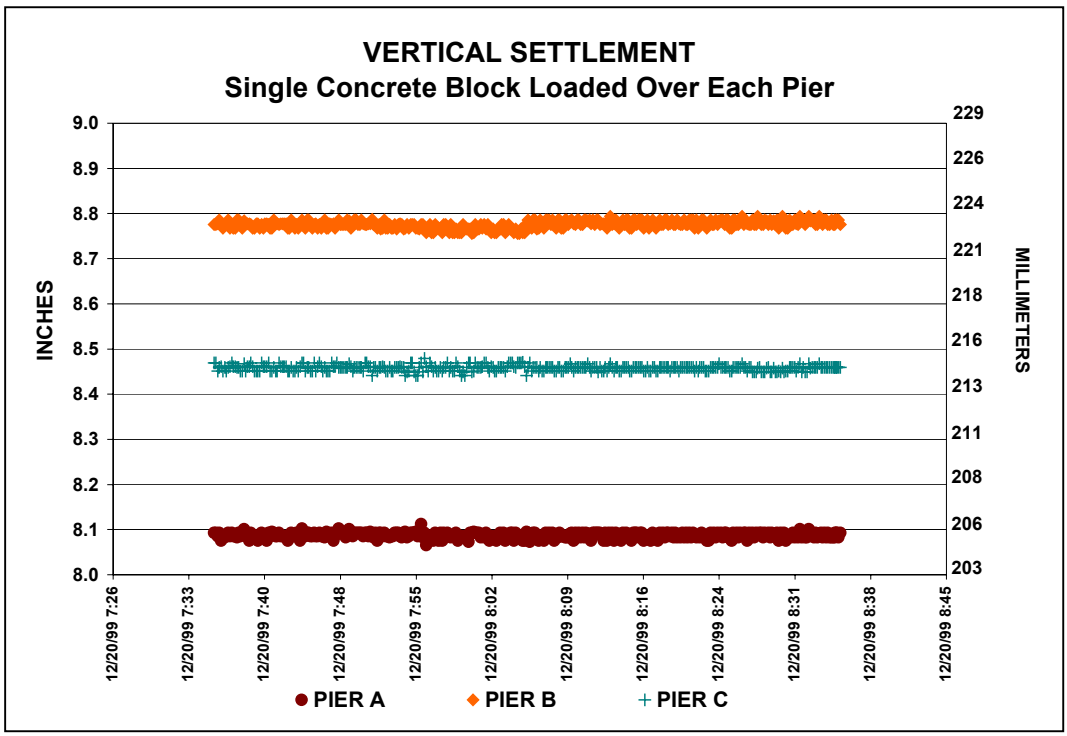

Figure 3.29 Pier Settlement at -4°C with Single Concrete Block Placed over Each Pier

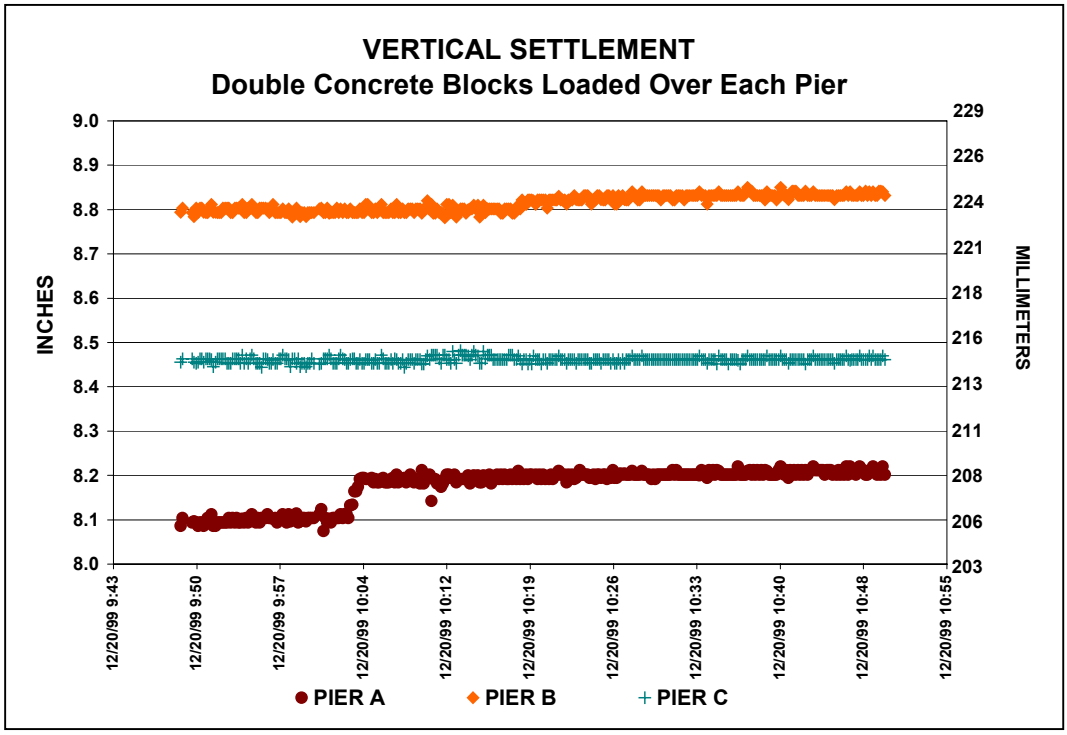

Figure 3.30 Pier Settlement at -4°C with Two Concrete Blocks Placed over Each Pier

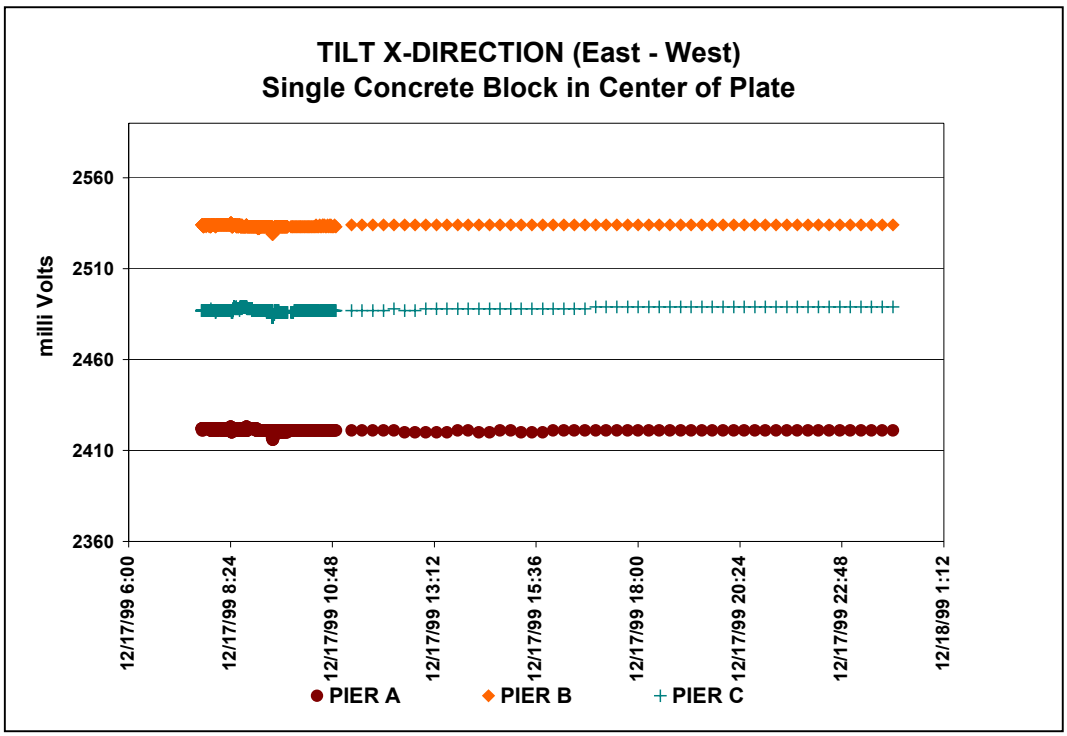

Figure 3.31 Tilt Readings for X-Direction for Single Block in Center of Plate

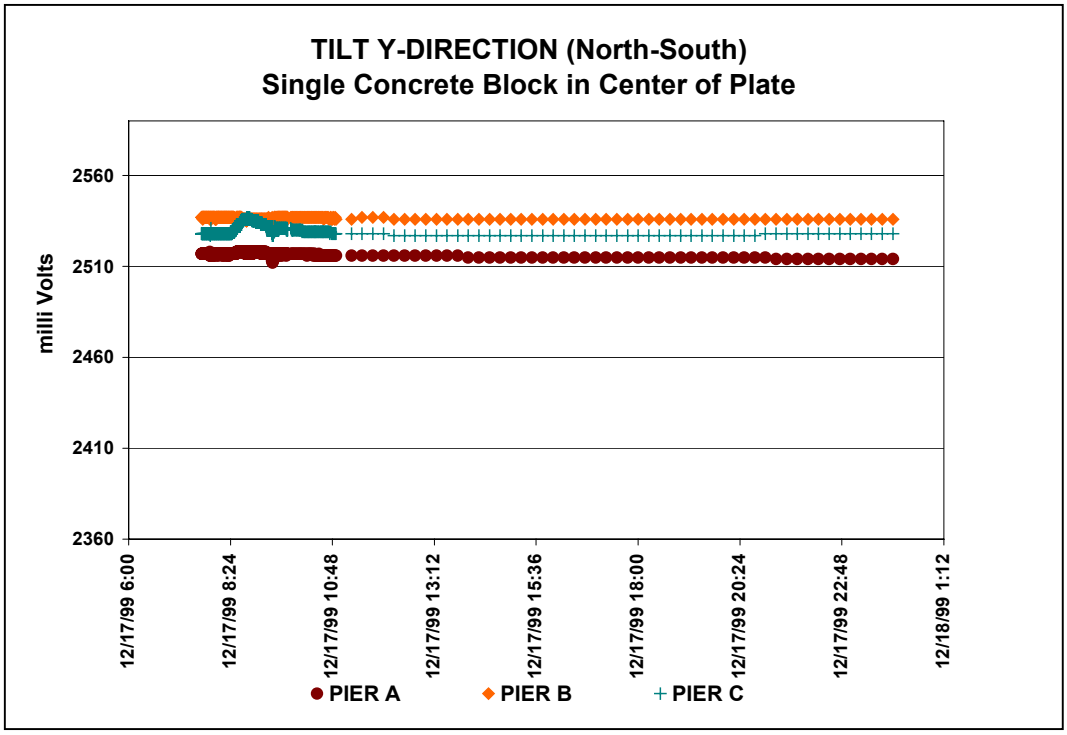

Figure 3.32 Tilt Readings for Y-Direction for Single Block in Center of Plate

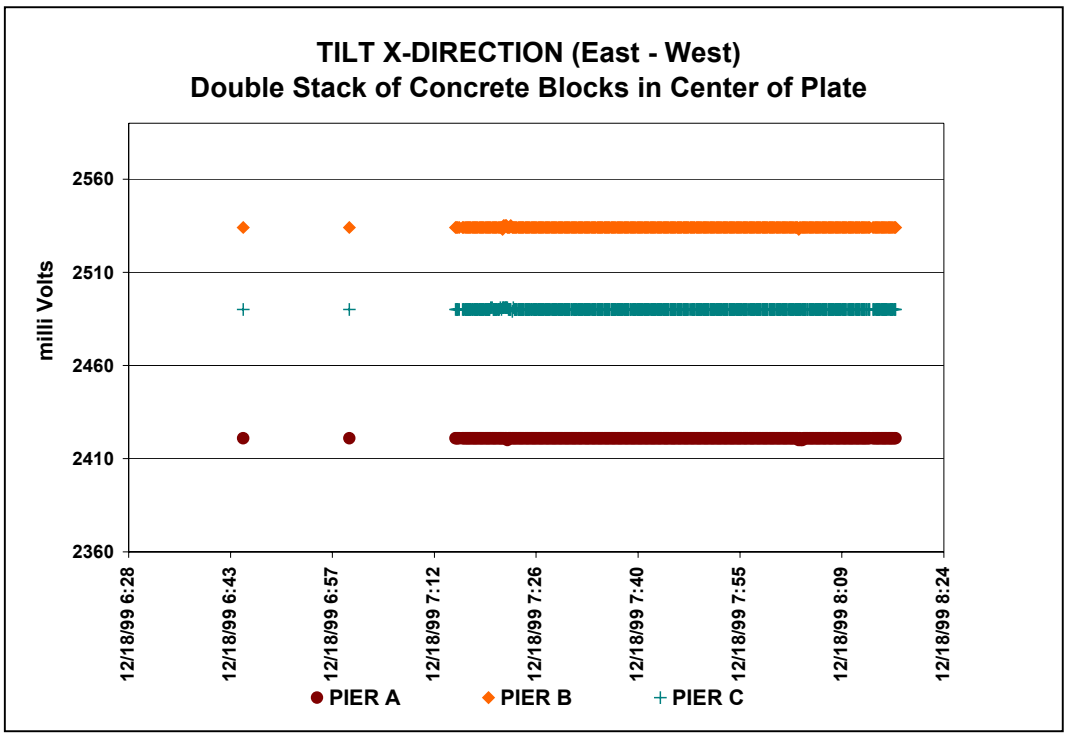

Figure 3.33 Tilt Readings for X-Direction for Two Blocks in Center of Plate

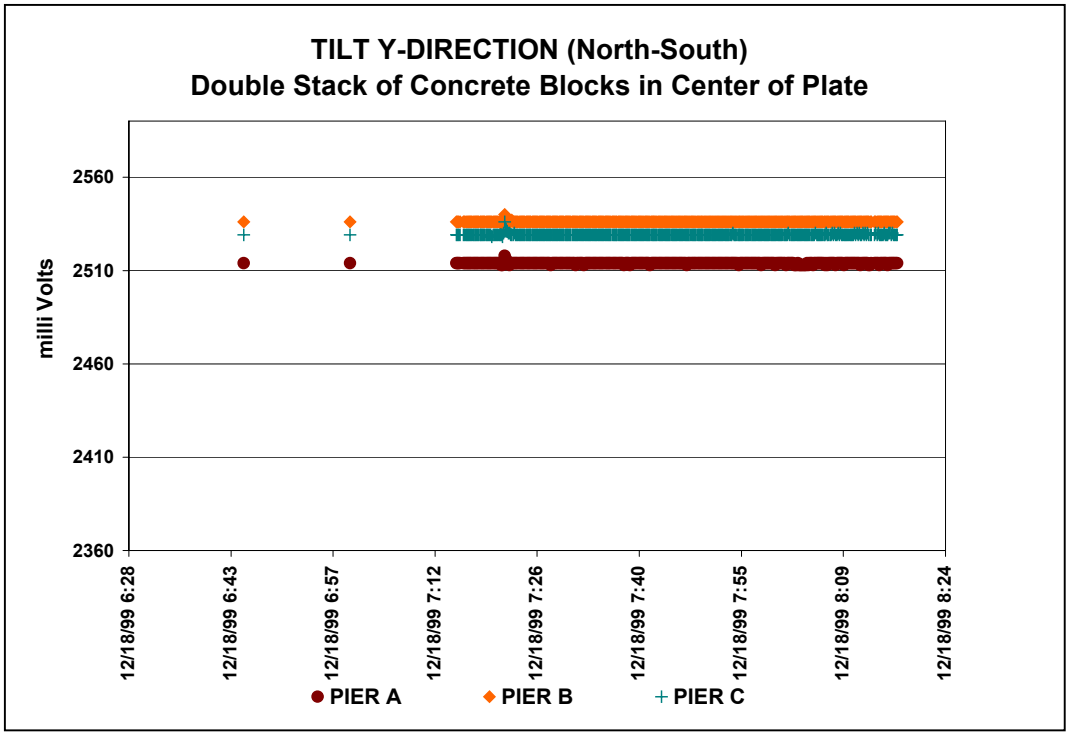

Figure 3.34 Tilt Readings for Y-Direction for Two Blocks in Center of Plate

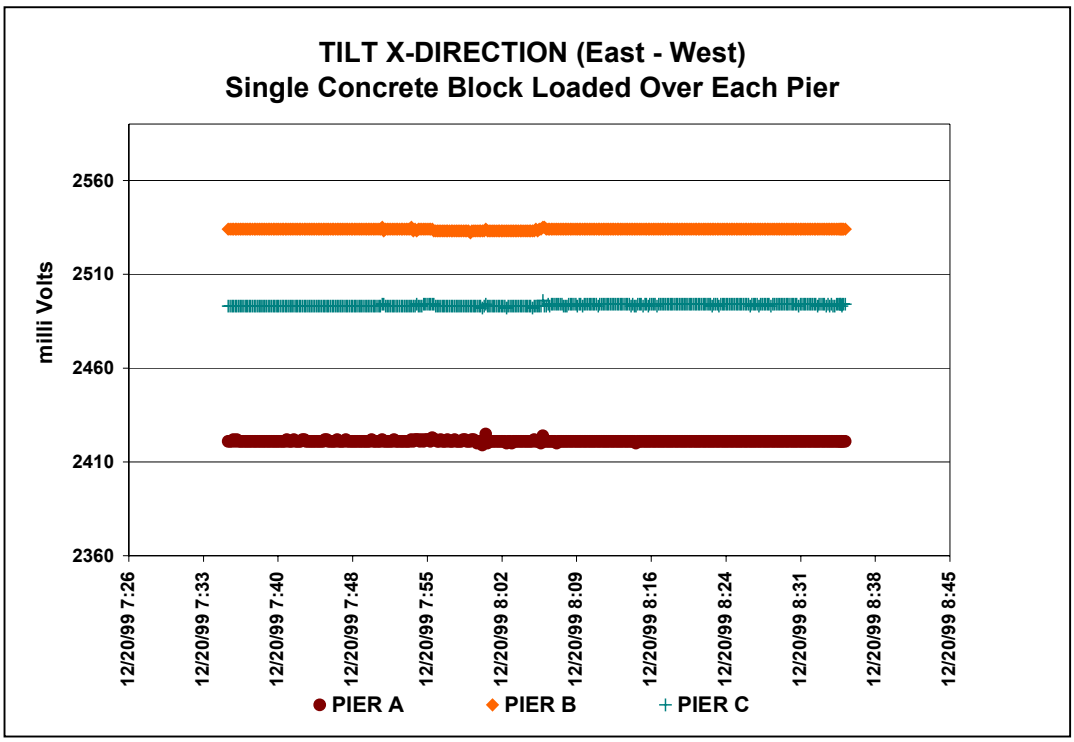

Figure 3.35 Tilt Readings for X-Direction for Single Block over Each Pier

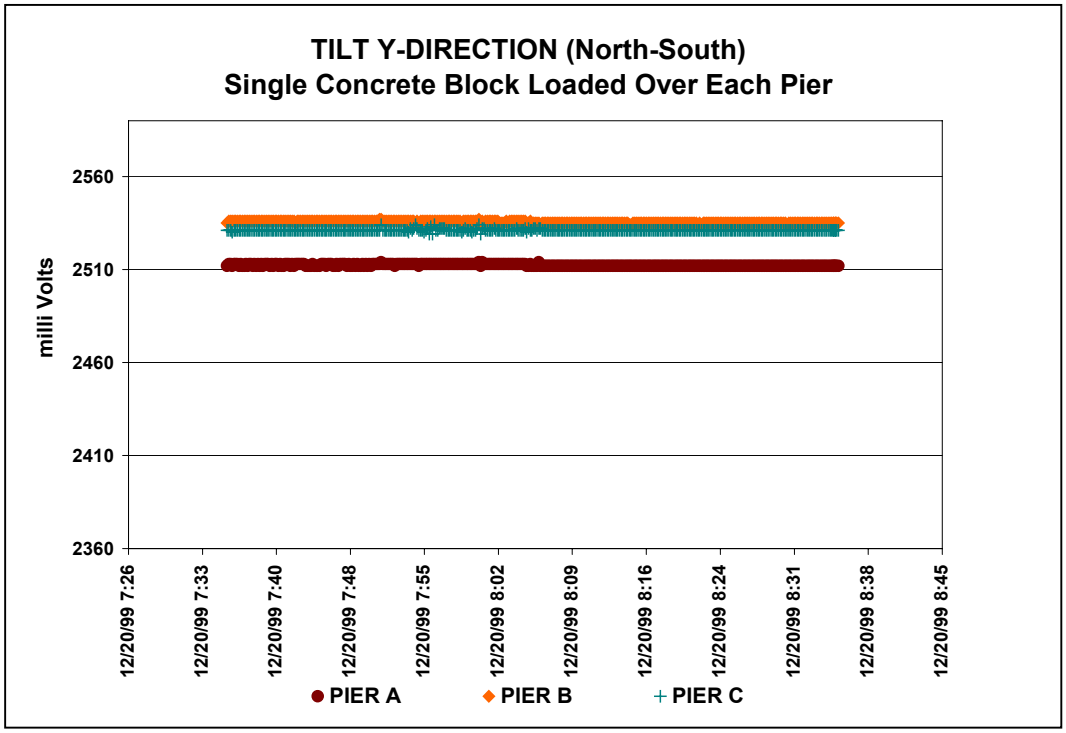

Figure 3.36 Tilt Readings for Y-Direction for Single Block over Each Pier

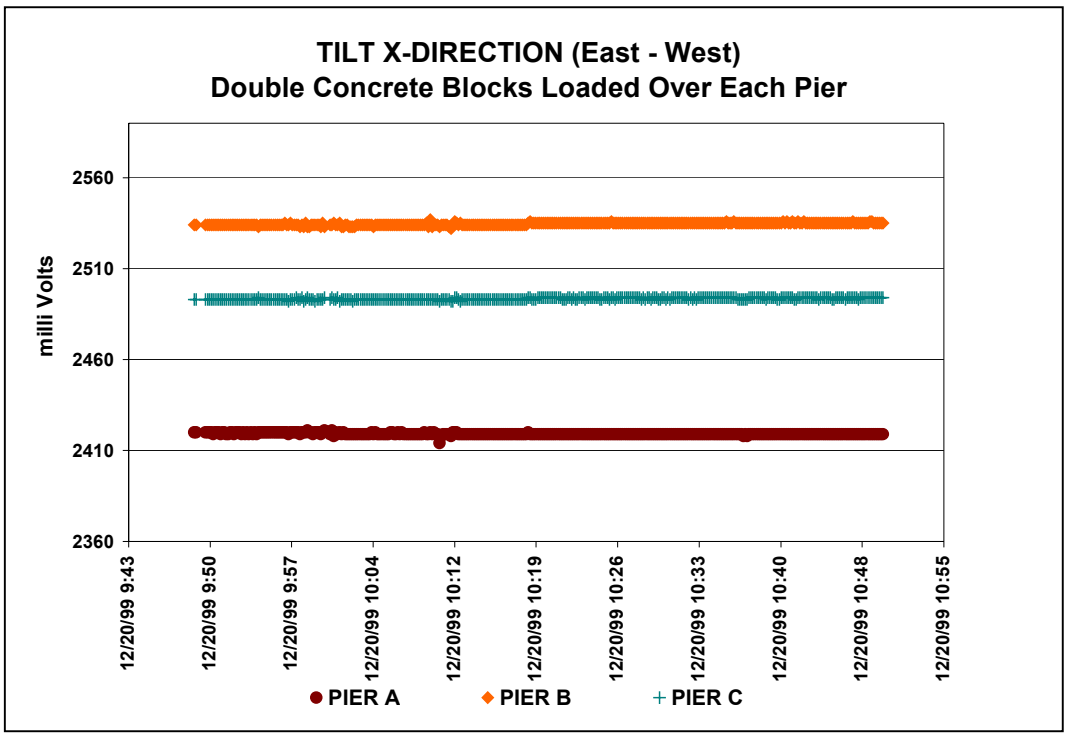

Figure 3.37 Tilt Readings for X-Direction for Two Blocks over Each Pier

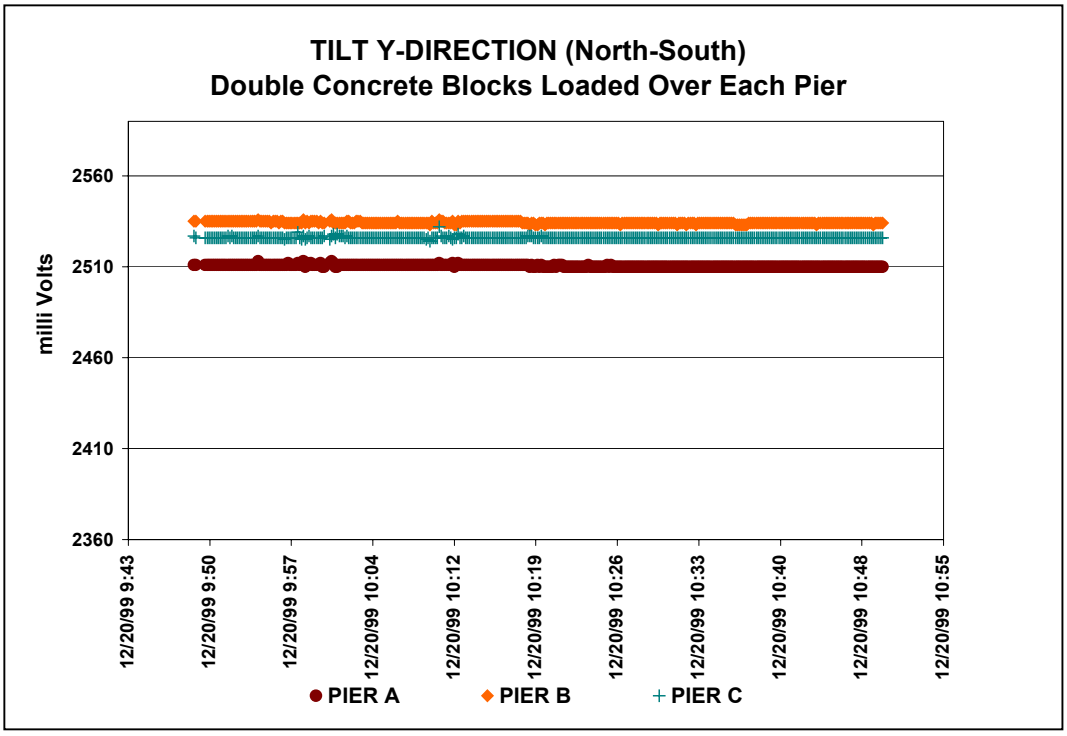

Figure 3.38 Tilt Readings for Y-Direction for Two Blocks over Each Pier

Table 3.7. Initial Tilt Meter Readings at Start of Test

Pier Location	X (mV)	Y (mV)
A	2,419	2,537
B	1,889	2,824
C	2,419	2,362

3.4.2 Test at –1°C

Beginning January 3, 2000 the temperatures of the panels were increased to -1°C (30°F) to warm the soil throughout the test cell. The thermistor temperatures were monitored regularly until a uniform soil temperature of approximately -1°C (30°F) was achieved. On March 7, 2000 the "warm frozen ground testing" procedure began using the same sequence as the test at –4°C. The loading portion of the test concluded on May 8, 2000 with the removal of all blocks and the steel plate. The data collection system continued to monitor the readings overnight. No further changes were seen in the data, and the test was discontinued.

While loading the steel plate on March 6, 2000, it came in contact with Pier C, causing it to tilt slightly, by less than 12.5 mm (0.5 in). An attempt was made to straighten the pier while the plate was placed, but the pier moved back out of alignment.

On March 9, 2000 the single center block was placed on the steel plate (Figure 3.39). The data suggested some movement in Pier C, so the test continued until March 13, when it appeared that any movement had stopped and the second block was stacked on top of the first (Figure 3.40). This block arrangement was held until April 5, when the settlement stabilized. Then the single blocks were placed over each pier. When no change was evident in the data, the second layer of blocks was added on April 7 (Figures 3.41 and 3.42). The piers remained this way until May 5, when all blocks and the steel plate were removed from the piers. The data collection system continued to monitor the piers for any rebound. No rebound was present in the data and the test was discontinued.

Results from the tilt meters are given in Figures 3.43 to 3.50. Both measurements in distance and tilt show some activity during the testing. For example Figure 3.42 shows pier A and B moving up 6 and 4 mm (0.24 and 0.16 in) respectively and pier C moving down 5 mm (0.20 in), which does not make sense regarding creep. The tilting of the piers was less than 56mV that is less than one degree.

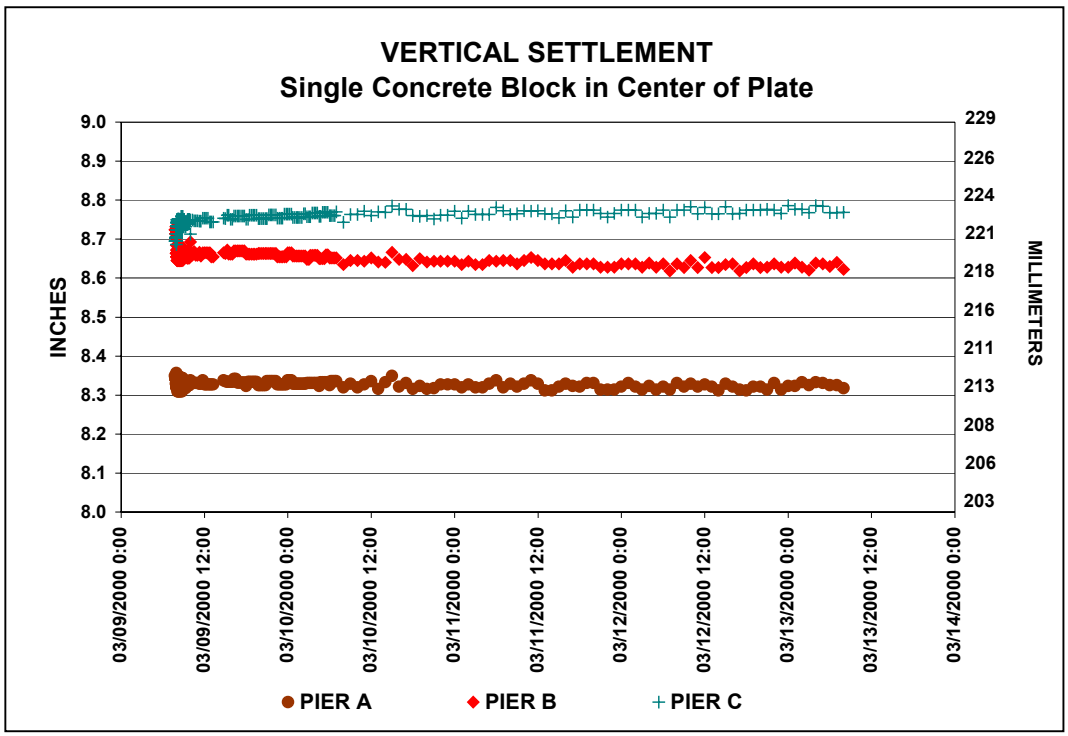

Figure 3.39 Pier Settlement at -1°C with Concrete Block in Center of Steel Plate

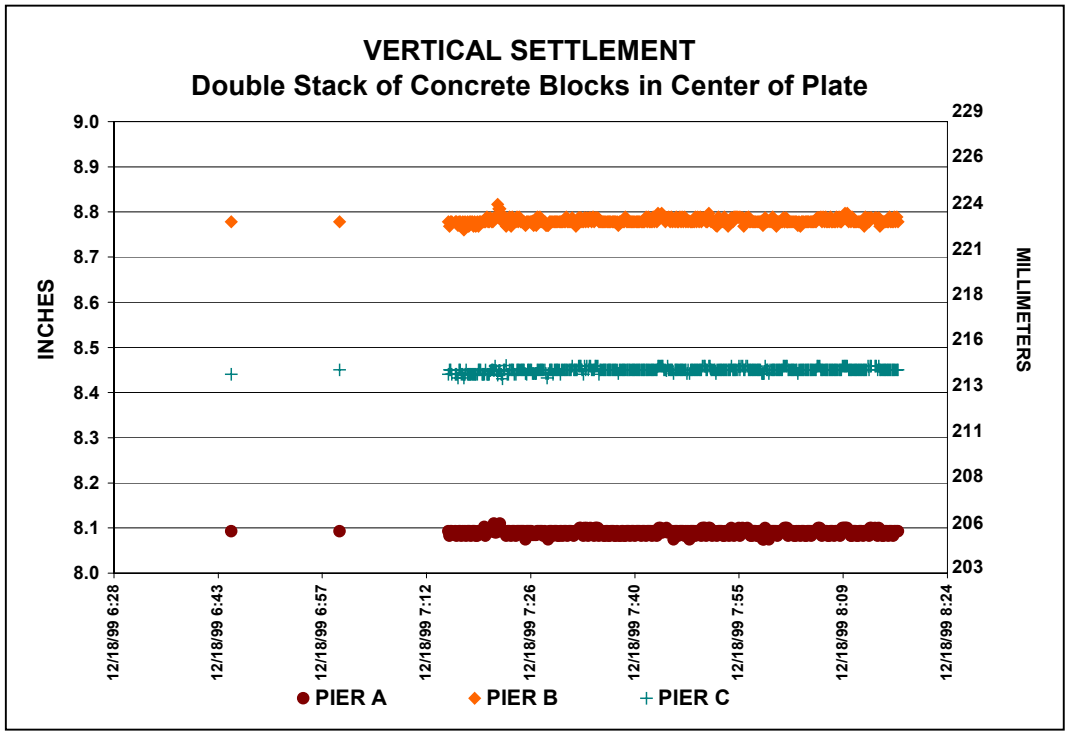

Figure 3.40 Pier Settlement at -1°C with Two Concrete Blocks in Center of Steel Plate

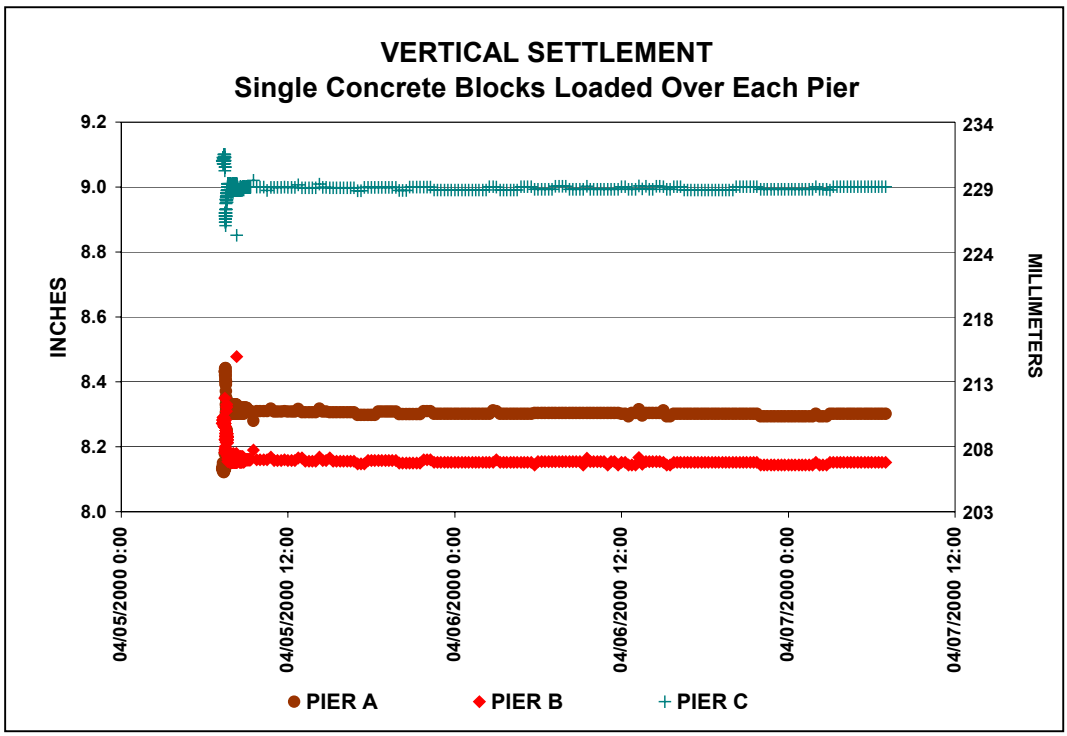

Figure 3.41 Pier Settlement at -1°C with Concrete Block Placed over Each Pier

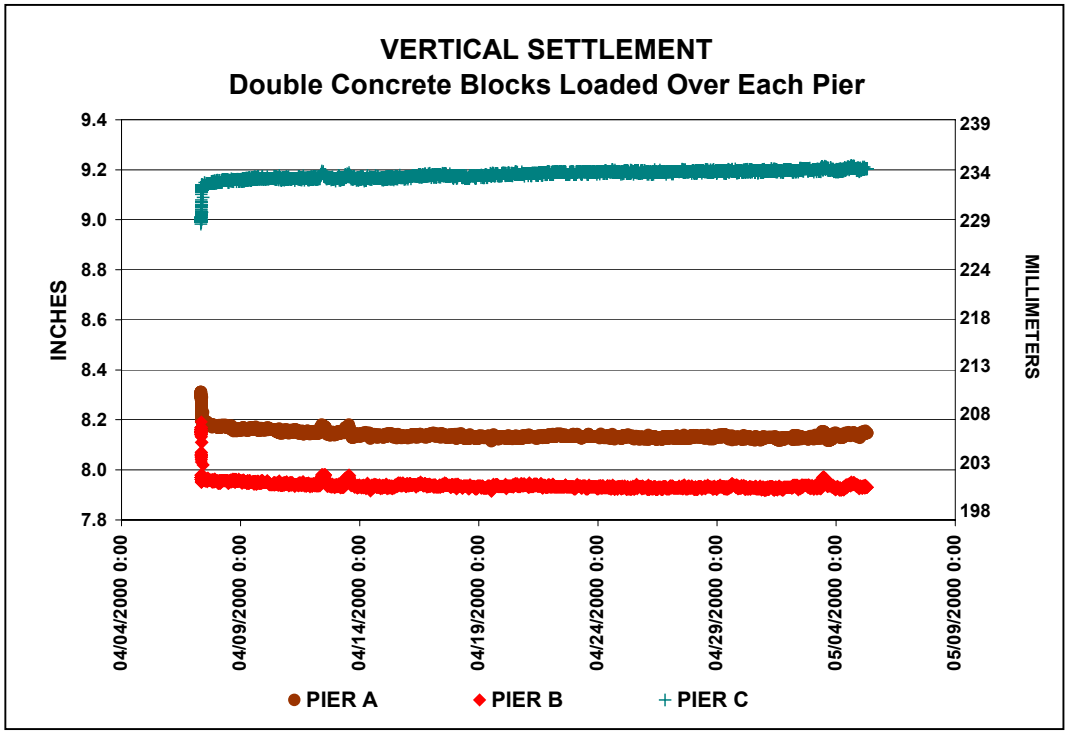

Figure 3.42 Pier Settlement at -1°C with Two Concrete Blocks Placed over Each Pier

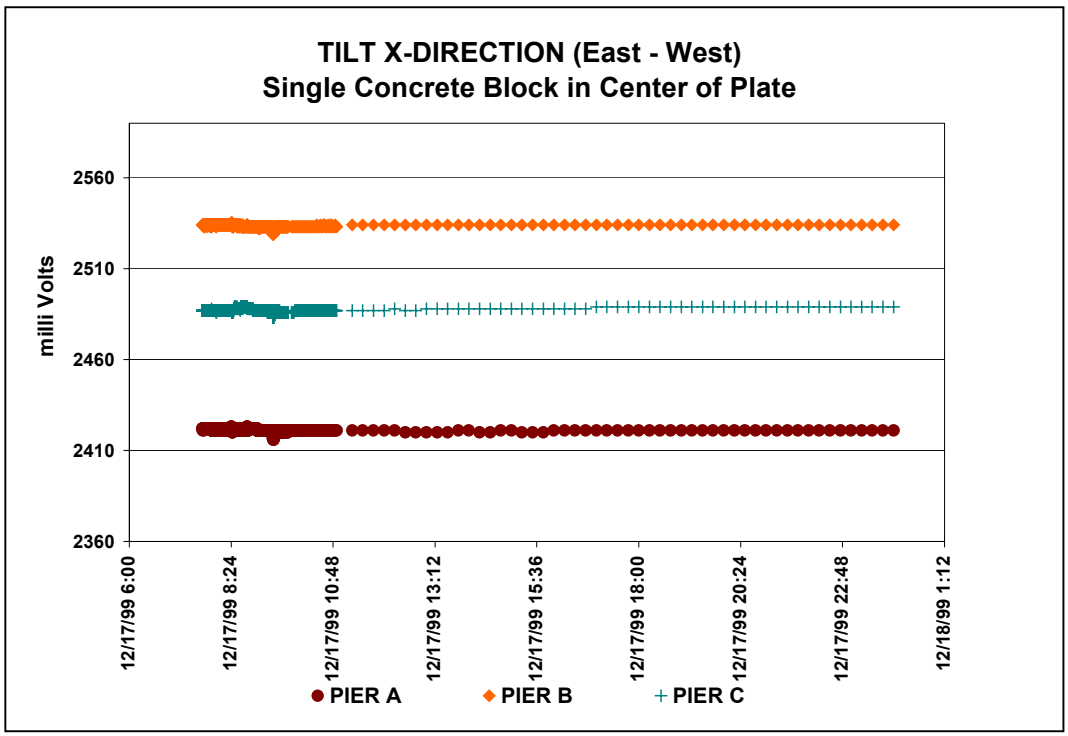

Figure 3.43 Tilt Readings for X-Direction for Single Block in Center of Plate

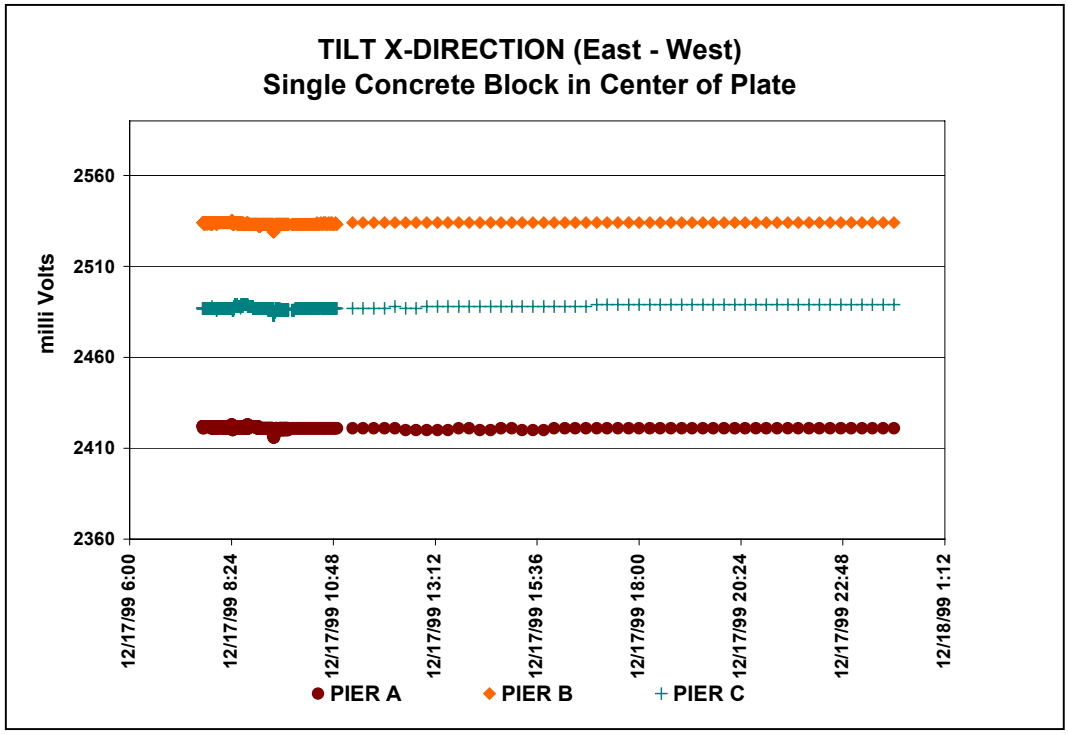

Figure 3.44 Tilt Readings for Y-Direction for Single Block in Center of Plate

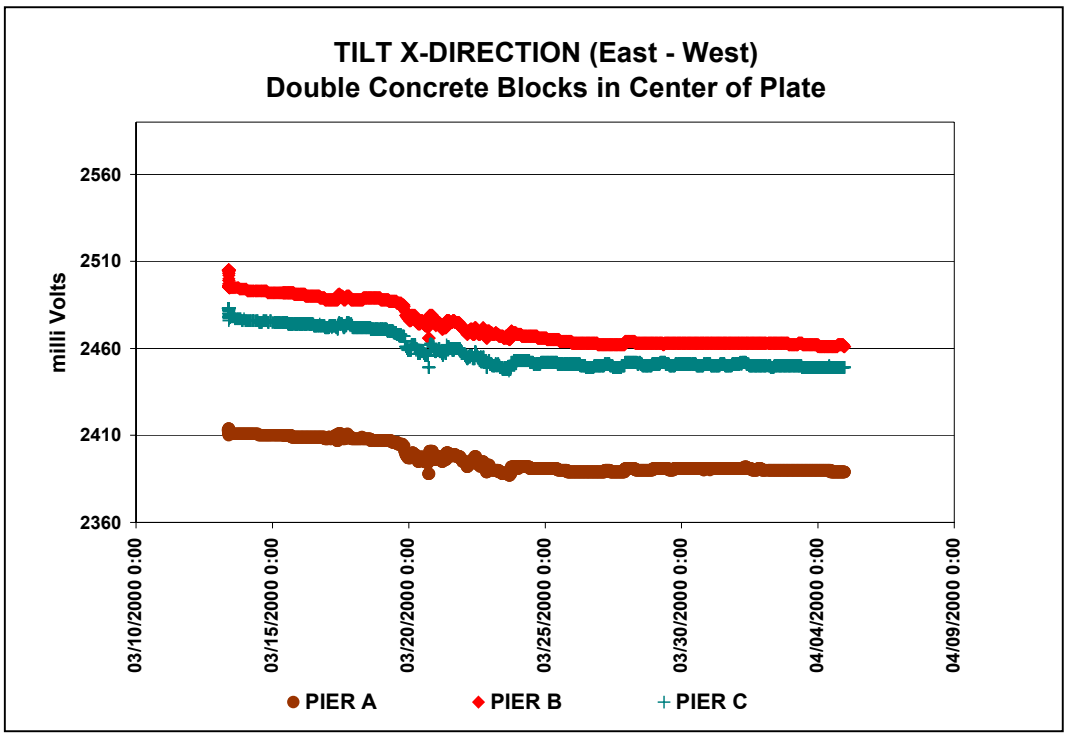

Figure 3.45 Tilt Readings for X-Direction for Two Blocks in Center of Plate

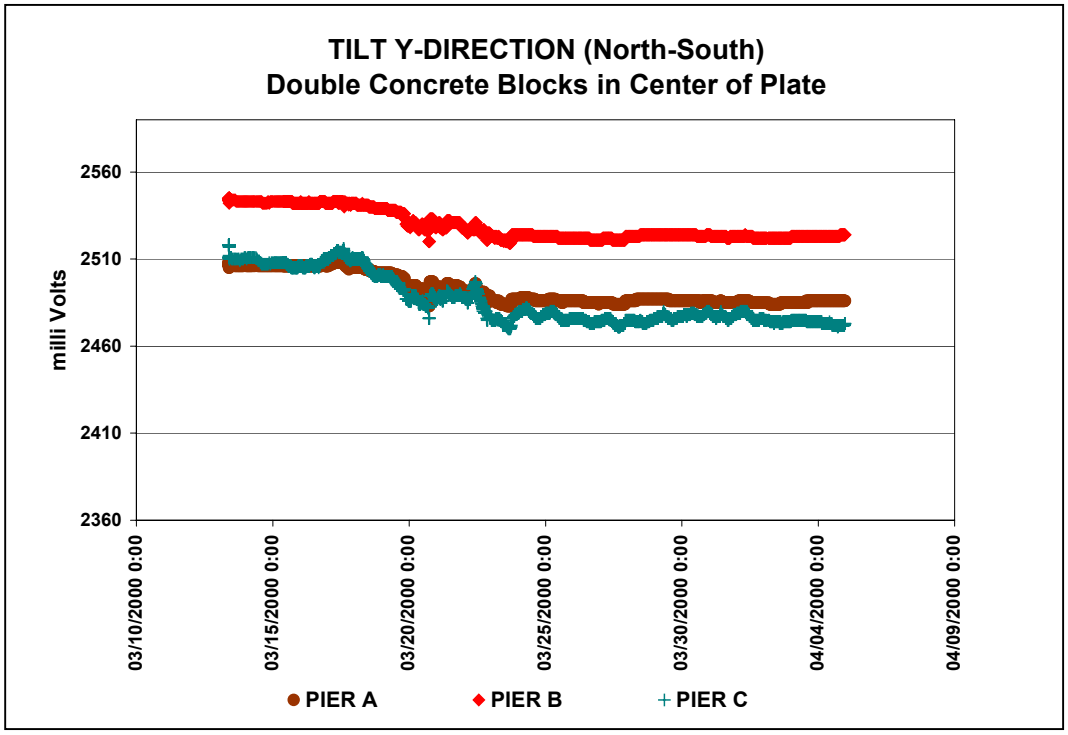

Figure 3.46 Tilt Readings for Y-Direction for Two Blocks in Center of Plate

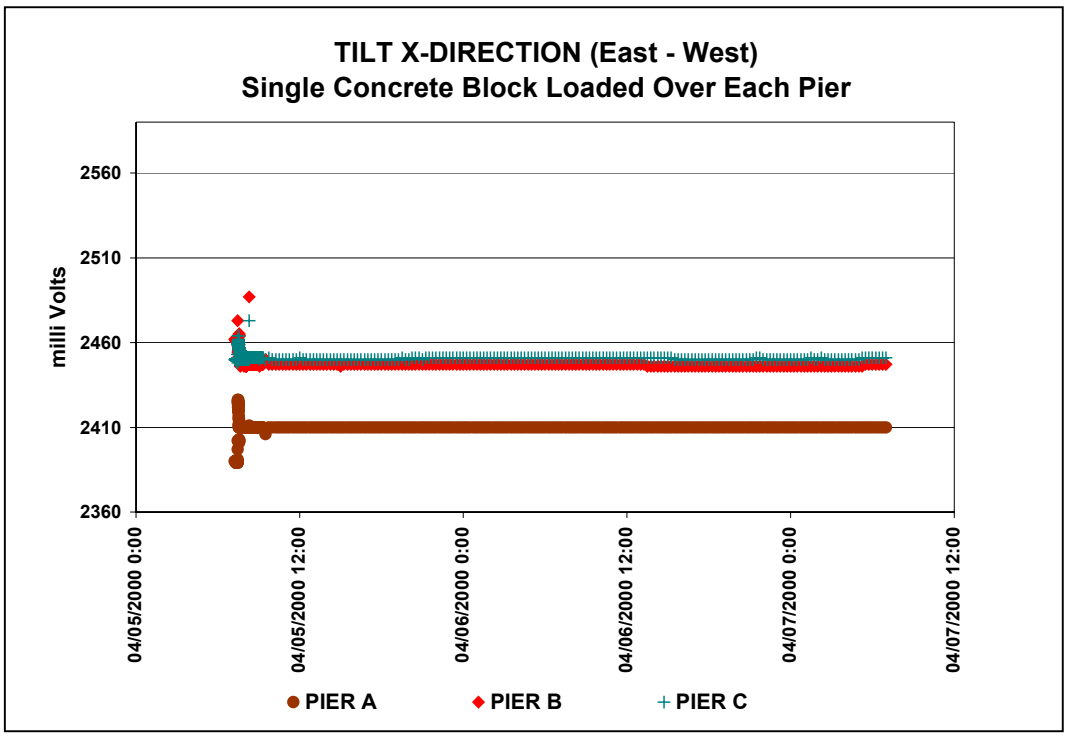

Figure 3.47 Tilt Readings for X-Direction for Single Block over Each Pier

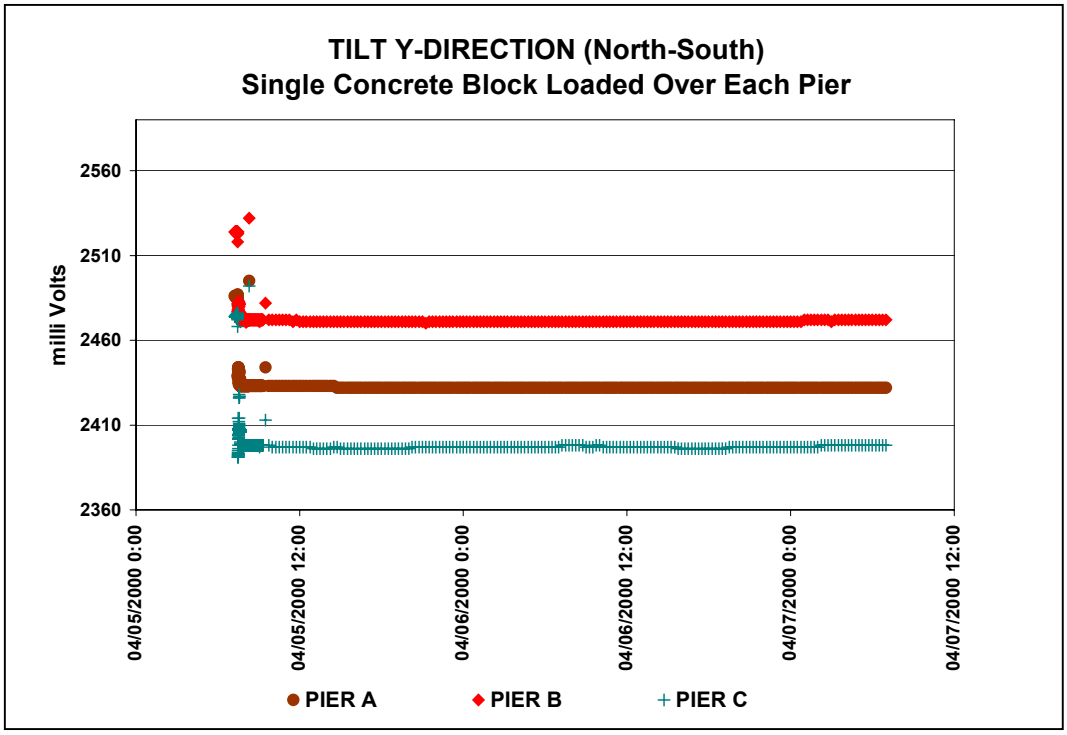

Figure 3.48 Tilt Readings for Y-Direction for Single Block over Each Pier

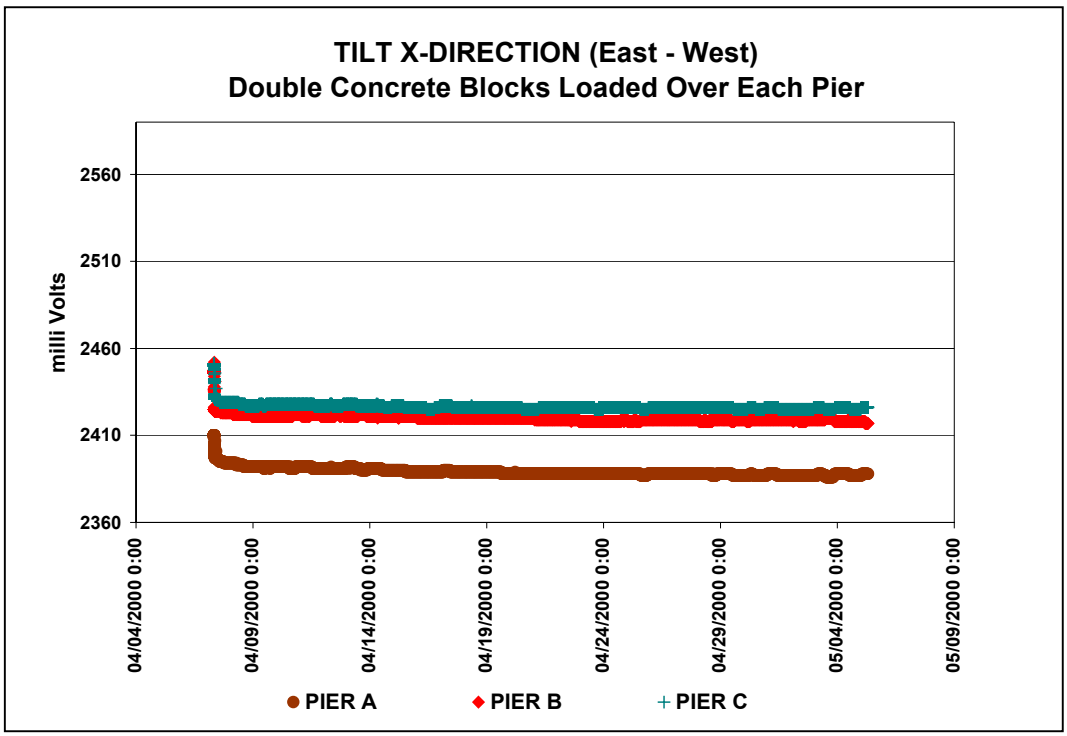

Figure 3.49 Tilt Readings for X-Direction for Two Blocks over Each Pier

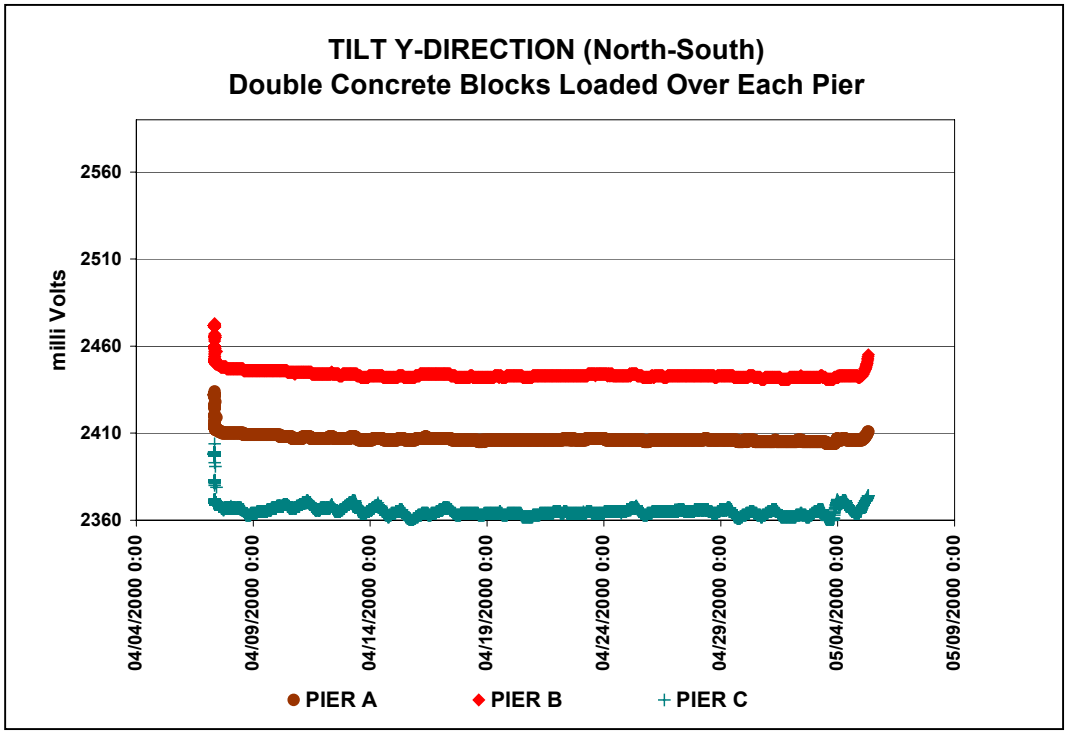

Figure 3.50 Tilt Readings for Y-Direction for Two Blocks over Each Pier

3.5 Conclusions for CRREL Experiment

The following conclusions were drawn from the FERF experiment:

- The piers did not settle or tilt at -4°C.
- The results for the -1°C test indicated some movement, which may be the result of uneven temperatures on the soil basin and partial thaw settlement. The vertical movement of piers was in order of a few millimeters up and down and the piers tilted less than one degree.
- The FEA models could not be calibrated using the test results, because of the uneven temperatures in the test cell and the short loading times.
- Installation of the piers in the frozen ground proceeded without any problems.

3.6 References for CRREL Experiment

AccuStar® II Dual Axis Clinometer, Operating Instructions and Installation Information, North American Operations, Lucas Control Systems, 1000 Lucas Way, Hampton, VA 23666.

U.S. Army Corps of Engineers, 1997, *Technical Instructions: Airfield Pavement Evaluation*, TI 826-01, Engineering Division, Washington D.C.

Sonic OMNI-BEAM™, Banner Engineering Corp., 9714 10th Avenue No., Minneapolis, MN 55441.

4. FIELD STUDY

4.1 Introduction

Helical pier installations have become very common in the past few years in permafrost construction. As their effectiveness, particularly in ice-rich areas, has been demonstrated their utilization has become routine.

Table 4.1 lists examples of some of the helical pier installations in permafrost in "Bush Alaska" in the past few years. Piers have been used as foundations in frozen ground for a variety of construction projects, boardwalks, fences, utilidors, and arctic pipe. As evident from Table 4.1, thousands of helical piers are currently installed in Alaska. The primary sources for this field information are the State of Alaska Department of Environmental Conservation Village Safe Water (VSW) and the Alaska Native Tribal Health Consortium, Department of Environmental Health and Engineering (ANTHC, DEHE).

Table 4.1 Examples of Helical Pier Installations in Rural Alaska

Year	Location	Comments
1996	Kiana	Fence installation, pilot hole and backhoe, Chance piers
1998	Selawik	Fence, 1,224 Dixie brand piers
	Noorvik	Arctic pipe installation, 500 piers
1999	Selawik	Fence, 2,400 piers
	Tuntutuliak	Boardwalk to sewage lagoon
2000	Chignik	Fence around lagoon, 24 piers, not a permafrost area
2001	Eek	Planned sewage lagoon fence, 180 piers
	Selawik	Arctic pipe and service lines to homes, 500 piers
2000/2001	Chefornak	Boardwalk, summer installation with skid loader

4.2. Installations

Helical piers can be installed any time of year. Installation is usually easier in the fall when the ground is frozen before significant snow buildup. Summer installation in wet areas can be challenging due to the soft ground and surface water. Installation in wet areas can be conducted with ground mats and proper selection of the installation equipment.

Piers are installed by auguring them into the ground. Typically, a backhoe or skid loader is used with a rotating power head. The rotating head can be a specially designed tool or can be made by modifying an existing rotating head. The amount of vertical force necessary depends upon the soil conditions and the temperature of the permafrost and must determined in the field by the installer. Colder, rockier soils require more pressure to be applied to the pier as it is augured.

Neither VSW nor ANTHC drill pilot holes for the piers. For some of the first pier installations pilot holes were air-drilled to ensure that the piers would be straight and plumb. Installers have found that piers can be installed correctly without pilot holes (Dixon, 2001).

Design factors typically used are relatively simple. Besides load determination the critical factor is the depth of the active layer. If the pier helix is founded well below the active layer a solid, long lasting foundation is almost certain. The diameter of the steel rod portion of the pier is too small to provide enough surface area for heaving soils to lift the pier. Therefore, piers remain in place without any displacement or jacking.

Utilidors and arctic pipe are traditionally installed on grade or on posts with a short life expectancy. Heat loss from on-grade utilidors melts the permafrost within a few years causing displacement of the utilities that often makes them unusable. Figure 4.1 and Figure 4.2 show typical on-grade utilidors. Posts also perform poorly in frozen ground because of jacking. Therefore, the VSW and ANTHC prefer helical piers as foundations for gravity and vacuum sewage lines in arctic pipe. Grade is critical for these sewage lines and helical piers have provided a long-lasting, stable foundation in cold, ice-rich permafrost without requiring adjustment.

More and more helical piers are used for non-frost jacking fence post anchors. They have higher initial cost than posts with lateral supports laid on grade, but the longer service life and reduced maintenance operations makes them an economical foundation. The use of helical piers could revolutionize housing foundations in permafrost as well as seasonal frost areas. The characteristics, such as ease and speed of installation, no curing time and no frost jacking make helical piers very attractive foundations and it is only a question of time when they full potential is realized.

Figure 4.1 Utilidor on Grade in Permafrost Area, Noorvik, Alaska (ANTHC, DEHE)

Figure 4.2 Damaged Utilidor on Grade, Noorvik, Alaska (ANTHC, DEHE)

4.3 Field Applications

ANTHC has utilized helical piers in numerous installations throughout rural Alaska. Examples in this report are in the villages of Noorvik, Kiana, and Selawik in northwest Alaska near Kotzebue Sound where permafrost is continuous and considered cold. These villages can be located on the map in Figure 4.3.

Figure 4.3 Location of Villages in State of Alaska (Grolier Encyclopedia, 2001)

Helical piers are the foundation for the arctic pipe installation in Noorvik. Originally, the sewage pipes were in a utilidor on grade. Noorvik is in a very ice-rich permafrost area, 50 to 400% ice, and the on-grade installation caused severe thaw subsidence and chronic malfunctions of the vacuum sewage line. In 1998, new arctic pipe was installed using helical piers with tremendous success. The grade-sensitive sewage vacuum system has operated as designed. Photos of the installation at Noorvik are shown in Figure 4.4 and Figure 4.5. Figure 4.6 is the finished utilidor installation in Noorvik.

Figure 4.4 Helical Piers in Noorvik, Alaska Installed as Foundations for Arctic Pipe Sewage Installation.
The Arctic Pipe Contains a Vacuum Sewage Line. (ANTHC, DEHE)

Figure 4.5 Arctic Pipe with Helical Piers as a Foundation in Noorvik, Alaska (ANTHC, DEHE)

Figure 4.6 Finished Utilidor on Helical Piers in Noorvik, Alaska (ANTHC, DEHE)

Typical installations consist of a 1.68 m (5.5 ft) pier with a 2.13 m (7 ft) extension. The active layer in the Noorvik area is about 0.6 m (2 ft) thick and this pier length has proven to be adequate to firmly anchor in the permafrost. The pier is screwed in until a stub is left at the surface and the post or tubing that is necessary for the construction is bolted to the stub. Figure 4.7 and Figure 4.8 are the details for typical pier installation and supports. These designs were used in Noorvik.

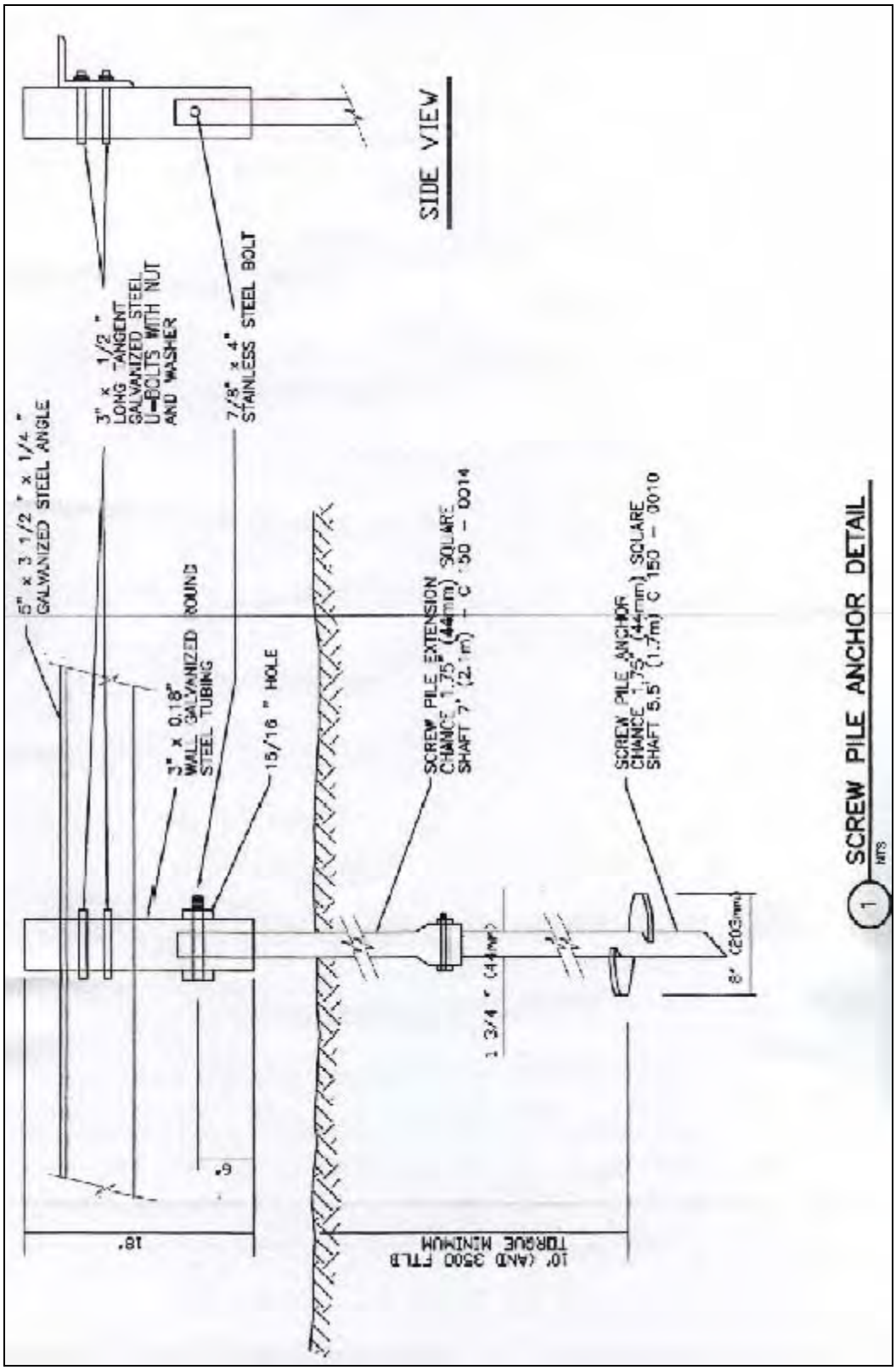

Figure 4.7 Typical Pier Detail (ANTHC, DEHE)

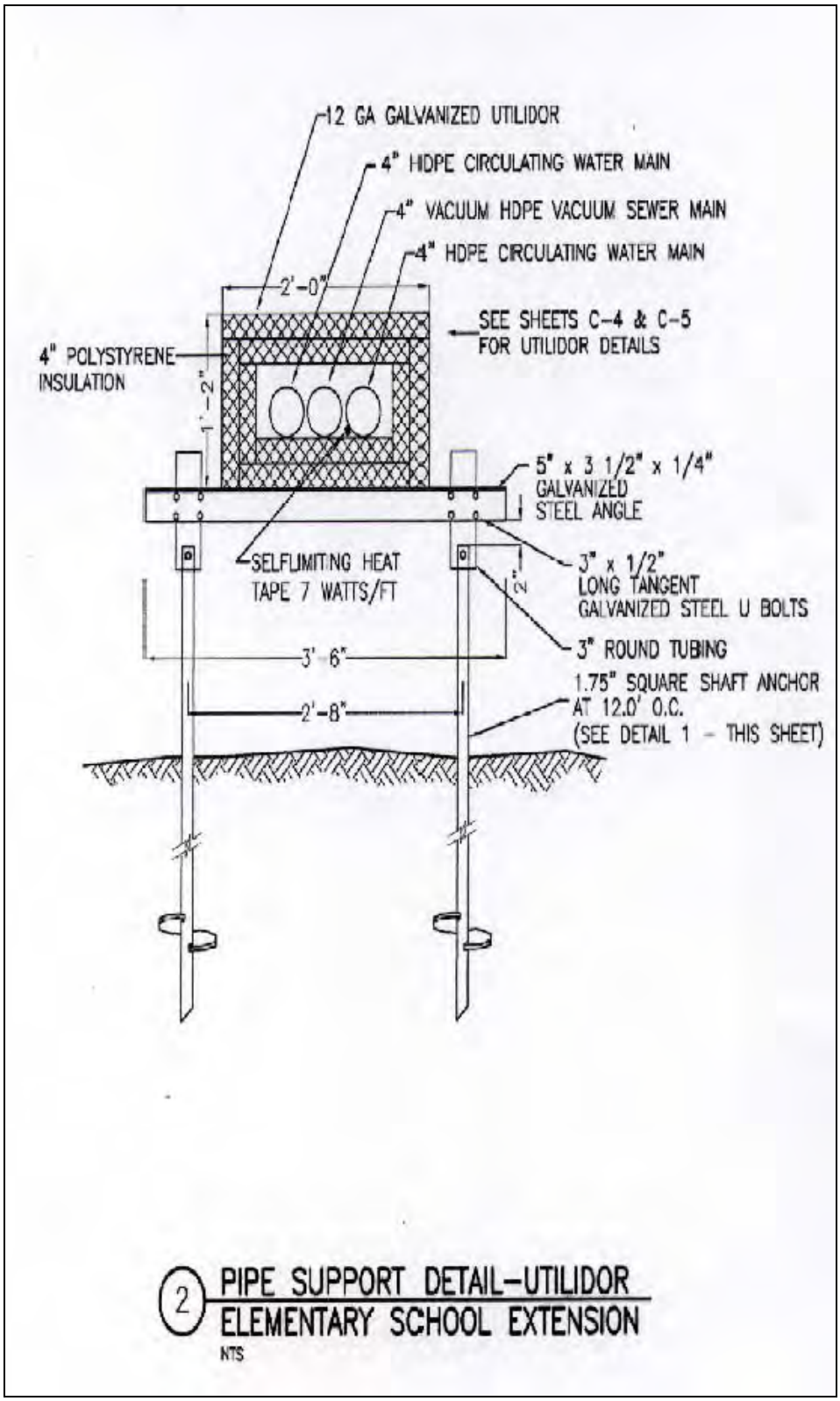

Figure 4.8 Typical Detail for Helical Piers as Used in Noorvik for the Utilidor and Arctic Pipe Installation (ANTHC, DEHE)

The village of Kiana is built on cold, ice-rich permafrost. An extensive fence project was built in 1996 using helical piers as the foundation for the posts. As of this writing (December, 2001) the piers remain straight and plumb. The fence is shown in Figure 4.9 in a photo taken in 1998. The installation for the fence piers are the same as for the utilidors with line or corner posts bolted to the pier shafts.

Figure 4.9 Fence Constructed in Kiana in 1996 (ANTHC, DEHE)

VSW has projects in several villages in the Kuskokwim Delta. Permafrost in this area is warm and discontinuous. Pier installations have been very successful when compared to traditional techniques. But, because of the nature of the discontinuous permafrost and variations in the depth of the active layer there are more instances of jacking or heave of the piers.

In Chefornak, helical piers were used to construct a boardwalk during summer. A skid loader with a drive head installed the piers while advancing along the boardwalk as it was constructed. Construction advanced across the swampy area in 1.8 m (6 ft) segments (Menough, 2001). The boardwalk in Chefornak will have piers replaced in the next year; they were not installed deeply enough. Inconsistent soils and thus a great variation in active layer depth in the area are the likely cause of the problem. Figure 4.10 and Figure 4.11 show the installation of the Chefornak boardwalk.

Figure 4.10 The Summer Installation of the Boardwalk in Chefornak. (VSW)
The Power Head on the Skid Loader Used to Install the Piers can be seen at the Right.

Figure 4.11 Installation of the Boardwalk in Chefornak (VSW)

In the village of Tuntutuliak helical piers are the foundation for a boardwalk. Tuntutuliak is subject to fall flooding caused by tidal surges with high winds. The boardwalk itself has not endured the flooding well. The piers have been very stable with the exception of a few located in the transition area between the permafrost soils and a lagoon. In that area the piers were not installed deeply enough. The active layer thickness is much greater in the area closer to the lagoon (Burleigh, 2001).

4.4 Conclusions for Field Study

Helical piers have been used in a variety of projects in frozen ground in rural areas of Alaska. They have been successful when installed deep enough below the active layer into the permafrost. They have carried the applied loads without failures and resisted the forces of heaving and jacking.

Installation of helical piers is more expensive than installation of utilities on grade or on posts. However, since these traditionally used methods are simply not working, the long-term performance of helical piers justifies the expense, particularly, for grade-sensitive structures (Dixon, 2001).

4.5 References for Field Study

Burleigh, Roger, November 2001, Interview, State of Alaska DEC-VSW.

Dixon, Matthew, November 2001, Interview, ANTHC.

Grolier Encyclopedia, 2001, *Multimedia Encyclopedia Deluxe Edition,* Scholastic.

Menough, Jon, December 2001, Interview, State of Alaska DEC- VSW.

Schubert, Dan, November 2001, Interview, GV Jones & Associates.

5. DEVELOPMENT OF FINITE ELEMENT MODEL

5.1 Introduction

Helical piers come in different types and shapes. Typical configurations of helical piers are shown in Figure 5.1. Current design methods for determining the capacity of helical piers are based upon very simple formulas that assume uniform stress distribution on helixes (Figure 5.1). These formulas may or may not be conservative (Equation 2.1, Figure 2.1). Some research has been conducted to describe the overall capacity and displacement of helical piers subjected to vertical and lateral loading (Narasimha Rao and Prasad, 1993, Prasad and Narasimha Rao, 1996, and Ghaly et al., 1991). Much less has been done to examine the distribution of stresses in the soil surrounding these piers, their behavior under prolonged loading in frozen ground, or the stresses within a typical helical pier during installation or under normal working loads.

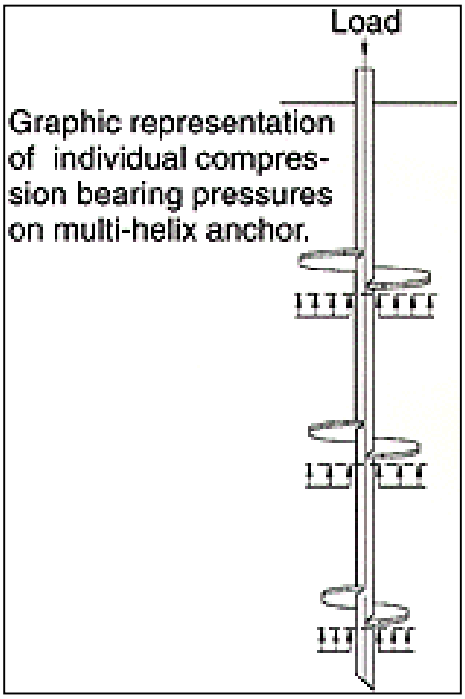

Figure 5.1. Simplified Distribution of Bearing Pressure (A. B. Chance Co. 1996)

The purpose of developing Finite Element Analysis (FEA) models is to investigate the behavior of helical pier foundations in frozen ground. Problems related to frozen ground include the risk that the piers will break during the installation, instantaneous strength, stability failure, and long-term creep failure in the frozen ground.

The complex geometry of helical piers is modeled precisely. Four objectives were established to complete this study:

1) Analyze displacement and stress distribution in frozen soil due to an axial load (instantaneous failure mode),

2) Analyze the stresses within the pier structure when it is subjected to this load, (instantaneous failure mode),

3) Provide a detailed analysis of the stresses within the pier during installation (installation failure mode),

4) Investigate long-term creep settlement behavior in frozen ground (excessive settlement failure mode).

A FEA program, called ANSYS, was chosen to model all four of these situations for its ability to model complex, nonlinear, three-dimensional conditions. The following four components were needed to do this:

1) Large Model: This model will analyze the soil stresses and displacements immediately after the pier is subjected to its design load. This data is also critical for the development of more detailed analysis using sub-modeling techniques.

2) Small Model: The small model is a sub-model of the large model. It will analyze the stresses developed within the spiral structure by using results from the large model analysis.

3) Installation Failure Model: A detailed model of the spiral structure subjected to a torsional load during installation will provide insight into the failure mechanism of helical piers during construction.

4) Creep Model: Creep analysis will be conducted to determine the long-term displacement and soil stress in frozen ground.

The FEA program ANSYS provides a variety of functions and features for modeling of complicated conditions. However, little data exists for the displacement of helical piers and the surrounding soil when subjected to axial compressive loads. Therefore, it was planned that these results would be compared with physical tests to be conducted at the U.S. Army Corps of Engineers Cold Regions Research and Engineering Laboratory (CRREL) in Hanover, New Hampshire. The analysis results will be used to develop installation guidelines, and to create design curves for frozen ground in the future design work.

5.2 Basic Assumptions for Finite Element Analysis

The following sections describe the needed material properties and basic assumptions used in the analysis.

5.2.1 Geometric Considerations

The three-dimensional elements consist of several parts, a cylindrical soil column, a circular steel plate that represents the pier itself, and finally a steel pipe that represents the shaft

from the pier to the top of the soil. A three-dimensional analysis was chosen because it allows the general results to be applied to a sub-model with more specific geometry.

In the Large Model and the Creep Model a cylinder-shaped column of soil was chosen because it is the easiest volume of soil to model in a cylindrical coordinate system. Based on the Theory of Elasticity, the physical size of the soil column was based on the vertical stress distribution under the center a circular plate. Since the soil column cannot be modeled as an infinite space, such as the actual Earth, the model was designed to allow the stress in the soil to fully develop with stress distribution at the bottom of the volume being less the 1% of the assumed uniform distributed pressure beneath the helix. This guarantees that the fixed boundary conditions at the bottom of the model will have a negligible effect on results. Thus for a 203 mm (8 in) diameter helix, a soil minimum depth of 1,245 mm (49 in) is required under the pier to achieve desired stress, strain and deformation levels. However, to further guarantee no interference from the boundaries a depth of 2,286 mm (90 in) was selected. This resulted in a theoretical maximum vertical stress only 0.30% of the assumed uniform distributed pressure beneath the helix. Furthermore, the additional depth helped create a convenient geometric expansion of the model element sizes. The 1,626 mm (64 in) diameter of the cylinder was established in a similar manner. A steel circular plate was chosen over an actual helix because the general behavior is the same and a circular plate saves considerable time in model development and actual analysis time. Also, steel pipe models the actual load-bearing element, and is used to transmit the load from the soil surface to the pier.

5.2.2 Frozen Soil Material Properties and Yield Criteria

In addition to the geometry of the model, physical properties of the soil had to be included in the model. A basic elastic-plastic model is used to represent the response of frozen soil. The frozen-soil parameters used in the model development are given in Table 5.1.

Table 5.1. Soil Parameters Used for Development of Models

Youngs Modulus	MPa	1,800
	ksi	261
Poisson's Ratio		0.35
Unit Weight	kN/m^3	20
	pcf	130
Friction Angle		20
Cohesion	kPa	34.5
	psi	5

The program used allows for numerous methods for non-linear analysis. The Drucker-Prager yield criterion was used to describe the yield surface for the soil elements and to most accurately model the three-dimensional elastic-plastic properties of the soil. The Drucker-Prager criterion is preferred because it accounts for internal friction angle as well as cohesion, which allows hydrostatic stress to have an influence on yielding using the outer cone approximation to the Mohr-Coulomb law. The criterion creates a yield surface for the principal stresses within the

soil volume that is based on the internal friction angle of the soil and its cohesion. The material response is elastic-perfectly plastic. The yield surface is defined in Figure 5.2. The material constant is:

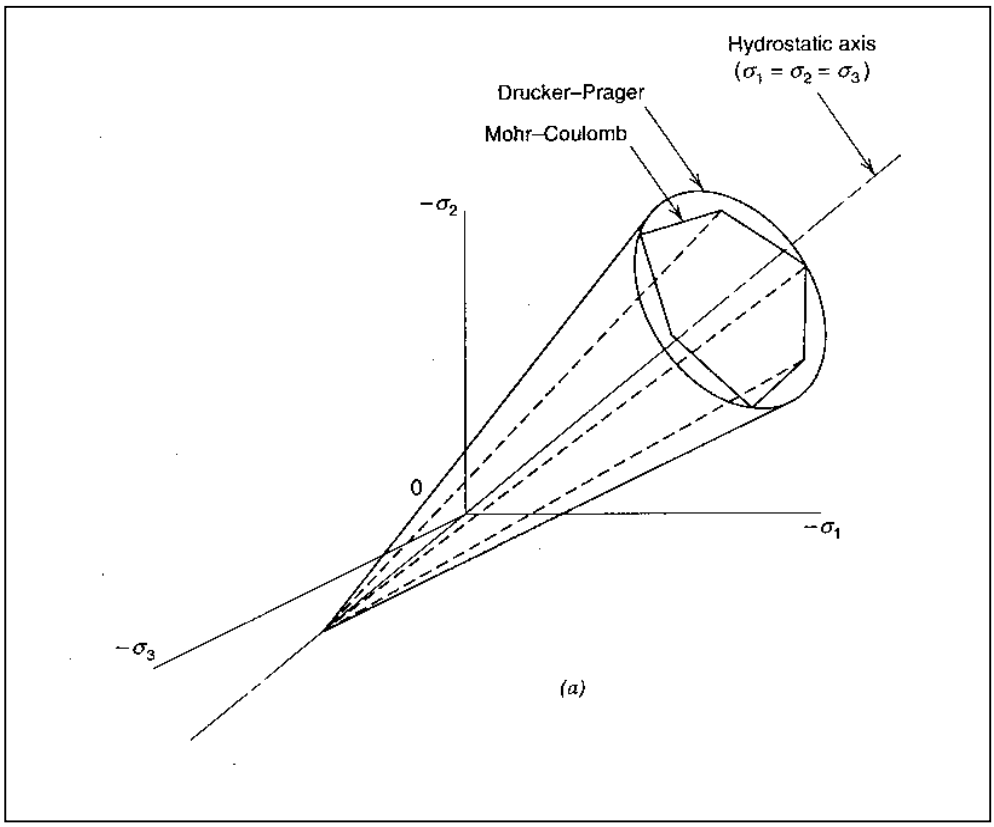

Figure 5.2 Drucker-Prager Circular Cone Yield Surface

$$\beta = \frac{2\sin\phi}{\sqrt{3}(3-\sin\phi)} \qquad \text{Equation 5.1}$$

where ϕ = the angle of internal friction.

The material yield parameter is:

$$\sigma_y = \frac{6c\cos\phi}{\sqrt{3}(3-\sin\phi)} \qquad \text{Equation 5.2}$$

where c = the cohesion value for the material.

The yield criterion is:

$$F = 3\beta\sigma_m + \left[\frac{1}{2}\{s\}^T[M]\{s\}\right]^{\frac{1}{2}} - \sigma_y = 0 \qquad \text{Equation 5.3}$$

where $\{s\}$ = the deviator stresses,

$$\sigma_m = \frac{1}{3}(\sigma_x + \sigma_y + \sigma_z) \text{ , and} \qquad \text{Equation 5.4}$$

[M]= a constant scalar matrix.

5.2.3 Steel Material Properties and Yield Criteria

The spiral and central column were modeled using the material properties for steel - Bilinear Isotropic yield criteria. Figure 5.3 shows the concept of the material model. When stress in steel is lower than the yield level, the behavior of steel is linearly elastic. The bi-linear isotropic yield criteria are for the plastic behavior when stresses in steel reach the yield level. In the FEA models, the following parameters were used for the bi-linear yield surface:

σ_y = 345 MPa (50 ksi)
E = 200,000 MPa (29,000 ksi)
E_t = 10,000 MPa (1,450 ksi)

A typical geometry chosen for a pier includes a 76 mm (3 in) outer diameter pipe section with 13 mm (0.5 in) wall thickness for the pipe; and a 254 mm (10 in) diameter, 13 mm (0.5 in) thick plate for the spiral. In the Large and Creep Model, the spirals were modeled using flat plates, which did not account for any pitch that would be present in the actual conditions. This was done to limit the overall number of elements in the large models and to simplify model construction. The effect of pitch was assumed to be negligible in determining the overall capacity of a pier. The element and material properties used in these models appear in Table 5.2.

Table 5.2. Pier Properties and FEA Parameters

Material	E (MPa)	ν	ρ (kN/m^3)	Element Type	Nodal DOF
Steel shaft	200,000	0.3	77.0	Beam	6
Steel plate	200,000	0.3	77.0	Shell	6

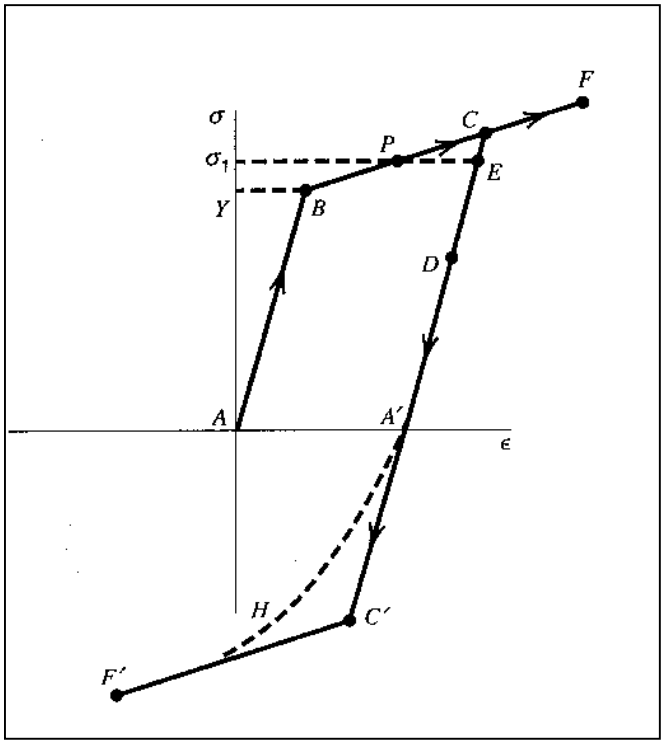

Figure 5.3 Bi-linear Isotropic Material Non-linearity

5.2.4 Creep Formula and Parameters

To analyze the effects of creep, a creep formula was used with the addition of creep parameters to simulate secondary creep effects over a period of time. The creep equations were determined based on previous research by Ladanyi and Johnston (Johnston and Ladanyi, 1974; Ladanyi and Johnston, 1974; and Ladanyi, 1983), and were selected to provide an upper bound for creep effects. The creep formula is as follows:

$$\dot{\varepsilon}_e = \dot{\varepsilon}_c \left(\frac{\sigma_e}{\sigma_{cu\theta}} \right)^n \qquad \text{Equation 5.5}$$

Where: $\dot{\varepsilon}_e$ = reference strain rate,
n = creep parameter,
σ_e = equivalent stress,
$\sigma_{cu\theta}$ = creep modulus corresponding the reference strain rate.

5.3 Sample Analyses on Stress, Strain and Deformation for Helix and Soil

The following sections contain examples of the work to describe how the analysis was conducted.

5.3.1 Soil Stress-Strain and Deformation Analyses – Large Model

Two large-scale models were created using a cylindrical volume of soil with a helical pier at the center: 1) Test Model to simulate the testing conditions at the CRREL, and 2) Deep Model to simulate conditions in the field. The soil cylinder of the Test Model had an overall diameter of 1,270 mm (50 in) and an overall depth of 3,048 mm (120 in). The Deep Model was used to investigate the effects of boundary interactions within the model. In this model the diameter remained 1,270 mm (50 in), but the depth was extended to 5,588 mm (220 in). In both models, the pier's total embedded depth was 2,286mm (90 in) and each had two 254 mm (10 in) diameter helices spaced 762 mm (30 in) apart.

The geometry chosen for the pier includes an 89 mm (3½ in) outer diameter pipe section with 13 mm (½ in) wall thickness for the shaft; and a 254 mm (10 in) diameter, 13 mm (½ in) thick plate for the spiral. For this large-scale model, the spirals were modeled using flat plates. This was done in order to limit the overall number of elements in the model.

Figure 5.4 shows the geometry of the Test Model (Figures a and b are given in different scales for convenient viewing). A three-dimensional brick element was used to represent soil. The FEA mesh was carefully designed to keep all bricks in good shape/aspect ratio, and to provide reasonable connection with soil model while granting efficient computational time.

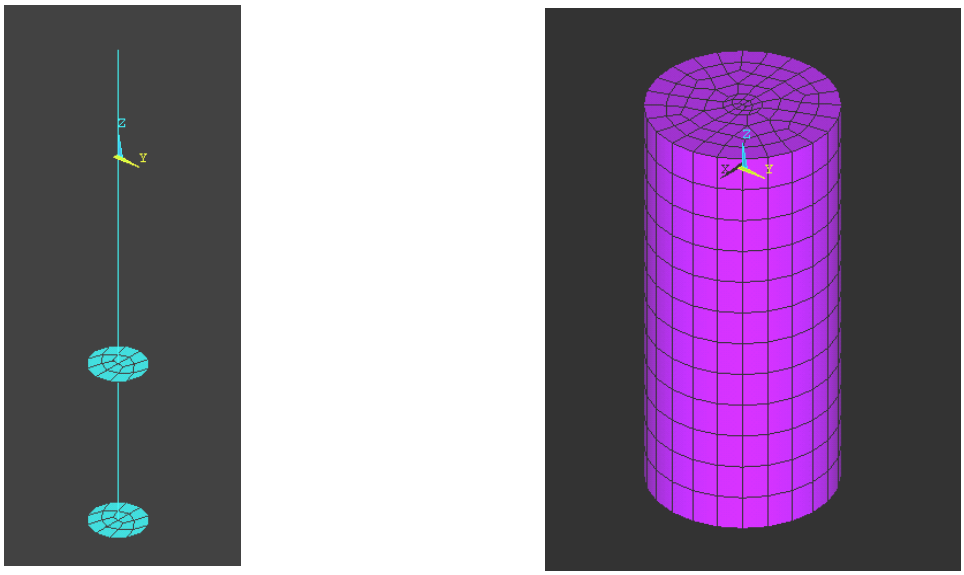

(a) FEA Model of Helical Piers (b) FEA Model of Soil Volume

Figure 5.4 FEA Meshes for Helical Piers and Soil Volume (not in same scale)

Boundary conditions for Test and Deep Models included translational restraint in the horizontal directions for the sides of the soil cylinder and full restraint for the bottom of the soil cylinder.

Figure 5.5 shows the vertical soil displacement from the sample calculation for the Test Model due to an ultimate axial load of 89 kN (20 kip). It is clear that the vertical displacement is concentrated near the pier. A relatively small vertical displacement can be attributed to the effects from shallow boundary conditions. The maximum displacement was 69 mm (2.72 in) which occurred in the soil around the helical pier.

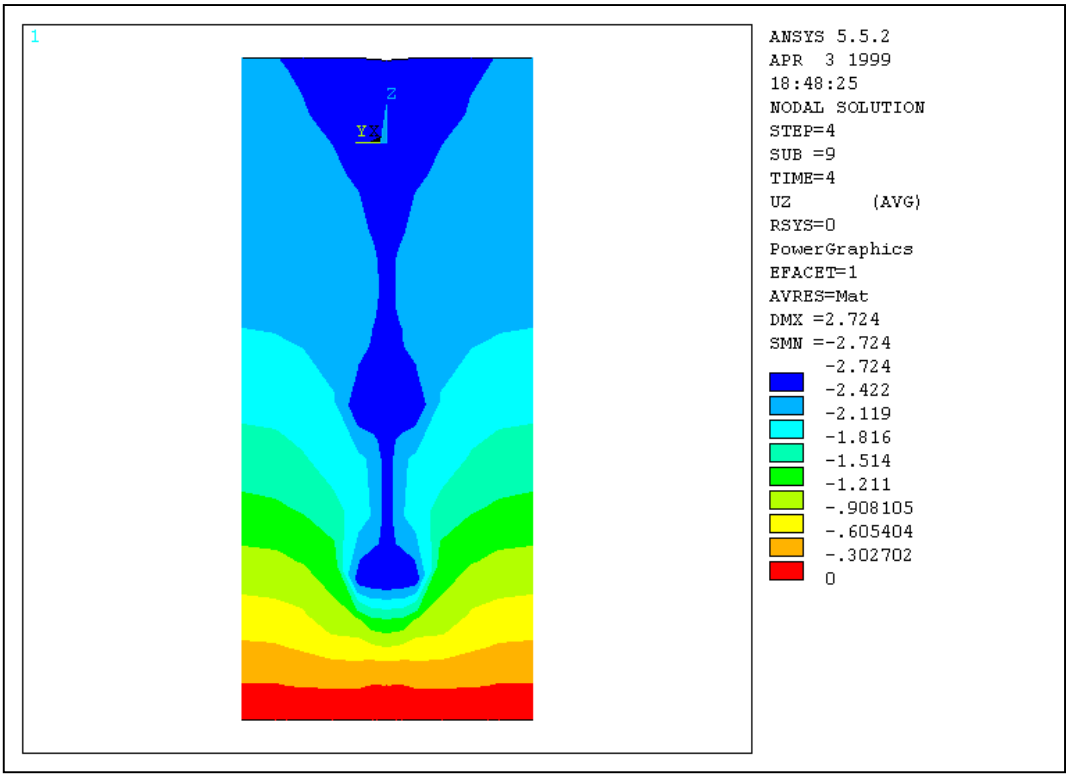

Figure 5.5 Vertical Displacement in Soil for Shallow Model Due to Axial Load 89 kN (20 kip)

Figure 5.6 shows the vertical soil stress for Test Model under an ultimate axial load of 89 kN (20 kip). Small vertical tension stresses were developed above both plates with magnitudes up to 27 kPa (4 psi). These stresses are consistent with adhesion between the soil and the pipe or plate elements in this region and were limited by the Drucker-Prager yield criteria. The soil displacement due to the applied load and soil self-weight was greatest at points near the pier as would be expected. The small cohesion strength used in this model limited the ability of the soil elements to transfer shear outward from the pier, resulting in a very localized displacement of the pier. Soils with greater cohesive characteristics would be expected to undergo more uniform displacements over a wider area although high cohesion values are not consistent with long-term loads on frozen ground.

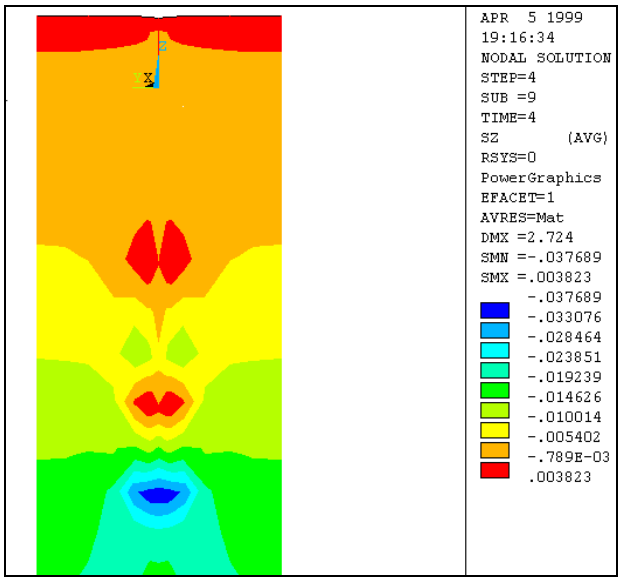

Figure 5.6 Vertical Stress Distributions within Soil Volumes (ksi)-Test Model

It is evident from the vertical stress distribution that the axial load is not equally divided between the two spirals (even after accounting for the effect of overburden pressure). In the case under consideration, the top spiral shares only about 25% of total load; while the bottom one shares about 75% of total load. However, in the current simplified design formula, it is assumed that vertical response stresses in soil under all spirals are the same for cohesive soils and increased only by the overburden pressure for granular soils (Figure 5.1 and Equation 2.1). Based on the current design method, the upper spirals may be over-designed, while the bottom spiral may be under-designed.

Another result seen from Figure 5.6 is that the vertical stresses were concentrated within an area of about three times the radius of the spiral. It can be considered that the "Effective Area" for each helical pier is about three times the radius of the spiral. This supports the recommendation by A. B. Chance Co. (1996) for the spacing between the piers being at least 3 times the helix diameter.

According to the design equations, Equation 5.1 and 5.2, using the cohesion c = 34 kPa (5 psi) and the angle of internal friction ϕ= 20° for frozen silt, the ultimate pier capacity would be about 42 kN (9.5 kip). Axial loads ranging from 0 to 111 kN (25 kip) were applied to investigate the full range of conditions from no load to greater than the capacity of the soil.

Figure 5.7 shows the vertical stress in soil in the Deep Model due to an axial load 89 kN (20 kip). The vertical stresses distribution in the Deep Model was similar to that in the Test Model. However, the soil displacement was significantly different between the models, as shown in Figure 5.8. The displacement in soil distributed more evenly in the Deep Model. In the case of a shallower Test Model, the maximum displacement due to soil self weight and applied load was 69 mm (2.72 in), while the maximum displacement in the case of the Deep Model was 247 mm (9.72 in), which is 3.6 times greater than for the Test Model.

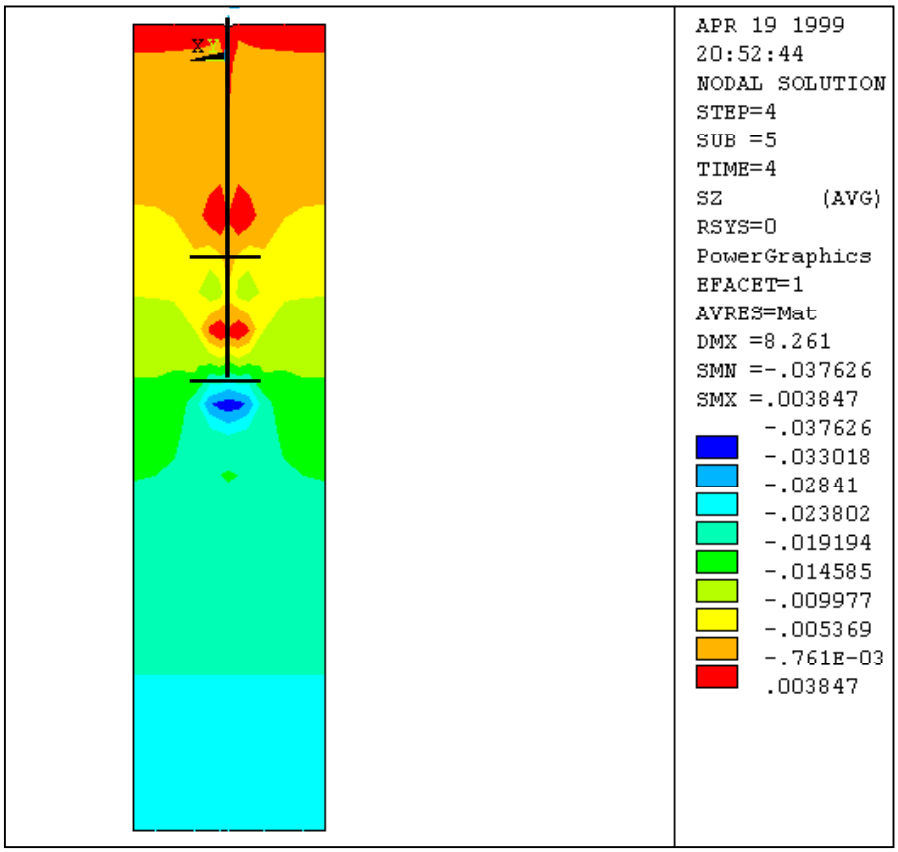

Figure 5.7 Vertical Stress Distributions within Soil Volumes (ksi) -Deep Model

The stress results of both of these analyses (Test and Deep Model) indicated that the vertical compressive reaction stresses developed within the soil immediately after placement of an 89 kN (20 kip) load were not distributed evenly between the plates. The stresses were concentrated at both the top and bottom plates, though the stress at the bottom plate was significantly higher. The vertical compressive stress reached 260 kPa (38 psi) under the bottom plate and only 85kPa (12 psi) under the top plate. The reason for this may be attributed to the stiffness of the steel central column. The steel shaft is relatively very stiff between the two spiral plates, resulting in almost no shortening under the loading condition. The soil deformation between two plates is mainly controlled by the steel deformation. Very small soil deformation would provide very small reaction stresses. The results for the same load in the Deep Model produced nearly identical stress distributions in the soil near the pier (Figure 5.7).

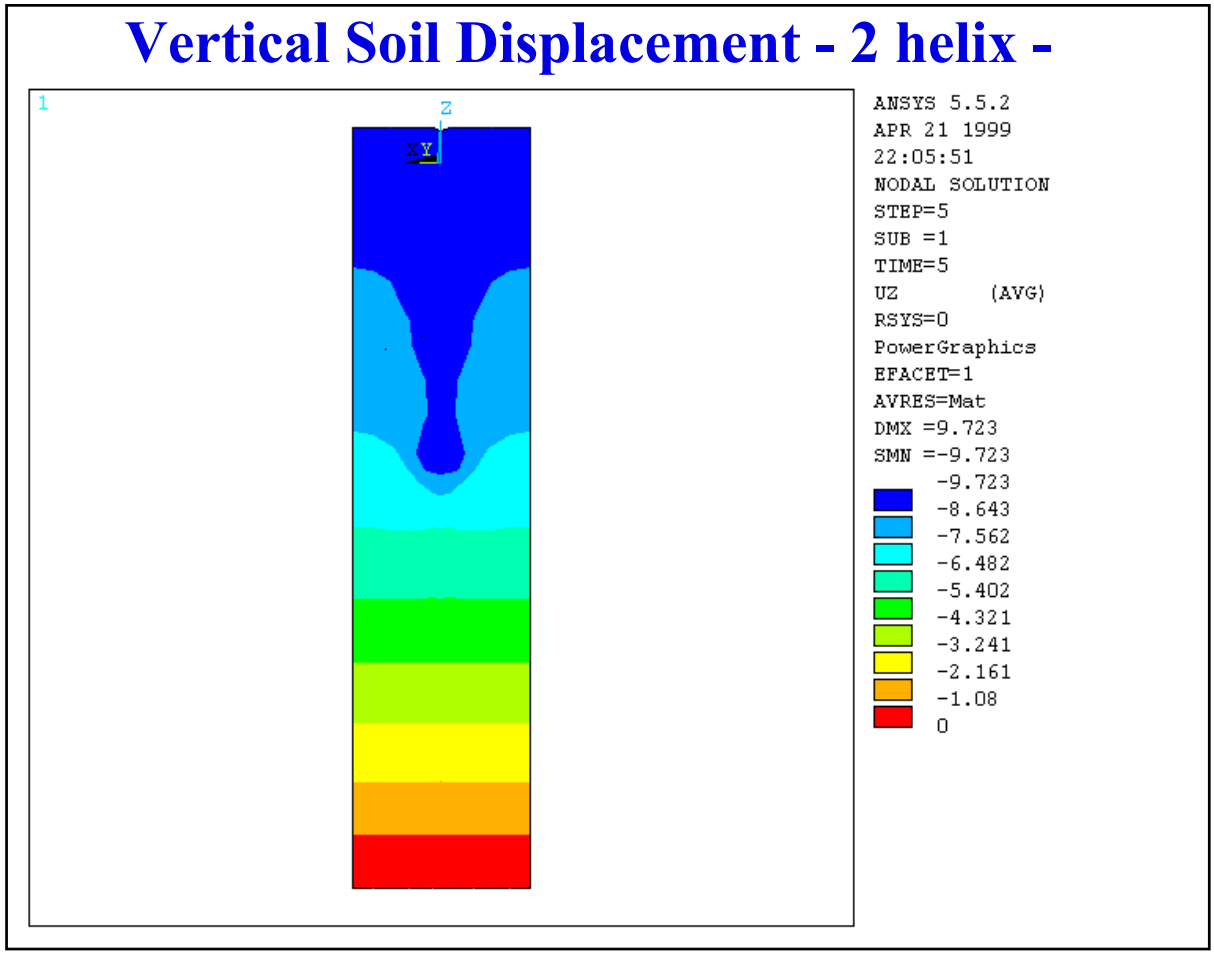

Figure 5.8 Vertical Soil Displacement Distribution - Deep Model

The vertical compressive stresses were concentrated within an area of about three times the radius of the spiral section and expanded outward and downward from the bottom of the pier. In the case of two helix plates, a spacing of three times or more the plate diameter between helixes is necessary to prevent soil failure.

In addition to above the sample analysis, a special model was created for the purpose of verifying the effect of distance between spiral plates. In this model, four plates were closely connected to the central shaft at distances of 1-2 times the diameter of the helix.

The results of this analysis also indicated that the reaction stresses developed within the soil immediately after placement of a 156 kN (35 kip) load were not distributed evenly among the plates. The reaction stresses directly below the bottom plate were much higher than in other regions. The stress in this region was 258 kPa (37.50 psi), which is six times higher than similar reaction regions above it. The fact that there was little significant contribution from the upper three spirals is likely to be caused by the confinement of the soil between the plates, which allows the soil in that volume to move for the most part, as a unit. Compressive stresses were

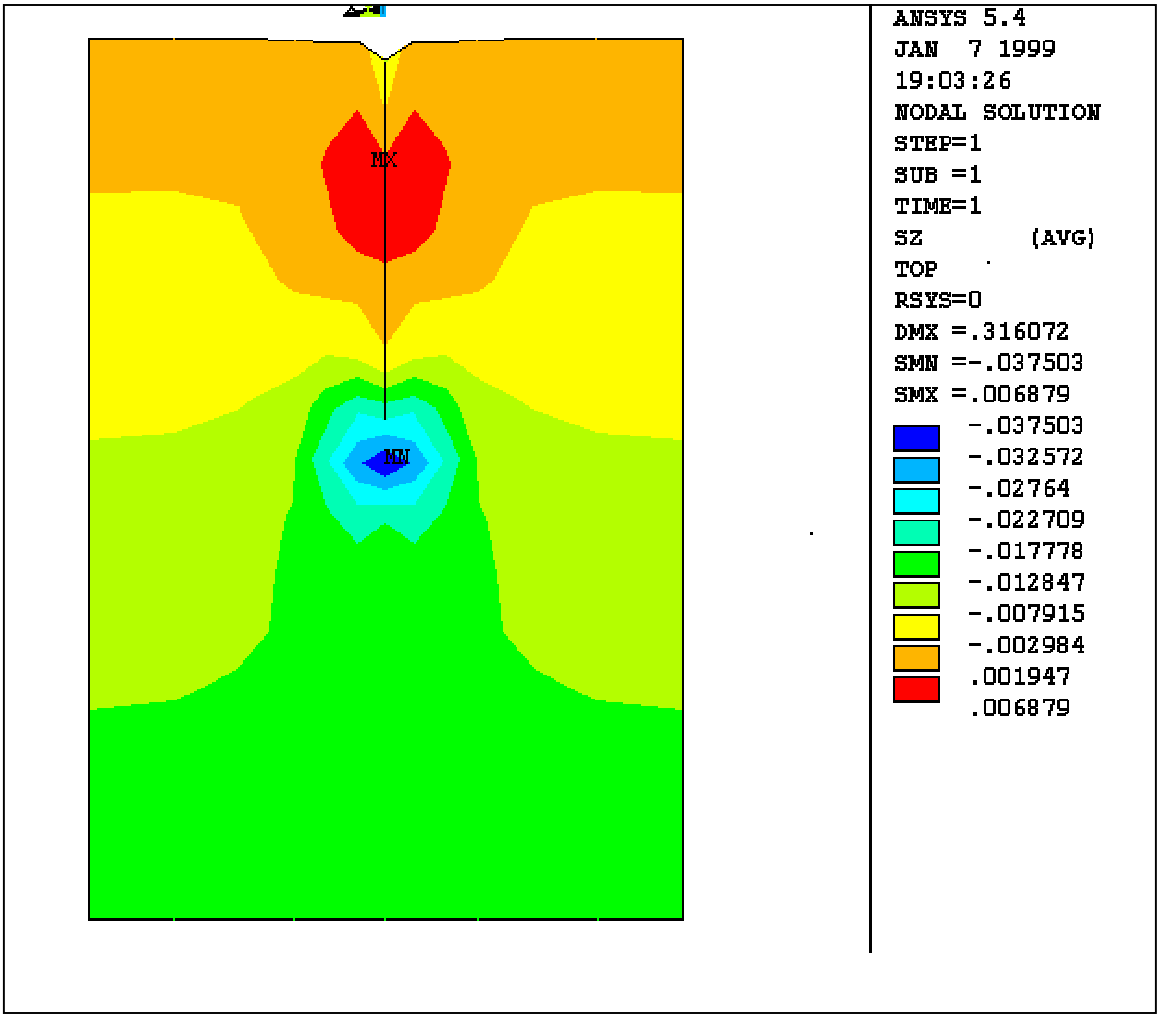

Figure 5.9 Vertical Stress Distribution in the Soil Volume (Test Model with Four Closed Helixes)

concentrated within an area of about three times the radius of the spiral section and expanded outward and downward from the bottom of the pier. The vertical stress distribution can be seen in Figure 5.9. Some tension stress was developed above the top plate with magnitudes up to 47 kPa (6.88 psi). These stresses are caused by adhesion between the soil and the pipe or plate elements in this region, and were limited by the Drucker-Prager yield criteria.

The soil settlement due to the applied load, shown in Figure 5.10, was greatest near the pier. This is a result of the small cohesion value used in this model, which reduced the ability of the soil elements to transfer shear outward from the pier. The maximum settlement of 8 mm (0.316 in) occurred at the top of the pier and the pier was displaced relatively rigidly. The plate deformation was not of any significant interest in this model, however it was analyzed much more closely in the detailed models.

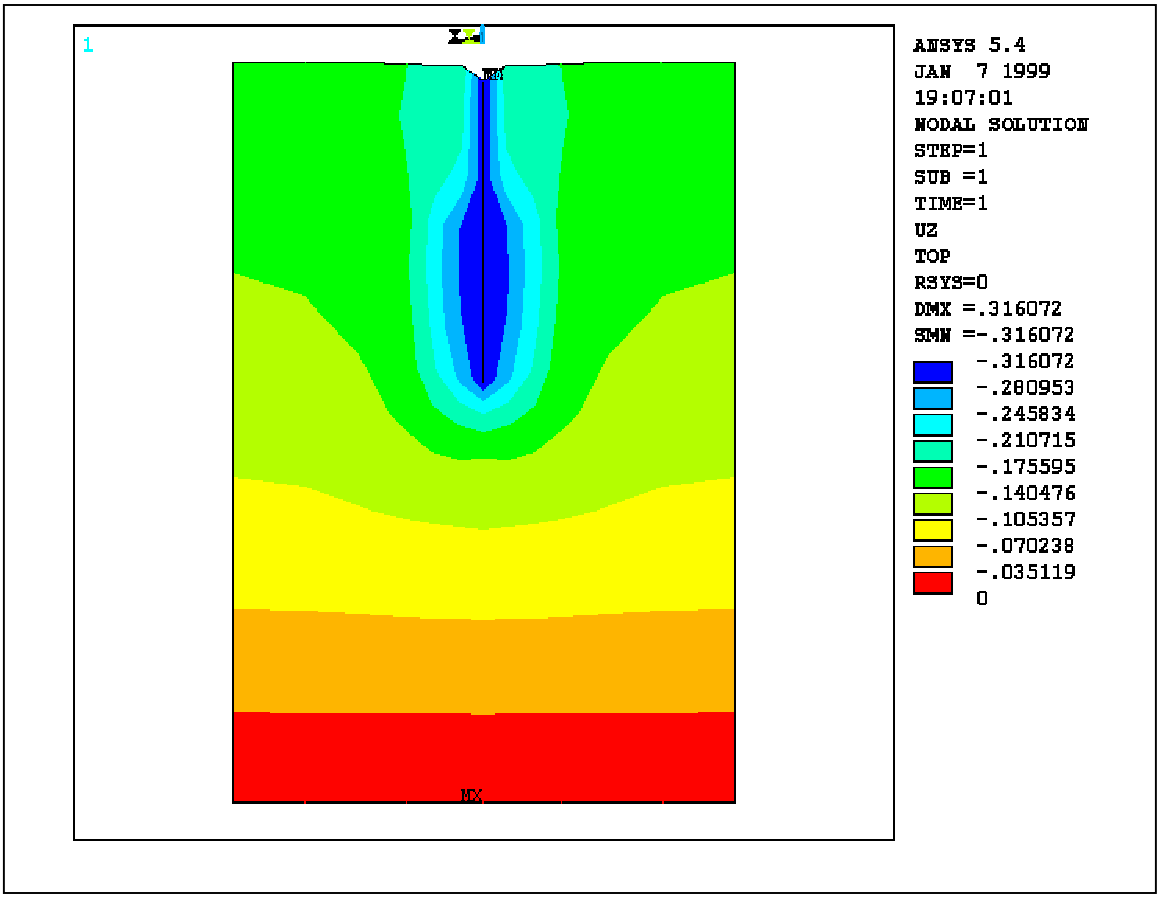

Figure 5.10 Vertical Displacement Distribution in the Soil Volume (Test Model with Four Closed Helixes)

5.3.2 Soil Stress-Strain and Deformation Analyses – Sub Models

The small model was used to analyze the local stresses in the immediate vicinity of the spiral structure as well as the stresses within the spiral itself. The pipe and spiral were modeled with the actual geometry of the spiral shape and dimensions of the pier structure using shell elements. The boundaries of the soil volume used for the sub-model were chosen far enough from stress concentrations to avoid modeling errors resulting from the simplification of the pier structure in the large-scale model. The resulting model was a 381 mm (15 in) diameter cylinder with a depth of 254 mm (10 in). The calculated displacements from the coarse model's results were imposed on the boundaries of the sub-model so the local behavior within the sub-model could be determined with greater accuracy. This method was used to analyze the local behavior of the spiral structure.

Figure 5.11 shows the FEA mesh on a sub-model of a helical pier with the following parameters: Soil: 381 mm (15 in) diameter, depth = 254 mm (10 in), helix: 76 mm (3 in) diameter shaft, 254 mm (10 in) diameter spiral, 13 mm (0.5 in) steel plate.

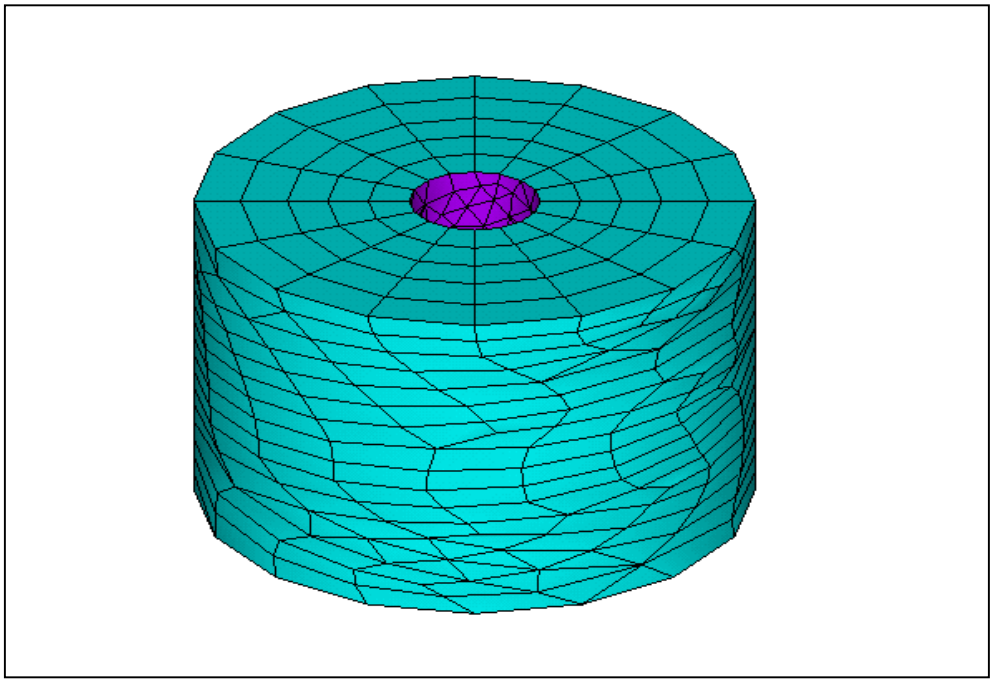

(a) Soil Volume of the Sub-Model

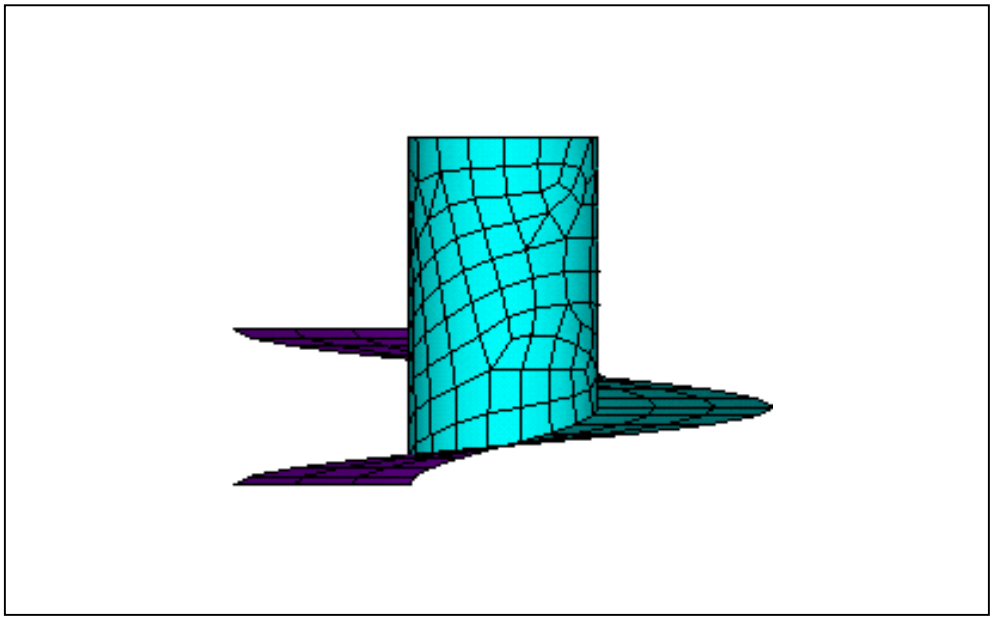

(b) Front View of FEA Mesh on a Part of Helix

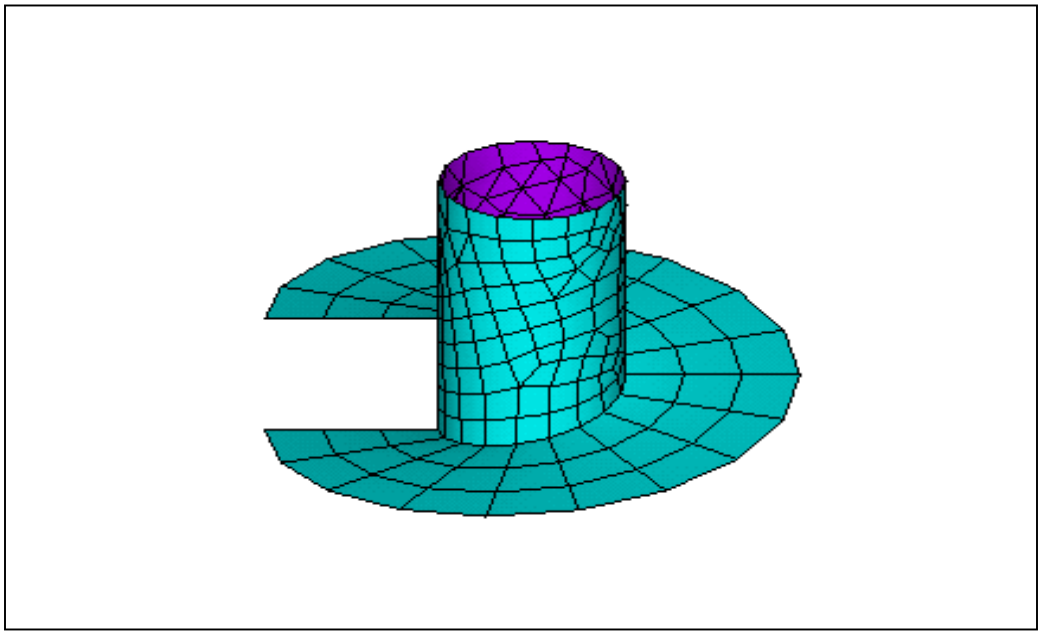

(c) Isometric View of FEA Mesh on a Part of Helix

Figure 5.11 FEA Sub Model of Helical Piers

The sub-model analysis results are shown in Figures 5.12 and 5.13. The vertical stress distribution in soil at the bottom spiral due to an axial load of 89 kN (20 kip) is shown in Figure 5.12. The complicated vertical compressive stress distribution can be seen from the stress contour, compared with simplified design assumption. The vertical stress distribution in soil at the bottom spiral is shown in Figure 5.13. The maximum vertical stress was 308 kPa (44.69 psi) below the outer edge of the spiral.

The sub-modeling technique also provides a closer investigation for stress distribution in steel helical piers. Figure 5.14 and Figure 5.15 provide von Misses stress distribution in a typical spiral plate from different viewpoints. The von Misses stress is the most intense at the junction between the plate and the pipe section. The maximum von Misses stress was 110 MPa (15.95 ksi) at a point 90° along the spiral from its cutting edge. The reason for the maximum von Misses stress occurring at that location is possibly due to the biaxial bending condition. This information and corresponding data will be very useful for estimating stresses in welding for manufacture design purposes.

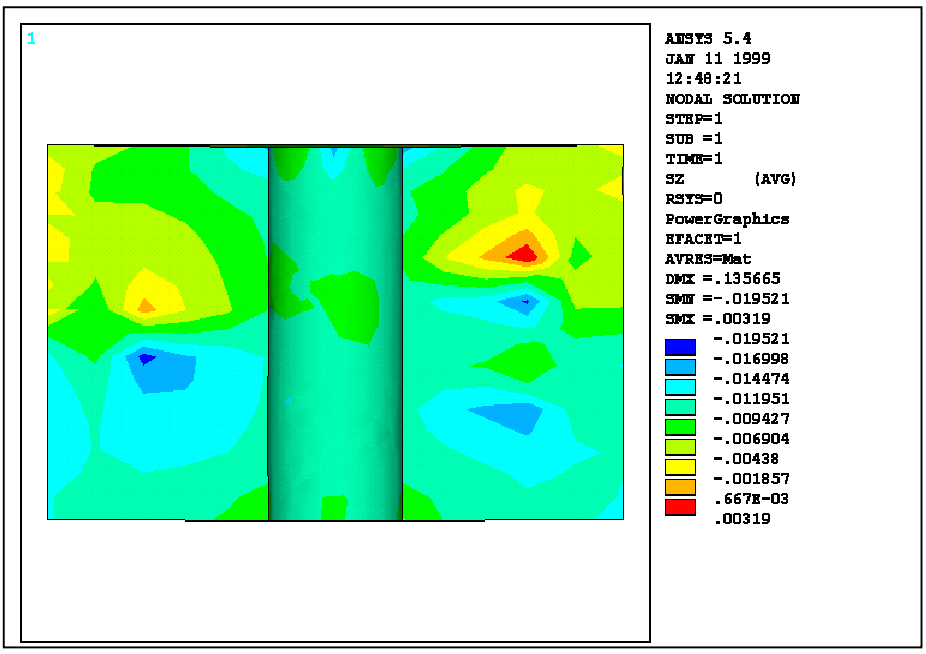

Figure 5.12 Vertical Stress Distribution in Soil at Bottom Spiral

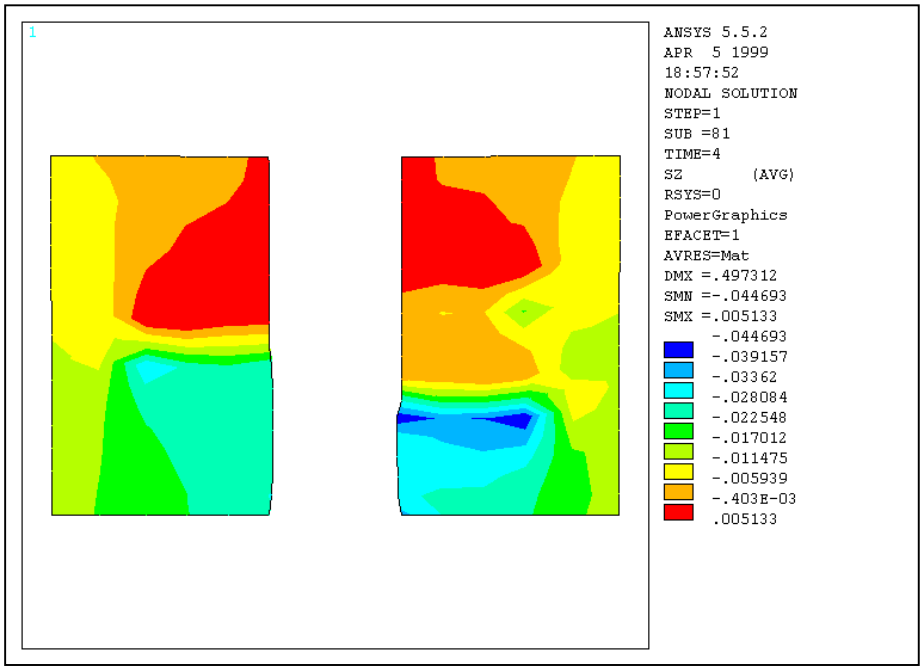

Figure 5.13 Vertical Stress Distribution in Soil at Bottom Spiral

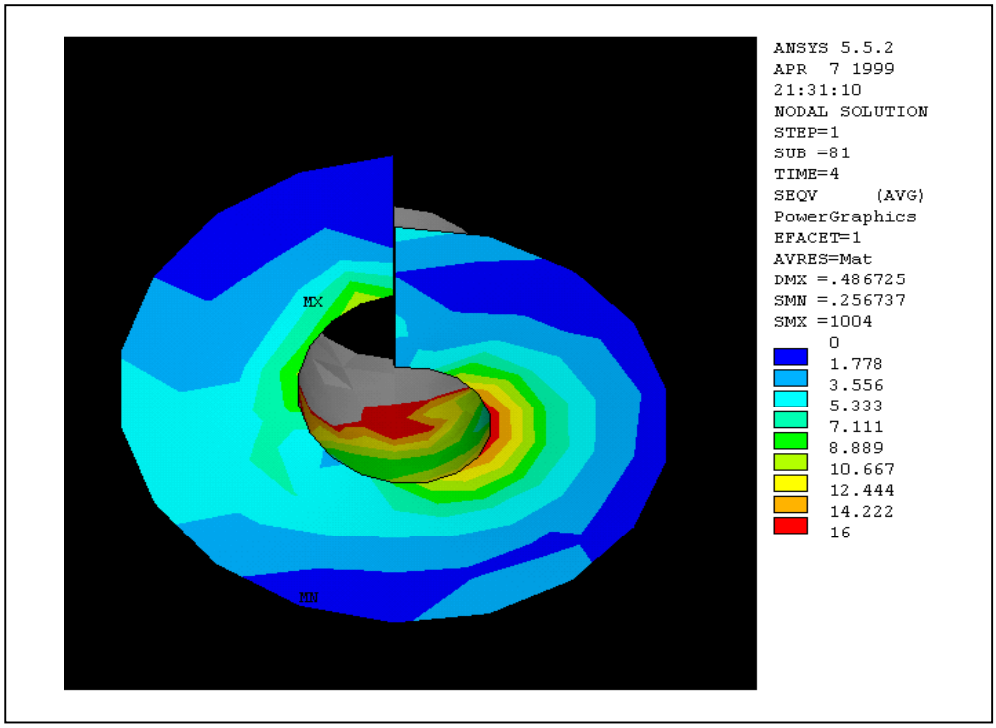

Figure 5.14 von Misses Stress Distribution in a Typical Spiral Plate – View I

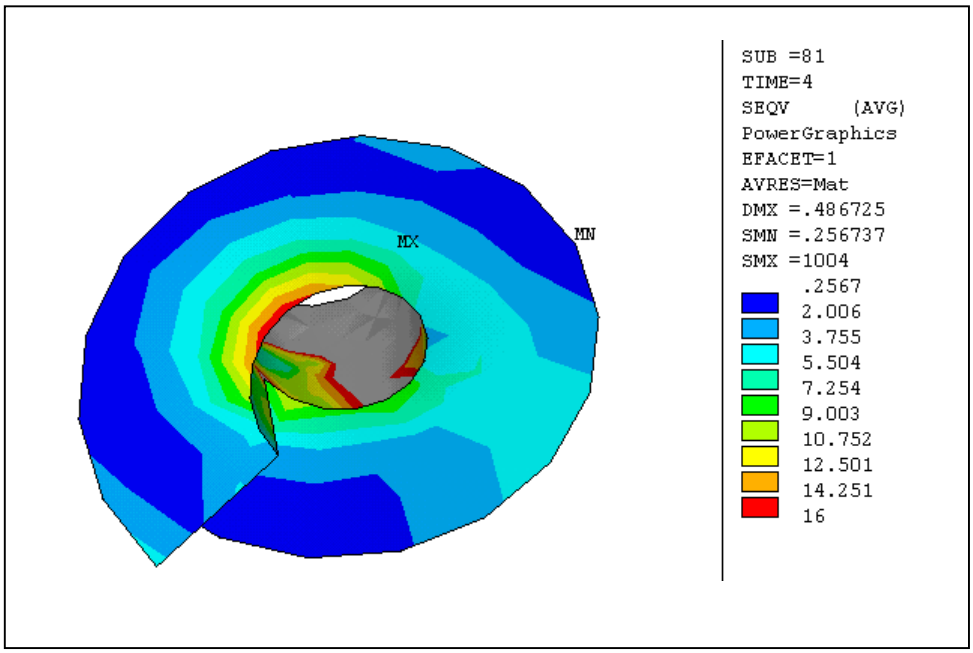

Figure 5.15 von Misses Stress Distribution in a Typical Spiral – View II

5.3.3 Installation Strength Analyses

An installation failure FEA model was created to simulate a critical failure during installation when the spiral encounters a hard rock, ice lens or other significant obstacle. The model used the same detail of the spiral structure as the Small Model but contained no soil elements. The spiral structure was restrained horizontally at an area of the outermost end of the bottom of the spiral and the bottom of the pipe was restrained against translation in the vertical direction as well as rotation about all but the vertical axis. A torque was applied at the top of the pipe section with a magnitude of 1,465 kN-m (90 kip-in), which is in the range used during installation of these piers (A. B. Chance, 1996). The spiral was modeled using the same material properties as in the Small Model with the addition of Bilinear Isotropic yield criteria (see Figure 5.3) including σ_y = 345 MPa (50 ksi) and E_T = 10,000 MPa (1,450 ksi). This yield criterion allows for both elastic and plastic deformation of the elements. This model used shell elements with 4 nodes and 6 degrees of freedom at each node.

The helix and the center tube were modeled by shell elements. The special shape of the helix made the FEA meshing very difficult. Several meshing techniques were used. The final FEA mesh shown in Figure 5.16 for the helix and central tube was carefully designed with most elements having good shapes and aspect rations which is significant important for accurate computational results.

Figure 5.17 shows a typical Installation Failure Model by FEA. The results from this model show clearly that large stresses will develop at the weld between the spiral and the pipe. These stresses, reaching almost 500 MPa (72.5 ksi), are sufficient to yield the steel. This stress is highly concentrated at the bottom end of the connection and rapidly dissipates within an inch of this point.

The stress developed in the steel tube is much smaller than that in the helix. From the stress contours in Figure 5.17 it is clear that the von Misses stress is highly concentrated at the connection near the leading edge. Stress level in this small area is several times higher than the average stress in the entire helix. These results are consistent with some, although rare, failure cases reported during installation procedure.

The developed FEA can be utilized in providing the accurate maximum stress under a certain torque, or the maximum allowable torque without material failure.

5.3.4 Frozen Ground Creep Analyses

The Test Model was used in the development of a “creep model.” The material properties used were same as the previous models with the addition of creep parameters to simulate secondary creep effects over the period of two years. The computed design load of 22 kN (5 kip) was applied axially at the top of the pier.

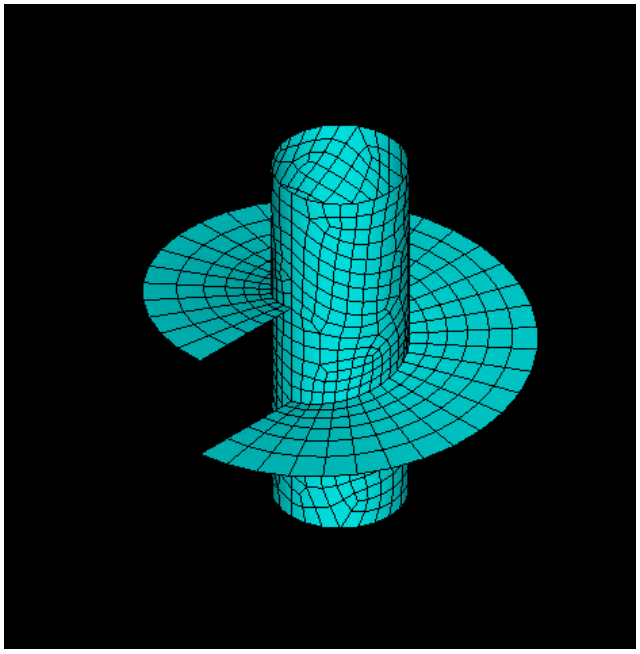

Figure 5.16 Typical FEA Mesh of Helix and Central Tube

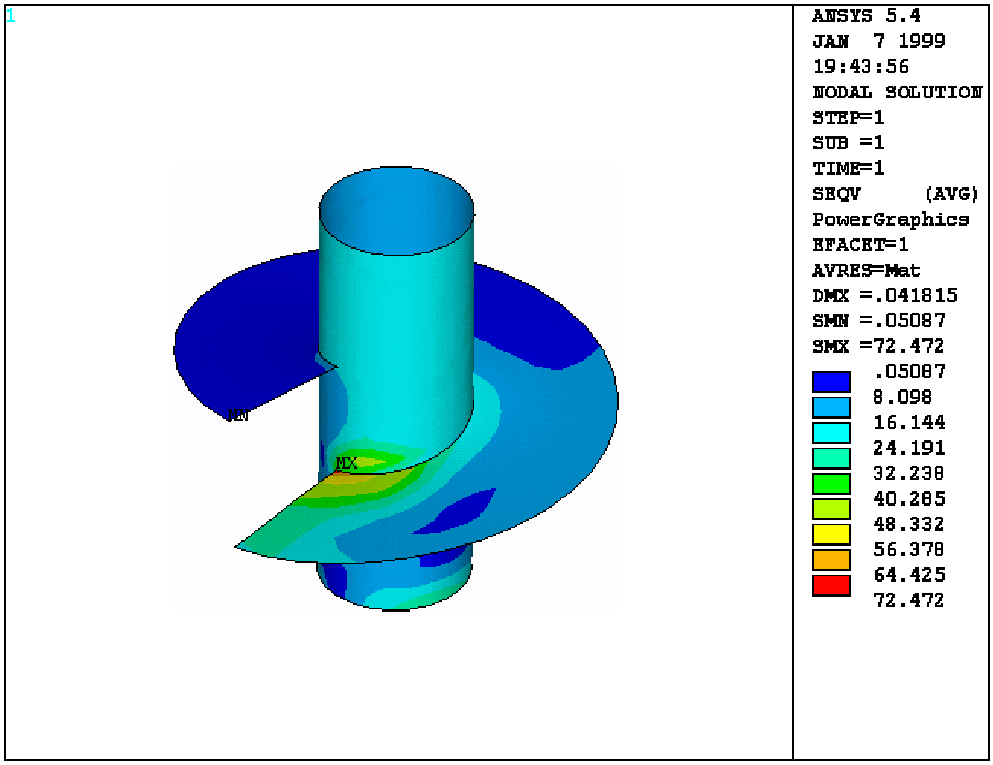

Figure 5.17 von Misses Stress (ksi) Due to Installation Torque = 1,465 kNm (90kip-in)

The soil parameters used in this model are: friction angle, $\phi = 31°$, c = 34 kPa (5 psi), unit weight = 20 kN/m^3 (130 pcf), reference strain rate = 0.01 yr^{-1}, creep modulus = 38 kPa (5.5psi), creep parameter n = 3.

According to original plan, the creep calculation results would compare with that from the lab testing, therefore, creep calculations used the same dimension of soil model compatible with the lab setup. Figure 5.18 shows the creep displacement due to a constant axial load 22 kN (5 kip) for 2 years for Test Model.

The displacement results provided apply only to secondary settlement conditions and do not account for primary or tertiary settlement. The initial settlement under the load was 30 mm (1.2 in) and increased to 40 mm (1.6 in), about 133% of the initial settlement over the course of two years. Some nonlinear displacement can be seen in Figure 5.18, indicating the possibility of boundary interaction between the base of the pier and the bottom of the soil volume. This effect should not been seen if Deep Model was used.

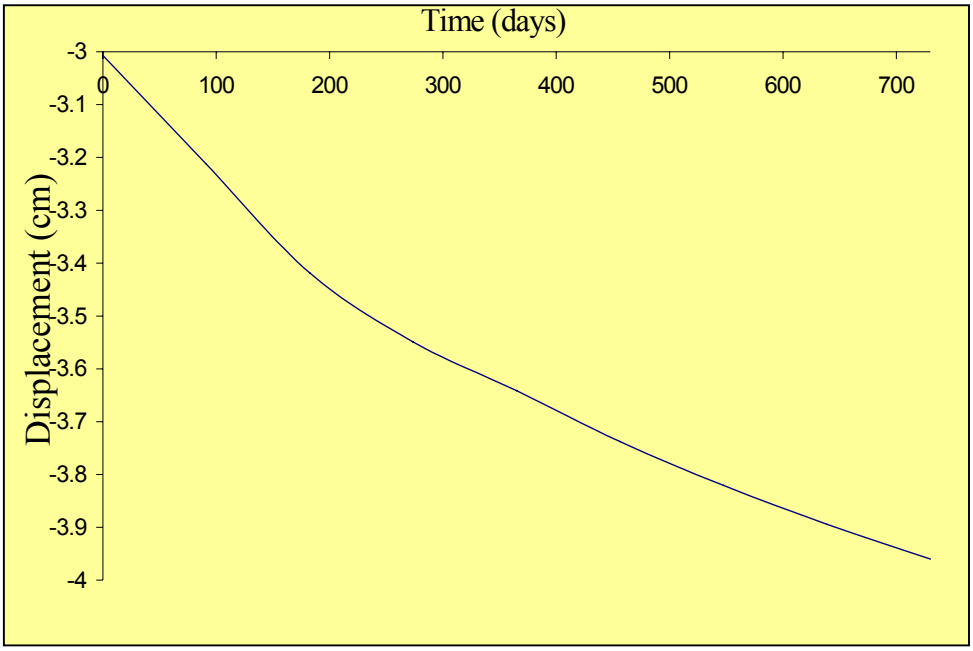

Figure 5.18 Creep Displacement Time History for a Shallow Model

The creep formula used in this study was based on equivalent von Misses stress due to surcharge on the soil. The FEA program will provide creep displacement due to total von Misses stress. Therefore, an approximation in the creep calculation is made on the correction for creep due to self-weight of the soil. Since the creep behavior of the system is nonlinear, it is mathematically incorrect to simply subtract the creep due to self-weight from the total creep. In addition, if self-weight of the soil were not used in the model, then the equivalent stress developed would not be accurate or reliable. Since the purpose of the research is to determine the

creep due to surcharge on the pier, it is necessary to account for the additional creep due to self-weight of the soil. However, creep analysis based on the weight of the soil only showed minimal displacement of the pier. Given that the displacement was so small, it was decided that the creep due to self-weight would be subtracted out as though it were a linear behavior. Since the research deals with the general behavior of a large area around the pier that is not dependent on extraneous accuracy, this approximation is appropriate for this analysis. It was recognized that this is not theoretically or mathematically correct, but there was no better way to do it. It seems to have no effect on the general results, though there are some anomalies in the data that may be related to this approximation.

Figure 5.19 shows the displacement time history for Deep Model with correction of self-weight effects. The maximum net settlement of the Deep Model was 139 mm (5.49 in), which occurred under a 111 kN (25 kip) axial load, with the pier being displaced relatively rigidly. Figure 5.19 depicts the soil surface profile of Deep Model under various applied loads ranging from 0 kN to 111 kN. The initial displacement of the soil was due to the application of its self-weight only. The pier did not settle uniformly with the soil volume, consequently a bulge is evident at the surface of the soil. The gross displacement can be seen on the vertical axis and the net displacement, due to the applied load only, of the pier is indicated for each load step that was analyzed.

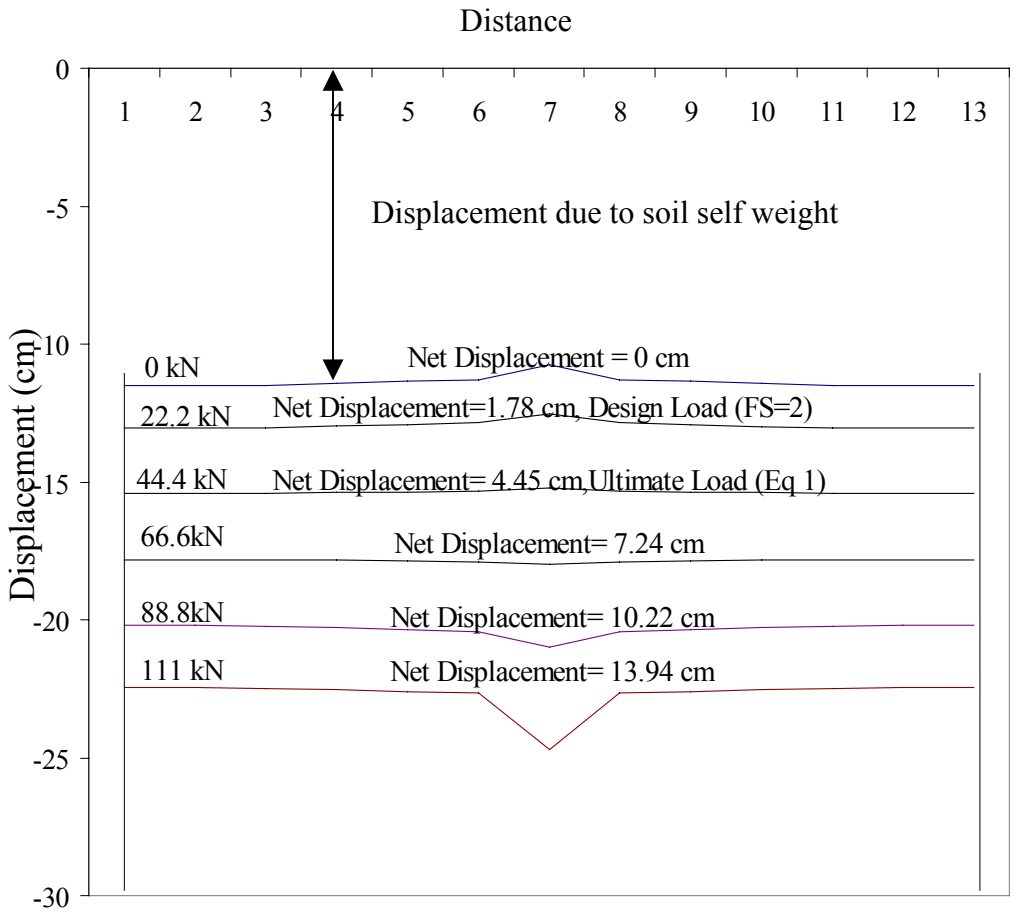

Figure 5.19 Surface Profile of the Deep Model Due to Various Loads

For piers with multiple helixes under small stress conditions, settlements due to applied loads will be almost the same as for corresponding single helix piers. However, under large stress conditions, the settlement is reduced with multiple helixes.

For the small stress condition, the stress results of two-helix pile indicated that the vertical compressive reaction stresses developed within the soil immediately after placement of the load were not distributed evenly between the plates. The stresses were concentrated at both the top and bottom plates, though the stress at the bottom plate was significantly higher. The reason for this may be attributed to the stiffness of the steel central column. The steel shaft is relatively very stiff between the two spiral plates, resulting in almost no shortening under the loading condition. The soil deformation between the two plates is mainly controlled by the steel deformation. Very small soil deformation would provide very small reaction stresses.

In addition to above sample analysis, a special model was created for the purpose of verifying the multi-helix effects of spiral plates. In this mode, four plates were connected to the central shaft. The results of this analysis indicated that the reaction stresses developed within the soil immediately after placement of the load were not distributed evenly among the plates. The reaction stresses directly below the bottom plate were several hundred percentages higher than in other regions. The fact that there was little significant contribution from the upper three spirals is likely to be caused by the confinement of the soil between the plates**,** which allows the soil in that volume to move for the most part, as a unit. To mobilize the soil strength the helixes need to be located at an adequate distance from each other. The study results show that a distance of three helix diameters between the helixes reduces creep under large stress.

The analysis results are consistent with the theoretical prediction. Based on *Newtonian Mechanics* for purposes of analyzing the statics or dynamics of a body, consider a force system whose force and moment resultants are identical. The force resultants, while equivalent, need not cause an identical distribution of strain, owing to a difference in the arrangement of the forces. In addition, *Saint-Venant's principle* permits the use of an equivalent loading for the calculation of stress and strain. This principle states that, if an actual distribution of forces is replaced by a statically equivalent system, the distribution of stress and strain throughout the body is altered only near the regions of load application. Comparing single helix and multi-helix cases under the same load, the resultant reaction forces from the single helix and the multi-helix are the same. The stress and strain distributions are mainly identical in most of regions except near the helixes. The soil settlements are controlled by the soil deformation in most regions, not by the small region near the helixes. Therefore, the pile settlements are mainly the same in case of single-helix and multi-helix cases. However, stresses and strains in the area near the helixes are not the same in the cases of single and multi-helixes, which affects the stresses and strains within helixes.

For the large stress condition, due to the yielding of the soil under the bottom helix, the redistribution of stress is expected. When stresses in the soil under the bottom helix reach the yield level, the top helix would pick up more load. As a result, stresses are distributed more evenly between helixes and the average stress is smaller than that of the single helix condition. Therefore, the double helix will help to decrease the total creep settlement.

5.4 Summary of FEA

The findings from the development and the analysis of the FEA results are the following:

- The FEA model results will increase understanding of helical piers in various soil conditions as well as provide insight into design and installation considerations.
- The installation failure FEA model displayed the stresses encountered during installation of the pier system. The stress concentration that occurred at the bottom of the weld was very similar to known, but rare, failure mechanisms for helical piers. This information can be used to design better connection geometry at this critical location and emphasizes the need of good quality control during pier manufacturing.
- The FEA models provided valuable information regarding the distribution of stress and displacement within the soil. This stress may or may not depend on the geometry of the pier system in question. However, it does indicate that the soil reaction pressure is not equally distributed between two helices, and that the closely spaced spiral structures, even with three-helix-diameter spacing, will not provide significant increases in the overall capacity of the pier. As can be seen from the analysis of the two spirals spaced far enough apart in this pier system, only the bottom one contributes to any large extent to the pier's capacity. Soil stress is not uniformly distributed under helixes as assumed by Equation (2.1). However, creep settlement under heavy loads and warm frozen temperatures is reduced by adding a second helix at least three helix diameters apart from the bottom helix.
- The detailed helix FEA models provided a close examination of the stresses within the spiral during the application of design loads. The highest stresses were encountered at the top and bottom ends of the spiral welds. This information can be used to make changes to the design of these structures if necessary as well as provide a more detailed picture of the physical situation encountered by helical structures embedded in soil.
- The creep FEA analysis indicated the creep behavior of helical piers in frozen ground and provides valuable insight into the magnitude of settlement that can be expected over extended periods of time. The creep deformation is not significantly different between piers with single or multiple helixes under small loads and cold under any load in cold frozen ground, but increases with the load and warming temperature.
- According to original plan, to validate the model, these results would have been compared with physical tests conducted at CRREL. The authors felt that the non-uniform test temperature and short loading time at the CRREL resulted in test results that could not be used to calibrate the FEA models.

5.5 References for Finite Element Modeling

A. B. Chance Co., 1996, *Helical Pier Foundation System Technical Manual*, Bulletin 01-9601, Rev. 7/96, pp.2-7.

Das, B. M., 1998, *Principles of Foundation Engineering*, PWS Publishing, Fourth Edition.

Ghaly, A., Hanna, A., Ranjan, G. and Hanna, M., 1991, "Helical Anchors in Dry and Submerged Sand Subjected to Surcharge," *Journal of Geotechnical Engineering*, Vol. 117, No. 10, pp. 1463-1470.

Johnston, G.H. and Ladanyi, B., 1974, "Field Tests of Deep Power-Installed Screw Anchors in Permafrost," *Canadian Geotechnical Journal,* Vol. 11, No. 3, pp.348-358.

Ladanyi, B. and Johnston, G.H., 1974, "Behavior of Circular Footings and Plate Anchors Embedded in Permafrost," *Canadian Geotechnical Journal,* Vol. 11, pp.531-553.

Ladanyi, B., 1983, "Shallow Foundations on Frozen Soil: Creep Settlement," *Journal of Geotechnical Engineering,* Vol. 9, No. 11, pp.1434-1448.

Narasimha Rao, S. and Prasad, Y.V. N., 1993, "Estimation of Uplift Capacity of Helical Anchors in Clays", *Journal of Geotechnical Engineering*, Vol. 119, No. 2, pp. 352-357.

Prasad, Y.V. N. and Narasimha Rao, S., 1996, "Lateral Capacity of Helical Piles in Clays," *Journal of Geotechnical Engineering*, Vol. 122, No. 11, pp. 938-941.

6. DESIGN GUIDELINES

6.1 Development of Design Guidelines

The design guidelines are developed on the basis of the finite element analysis. For frozen ground, the dictating design criterion is the settlement due to the creep of the ice in the ground. The guidelines obtainable in the following sections are results from the Large Model (Deep Model) creep analysis. Input parameters for the analysis include material properties for the pier and the soil. The soil parameters include the strength parameters and creep parameters. These are functions of soil type, water content, unfrozen water content, and soil temperature. They vary greatly depending from location and season, and therefore, general guidelines cannot be provided for typical soil types, e.g. for sand, silt or clay. The following sections describe an example of design of helical piers for a silty soil at three different temperatures. To analyze any other soil, the engineer needs to contact the authors for FEA runs to produce the creep curves.

6.2 Materials and Model Dimensions:

The soil properties for the silty soil are given in Table 6.1. The pier has a pipe shaft with 90 mm (3.5 in) outer diameter and 13 mm (0.5 in) thick wall, and a 203 mm (8 in) diameter, 13 mm (0.5 in) thick plate for a single spiral. For the large-scale model, the spiral is modeled as a flat plate in order to limit the number of elements in the model. The element and material properties for steel appear in Table 5.2. The soil surrounding the helical piers is modeled as a cylindrical volume. The dimensions used in the final analysis models are given in Table 6.2 and Figure 6.1.

Table 6.1. Soil Properties for Silty Soil

	Unit	Temperature		
		-1°C	-5°C	-10°C
Unit Weight	**kN/m3**	19.07	19.07	19.07
	psf	119	119	119
Cohesion	**kN/m2**	2413	6206	9653
	psi	350	900	1400
Friction Angle	**°**	25	25	25
Creep Parameter, n		2.04	2.04	2.04
Creep Parameter, $\dot{\varepsilon}_c\left(\frac{1}{\sigma_{cu\theta}}\right)^n$	**1/(h MPa^n)**	$3.81*10^{-7}$	$5.49*10^{-8}$	$1.85*10^{-8}$
	1/(s ksi^n)	$5.44*10^{-9}$	$7.84*10^{-10}$	$2.64*10^{-10}$
Young's Modulus	**kPa**	1800	7400	14400
	psf	37594	154553	300752
Poisson Ratio		0.2	0.2	0.2

Table 6.2 Dimensions of Final Calculation Models

	H_1[1] (mm)	H_2 (mm)	H_3 (mm)	H (mm)	r (mm)	R (mm)
Single Helix Model	1270	-	2286	3556	203	1651
Double Helix Model	1270	610	2286	4166	203	1651

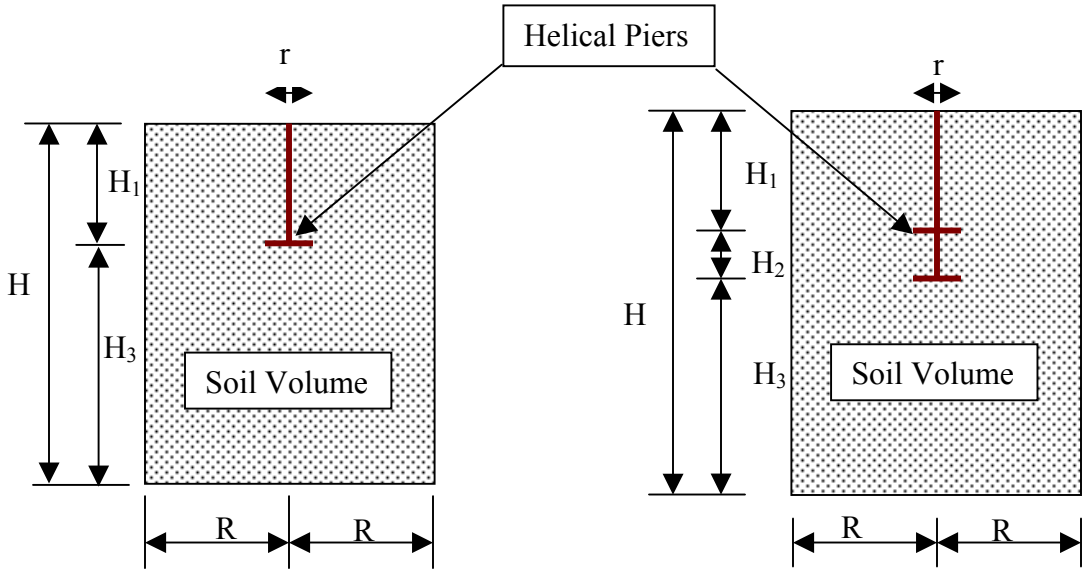

(a) Single Helix Model (b) Double Helix Model

Figure 6.1 Model Dimensions

6.3 Analysis Results

The results of the FEA analysis are given in Table 6.3. Creep settlement (displacement) as a function of temperature is plotted in Figures 6.2 to 6.7. For the given soil, the creep displacement under various design loads is less than 3 mm (0.12 in) at temperatures from –1 to -10°C, which is less than a typical allowable settlement.

[1] Pier manufacturers may recommend a larger minimum depth that could be conformed without affecting the creep curves significantly.

Table 6.3. Results of FEA Analysis for Silty Soil

	Displacement (mm)							
Time	-1°C Single				-5°C Single			
(years)	28kN	56kN	83kN	111kN	28kN	56kN	83kN	111kN
0.00	-0.05	-0.11	-0.16	-0.21	-0.02	-0.04	-0.07	-0.09
0.02	-0.05	-0.11	-0.16	-0.22	-0.02	-0.05	-0.07	-0.09
0.08	-0.05	-0.11	-0.18	-0.24	-0.02	-0.05	-0.08	-0.11
0.49	-0.06	-0.14	-0.24	-0.34	-0.03	-0.07	-0.11	-0.16
1.00	-0.07	-0.17	-0.29	-0.42	-0.03	-0.08	-0.13	-0.19
2.00	-0.09	-0.21	-0.37	-0.57	-0.04	-0.10	-0.16	-0.24
3.00	-0.10	-0.25	-0.45	-0.69	-0.04	-0.11	-0.19	-0.27
5.00	-0.11	-0.31	-0.59	-0.92	-0.05	-0.13	-0.22	-0.33
10.00	-0.16	-0.46	-0.87	-1.39	-0.06	-0.16	-0.28	-0.43
15.00	-0.19	-0.58	-1.11	-1.77	-0.07	-0.19	-0.34	-0.52
20.00	-0.23	-0.69	-1.32	-2.10	-0.08	-0.21	-0.39	-0.61
25.00	-0.26	-0.79	-1.51	-2.39	-0.09	-0.24	-0.44	-0.69
	Displacement (mm)							
Time	-10°C Single				-1°C Double			
(years)	28kN	56kN	83kN	111kN	28kN	56kN	83kN	111kN
0.00	-0.01	-0.03	-0.04	-0.06	-0.05	-0.11	-0.16	-0.21
0.02	-0.01	-0.03	-0.04	-0.06	-0.05	-0.11	-0.16	-0.22
0.08	-0.02	-0.03	-0.05	-0.07	-0.05	-0.11	-0.17	-0.24
0.49	-0.02	-0.04	-0.07	-0.10	-0.06	-0.14	-0.23	-0.33
1.00	-0.02	-0.05	-0.09	-0.13	-0.07	-0.17	-0.27	-0.39
2.00	-0.03	-0.06	-0.11	-0.16	-0.08	-0.20	-0.33	-0.49
3.00	-0.03	-0.07	-0.13	-0.18	-0.09	-0.22	-0.38	-0.56
5.00	-0.03	-0.09	-0.15	-0.22	-0.10	-0.26	-0.46	-0.69
10.00	-0.04	-0.11	-0.19	-0.28	-0.13	-0.34	-0.61	-0.94
15.00	-0.05	-0.12	-0.21	-0.32	-0.15	-0.41	-0.74	-1.15
20.00	-0.05	-0.14	-0.24	-0.35	-0.17	-0.46	-0.86	-1.32
25.00	-0.06	-0.15	-0.26	-0.39	-0.18	-0.52	-0.96	-1.48
	Displacement (mm)							
Time	-5°C Double				-10°C Double			
(years)	28kN	56kN	83kN	111kN	28kN	56kN	83kN	111kN
0.00	-0.02	-0.04	-0.07	-0.09	-0.01	-0.03	-0.04	-0.06
0.02	-0.02	-0.05	-0.07	-0.09	-0.01	-0.03	-0.04	-0.06
0.08	-0.02	-0.05	-0.08	-0.11	-0.01	-0.03	-0.05	-0.07
0.49	-0.03	-0.07	-0.11	-0.16	-0.02	-0.04	-0.07	-0.10
1.00	-0.03	-0.08	-0.13	-0.19	-0.02	-0.05	-0.09	-0.13
2.00	-0.04	-0.10	-0.16	-0.24	-0.03	-0.06	-0.11	-0.16
3.00	-0.04	-0.11	-0.19	-0.27	-0.03	-0.07	-0.13	-0.19
5.00	-0.05	-0.13	-0.22	-0.32	-0.03	-0.09	-0.15	-0.22
10.00	-0.06	-0.16	-0.27	-0.40	-0.04	-0.11	-0.19	-0.28
15.00	-0.07	-0.18	-0.31	-0.46	-0.05	-0.12	-0.21	-0.31
20.00	-0.08	-0.20	-0.34	-0.51	-0.05	-0.14	-0.24	-0.34
25.00	-0.08	-0.21	-0.37	-0.55	-0.06	-0.15	-0.25	-0.37

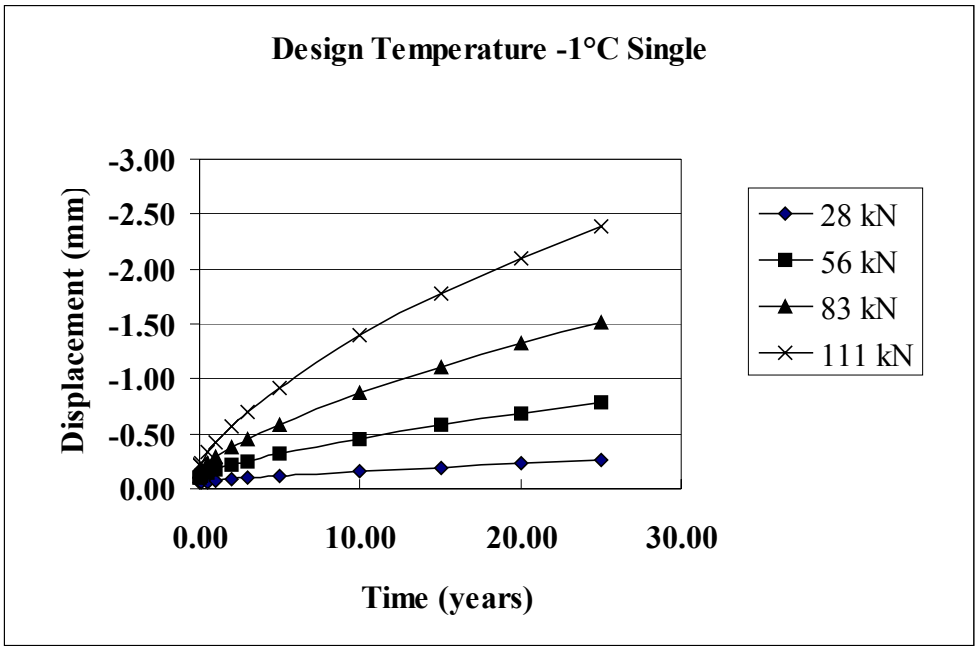

Figure 6.2. Creep Displacement for Single Helix Pier at Design Temperature of –1°C

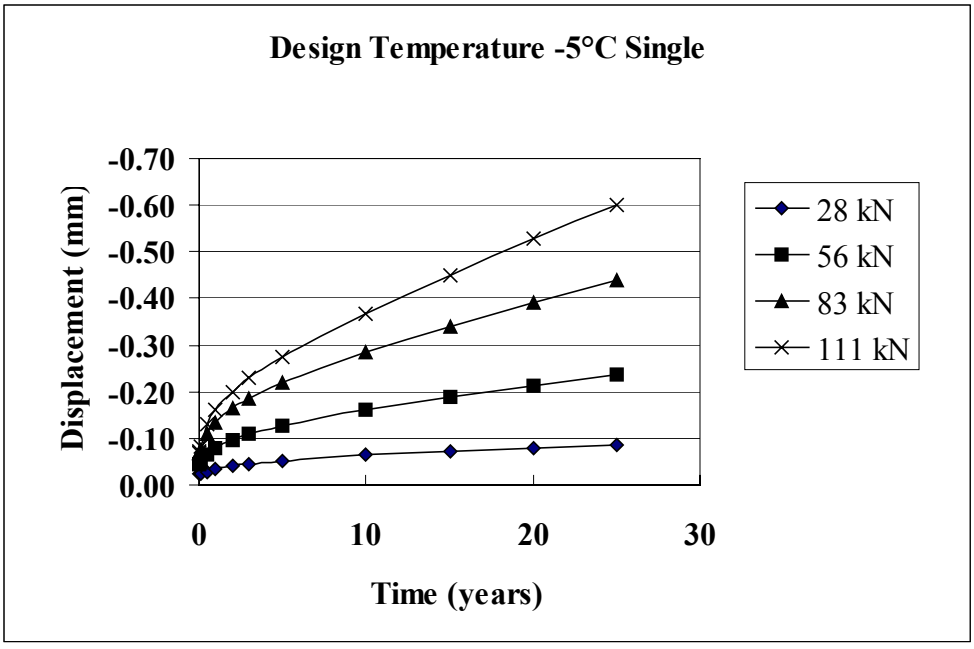

Figure 6.3. Creep Displacement for Single Helix Pier at Design Temperature of –5°C

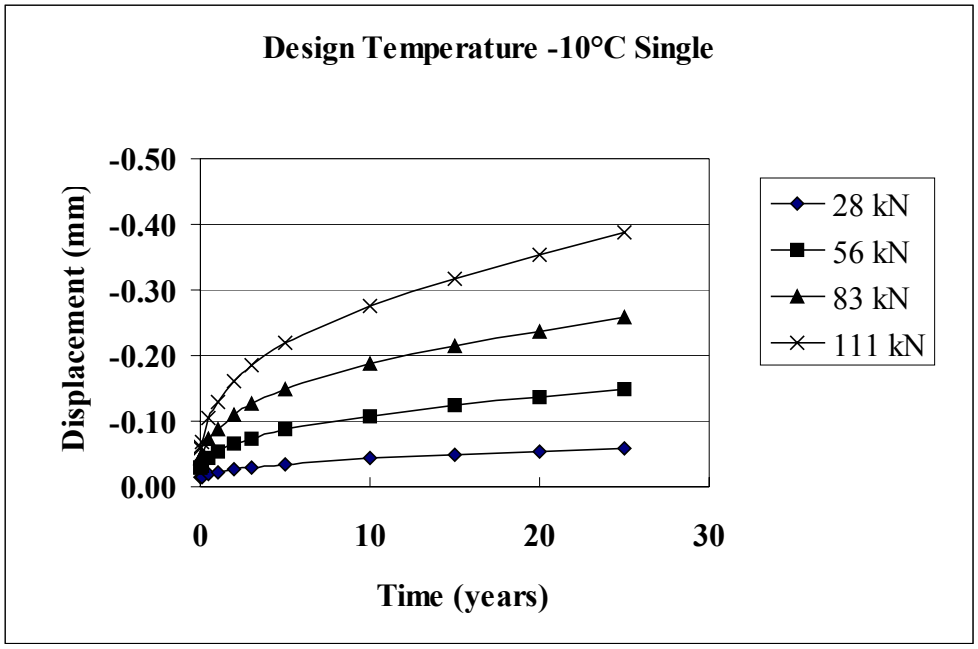

Figure 6.4. Creep Displacement for Single Helix Pier at Design Temperature of –10°C

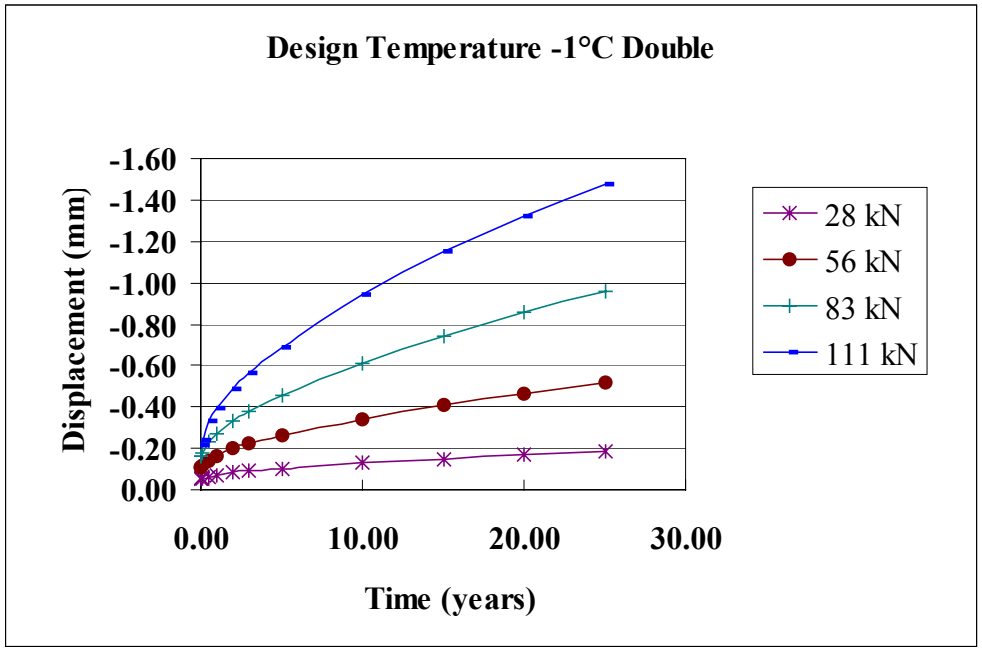

Figure 6.5. Creep Displacement for Double Helix Pier at Design Temperature of –1°C

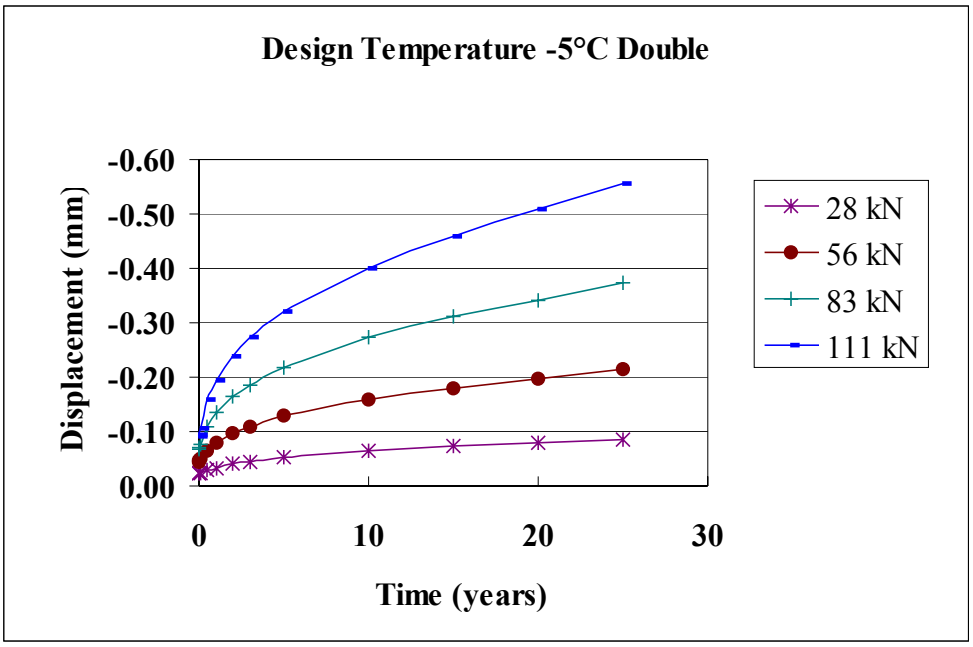

Figure 6.6. Creep Displacement for Double Helix Pier at Design Temperature of –5°C

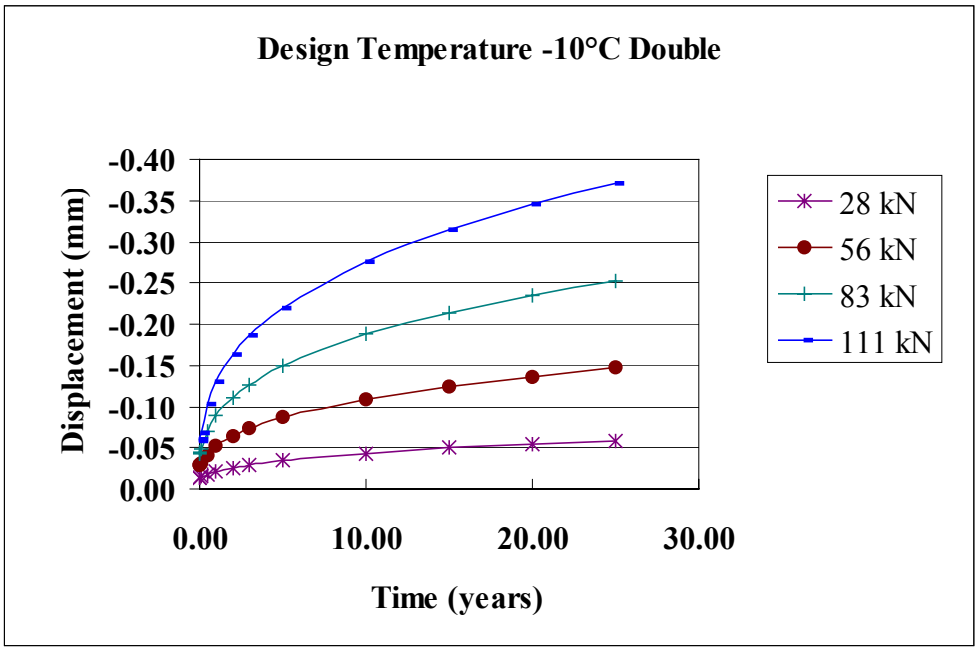

Figure 6.7. Creep Displacement for Double Helix Pier at Design Temperature of –10°C

6.4 Design Example

In order to design helical piers in the given frozen silt, the following information is needed: design temperature and allowable displacement after 25 years or less. When this information is obtained, the following steps will be performed:

1. Select the proper chart matching the design temperature.
2. Select design life and maximum allowable displacement.
3. Select a design load that yields a predicted displacement that is smaller than the allowable displacement.

The following example illustrates the design method:

Example: Design a single helical pier foundation for a 100 m (328 ft) long wall with a design load of 20kN/m (1,370lb/ft). Use a pier with allowable capacity of 111 kN (25,000 lb). Design temperature is –1°C (30.2°F) and the allowable displacement after 20 years is a) 25 mm (1 in), b) 1.5 mm (0.06 in, (small displacement is selected for illustration).

Solution:

a) Select the chart matching –1°C (Figures 6.2 and 6.5, or 6.8 and 6.9). Note that all loads yield smaller displacement than the allowable of 25 mm. Then, for the most economical design, select a design load of 111 kN per pier. The required spacing between the piers becomes 111kN/(20kN/m) = 5.55 m (18.2 ft). If the structural considerations allow this, the total number of the piers is 100m/(5.55m/pier) + 1 pier = 19 piers.

b) Select the chart matching –1°C for a single pier (Figures 6.2 or 6.8). If the piers were loaded to their capacity of 111 kN, the allowable displacement of 1.5 mm would be exceeded in 11 years. Consequently the piers need to be loaded by a smaller load. After 20 years a load of 83 kN (18,750 lb) per pier would yield 1.3 mm displacement that is smaller than the allowable maximum displacement and is therefore acceptable. To obtain a load of 83 kN per pier, the spacing between the piers becomes 83kN/(20kN/m) = 4.15 m (13.6 ft) and the total number of the piers is 100m/(4.15m/pier) + 1 pier = 25 piers. Again, check if the 4.15 m (13.6 ft) spacing meets the structural requirements. See Figure 6.8 for an illustration of this design example.

Check if piers with double helix would yield in more economical design. Select the chart matching –1°C for a double pier (Figures 6.5 or 6.9). Again, all loads yield smaller displacement than the allowable of 25 mm. Then, for the most economical design, select a design load of 111 kN per pier. The required spacing between the piers becomes 111kN/(20kN/m) = 5.55 m (18.2 ft). If the structural considerations allow this, the total number of the piers is 100m/(5.55m/pier) + 1 pier = 19 piers. Check if 19 double helix piers are less expensive than 25 single helix piers. See Figure 6.9 for an illustration of this design example.

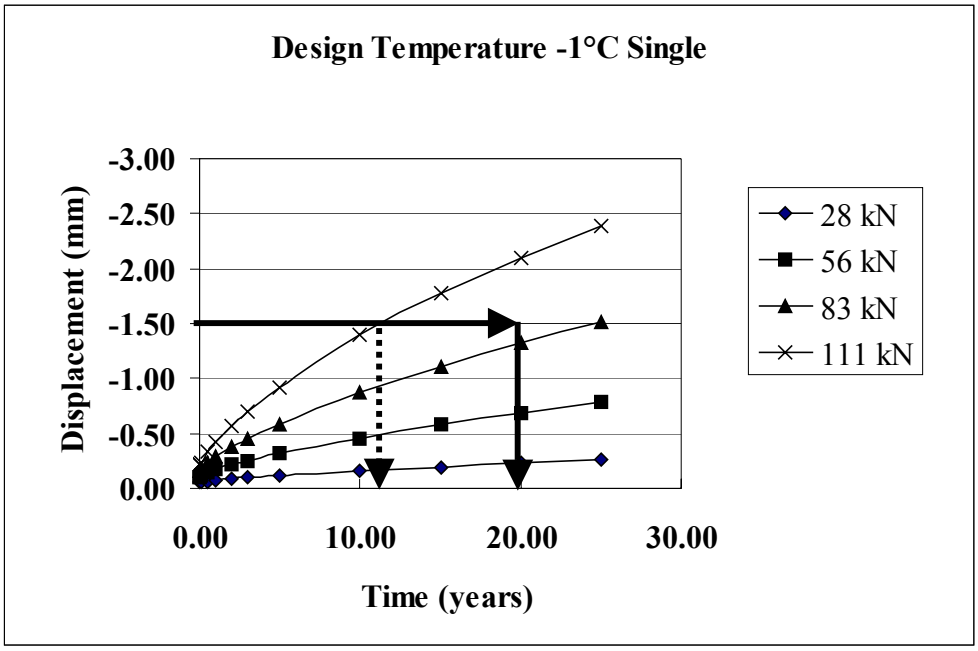

Figure 6.8. Design Example for Single Helix Pier at –1°C

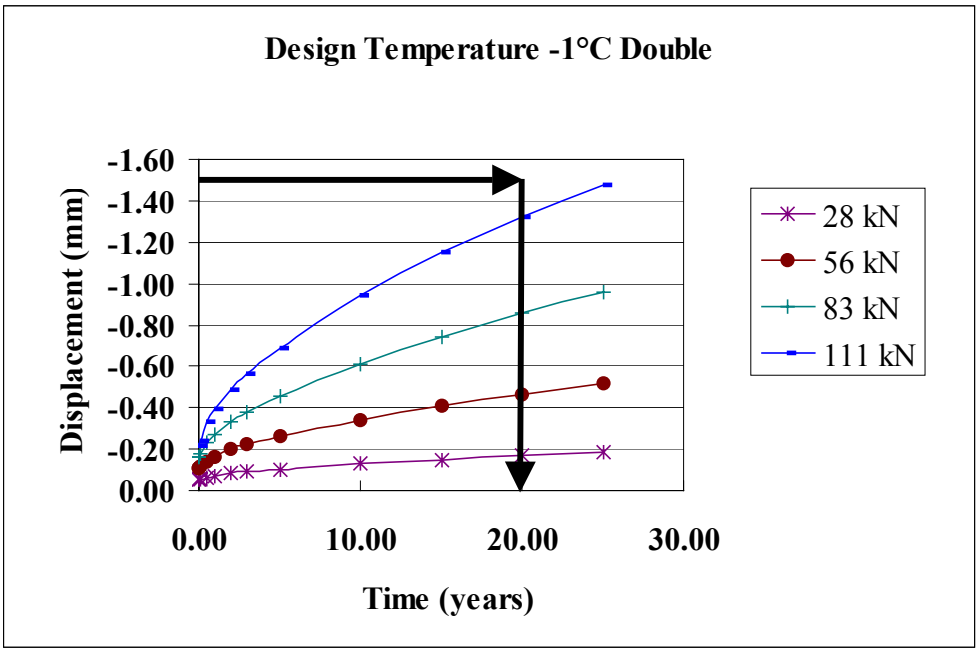

Figure 6.9. Design Example for Double Helix Pier at –1°C

6.5 Conclusions and Recommendations for Design

Even if specific design guidelines for frozen ground have not been in existence before, the piers are used successfully as a foundation for boardwalks and utilidors. However, engineers have been hesitating to specify helical piers as building foundations, because of the lack of design guidelines. The design method suggested here is very simple and helpful in designing piers for a given frozen soil. The design curves do not apply to any other soil than that given in Table 6.1, and even if the given creep displacements are insignificant, other soil properties may produce larger settlements. To properly design any foundations in frozen ground, the engineer still needs the creep parameters for the foundation soil. These parameters are not readily available for the engineering community. Therefore, actual soil testing needs to be conducted for various soils to create a library or database of soils encountered in cold regions. These tests would include strength parameters in thawed conditions, and creep and strength parameters at several frozen temperatures under various loads. Currently, to analyze any other soil, the engineer needs to contact the authors for FEA runs to produce the creep curves.

7. CONCLUSIONS AND RECOMMENDATIONS

7.1 Conclusions

The Evaluation of Helical Piers for Use in Frozen Ground project included a comprehensive literature review, field study, full-scale test at the CRREL, development of finite element models and creating design guidelines. The following findings were obtained during the work:

According to Literature Review, the design and performance of helical anchors and piers in warm soils is analyzed using simple formulas that predict the field behavior adequately. However, the behavior of warm soils differs greatly from the behavior of frozen ground. The extent to which design principles for helical piers in warm soil applications are applicable to frozen ground is not currently understood. The behavior of piles in frozen ground is routinely estimated using adfreeze strength along the pile length. The design principles and mechanics for adfreeze piles cannot be directly applied to helical piers.

The findings from the full-scale test at CRREL indicated that the piers did not move at -4°C under loads from 5.1 to 40.7 kN (1146 to 9140 lb). The results for the -1°C test indicated some movement, which was interpreted as a result of uneven temperatures on the soil basin and partial thaw settlement. The FEM could not be calibrated using the test results, because of the uneven temperatures in the test cell and the short loading times. Installation of the piers in the frozen ground proceeded without any problems.

The field study showed that the helical piers have been used by thousands in a variety of projects in frozen ground in rural areas of Alaska. They have performed very well when installed below the active layer in cold, continuous permafrost. When firmly anchored in the permafrost they have resisted the forces of heaving and jacking. Results are also good in warm discontinuous permafrost, but there are more instances of heaving and jacking of the piers.

The developed FEA model results will increase understanding of helical piers in various soil conditions as well as provide insight into design and installation considerations. The installation failure FEA model displayed the stresses encountered due to torque during installation of the pier system. The stress concentration that occurred at the bottom of the weld was very similar to known, but rare, failure mechanisms for helical piers. This information can be used to design better connection geometry at this critical location. The FEA models provided valuable information regarding the distribution of stress and displacement within the soil. According to the analysis, the soil stress is not uniformly distributed under helixes. Also, the analysis indicates that the soil reaction pressure is not equally distributed between the helixes. Only the bottom helix contributes to any large extent to the pier's capacity.

The detailed helix FEA models provided a close examination of the stresses within the spiral during the application of vertical design loads. The highest stresses were encountered at the top and bottom ends of the spiral welds. This information can be used to make changes to the design of these structures if necessary as well as provide a more detailed picture of the physical situation encountered by helical structures embedded in soil.

Finally, the creep FEA analysis indicated the creep behavior of helical piers in frozen ground and provides valuable insight into the magnitude of settlement that can be expected over extended periods of time. The creep deformation is not significantly different between piers with single or multiple helixes.

According to original plan, to validate the FEA models, the results would have been compared with physical tests conducted at CRREL. The authors felt that the non-uniform test temperature and short loading time at the CRREL resulted in test results that could not be used to calibrate the FEM.

The design method suggested includes simple design curves that are helpful in designing piers for a given frozen soil. To analyze creep of helical piers in any other soil, the engineer needs to contact the authors for FEM runs to produce the creep curves.

7.2 Recommendations

Based on the literature review, field study, and the FEM results, it is concluded that the helical piers are suitable foundations for frozen ground. Their use is highly recommended for their ease of transportation and installation, small ground disturbance, resistance to pile jacking, and stability. It is recommended that foundation engineers and research and development engineers for pier manufacturers utilize the developed FEM.

7.3 Future Research Needs

The engineer has to contact the authors for design of a specific foundation in a given soil and design temperature. It would be more convenient if general design curves existed for a variety of soils at different design temperatures. Therefore, it is recommended that frozen soil properties would be determined for a multitude of typical foundation soils in Alaska and other cold regions.

Since the CRREL experiment could not be used to calibrate the FEM, additional tests are recommended for creep observations at controlled temperatures.

ACKNOWLEDGEMENTS

This research project was cooperation between the Alaska Science and Technology Foundation (ASTF), University of Alaska Anchorage (UAA), Alaska Foundation Technology, Inc (AFT) and U.S. Corps of Engineers Cold Regions Research and Engineering Laboratory (CRREL). The cash funding for the project was provided by the ASTF, while the UAA, AFT and CRREL provided in-kind contributions. The driving force behind the project was the AFT, a Chance® distributor, without whose persistence none of the work would have been possible. The authors, Dr. Zubeck and Dr. Liu would like to thank all participants for their financial support. They would also like to thank Tom Metlicka from AFT for his help throughout the project and for installing the piers at the CRREL, Dr. Vincent Janoo and Robert Eaton from CRREL for conducting and reporting the CRREL experiment, graduate student Lynn Aleshire for her remarkable contributions to the literature review and field study, students Sean Baginsky and Paul Kendal for their finite element analysis work and Todd Verdick for his help in the CRREL experiment. Gary Bowen was very helpful throughout the project in providing guidance and comments. Warm thanks also goes to Dan Schubert and Matt Dixon from the Alaska Native Tribal Health Consortium, Department of Environmental Health and Engineering, Roger Burleigh and Jon Menough from the State of Alaska Department of Environmental Conservation Village Safe Water for their tremendous help in the field study.

Appendix D

Troubleshooting Communications in Buckland

Specialty Electric

P.O. Box 2023 Homer, Alaska

9-17-19

Troubleshooting and Analysis Buckland Power Plant Remote Access System

Buckland power plant remote access system basic description, current system:

To provide remote access to the Buckland power plant control system a modem supplied by the satellite provider Viasat is used as the ISP, internet service provider. The Cisco firewall/router does not use a VPN. The Viasat modem supplies a static IP address that is used by the Cisco firewall/router. The Cisco firewall/router model #ASA5505 supplies a login that allows access to the Buckland power plant control system. The satellite modem/router can only provide this static IP address when switched to bridge mode in settings. The Cisco router is connected to port #0 of the satellite modem/router by an Ethernet cable, the Cisco firewall/router needs to receive the static IP address provided by Viasat to maintain remote accessibility. If the Viasat router factory resets and fails to send the proper IP address, the Cisco firewall/router is no longer accessible remotely and the whole remote access system fails. All operator control stations, wind turbine communications, SMA communications, and the EPS main control system switchboard server are all plugged into the Cisco firewall/router Ethernet ports #1 through 7. Note: if power is disrupted to the Cisco firewall/router all remote communication and internal communication that are connected to the Cisco firewall/router will fail due to to current network topology.

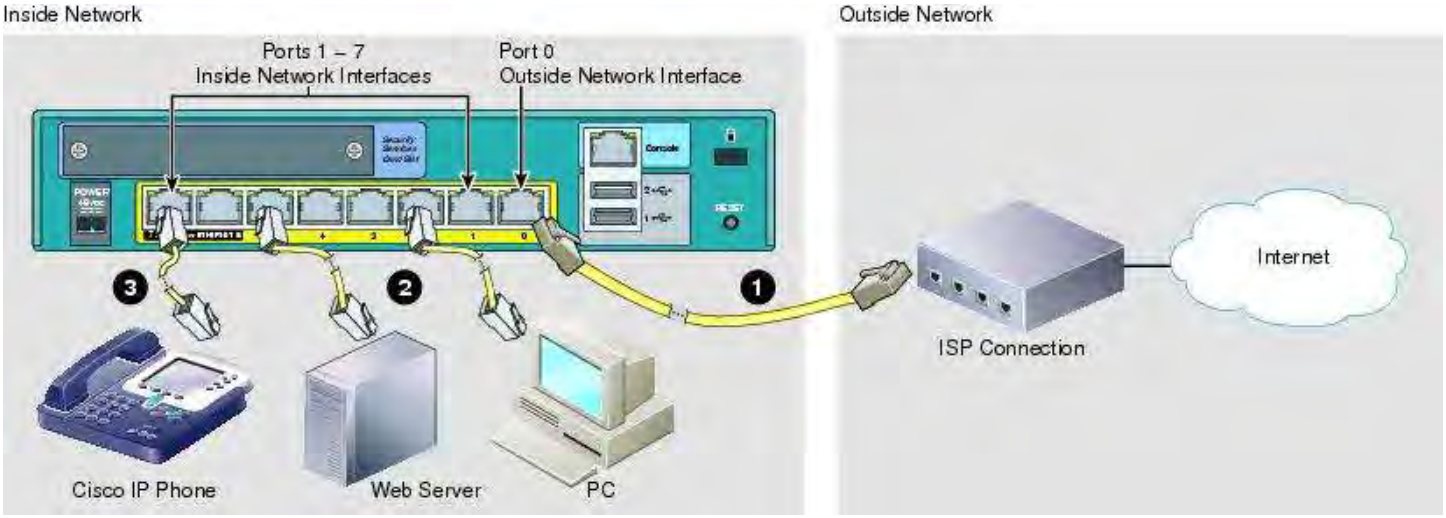

Current Remote communications issues:

1. Remote communications has been observed to fail multiple times due the satellite modem/router being factory reset. It is possible the router was tampered with. Remote communications fail due to the satellite modem switching out of bridge mode when it is factory reset. The static IP address cannot be supported when the satellite modem/router is not in bridge mode. The satellite modem then has to be manually configured onsite in order to switch back to bridge mode to provide a static I.P. Address. The Cisco firewall/router also has to be manually reset to take the static I.P address.

2. Remote communications has failed recently with the satellite modem/router appearing to be still in bridge mode with the static IP address assigned correctly. The issue is still being investigated, could be a loose Ethernet cable connection between the Cisco firewall/router and the Viasat satellite modem/router.

Specialty Electric

P.O. Box 2023 Homer, Alaska

9-19-19

Buckland Power Plant SCADA System Improvements

System Improvements Made on Service/Integration Trip to City of Buckland 09-04-19 – 09-09-19:

1. Created a digital schematic drawing to establish a clear up to date outline of the current system and distributed it throughout the facility. The up to date drawing will allow operators and technicians to have a better understanding of the full system and streamline communications on the subject.

2. Operators reported network communication errors between the Belkin router, SMA Data Manger, Cisco firewall/router, Viasat satellite modem/router, ABB micro-grid controller, SMA diagnostic laptop and the Sunny Boy Inverters. Investigated the communication network between the associated devices. Worked with SMA and ABB to solve the network communications issues. Tested the communications network by pinging each Sunny Boy Inverter from the ABB operator computer. Solved networking issues and stabilized the communications network.

3. Performed a health assessment on the overall back up power systems for the Buckland power plant control system. Recommendations documented.

4. Verified the functionality of the GCI cellular high speed data connectivity inside the power plant. With further integration, cellular connectivity could now be used to provide remote access instead of satellite. This could reduce data cost and increase network dependability. Will provide document detailing integration plan and option.

5. Assessed installation of network router, Cisco firewall/router, wind turbine Ubiquity antenna power over Ethernet converter, satellite modem/router cables, EPS network cable and wind turbine computer network cable. Developed plan to re-negotiate a more effective installation.

6. Re-established remote communications to power plant control system. Coordinated with the satellite provider Viasat's communications expert Mr. Ingemar Mathiasson to determined connectivity. Evaluated remote communication infrastructure with Will Galton Senior Project Manager and Jon Jaeger Senior Microgrid Application Engineer of ABB. Created a plan to change the remote communications over to a Virtual Private Network utilizing the Cisco firewall/router to increase reliability and cyber security.

7. Initiated a plan with Jon Jaeger Senior Microgrid Application Engineer of ABB and made a integration assessment based on current infrastructure to install a dedicated smart data logging system for the City of Buckland.

Appendix E

Design Documents

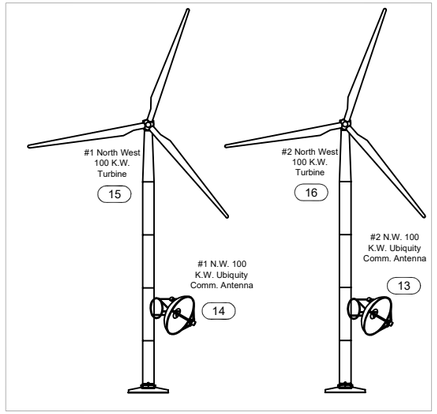

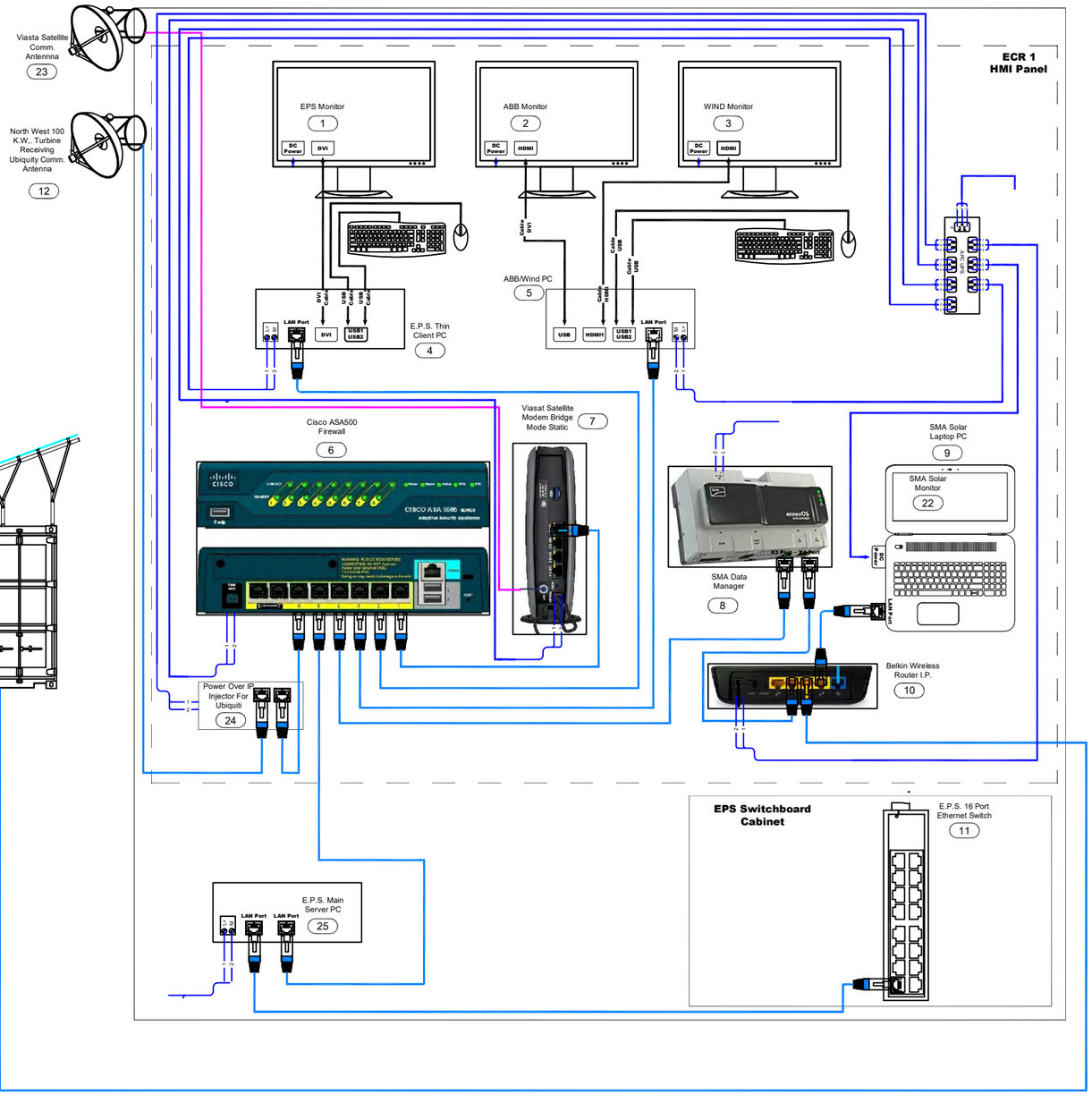

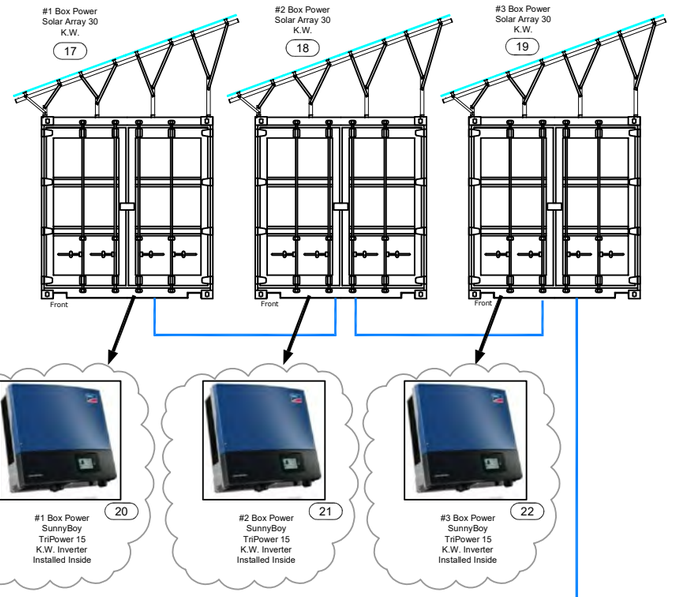

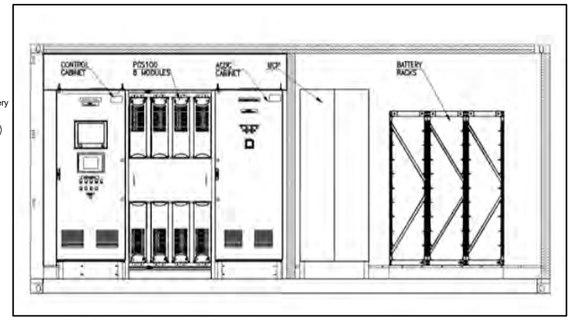

Drawn By:	Checked By:	Approved By - Date:	Filename:	Date:	Scale:
MRM				08/02/18	None

Specialty Electric

Marine, Microgrid, Industrial, Yachts

P.O.Box 2023
Homer, Alaska

Ph: (907)399-1625
Ph2: (985)264-7023

Buckland Complete System Integration Drawing Data and Power - For Material Estimate Only

Drawing Number:	Edition:	Sheet:
SCT000	-	1 of 1

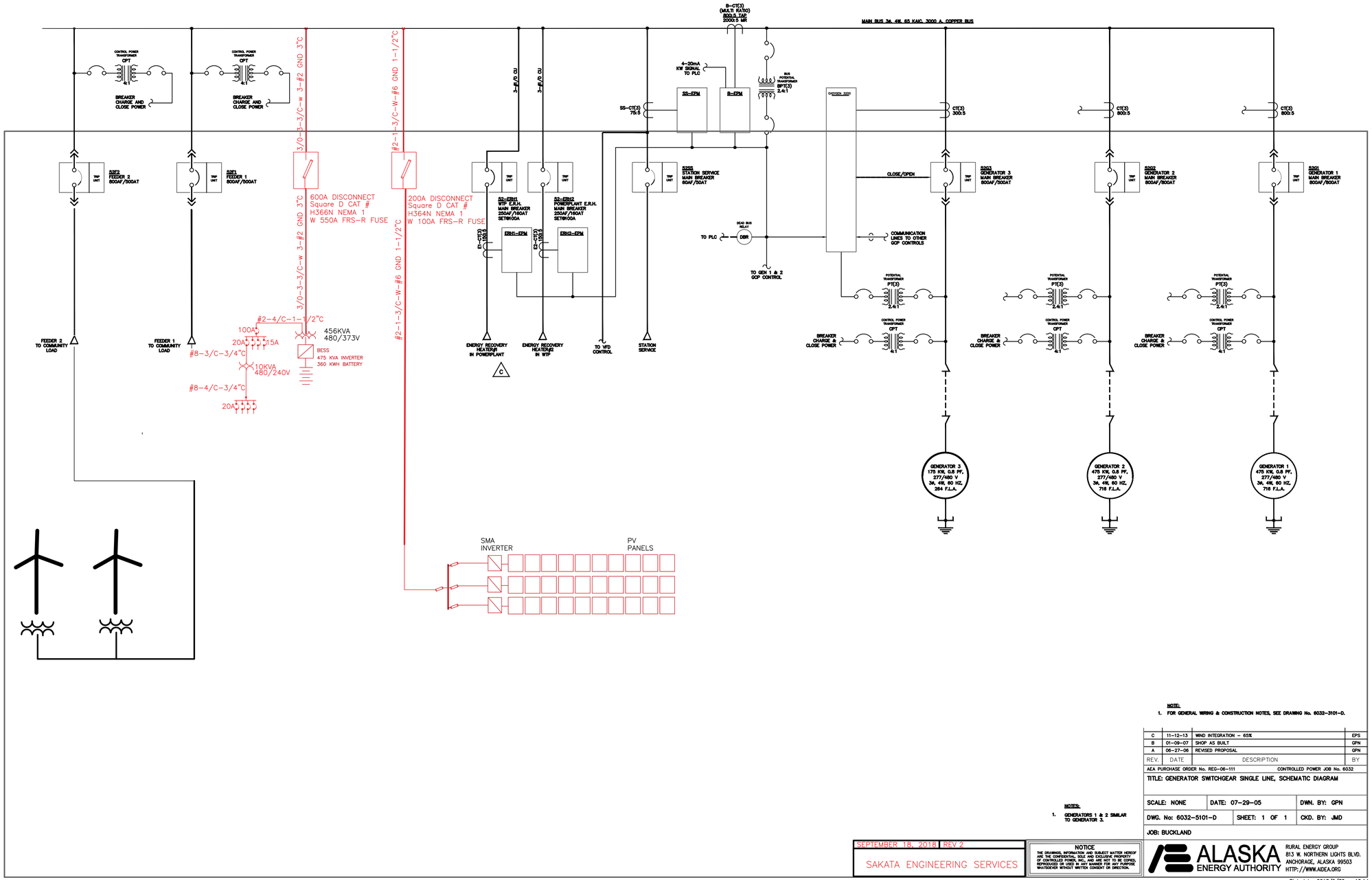

NOTE:
1. FOR GENERAL WIRING & CONSTRUCTION NOTES, SEE DRAWING No. 6032-3101-D.

NOTES:
1. GENERATORS 1 & 2 SIMILAR TO GENERATOR 3.

REV.	DATE	DESCRIPTION	BY
C	11-12-13	WIND INTEGRATION – 65%	EPS
B	01-09-07	SHOP AS BUILT	GPN
A	06-27-06	REVISED PROPOSAL	GPN

AEA PURCHASE ORDER No. REG-06-111 — CONTROLLED POWER JOB No. 6032

TITLE: GENERATOR SWITCHGEAR SINGLE LINE, SCHEMATIC DIAGRAM

SCALE: NONE	DATE: 07-29-05	DWN. BY: GPN
DWG. No: 6032-5101-D	SHEET: 1 OF 1	CKD. BY: JMD
JOB: BUCKLAND		

SEPTEMBER 18, 2018 | REV 2

SAKATA ENGINEERING SERVICES

ALASKA ENERGY AUTHORITY
RURAL ENERGY GROUP
813 W. NORTHERN LIGHTS BLVD.
ANCHORAGE, ALASKA 99503
HTTP://WWW.AIDEA.ORG

Plot date: 2013/9/30 – 12:14

General Notes

No.	Revision/Issue	Date

Firm Name and Address

Project Name and Address

#####
#####
#####
#####

Project #####

Date 9/18/2018

Scale As Noted

Sheet

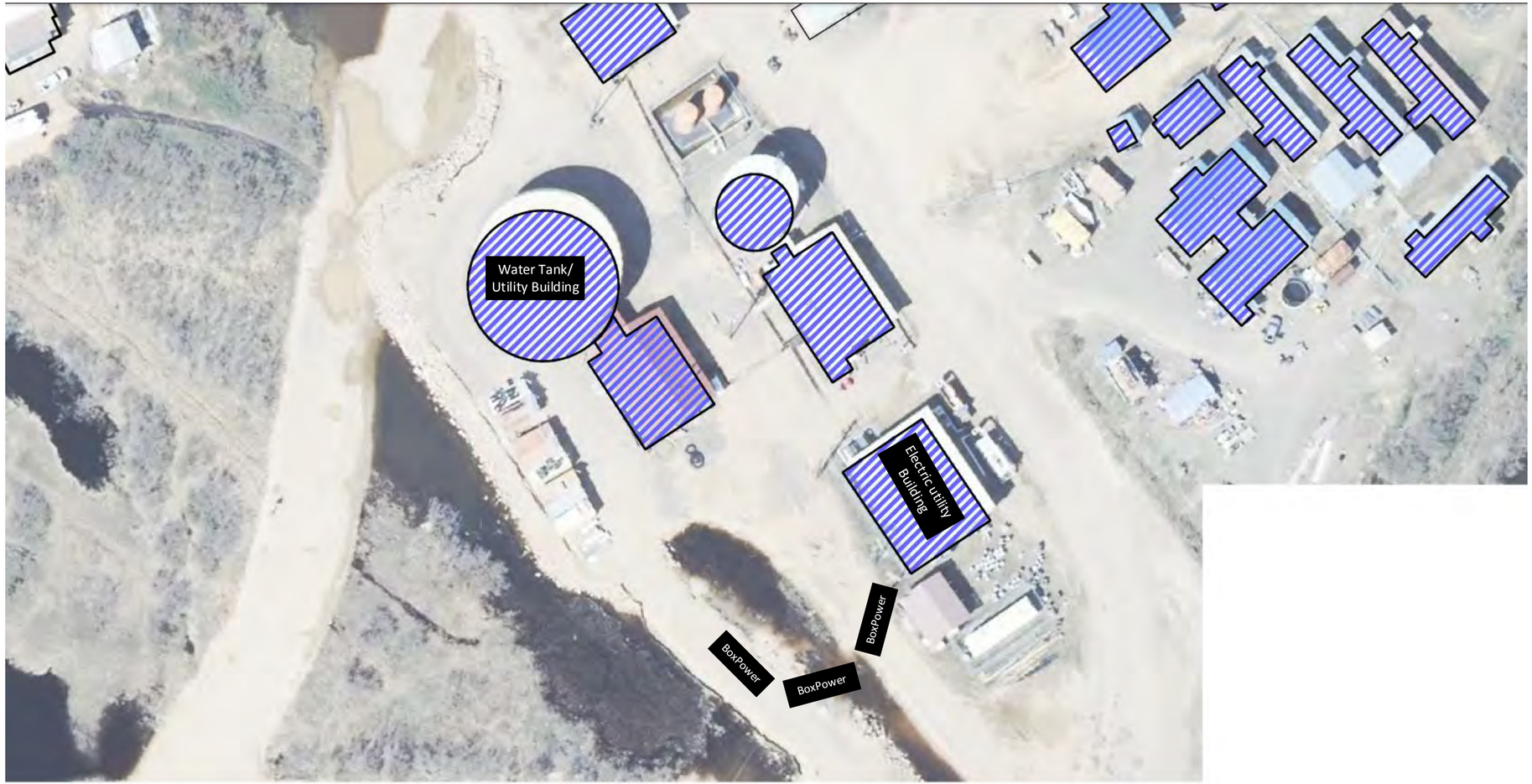

Buckland Site Layout

Deering - Planning Dimensions for Container Layout

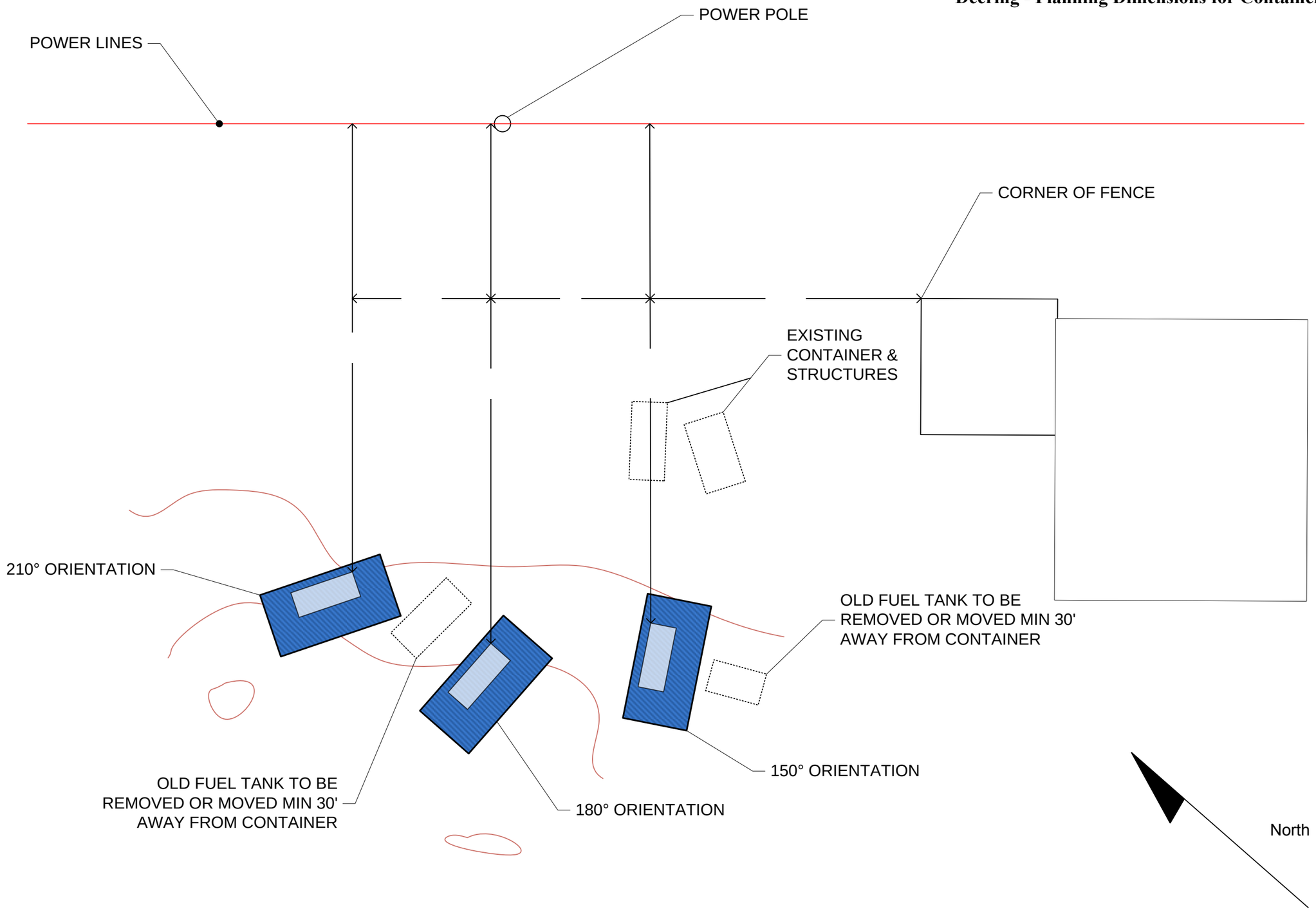

SCALE
1" = 30'

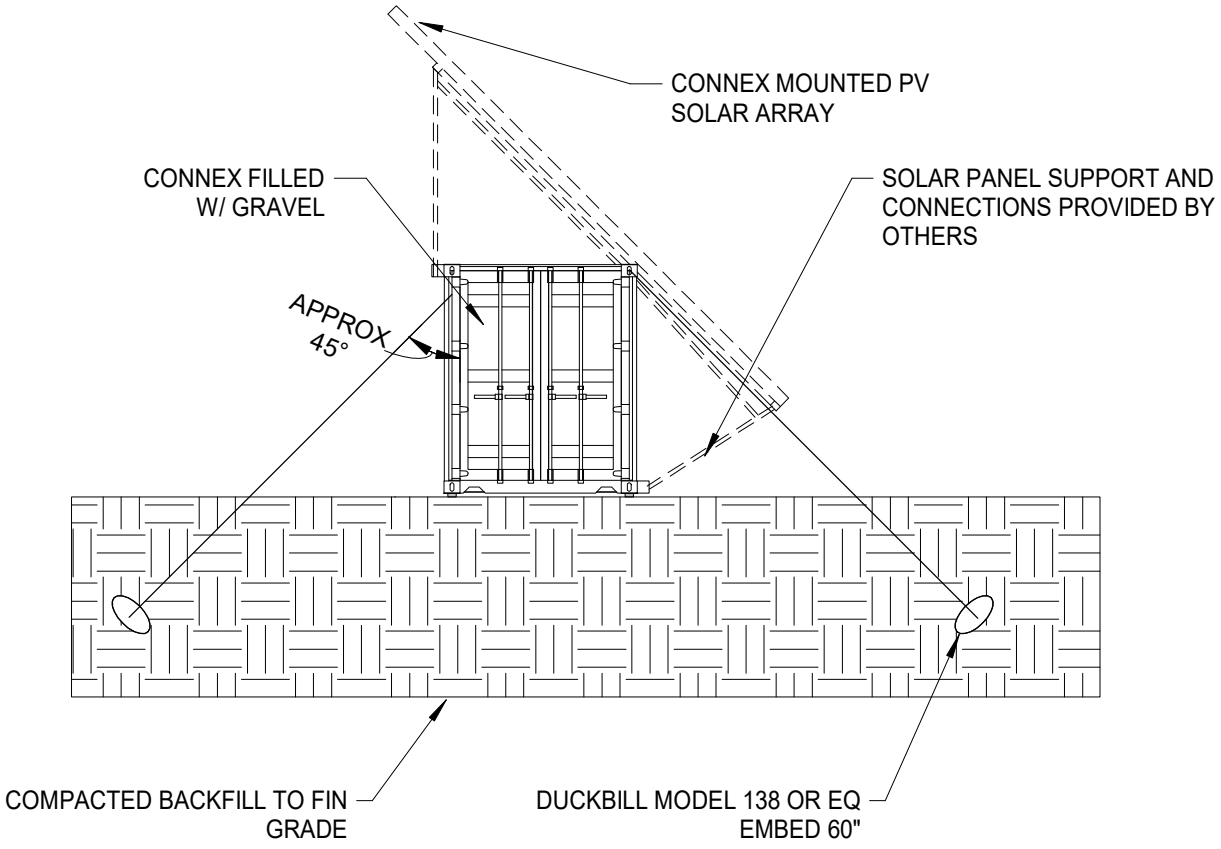

1506 WEST 36th AVENUE
ANCHORAGE, AK, 99503
PHONE: 907.561.1011
FAX: 907.563.4220
WWW.PNDENGINEERS.COM

P N D
ENGINEERS, INC.

PROJECT: **DEERING SOLAR ARRAY**

TITLE: FOUNDATION PLAN AND DETAILS

DRAWN BY:	DL			SHEET NO:
DESIGNED BY:	DL	DATE:	05/29/19	**S1.0**
CHECKED BY:	JG	PROJECT NO:	191088	

Appendix F

Project Documents

Photovoltaic PV101

SOLAR ENERGY INTERNATIONAL

Educate. Engage. Empower.

NANA

Northwest Arctic Borough Incorporated June 2, 1986

Kotzebue Electric Association

USDA

Southeast Conference

ATC

Alaska Technical Center
June 18-22, 2018

ATC is excited to provide the Photovoltaic 101 Workshop opportunity with our business industry partners:

Solar Energy International, USDA, Southeast Conference, NANA Regional Corporation, KEA, Northwest Arctic Borough

Please contact Erica Nelson enelson@nwarctic.org or Georgie Phillips gphillips@nwarctic.org for more information (907)442-1500

PV101 Workshop

Solar Energy International to provide the following:

- Customized, in-person technical IREC Accredited training with two SEI instructors. The training counts for educational hours through NABCEP.
- Participant materials including a notebook of lessons, quizzes and exercises, and a Solar Electric Handbook: Photovoltaic Fundamentals and Applications or NEC
- Records of Completion for each person who successfully completes the training.
- SEI will provide limited hands-on training equipment, as needed

Students who complete the PV101 workshop will be able to perform the following:

- Differentiate between various renewable energy sources and types of systems
- Perform power and energy calculations
- Evaluate utility bills and rate plans, perform a load analysis for a grid-direct system, and compare system production to energy consumption
- Describe energy efficiency measures that can be implemented to reduce electricity usage and PV system size
- Analyze different net metering rules, rebates, and incentives that affect the final cost of a PV system
- Diagram and list the features, applications, and components of the following PV system types: DC direct, stand-alone, grid-direct, and grid-tied with battery back-up
- Obtain and apply specifications for PV modules and determine their performance given various environmental and operating conditions
- Identify various types of digital multimeters and explain how to use them safely
- Diagram and determine the power, current, and voltage characteristics of PV modules in different series and parallel configurations
- Determine the magnetic declination, define azimuth and altitude angle and evaluate the shade potential for a given site
- Estimate energy production of a PV system based on location specifics including orientation and tilt angle
- List the pros and cons of different mounting systems (ground, pole, roof, and trackers) and determine the number of modules that can fit in a given roof space
- Given specific site criteria, evaluate what type of inverter is appropriate
- Decipher balance-of-system equipment specification sheets to determine the critical information needed for system design
- Design a residential grid-direct system including the array, inverter, circuit conductors, an overcurrent protection
- Define equipment grounding, system grounding, and components and conductors used for grounding
- Identify the following wires and components on schematics of residential grid-direct systems: disconnects, inverter, equipment grounding conductors, ungrounded conductors, grounded conductors, the grounding electrode(s), and the AC and DC system ground
- Identify potential safety hazards and the proper personal protective equipment for working on grid-direct PV systems
- List the order of installation, commissioning, and decommissioning of a grid-direct PV system